CHAPTER 46

Conducting Polymers: Electrical Conductivity

Arthur J. Epstein

*Department of Physics and Department of Chemistry, The Ohio State University, Columbus, OH 43210–1117*

46.1 INTRODUCTION

For the past 50 years, conventional insulating polymer systems have been increasingly used as substitutes for structural materials such as wood, ceramics, and metals because of their high strength, light weight, ease of chemical modification/customization, and processibility at low temperatures [1]. In 1977, the first electrically conducting organic polymer, doped polyacetylene, was reported [2], spurring interest in "conducting polymers [3]." The common electronic feature of pristine (undoped) conducting polymers is the π-conjugated system which is formed by the overlap of carbon p_z orbitals and alternating carbon–carbon bond lengths [4–6], shown schematically in Fig. 46.1. (In some systems, notably polyaniline, nitrogen p_z orbitals and C_6 rings also are part of the conjugation path.) Figure 46.2 shows the chemical repeat units of pristine forms of several families of conducting polymers, i.e., *trans-* and *cis-*polyacetylene [(CH)$_x$], poly (1,6-heptadiyne), the leucoemeraldine base (LEB), emeraldine base (EB), and pernigraniline base (PNB) forms of polyaniline (PAN), polypyrrole (PPy), polythiophene (PT), poly

(*p*-phenylene) (PPP), poly(*p*-phenylene vinylene) (PPV), polypyridine (PPyr), and poly (*p*-pyridyl vinylene) (PPyV). The electronic ground states of these systems are varied. Undoped *trans-*(CH)$_x$ has a twofold degenerate insulating ground state stabilized by the electron–phonon interaction (Peierls instability) [7] and contributions due to Coulomb repulsion [8–12]. Poly(1,6-heptadiyne) [13] and the pernigraniline oxidation state of PAN [14–16] and their derivatives also have degenerate ground states; that is, single and double bonds (benzenoid and quinoid rings for pernigraniline base polymer) can be interchanged without affecting the ground state energy. The remaining polymers illustrated in Fig. 46.2 and their derivatives have nondegenerate ground states; that is, interchange of single and double bonds leads to electronic structures of different energy [7].
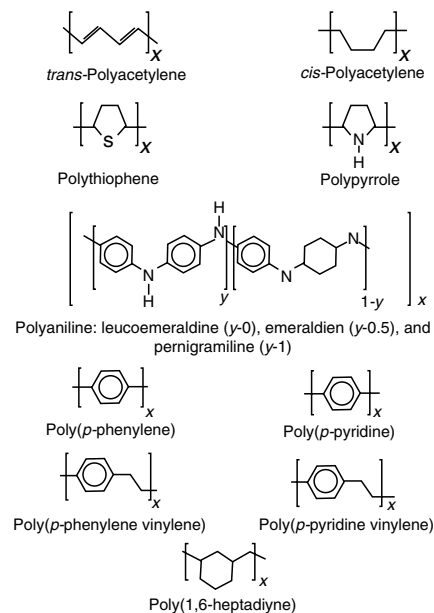
The conductivities of the pristine polymers are transformed from insulating to metallic through the process of doping, with the conductivity increasing as the doping level increases. Both n-type (electron donating) and p-type (electron accepting) dopants have been utilized to induce an insulator–metal transition in electronic polymers [2–7]. The
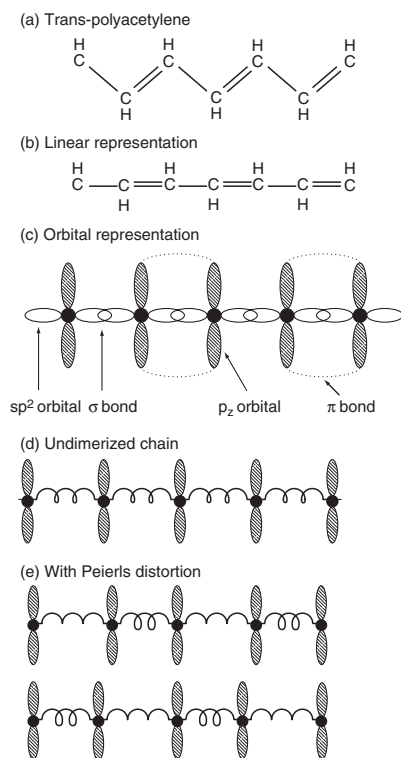
FIGURE 46.1. (a) Chemical structure of *trans*-polyacetylene [$(CH)_2$]. (b) Linear representation. (c) Orbital diagram of the carbon backbone with the sp^2 orbitals of adjacent carbons overlapping to from σ-bonds. The p_z orbitals form π-bonds between alternating pairs of atoms to create a conjugation path that allows electrons to exist in delocalized states over the chain. (d) Chain idealization in which the σ-bonds are represented as springs that exert a restoring force on the atoms. Here the chain is drawn in the ground state neglecting the effects of Peierls instability. (e) Peierls distortion due to electron-phonon coupling causes the chain to become dimerized with two degenerate ground state phases. © (1986) from [4]. Reproduced by permission of Routledge/Taylor & Francis Group, LLC.

FIGURE 46.2. Repeat units of several electronic polymers.

doping procedures differ from conventional ion implantation used for three-dimensional semiconductors. The doping process for polymers is carried out electrochemically or by exposing the films to vapors or solutions of the dopant [4]. Unlike substitutional doping, as occurs for conventional semiconductors, in electronic polymers the dopant atoms are positioned interstitially between chains, and donate charge to or accept charge from the polymer backbone [2,4,17]. The polymer backbone and dopant ions form new three-dimensional structures. There is a rich variety in these structures, with differing structures occurring for different dopant levels, different structures for different processing routes, and varying degrees of local order [18–20].

The negative or positive charges initially added to the polymer chain upon doping do not simply begin to fill the rigid conduction or valence bands, immediately causing metallic behavior. The strong coupling between electrons and phonons causes lattice distortions around the doped charge [7]. For the degenerate ground states, charges

added to the backbone through doping or photoexcitation are stored in soliton and polaron states [5–7,21–24]. For nondegenerate systems, the charges introduced by low doping or photoexcitation are stored as polarons or bipolarons (PT [25–30], PPy [26,31–34], PPV [35–37], PPP [38–40], and polyaniline [41,42]). Photoexcitation also leads to generation of neutral solitons [43,44] and neutral excitons [44–51]. At heavy doping of *trans*-polyacetylene, a soliton lattice that essentially overlaps the valence and conduction band is proposed to form [52,53]. For nondegenerate polymers, heavier doping to the metallic state results in polarons interacting to form a "polaron lattice" or partly filled energy band [54–56]. Some models suggest equilibrium between polarons and bipolarons [33,37,40].

In contrast to the n- and p-type doping processes applied to polyacetylene, polypyrrole, polythiophene, leucoemeraldine base, etc. for polyaniline emeraldine base (EB) form, the conductivity varies with proton (H^+ ion) doping level. In the protonation process, there is no addition or removal of electrons to form the conducting state [54]. Figure 46.3 schematically demonstrates the equivalence of protonic acid doping of emeraldine base and p-doping of leucoemeraldine base to form the conducting emeraldine salt. Similar electronic behavior has been observed for protonic acid doped PAN [54,55,57–60] as for the other nondegenerate ground state systems. Polarons are important at low doping, and, for doping into the metallic state, a polaron lattice forms [54,55,61]. Bipolarons are formed in less ordered regions [62].

Doped polyacetylene has been the prototype system since the initial report of the achievement of a conductivity of $\sigma \sim 100\,\text{S/cm}[100\,(\Omega\cdot\text{cm})^{-1}]$ upon doping with iodine and other donors and acceptors [2]. Subsequently, $(CH)_x$ was synthesized by alternate routes [63–69] that yielded higher conductivities upon doping. The room temperature
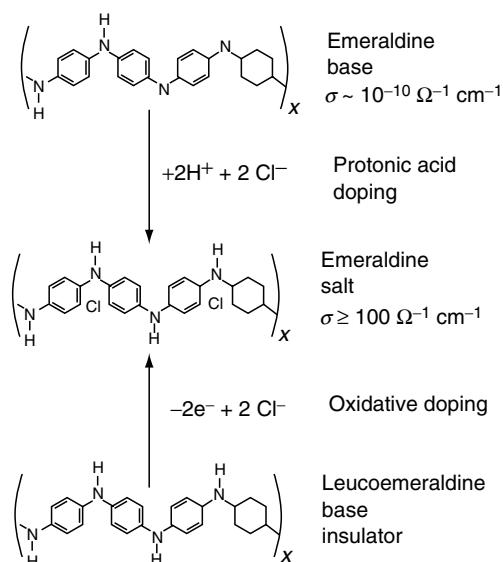
FIGURE 46.3. Illustration of the oxidative doping (p-doping) of leucoemeraldine base and protonic acid doping of emeraldine base, leading to the same final product, emeraldine salt (After Ref. [54]).

dc conductivity (σ_{DC}) for doped films of some of these new materials has been reported to be as high as $\sim 10^5 \, \text{S/cm}$ [63,64], rivaling that of traditional metals ($\sigma_{DC} \sim 10^4 - 6 \times 10^5 \, \text{S/cm}$). Recent advances in the processing of other conducting polymer systems has led to improvements in their σ_{DC}, to the range of $\sim 10^3$–10^4 S/cm [3,63–65,70–72], renewing interest in the properties of the polymer metallic state. It is noted that the absolute value of the highest conductivities achieved remains controversial. With theses improvements in σ_{DC}, many traditional signatures of an intrinsic metallic nature have become apparent, including negative dielectric constants, a Drude metallic response [73–75], temperature independent Pauli susceptibility [61,62,75–79], and a linear dependence of thermoelectric power on temperature [80,81]. However, the conductivities of even new highly conducting polymers, though comparable to traditional metals at room temperature, generally decrease as the temperature is lowered. Some of the most highly conducting samples remain highly conducting though, even in the millikelvin range [70,82].

Since there is still a great diversity in the properties of materials synthesized by even the same synthetic routes, in presenting properties of these polymers, correlated structural, transport, magnetic, and optical studies of the same materials are emphasized. In this chapter, the intrinsic properties of the metallic state of a broad class of conducting polymers will be reviewed with emphasis on the universality in the observed behaviors. Throughout the article, the correlation of x-ray, dc and ac transport, optical, and magnetic measurements will be stressed to demonstrate the relationships where such correlated data is available. On those systems where the correlated results are not available, the available data will be summarized.

The outline for the chapter is as follows. A brief overview of conductivities of various conducting polymers is presented in Section 46.2. This section summarizes models for the insulator–metal transition, localization, and metallic conductivity. In Section 46.3, the structural results of x-ray diffraction studies are introduced. Section 46.4 surveys the metallic density of states of highly conducting polymers. The results of temperature-dependent dc conductivity, thermoelectric power, and microwave dielectric constant are reviewed in Sections 46.5, 46.6, and 46.7, respectively. In Section 46.8, the optical properties of the highly conducting state are presented. A discussion of the ultimate conductivity of conducting polymers including resonance quantum transport in doped conducting polymers is given in Section 46.9. Section 46.11 introduces new morphologies of conducting polymers such as fibers. Applications of conducting polymers including an electric field effect are introduced in Section 46.10. The last two sections are a summary and a glossary of frequently used terms in the chapter.
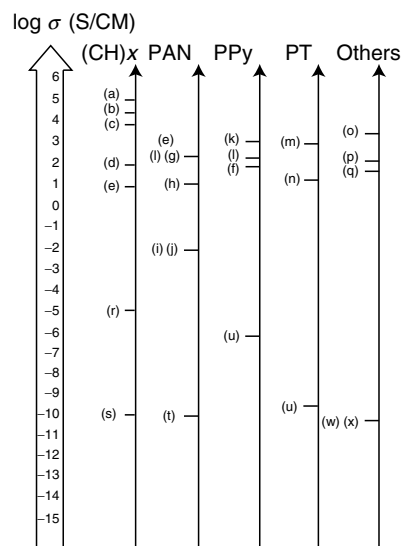
46.2 CONDUCTIVITY

46.2.1 Overview of Conductivity of Conducting Polymers

Figure 46.4 presents representative values of the room temperature conductivities reported [17,63–65,71–73,83–98] for the most widely studied doped conducting polymers. Also indicated is the dopant utilized for each value shown. The conductivities of each of these systems increase by more than ten orders of magnitude upon doping the pristine polymer. Further studies of the room temperature conductivities of these polymers and their derivatives and copolymers yield values of the dc conductivities within the ranges shown in Fig. 46.4.

46.2.2 Models of Insulator–Metal Transition

Many efforts have been made to account for the insulator–metal transition that occurs with an increasing doping level in conducting polymers. The richest area of theoretical work concerning the insulator–metal transition is for polyacetylene, which has been studied for the longest time. One of the simplest approaches is to include only the nearest neighbor overlap (leading to a one-dimensional energy band) and the electron–phonon interaction in the starting Hamiltonian [7,21–23]. Within this model, a metallic state is not stable for an isolated one-dimensional chain due to the formation of a Peierls distortion [99] yielding an energy gap at the Fermi level. Negative (n-type) or positive (p-type) doping leads to formation of negatively or positively charged solitons that form completely filled or empty bands [7]. The Su–Schrieffer–Heeger (SSH) Hamiltonian frequently has been used as the starting point for adding additional interactions. Mele and Rice suggested [100] the

log σ (S/CM)

FIGURE 46.4. Overview of conductivity of conducting polymers at room temperature. (a) stretched $[CH(I_3)]_x$ (from Ref. [63]), (b) stretched $[CH(I_3)]_x$ (from Ref. [64]), (c) $[CH(I_3)]_x$ (from Ref. [65]), (d) $[CH(I_3)]_x$ (from Ref. [17]), (d') $[CH(I_3)]_x$ (from Ref. [83]), (e) stretched PAN–HCl (from Ref. [71]), (f) PAN–CSA from *m*-cresol (from Ref. [84]), (g) PAN–CSA from *m*-cresol (from Ref. [73]), (h) PAN derivative: poly(*o*-toluidine) POT-CSA fiber from *m*-cresol (from Ref. [85]), (i) POT-HCl (from Ref. [86]), (j) sulfonated PAN (from Ref. [87]), (k) stretched $PPy(PF_6)$ (from Ref. [88]), (l) $PPy(PF_6)$ and (l') PPy(TsO) (from Refs. [74,89]), (m) iodine doped poly(dodecylthiophene) (from Ref. [72]), (n) $FeCl_4$ doped PT (from Ref. [90]), (o) $PPV(H_2SO_4)$ (from Ref. [91]), (p) $PPP(AsF_5)$ (from Ref. [92]), (q) $^{84}Kr^+$ implanted (polyphenylenebenzobisoxazole) (from Ref. [93]), (r) undoped *trans*-$(CH)_x$ (from Ref. [94]), (s) undoped *cis*-$(CH)_x$ (from Ref. [95]), (t) undoped PAN (EB) (from Ref. [96]), (u) undoped PPy (from Ref. [97]), (v) undoped PT (from Ref. [90]), (w) undoped PPV (from Ref. [98]), (x) undoped PPP (from Ref. [92]). The conductivity reported from undoped polymers should be considered an upper limit due to the possibility of impurities.

commensurate charge density wave (CDW) to incommensurate CDW transition model. This model introduced a wide soliton band between the conduction and valence bands as the doping level is increased. In this model, disorder plays an important role to close the incommensurate Peierls gap and convert the system into a conductor. As the most highly conducting doped polymers are the most ordered, this mechanism is unlikely. Kivelson and Heeger later proposed that for polyacetylene there is a first-order transition from the soliton lattice to the polaron lattice with increased doping [101]. Though a charged polaron band would be a half-filled band and thus metallic (in the absence of a further Peierls transition), later studies suggested that the infrared data was inconsistent with this model [102–104].

Conwell and others have proposed that when long-range Coulomb interactions and screening are taken into account, the soliton band in *trans*-$(CH)_x$ overlaps the valence and conduction bands, giving a metallic state [52,53]. In contrast, Kivelson and Salkola have focused on the interchain

interaction, which they show can lead to a simple metallic system with no residual Peierls interaction [105]. Baeriswyl and others, have shown that in some limits the Coulomb interaction is sufficient to close the Peierls gap, giving a metallic state as well [8]. Epstein *et al.* proposed that a disordered conducting state (not the metallic state) is stabilized in the presence of three-dimensional disorder [83]. Other more exotic schemes for the transition to the metallic state also have been proposed [106–109]. For the nondegenerate ground state conducting polymers, more emphasis has been placed on an empty (p-doped) or filled (n-doped) bipolaron energy band overlapping the valence or conduction band, respectively, giving rise to the metallic behavior [56]. Alternatively, a partially filled polaron (band) lattice metallic state [26,31,54–56,61,110,111] has been proposed for some materials. The role of resonant quantum tunneling is discussed in Section 46.9.2.

46.2.3 Models for Localization and Metallic Conductivity

Much work has also focused on the nature of the carriers in the highly doped metallic state. Even though there are a high density of conduction electrons at the Fermi level for the highly doped state, the carriers may be spatially localized so they cannot participate in transport except through hopping. The prime source of localization which has been studied is structural disorder in the polymers [18]. X-ray studies of these systems show that they are generally of modest crystallinity, with regions of the material that are more ordered while other regions are more disordered. Also, the fibrillar nature of many of the conducting polymers may lead to localization by reducing the effective dimensionality of the electrons delocalized in a bundle of polymer chains [112].

In a perfect crystal with periodic potentials, electron wave functions form delocalized Bloch waves [113]. Impurities and lattice defects in disordered systems introduce backward scattering. Anderson studied this phenomenon in terms of a localization effect and the disorder induced metal–insulator transition [114]. It is well known that the electronic structure of the system strongly depends on the degree of disorder. The energy fluctuation in the random potentials broadens the bandwidth and creates smooth "band tails." Due to these band tails, the original band gap between the conduction and the valence bands of a semiconductor may be closed. The ramifications, a finite density of states $N(E_F)$ produced at the Fermi level E_F between mobility edges, were discussed by Mott [115]. When the Fermi level lies in the localized region, the conductivity at zero temperature is zero even for a system with a finite density of states. The Mott variable range hopping (VRH) model is applicable to systems with strong disorder such that ΔV (disorder energy) $\gg B$ (band width) [115]. The general form of the temperature dependent conductivity of Mott's variable range hopping model is described as

$$\sigma = \sigma_0 \exp\left[-\left(\frac{T_0}{T}\right)^{1/d+1}\right], \qquad (46.1)$$

where d is the dimensionality and, for three-dimensional systems, $T_0 = c/k_B N(E_F)L^3$ (c is the proportionality constant, k_B the Boltzmann constant, and L the localization length). It is noted that for use of Eq. (46.1) for $d = 1$ refers to quasi-one-dimensional variable range hopping. In this case the charge carriers may hop to a near neighbor chain allowing avoidance of particularly high barriers due to disorder or chain ends. If the charges may hop only along the one-dimensional disordered chain then Eq. (46.1) is replaced by

$$\sigma = \sigma_0 \exp\left[-\left(\frac{T_1}{T}\right)\right],$$

where T_1 represents the highest energy barrier encountered by the charge hopping along the isolated chain.

If the Fermi level is at an energy such that the electronic states are extended, then finite conductivity at zero temperature is expected. This model assumes that substantial disorder is homogeneous throughout the isotropic three-dimensional sample. For three-dimensional materials near the insulator–metal transition, the Ioffe–Regel condition, $k_F l \sim 1$ where k_F is the Fermi wavevector and l is the mean free path, is satisfied, implying a very short localization length and a very short scattering time. Other external parameters such as magnetic field or pressure can affect the localization/delocalization transition and the localization lengths. This model has received much experimental attention for doped [83,116–118] and ion implanted polymers [93].

In Mott's model, electron correlations are neglected as for the classical Fermi liquid. Efros and Shklovskii pointed out that the interactions between localized electrons and holes play an important role in the hopping transport, especially at low temperature [119], changing the expected temperature dependence of the conductivity to

$$\sigma = \sigma_0 \exp\left[-\left(\frac{T_0'}{T}\right)^{1/2}\right], \qquad (46.2)$$

where $T_0' = e^2/\varepsilon L$ (e is the electron charge and ε is the dielectric constant).

It is well known for a one-dimensional metallic chain that the localization of charge carriers arises for even weak disorder because of quantum interference of static backscattering [115]. In contrast, strong disorder (the mean free path is comparable with the Fermi wavelength) is required for localization in three-dimensional systems. This consequently requires a short transport time, and hence low σ_{DC} at room temperature. Anderson localization therefore is unlikely for the partially crystalline chain structured doped conducting polymers. The localization effects in the inhomogeneously disordered (partially crystalline) conducting polymers may originate from the one-dimensional localization in the disordered regions [73,120].

Prigodin and Efetov studied the insulator–metal transition of conducting polymers using a random metallic network (RMN) model [112] to represent weakly connected, fibrous bundles of metallic chains. In this zero temperature model, the phase transition is a function of the cross-sectional capture between fibers (α), and the product ($\rho = pR_{loc}$) of the localization radius (R_{loc}) and the concentration of crosslinks between fibers (p). The metallic state can be induced by strengthening the interchain (or interfibril) interaction (increasing α), increasing the density of crosslinks between fibers (increasing p), or increasing the localization length (increasing R_{loc}). This model, developed for contacts between fibers comprised of parallel polymer chains, can be generalized to the three-dimensional delocalization transition that occurs in inhomogeneously disordered (partially crystalline) nonfibrillar polymers: as the strength of connection between ordered or crystalline regions (α) is increased, the density of interconnections between ordered or crystalline regions (p) increases, and the localization length within the disordered regions (R_{loc}) increases.

The inhomogeneous disorder model was expanded [120] to account for the temperature dependence of the conductivity. Within this model, conduction electrons are three-dimensionally delocalized in the "crystalline" ordered regions (though the effects of paracrystalline disorder may limit delocalization within these regions [121]). In order to transit between ordered regions, the conduction electrons must diffuse along electronically isolated chains through the disordered regions where the electrons readily become localized. Phonon-induced delocalization increases the conductivity with increasing temperature. This model accounts for localized behavior at low temperature despite conductivities at room temperature in excess of the Mott minimum conductivity. Three-dimensional crystalline order facilitates delocalization. It has been shown [122] that nematic-like order can also increase delocalization, though less effectively.

For conventional metals, the electrical transport properties can be described by the Drude model [123,124] within which electrons are treated as free particles in a gas with a single scattering time τ. Despite its simplified assumptions, the Drude model explains high and frequency independent conductivity from dc to the microwave ($\sim 10^{10}$ Hz) frequency range, and a real part of the dielectric constant (ε_r) which is negative below the screened plasma frequency ($\omega_p^2 = 4\pi n e^2/m^*\varepsilon_b$; n is the density of carriers, m^* is the carrier effective mass, and ε_b is the background dielectric constant) [124]. Within the Drude model the real (ε_r) and imaginary part (ε_i) of the dielectric function are

$$\varepsilon_r = \varepsilon_b - \frac{\omega_p^2 \tau^2}{1 + \omega^2 \tau^2}, \qquad (46.3)$$

$$\varepsilon_i = \frac{\omega_p^2 \tau}{\omega(1 + \omega^2 \tau^2)}, \qquad (46.4)$$

where ω is the external frequency.

In low frequency limit ($\omega\tau \ll 1$), the Drude response can be deduced as

$$\varepsilon_r \cong \omega_p^2 \tau^2, \tag{46.5}$$

$$\varepsilon_i \cong \frac{\omega_p^2 \tau}{\omega}. \tag{46.6}$$

46.3 STRUCTURAL ORDER

Each of the conducting polymer systems exhibits different local structures and a wide range of local orders depending upon the synthesis and processing routes used [18]. The typical fraction of crystallinity and the crystalline coherence lengths for typical samples of three of the most intensively studied highly conducting polymer systems are given in Tables 46.1 and 46.2. The synthetic route, processing procedure, and dopant counterion also will affect the crystal structure as well as the percent crystallinity. For both p and n doping of polyacetylene, the polymer forms a number of different structures (stages) as a function of doping level [19,20,125]. Similar results are found for doped PPV [126]. There is less evidence for intermediate stages at various dopant/polymer stoichiometries for the other conducting polymers. Instead, data support formation of inhomogeneous regions of fully doped polymer which increase in number with increasing doping. Doped polyacetylene can be as much as 80–90% crystalline.

Polyaniline forms a rich set of structures dependent upon the processing sequence and dopant [18,62,127–132]. Generally, doped polyaniline obtained from solution in the doped (conducting salt) form exhibits a local crystalline order of type emeraldine salt-I, ES-I. In contrast, polyaniline obtained by doping powder or films cast as the base form

TABLE 46.2. *Typical percent crystallinity and crystallographic coherence lengths (ξ (Å)) for highly conducting polymer systems.[a]*

Highly conducting polymer	Crystallinity (%)	$\xi_\parallel^a$(Å)	$\xi_\perp^a$(Å)
T-$(CH(I_3)_y)_x$ [18,137][b]	~80	50	35
PPy-PF6 [18,136][c]	~50	20	20
PAN–CSA (*m*-cresol) [18][d]	~50	50	30

[a]The terms $\parallel$ and $\perp$ refer to parallel and perpendicular to the chain direction, respectively.
[b]T-$(CH(I_3)_y)_x$ is the heavily iodine doped Tsukamoto polyacetylene.
[c]PPy-PF6 is the hexafluorophosphate doped polypyrrole.
[d]PAN–CSA (*m*-cresol) is the camphor sulfonic acid doped polyaniline cast from *m*-cresol solvent.

from solution are of the ES-II types [62,122,131–133]. Both preparation methods lead to between a few percent and about 50% crystallinity dependent upon details of the processing route. In addition, there are significant differences in the type of local order to exist in the disordered regions between the crystalline ordered regions, varying from coil-like, to expanded coil-like, to more rod-like [133–135]. For undoped and doped polyaniline, short-range local order in the disordered regions resembles that in the ordered regions [18,133]. Table 46.1 summarizes the fraction of crystallinity and the x-ray coherence lengths of the various doped polyaniline systems, while Table 46.2 compares the fraction of crystallinity and x-ray coherence lengths for selected doped polyacetylene, polypyrrole, and polyaniline samples.

Similarly, the degree of local order varies for polypyrrole dependent upon the preparation method, with the degree of crystallinity varying from nearly completely disordered up to ~50% crystalline [18,136]. In contrast to polyaniline, the local order in the disordered regions of polypyrrole does not resemble that in the ordered regions [18].

The percent crystallinity for doped polyacetylene is usually larger than that of doped polyaniline or doped polypyrrole [18,137]. For each of these systems, the coherence length within the doped crystallographic regions generally is no more than 50–75 Å along the chain direction with smaller values in the perpendicular direction. It has been proposed that these coherent crystalline regions form metallic islands and the disordered weak links between more ordered regions are areas where conduction electrons are subject to localization, as expected for charges moving through isolated one-dimensional chains. That is, for each very highly conducting polymer system studied, there are regions of one-dimensional electronic character through which conduction electrons must pass [75]. The charge transport mechanism between the islands may be via phonon controlled hopping (resulting in insulating (i.e., dielectric) behavior at low temperatures) or direct or resonant quantum tunneling (resulting in a "metallic" behavior even to the millikelvin range).

TABLE 46.1. *Typical percent crystallinity and crystalline coherence lengths (ξ (Å)) of various polyaniline materials obtained from x-ray diffraction experiments.*

Materials	Crystallinity (%)	$\xi_\parallel$ (Å)	$\xi_\perp^b$ (Å)	$\xi_\perp^a$ (Å)
[i]XPAN-ES[a] (3.5×) [73,132]	~45	73	57	29
[h]XPAN-ES[a] (3.5×) [73,132]	~40	64	47	23
[h]XPAN-ES[b] (5.5×) [73,132]	~35	57	45	21
PAN-ES[b] (4×) [73,132]	~30	52	42	23
[n]XPAN-ES[b] (1×) [73,132]	<15		15	

[a]High molecular weight samples. XPAN-ES represents the "physically crosslinked" polyaniline emeraldine salt. Note that *i*, *h*, and *n* refer to intermediate, high, and noncrosslinked samples, respectively. The stretch ratio (l/l_0) is given in parentheses (e.g., 3.5×). Note that $\xi_\perp^a$, $\xi_\perp^b$, and $\xi_\parallel$ are obtained from full width at half maximums of (200), (010), and (002) ES-II reflections, respectively.
[b]Low molecular weight samples.

46.4 DENSITY OF STATES

Magnetic susceptibility studies identify the charge storage mechanism at low doping levels, as well as the density of states at the Fermi level and the density of localized "Curie" spins at higher dopant levels. For $(CH)_x$, spinless solitons dominate at low doping levels [76,78]. In contrast, spin 1/2 polarons and spinless bipolarons are present in nondegenerate systems at low doping levels [7,33,138]. At high doping levels, the highest conducting doped polyacetylene, polypyrrole, polyaniline, polythiphene, and polyparaphenylenes are reported to have finite densities of states at the Fermi level [$N(E_F)$]. Typical literature values of $N(E_F)$ [27,61,62,71,74–76,78,79,138–148] for each of these systems are presented in Table 46.3. Having the Fermi level in a partially filled conduction band results in Pauli susceptibility ($\chi_{Pauli} = 2\mu_B^2 N(E_F)$) and enables metallic conduction. The magnitude of χ_{Pauli} depends on the structural order and morphology of the polymers as this affects the uniformity of the doping. It is noted that the values of $N(E_F)$ in Table 46.3 have not been scaled to the percent crystallinity. Hence the intrinsic density of states in each of the ordered polymers may be larger than indicated.

For the earliest studied iodine doped Shirakawa [76,78,139] and Naarmann [140] $(CH)_x$, Fig. 46.5, $N(E_F) \sim 0.1$ states/eV-C for doping levels above $\sim$4–6% doping level. With the recently studied Tsukamoto [75,142] $(CH)_x$, which has a more compact morphology, a higher doping level was attained resulting in $N(E_F) \sim$0.2–0.3 states/eV-C, Fig. 46.5, indicating that the doping was more homogeneous.

For PAN, $N(E_F)$ is finite and has been shown to increase with the level of protonic acid doping and the volume fraction of crystalline material for both the ES-I, Fig. 46.6, and ES-II, Fig. 46.7, structure [61,62]. The $N(E_F)$ differ for ES-I HCl and ES-II HCl, being 0.26 states/eV-(C+N), and 0.083 states/eV-(C+N), respectively [143]. For highly conducting PAN–CSA (m-cresol) [79], $N(E_F) \sim 0.07$ states/eV-(C+N). Recently, a differently prepared stretched PAN doped with HCl was reported to have a much higher $N(E_F)$, ~ 1.4 states/eV-(C+N) [71]. Some solutions of PAN–CSA have been reported to have a Pauli-like susceptibility [144].

Highly conducting doped polypyrrole has a large χ_{Pauli} [74]. The samples initially studied typically had conductivities in the range of $\sim$ 1–10 S/cm with little crystallinity; for these materials, $N(E_F) \leq 0.01$ states/eV-C [145]. Later studies on BF_4 doped PPy [138,146] indicated $N(E_F) \sim 0.045$ states/eV-C, however, these films were not structurally characterized. A coordinated study of PPy doped with hexafluorophosphate [$PPy(PF_6)$] and toluene sulfonate [PPy(TsO)] [74] shows that for the more highly crystalline (50%), higher conductivity ($\sigma_{DC} \sim 300$ S/cm)$PPy(PF_6)$, $N(E_F) \sim 0.2$ states/eV-C, similar to what was found for highly conducting iodine doped Tsukamoto $(CH)_x$. For less crystalline (25%), lower conductivity ($\sigma_{DC} \sim 120$ S/cm) PPy(TsO), $N(E_F) \sim 0.05$ states/eV-C. Figure 46.8 contrasts the density of states [$N(E_F) = \chi_{Pauli}/2\mu_B^2$] and number of localized Curie-like spins measured for the PPy-PF_6 and PPy-TsO compounds [74]. The more metallic PPy-PF_6 clearly has the larger χ_{Pauli} and the smaller number of localized Curie spins (independent polarons).

For doped polythiophene, there is variation of the doping level attained with different dopants. For BF_4 doped PT [146], $N(E_F) \sim 0.05$ states/eV-C at the 4–8% dopant level. For $PT(AsF_6)$ [27], the doping is inhomogeneous until 26 mol% where $N(E_F) \sim 0.23$ states/eV-C.

For PPP, a metallic density of sates of $N(E_F) \sim 0.05$ states/eV-C has been reported for doping with AsF_6 [147].

TABLE 46.3. *Typical χ_{Pauli} and $N(E_F)$ for highly conducting polymer systems.*

Material	χ_{Pauli}	$N(E_F)$
$[CH(I_3)_y]_x$ [75,142,160]	1.1×10^{-5} emu/mol-C	0.33 states/eV-C
$[CH(I_3)_y]_x$ [76,139,140]	2.9×10^{-6} emu/mol-C	0.09 states/eV-C
$[CH(ClO_4)_y]_x$ [141]	3.3×10^{-6} emu/mol-C	0.11 states/eV-C
$[CH(ClO_4)_y]_x$ [139]	2.3×10^{-6} emu/mol-C	0.08 states/eV-C
$[CH(Na)_y]_x$ [139]	2.0×10^{-5} emu/mol-C	0.07 states/eV-C
PAN(HCl) ES-I [61,143]	7.9×10^{-6} emu/mol-(C + N)	0.26 states/eV-(C+N)
PAN(HCl) ES-II [62,143]	2.5×10^{-6} emu/mol-(C + N)	0.083 states/eV-(C+N)
PAN(HCl) [71]	4.0×10^{-5} emu/mol-(C + N)	1.4 states/eV-(C+N)
PAN(CSA) [79]	2.1×10^{-6} emu/mol-(C + N)	0.07 states/eV-(C+N)
PAN(SO_3) ("SPAN") [87]	1.7×10^{-6} emu/mol-(C + N)	0.06 states/eV-(C+N)
POT(HCl) [121]	3.9×10^{-6} emu/mol-(C + N)	0.13 states/eV-(C+N)
$PPy(PF_6)$ [74]	7.0×10^{-6} emu/mol-C	0.20 states/eV-C
PPy(TsO) [74]	1.8×10^{-6} emu/mol-C	0.05 states/eV-C
$PPy(BF_4)$ [146]	1.7×10^{-6} emu/mol-C	0.05 states/eV-C
$PT(AsF_9)$ [27]	7.5×10^{-6} emu/mol-C	0.23 states/eV-C
$PT(BF_4)$ [146]	1.5×10^{-6} emu/mol-C	0.05 states/eV-C
$PPP(AsF_6)$ [147]	1.5×10^{-6} emu/mol-C	0.05 states/eV-C
C_2H_5O-PPV(BF_4) [148]	$\leq 1 \times 10^{-6}$ emu/mol-C	0.03 states/eV-C
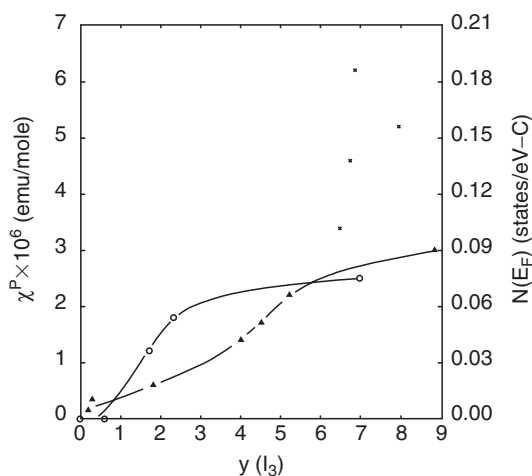
**FIGURE 46.5.** Pauli susceptibility and density of states as a function of I_3 doping level for an oriented ($I//I_0 \sim 6$) Naarmann polyacetylene (triangles) (N-$(CH)_x$) (from Ref. [135]), unoriented Shirakawa polyacetylene (circles) (S-$(CH)_x$) (from Ref. [140]), and Tsukamoto polyacetylene (x) (T-$(CH)_x$) (from Refs. [75,160]).

There are no reports in the literature concerning the temperature dependence of the susceptibility of doped PPV. However, if the reported room temperature magnetic susceptibility measured of BF_4 doped poly(2,5-diethoxy-p-phenylene–vinylene) [C_2H_5O-PPV(BF_4)] [143] is entirely due to a Pauli contribution, an upper estimate of $N(E_F)$ is 0.03 states/eV-C.

In sum, for each of these systems the metallic density of states at the Fermi level varies substantially. Where data are
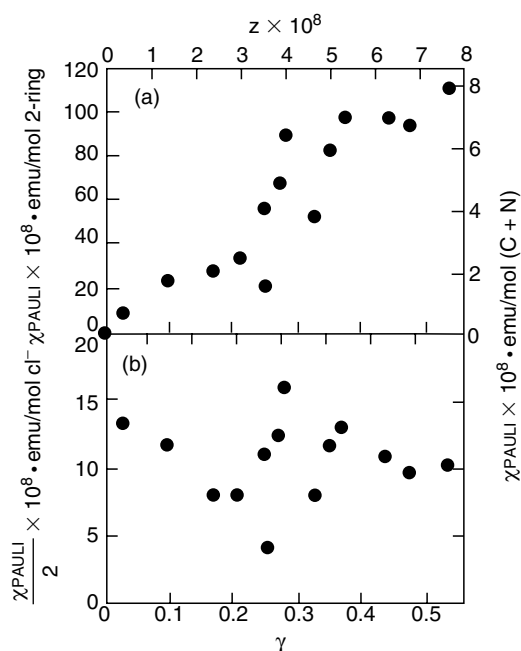
FIGURE 46.6. $N(E_F)$ versus doping level for PAN–HCl, ES-I structure. The lower curve presents χ_{Pauli} normalized to the doping level (from Ref. [61]).
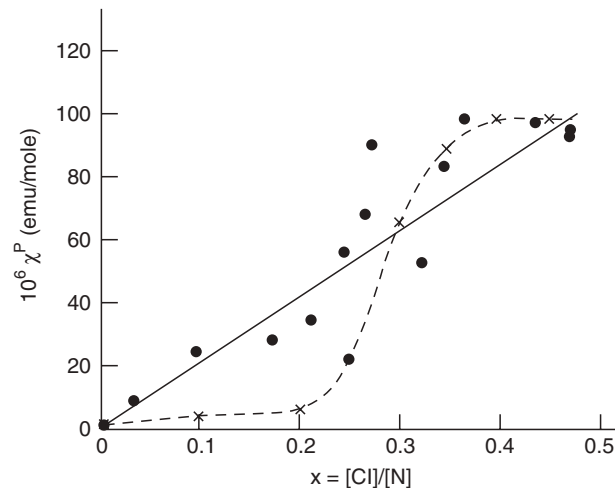
FIGURE 46.7. $N(E_F)$ versus doping level for PAN–HCl, ES-II structure (dashed line). The closed circles are for HCl doping of the ES-I structure (from Ref. [62]).

present, the Pauli susceptibility increases with increasing three-dimensional or nematic order.

46.5 TEMPERATURE DEPENDENT CONDUCTIVITY AND MAGNETORESISTANCE

46.5.1 Conductivity

The temperature dependent dc conductivity, σ_{DC} (T), provides a direct probe of the macroscopic charge conduction through the less conducting regions. Recent advances in chemical processing have resulted in higher crystallinity and conductivity for conducting polymers.

Ishiguro *et al.* reported the temperature dependent resistivity [ρ (T)] of heavily iodine doped $(CH)_x$ and hexafluorophosphate (PF_6) doped PPy down to mK range as function of aging (disorder), Figs. 46.9 and 46.10, respectively [70].
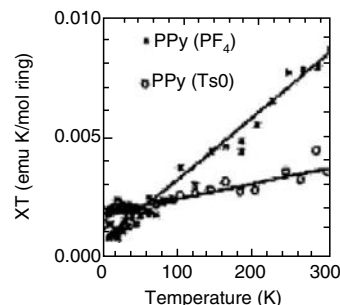
FIGURE 46.8. χ^T versus T for PPy-PF$_6$ and PPy-TsO (from Ref. [74]). Note that assuming $\chi = (\chi_{Pauli} + \chi_{curie})$ and that χ_{Pauli} is T independent while $\chi_{Curie} \propto T^{-1}$, PPy-PF$_6$ has the larger regions of metallic density of states while the PPy-TsO system has a great density if localized (independent polaron) spins.
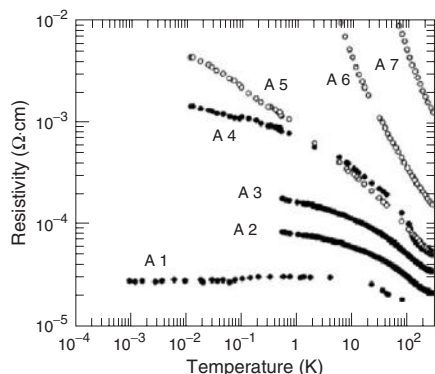
FIGURE 46.9. Temperature dependence of the resistivity for various heavily iodine doped poly-acetylenes represented in a log ρ versus log T scheme (from Ref. [70]).

FIGURE 46.11. σ_{DC} (T) for "crosslinked" PAN-ES, PAN–CSA (CHCl$_3$), and PAN–CSA (m-cresol) samples (from Ref. [73]). The dashed lines are based upon the quasi-1D VRH model. Note here "crosslinks" refers to physical crosslinks (microcrystalline regions) not chemical crosslinks (covalent bonds).

The highest σ_{DC} at room temperature reported in this study is $\sim 5 \times 10^4$ S/cm for I$_3$ doped T-(CH)$_x$ and $\sim 10^3$ S/cm for the highest conducting PPy(PF$_6$). For both of these materials, the conductivity decreases with decreasing temperature to a minimum at $T_{m\sim10\,K}$. Below T_m, σ increases by $\sim 20\%$ and then is constant to 1 mK. Some highly conducting preparations of PAN–CSA show similar behavior [82].

Hydrochloric acid as well as camphor sulfonic acid doped polyaniline prepared in chloroform often have log σ proportional to $T^{-1/2}$ as expected for quasi-one-dimensional variable range hopping (VRH), Fig. 46.11, [73,121,143]:
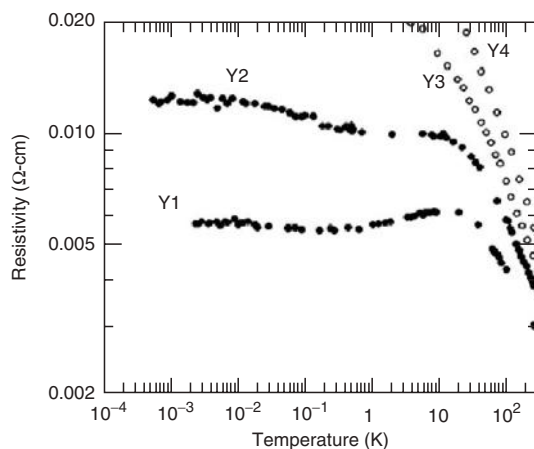
$$\sigma = \sigma_0 \exp[-(T_0/T)^{1/2}], \qquad (46.7)$$

where $T_0 = 16/[k_B N(E_F)L_z]$. Here L is the one-dimensional localization length and z the number of nearest neighbor chains. Generally, the higher conductivity samples have a weaker temperature dependence at low temperatures ($T_0 \sim 700–1,000$ K for $T < 80$ K), and lower conductivity

samples a stronger temperature dependence ($T_0 \sim 4,000$ K). The smaller T_0 for the more highly conducting samples has been associated with weaker localization due to improved intrachain and interchain order.

Higher conducting polyaniline films that were prepared from solutions of PAN and HCSA in m-cresol have an intrinsic metal-like temperature dependence at room temperature to ~ 200 K, below which the conductivity decreases slowly, Fig. 46.12. It was shown that this metal-like behavior

FIGURE 46.10. Temperature dependence of the resistivity for PF$_6$ and BF$_6$ doped polypyrroles represented in a log ρ versus log T scheme (from Ref. [70]).

FIGURE 46.12. Resistivity versus temperature for PAN–CSA (m-cresol). The inset shows the resistivity minima on an expanded scale (from Ref. [116]).

for $T > 200$ K can occur in the presence of one-dimensional localization when the phonon backscattering rate becomes larger than the impurity scattering rate [120]. A similar temperature dependence for conductivity has been reported for $FeCl_3$ doped polyacetylene [149].

For PAN–CSA [116,120], PPy(PF$_6$) [74,118], and iodine doped $(CH)_x$ [150], the proximity of the material to the insulator–metal transition can be gauged by the resistivity ratio $\rho(1.4\,K)/\rho(300\,K)$ and a plot of the reduced activation energy: $W = -T\,d\ln(\rho(t))/dT$ [151]. For a conductor close to the insulator–metal transition, the resistivity follows a power law behavior with T [152]; for a critical regime sample, the plot of log 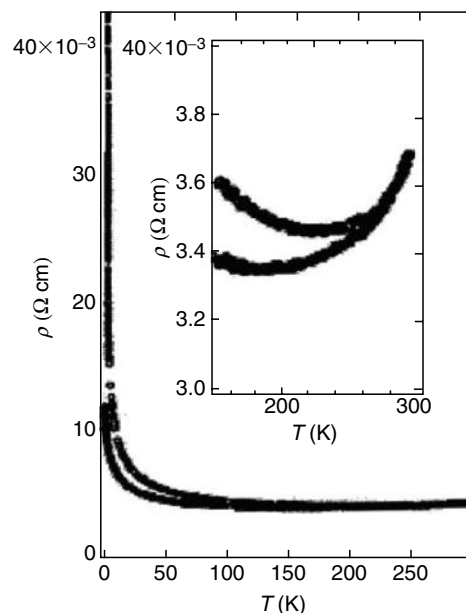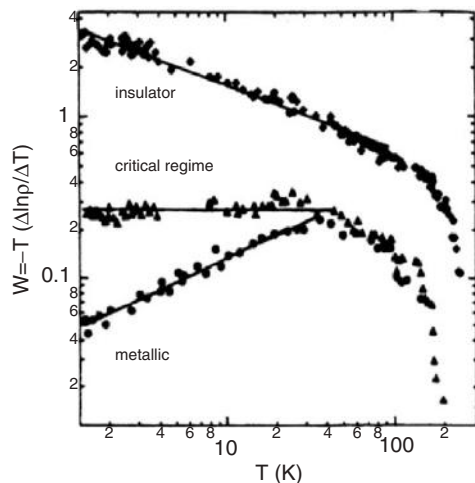W versus log T approaches $T = 0$ K at a constant value. The plot of log W versus log T for a critical sample provides a dividing line between the plot of log W versus log T for insulator hopping behavior which increases with decreasing T (i.e., the slope of log W versus log T is equal to γ if $\sigma \propto \exp(T_0/T)^\gamma$) and the plot of log W versus log T for metallic samples which decrease with decreasing T. The W plots for selected PAN–CSA materials are shown in Fig. 46.13.

46.5.2 Magnetoresistance

The charge transport can be changed in the presence of an external magnetic field because of the destruction of time-reversal symmetry, i.e., a total phase difference between two paths is created by the magnetic field [153]. The magnetoresistance is more easily detected at low temperature because of large localization effects. The fractional change of resistivity in the presence of a magnetic field, $\Delta\rho/\rho$, can be either positive or negative. A negative magnetoresistance can originate from localization effects caused by magnetic field-related dephasing. A field-dependent cutoff length $L_H = \sqrt{\hbar c/eH}$, where c is the speed of light, is important

at high magnetic fields [153]. A positive magnetoresistance is detected when the mobility edge E_c is shifted by the external magnetic field [154]. For an impurity conduction mechanism, the wave functions of the impurity electrons are compressed in the transverse direction by the magnetic field, leading to an enhancement of localization effects, which also induces a positive magnetoresistance [153].

Figures 46.14–46.16 show examples [116,118,155] of the magnetoresistance of doped polyacetylene, polypyrrole, and polyaniline samples at low temperatures. A wide range of behaviors is observed. The variation in magnetoresistance for conducting polymers is closely related to the magnitude and temperature dependence of the conductivity in the absence of a magnetic field. For highly conducting doped $(CH)_x$, a negative magnetoresistance is reported [81,155] for both the parallel and perpendicular directions (Fig. 46.14). This was attributed to quantum interference though the magnitude of the magnetoresistance in the parallel direction is relatively insensitive to the magnetic field. For highly conducting PPy(PF$_6$) and PAN–CSA materials, the magnetoresistance is usually positive, (Figs. 46.15 and 46.16), which was interpreted as a shift of the mobility edge in the presence of a magnetic field.
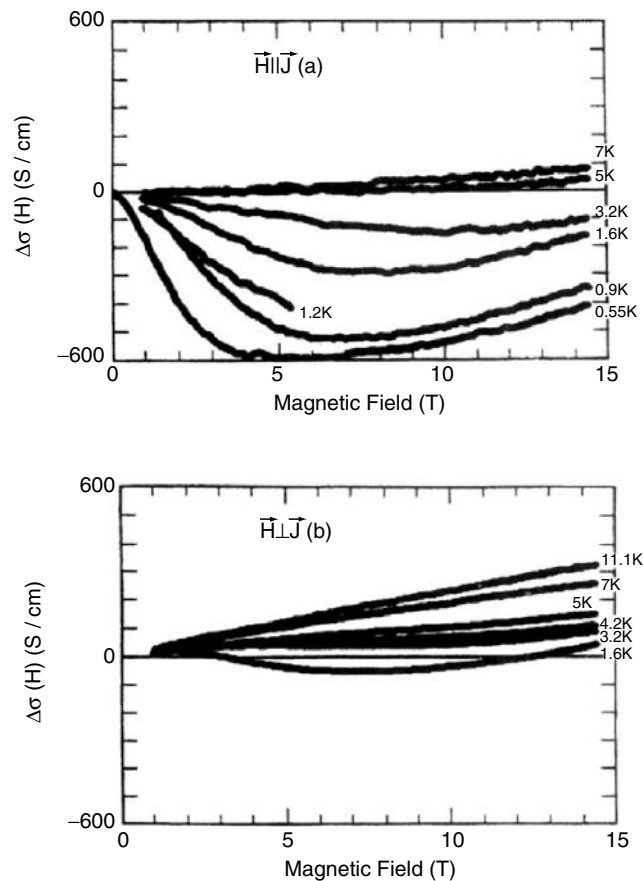
FIGURE 46.14. Magnetic field dependence of the conductivity increment $\Delta\sigma$ (H) at various temperatures for heavily iodine doped T-(CH)$_x$ (from Ref. [155]).

FIGURE 46.13. W plot for PAN–CSA (m-cresol) for samples in the insulating, critical, and metallic regime (from Ref. [116]).

(a)

(b)

FIGURE 46.15. $\Delta\rho/\rho$ versus H^2 for PAN–CSA (*m*-cresol): (a) In the critical regimes; [$\rho(T) \propto T^{-0.26}$, 4.2 K (solid circles), 2.5 K (solid diamonds), and 1.4 K (solid triangles); (b) in the insulating regime (follows three-dimensional VRH model), 4.2 K (solid circles), 2.5 K (solid diamonds), and 1.4 K (solid triangles)] (from Ref. [116]).

46.6 THERMOELECTRIC POWER

The results of the thermoelectric power experiments determine the sign of the conducting charge, either electron-like (for a negative thermoelectric power) or hole-like (for a positive thermoelectric power). In terms of band theory, the positive or negative thermoelectric power implies p-type or n-type doping of a system, respectivel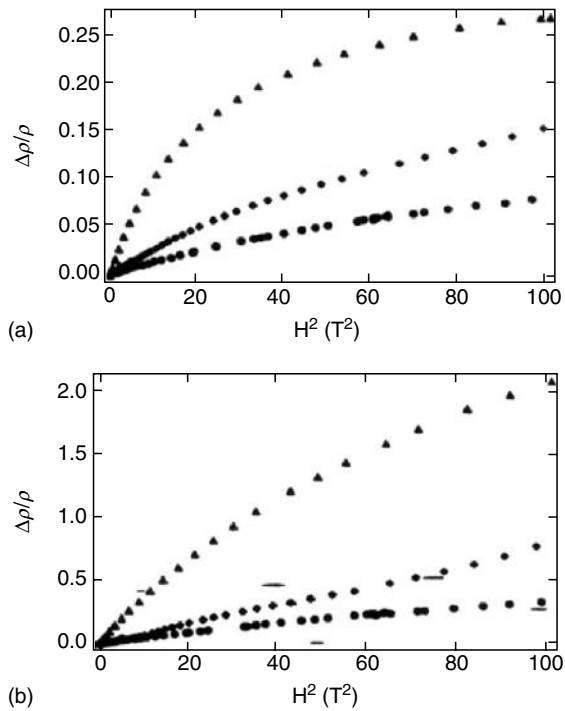y. For inhomogeneous conducting polymers, there are several different contributions to the total thermoelectric power [156,157].

When the conductivity is determined by the motion of charge carriers near the Fermi level, where states are metallic (delocalized), the thermoelectric power is [115]

$$S(T) = \frac{2\pi^2}{3} \frac{k_B^2 T}{e} \frac{d \ln N(E)}{dE} \bigg\|_{E=E_F}. \qquad (46.8)$$

Assuming a weak energy dependence of the density of states $N(E_F)$, the thermoelectric power increases linearly as the temperature increases.

When the conduction is determined by three-dimensional VRH, $S(T) \propto \sqrt{T}$ [115]. For a quasi-one-dimensional VRH case, the thermoelectric power due to the interchain motion is constant [143] while that due to intrachain hopping is $\propto 1/T$, similar to that of doped semiconductors [115].

Park *et al.* [80] and Javadi *et al.* [81] reported metallic thermoelectric power [$S(T) \propto T$] for heavily doped highly conducting polyacetylene (Figs. 46.17 and 46.18) though VRH-type $S(T) \propto \sqrt{T}$ had been reported earlier for poorly conducting polyacetylene [83]. Similarly, highly conducting forms of polyaniline and polypyrrole have $S(T) \propto T$, Figs. 46.19 [117,158] and 46.20 [154], while more disordered materials show nonlinear temperature dependent

FIGURE 46.16. Magnetoresistance of doped polypyrroles (from Ref. [70, 224]). The inset shows the magnetoresistance for a less highly conducting doped PPy than in the main figure.
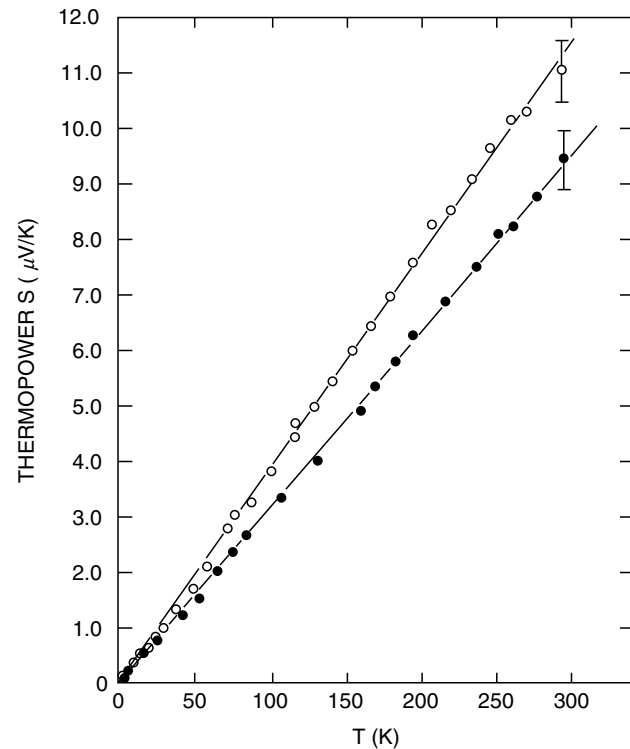
FIGURE 46.17. Temperature dependence of the thermoelectric power in unstretched (solid circles) heavily AsF$_5$ doped polyacetylene and stretched ($l/l_0 \sim 3.2$, open circles) ones (from Ref. [80(b)]).
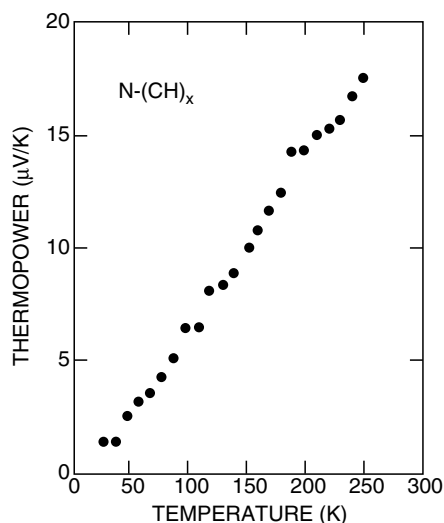
FIGURE 46.18. Thermoelectric power of stretched heavily iodine doped N-(CH)$_x$ film versus temperature measured parallel to the stretched axis (from Ref. [81]).

behavior, which might include the three-dimensional or quasi-one-dimensional VRH contributions. Figure 46.21 [143] shows the nonlinear $S(T)$ of some hydrochloride doped polyaniline materials.

46.7 MICROWAVE DIELECTRIC CONSTANT

The microwave frequency dielectric constant provides a measure of the charge delocalization in individual samples.
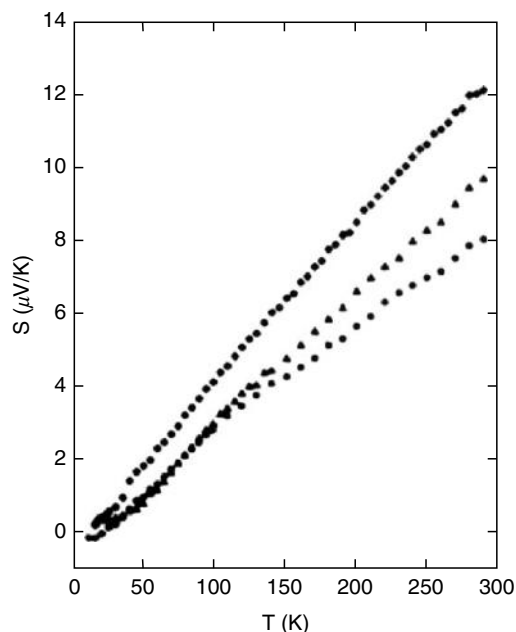
FIGURE 46.19. Temperature dependence of thermoelectric power of PAN–CSA (*m*-cresol) samples: different symbols refer to materials prepared in different casting conditions (from Ref. [117]).
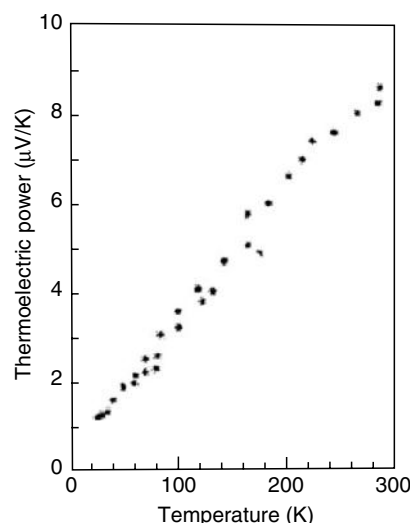
FIGURE 46.20. Temperature dependence of thermoelectric power of PF$_6$ doped polypyrrole (from Ref. [159]).

Figure 46.22 presents [73] the low temperature dielectric constant ε_{mw}, for a series of emeraldine hydrochloride samples plotted against the square of the crystalline coherence length, ξ (as measured by x-ray diffraction). For low temperatures, ε_{mw} is proportional to ξ^- independent of the direction of orientation of the sample with regard to the microwave frequency electric field. This demonstrates that the charge is delocalized three-dimensionally within the crystalline regions of these samples. Using a simple metallic box model [73,143],

$$\varepsilon = \varepsilon_\infty + (2^{9/2}/\pi^3)e^2N(E_F)L^2, \qquad (46.9)$$

and taking for the low temperature localization length the x-ray crystalline correlation length determined by x-ray diffraction, $N(E_F) \simeq 1.23$ state/(eV 2-rings) (0.088 state/eV-
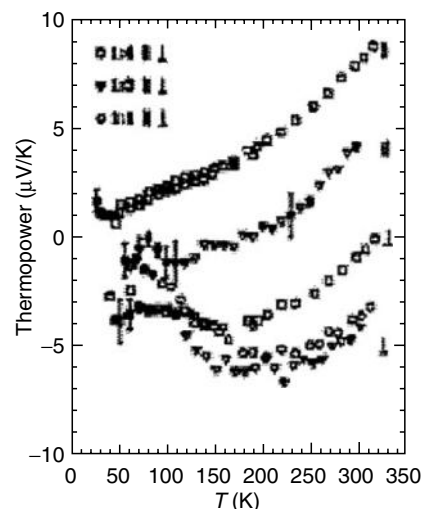
FIGURE 46.21. Comparison of temperature dependence of thermoelectric power of HCl doped PAN-ES samples (from Ref. [143]).
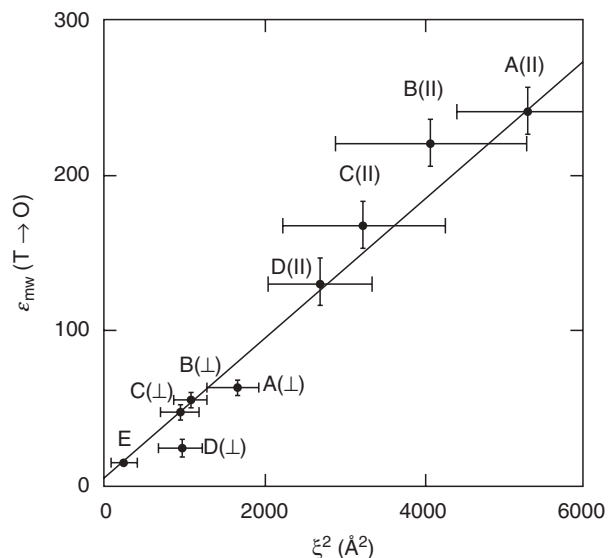
FIGURE 46.22. $\varepsilon_{mw}(6.5 \times 10^9\,\text{Hz}, T \to 0)$ versus ξ^2 for HCl doped PAN-ES ($\xi^2 = \xi_{\perp,\,a} \times \xi_{\perp,\,b}$) (from Ref. [73]).

(C+N)) for PAN–HCl. This compares very favorably with the value obtained from magnetic susceptibility experiments [61].

A positive microwave frequency dielectric constant is also found for modestly conducting iodine doped unstretched and modestly stretched Tsukamoto polyacetylene [75] and for unstretched PPy-TsO [74], Fig. 46.23(a) and (b). Using Eq. (46.9), the size of the low temperature metallic box, L, can be determined. Table 46.4 summarizes the low temperature microwave dielectric constant for typical modestly conducting doped polymers and the corresponding metallic box size calculated using Eq. (46.9). In each case L is approximately the size expected from x-ray diffraction studies of the structural coherence length, ξ.

An independent measure of the temperature dependence of the conduction electron localization length is obtained through study of the temperature dependence of the dielectric constant. For HCl doped PAN-ES samples with weaker localization in the disordered regions, $\varepsilon_{mw}(T)$ increases rapidly with increasing temperature to values in excess of 10^4 at room temperature, Fig. 46.23(c). In contrast, more localized samples have a weaker temperature dependence to the dielectric constant with $\varepsilon_{mw}(295\,\text{K}) < 2 \times 10^3$. Using Eq. (46.9) the room temperature localization length (L_{RT}) is estimated as ~1,000 Å and ~350 Å parallel and perpendicular to the chain direction, respectively, for these highly conducting materials [73]. This distance encompasses of order seven or more structurally coherent regions ("crystalline islands") in the parallel direction and four or more in the perpendicular direction. Such materials were described [73] as having mesoscopic metallic states at room temperature. In contrast, for modestly conducting materials, L_{RT} is less than or of order twice the distance between crystalline regions implying nearly isolated "metallic" islands.
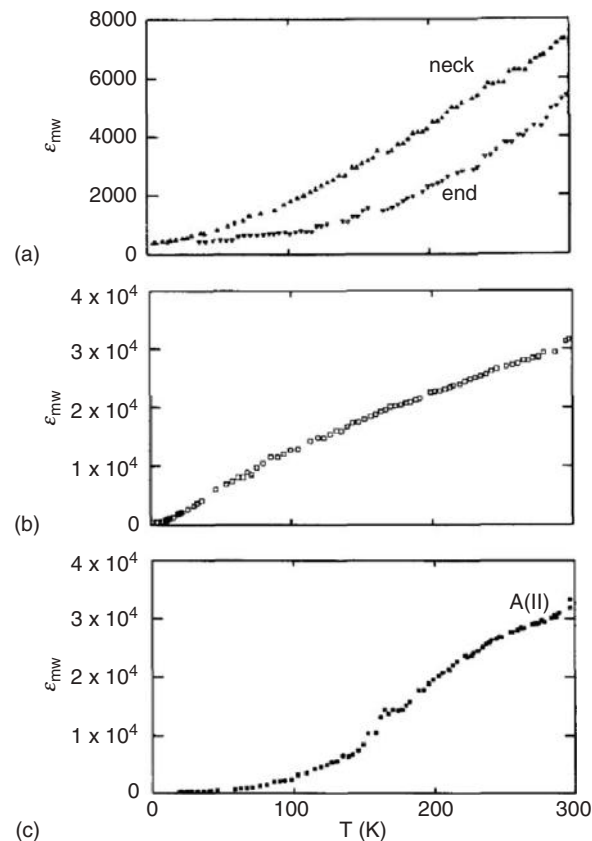
FIGURE 46.23. $\varepsilon_{mw}(6.5 \times 10^9\,\text{Hz})$ versus temperature for modestly conducting doped polymers. (a) I_3 doped Tsukamoto polyacetylene (unstretched end and modestly stretched neck portions of sample) (from Refs. [75,160]), (b) unstretched PPy-TsO (from Ref. [74]), and (c) intermediate "crosslinked" 3.5 times stretched HCl doped PAN-ES (from Ref. [73]).

The sign, magnitude, and temperature dependence of the 6.5×10^9 Hz dielectric constant for very highly conducting T-$[CH(I_3)_y]_x$ [75,160], PPy-PF$_6$ [74], and m-cresol prepared PAN–CSA [73] are quite striking, Fig 46.24. For example, PAN–CSA (m-cresol) has a metallic negative dielectric constant and features a maximum in microwave frequency conductivity at ~180 K [73]. A similar large and negative value of ε_{mw} and temperature dependence of ε_{mw} were determined for heavily iodine doped stretched Tsukamoto

TABLE 46.4. Low temperature dielectric constant, $\varepsilon_{mw}(T \to 0)$ and derived metallic box size, $L(T \to 0)$, compared to the x-ray diffraction determined coherence length, ξ, for typical modestly conducting polymers.

Modestly conducting polymer systems	ε_{mw} ($T \to 0$)	$L(T \to 0)$ (Å)	ξ(Å)
T-$(CH(I_3)_y)_x$ [75]	~400	~170	Not measured
PPy-TsO [74]	~20	~25	~15
PAN–CSA (CHCl$_3$) [73,75]	~30	~24	$\xi_\parallel$~35, $\xi_\perp$~25
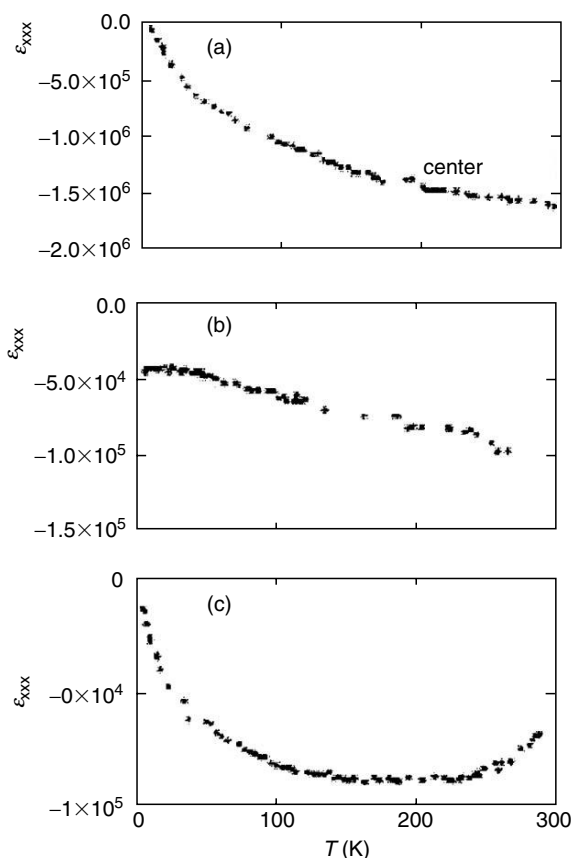
FIGURE 46.24. $\varepsilon_{mw}(6.5 \times 10^9 \, Hz)$ versus temperature for highly conducting doped polymers. (a) I_3 doped Tsukamoto polyacetylene (stretched central portion of sample) (from Ref. [160]), (b) unstretched PPy-PF$_6$ (from Ref. [74]), and (c) PAN–CSA (m-cresol) (from Ref. [73]). Note the large negative values of these dielectric constants.

polyacetylene [75,160] and PF$_6$ doped polypyrrole [74]. Using the Drude model [123,124] for low frequencies ($\omega\tau \ll 1$), a plasma frequency of $\omega_p = 0.015 \, \text{eV}(120 \, \text{cm}^{-1})$ and a room temperature scattering time of $\tau = 1.2 \times 10^{-11} \, s$ were calculated [73] for the PAN–CSA (m-cresol) system, though the exact values correlate with the sample preparation. Similar values are obtained for heavily iodine doped stretched Tsukamoto polyacetylene and PF$_6$ doped polypyrrole (Table 46.5). These values of ω_p are much smaller than

TABLE 46.5. *Typical low frequency plasma frequency and relaxation time obtained from microwave frequency measurements of very highly conducting polymers.*

Highly conducting polymer	$\omega_{p(cm^{-1})}$	τ (s)
T-(CH(I$_3$)$_y$)$_x$ (295 K) [75,160]	~200	~ 3.3×10^{-11}
PPy-PF$_6$ (265 K) [74]	~100	~ 3.0×10^{-11}
PAN–CSA (m-cresol) (295 K) [73,75,120]	~120	~ 1.2×10^{-11}

one expects from the usual Drude model. The small values of ω_p suggest that only a small fraction of the conduction band electrons participate in this low frequency plasma response. Similarly, the value of τ is two orders of magnitude larger than usual for an alkali, noble, or transition metal [124]. The origin of the anomalously large scattering time was suggested [120] to be the ineffectiveness of forward scattering of conduction electrons in the metallic state and the need for backward scattering (i.e., the Fermi surfaces of metallic polyaniline, polyacetylene, and polypyrrole are "open" as expected for highly anisotropic materials and backward scattering from k_F to $-k_F$ may be necessary for momentum relaxation).

The behavior of ε_{mw} for PAN–CSA of moderate conductivity (~200 S/cm) demonstrates [120] strikingly the effect of disorder (Fig. 46.25). A metal–insulator transition as a function of temperature is reflected in ε_{mw}. ε_{mw} crosses from huge and negative (Drude-type band transport) at room temperature to large and positive (insulating or "dielectric" behavior) at ~20 K. This behavior is ascribed [120] to phonon controlled delocalization. When the phonon scattering rate is larger than the impurity scattering rate, phonon scattering destroys the localization caused by impurity scattering. The presence of this effect is suggested to arise from the key role of one-dimensional chains electronically linking three-dimensional metallic regions in the polymer.
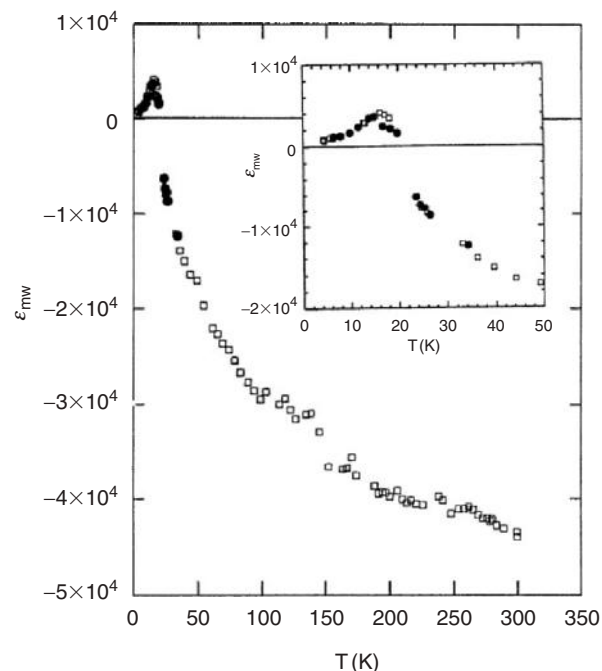
FIGURE 46.25. $\varepsilon_{mw}(6.5 \times 10^9 \, Hz)$ versus temperature for a sample of PAN–CSA (m-cresol) of moderate conductivity (~200 S/cm), demonstrating a metal–insulator transition as a function of temperature (from Ref. [120]).

46.8 OPTICAL ABSORPTION, TRANSMISSION, AND REFLECTION

The apparent semiconducting or insulating bandgaps for the undoped forms of each of the principal conducting polymers as obtained by visible/UV spectroscopy are listed in Table 46.6 [91,161–181], though for many of the nondegenerate polymers, the lower energy optical absorption may actually represent formation of excitons [49–52,181–184]. Upon low level doping, there is a systematic change in the optical properties depending on whether the ground state is degenerate or nondegenerate, with prominent signatures for solitons, polarons, and bipolarons. However, for the most highly doped ordered states, the conducting polymers show "metallic" absorption and reflection behavior.

Because the metallic state is so highly reflecting, it is often studied via reflectance from films. From such data, a Kramers–Kronig analysis provides all the optical constants of interest including the absorption coefficient, dielectric functions, and conductivity [185]. The real part of the dielectric function (ε_1) and the optical conductivity (σ_1) give insight into the localized or delocalized behavior of the conduction electrons. The measured frequency response can be compared with the Drude model for free electrons and other models for localized (bound) electrons [185]. Again, the universality of the electronic behavior of the systems with improving structural order, morphology, and doping is stressed. For the materials with the highest σ_{DC}, an increased fraction of the total oscillator strength (from conduction electrons) demonstrates free electron Drude response.

46.8.1 Optical Dielectric Function

For the conducting forms of doped polyacetylene and other conducting polymers, there are zero, two, three, or one zero crossings of the real part of the dielectric function (ε_1) as the frequency is decreased. For the least conducting materials, ε_1 remains positive for the entire optical frequency range (50–50,000 cm^{-1}), reaching values of several hundred at microwave frequencies. For higher conductivity materials, ε_1 crosses zero between 1 and 3 eV (the all-conduction-electron plasma response) and then becomes positive again below $\sim 1{,}000$ cm^{-1}, reaching values in excess of 10^4 at microwave frequencies. For the most metallic samples, two behaviors have been reported dependent upon the system. For doped PAN and PPy with modest $\sigma_{DC} \sim 400$ S/cm, ε_1 demonstrates the previous two zero crossings, and a third zero crossing occurs to negative values at a "delocalized conduction electron plasma frequency" of several hundred wavenumbers. For the most highly conducting doped polyacetylene, ε_1 crosses zero at the all conduction electron plasma frequency and remains negative to the lowest measured optical frequencies.

The optical response of iodine [83,106,162,186,187] and perchlorate (ClO$_4$) [106,188,189] doped (CH)$_x$ and PF$_6$ doped poly(methylthiophene) [190] have been well characterized, as have polyaniline samples (PAN–HCl [55,191,192] and PAN–CSA prepared in m-cresol [75,146, 193–196] and in solutions of m-cresol and chloroform [193,197]) and polypyrrole films (doped with PF$_6$ [74,89, 198,199], TsO [74,89,198], ClO$_4$ [166], and some sulfonated poly(β-hydroxyethers) [46,192].

Figure 46.26 shows ε_1 at room temperature for selected PAN samples. PAN–CSA (m-cresol) ($\sigma_{DC} \sim 400$ S/cm) has three zero crossings for ε_1 which correspond to two different plasma frequencies [193]. The higher energy zero crossing was assigned [75] to the plasma response of the whole conduction band, as the density of carriers (n) determined from the plasma frequency ($\omega_p^2 = 4\pi n e^2/m^*$; assuming m^*, the effective mass, is approximately the free electron mass) is in the range of the dopant density. There is a Lorentzian frequency dispersion at this ω_p indicating that the majority

TABLE 46.6. *Typical apparent "bandgap" values for the undoped conducting polymers. Both the absorption onset and peak are given.*

Material	Absorption onset (eV)	Absorption peak (eV)
(CH)$_x$ (*trans*) [161,162]	1.4	1.8
(CH)$_x$ (*cis*) [163]	~1.9	2.3
PAN (LEB) [164]	3.2	3.6
PAN (EB) [164]	1.6(3.0)	2.0(3.8)
PAN (PNB) [165]	1.8	2.3
PPy [166,167]	2.5	3.2
PT [168–171]	2.0	2.3–2.7
PPP [91,172–174]	3.1	3.43–3.7
PPV (old) [175–178]	2.4	2.9
PPV (new) [179]	2.25	2.46
PPyr [180]	2.9	3.3
PPyV [181]	2.5	3.0
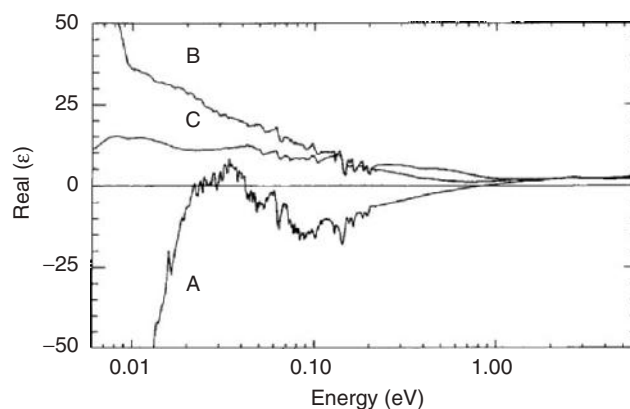
FIGURE 46.26. Real part of the room temperature dielectric response versus frequency for PAN–CSA(m-cresol) (A), PAN–CSA(chloroform/m-cresol) (B), and PAN–HCl IXL (C) (from Refs. [192,193]).

of the conduction electrons are localized or bound spatially, and require a finite amount of energy to be excited. At a lower frequency dispersion, ε_1 begins to become positive at $\sim 330\,\text{cm}^{-1}$ ($\sim$0.04 eV); this is a characteristic of the Lorentzian (localized) behavior. However, at $\sim 200\,\text{cm}^{-1}$ ($\sim$0.02 eV), ε_1 again crosses to negative values and grows increasingly negative with decreasing wavenumber. This plasma frequency shows Drude behavior with decreasing wavenumber and in fact appears approximately at the frequency predicted by the microwave estimates [73,74]. Similar zero crossings are reported for PPy(PF$_6$) ($\sigma_{DC} \sim 300\,\text{S/cm}$) [74,198,199] (Fig. 46.27).

Comparison of the plasma frequencies for the Drude electrons with the plasma frequencies for the whole conduction band for these polymers, assuming that the effective mass m^* is the same as that for the whole conduction band response, yields a ratio of the density of electrons contributing to the free response compared to the localized response of $\sim 10^{-3}$. Assuming even a tenfold increase in m^* for the lower frequency ω_p (as the delocalized electrons must traverse the disordered regions with presumably narrowed energy bands), only a small fraction ($\sim 10^{-2}$) of the conduction electrons are delocalized enough to show Drude behavior in PAN–CSA (m-cresol).

The frequency response of ε_1 for PAN–CSA prepared from chloroform and subsequently briefly exposed to m-cresol vapor ($\sigma_{DC} \sim 20\,\text{S/cm}$) [193] (Fig. 46.26) is characteristic of localized electrons. ε_1 is positive at all optical frequencies; the scattering due to disorder in these materials has broadened and washed out the dielectric zero crossings. Lorentzian dispersion due to a "localized polaron" [146] is evident in ε_1 around $12,000\,\text{cm}^{-1}$ (1.5 eV) and ε_1 for this material increases positively with decreasing wavenumber in the far IR, characteristic of a material with a small residual band gap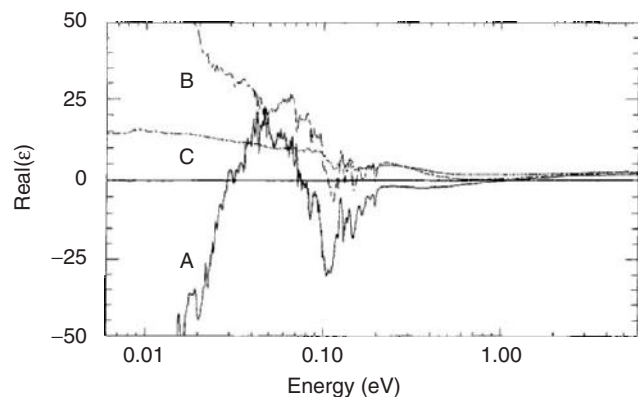 or localized carriers. Lower conductivity PAN–HCl [193] ($\sigma_{DC} \sim 10\,\text{S/cm}$) materials show even less dispersion with wavenumber. ε_1 for these materials is also positive over the whole range and shows only a modest increase in the IR, becoming nearly wavelength independent in the far IR.

Polarized optical measurements of the dielectric response of HCl doped stretched PAN samples are shown in Fig. 46.28. The dielectric response perpendicular to the stretch direction is characteristic of insulating behavior. Along the stretch direction, a strong plasma-like response is observed [191], indicating that the scattering times along the chain are much longer than those perpendicular to the chain. This indicates that on-chain partial delocalization develops first in these systems.

Doped polypyrrole demonstrates behavior similar to polyaniline for samples with lower conductivity and structural order. In Fig. 46.27, the more disordered PPy(TsO) ($\sigma_{DC} \sim 120\,\text{S/cm}$) [74,198] shows a more localized behavior than PPy(PF$_6$) as ε_1 remains positive throughout the optical frequency range. The carriers are weakly localized though as ε_1 increases rapidly in the far IR. For PPy(S-PHE) ($\sigma_{DC} \sim 10\,\text{S/cm}$) [46,192], there is very little dispersion in ε_1; it remains positive and small in the entire optical range, becoming nearly wavelength independent in the far IR.

ε_1 for the most highly conducting iodine and perchlorate doped polyacetylene samples remains negative but small for frequencies less than its all-conduction-electron plasma frequency of $\sim$3 eV through the far IR for light polarized both parallel and perpendicular to the stretched chain direction [187,188] (Fig 46.29) again supporting the three-dimensional nature of the metallic state in conducting polymer systems. Below $\sim$0.05 eV, ε_1 becomes increasingly negative, suggesting a Drude plasma frequency for the most delocalized electrons.

Summarizing, there is an evolution of the dielectric response with increasing order. For the most disordered, lowest conducting samples, ε_1 remains positive and shows very weak dispersion. As the order and conductivity of the materials increase, ε_1 first shows more dispersion at the plasma edge of the whole conduction band as the scattering time increases, possibly turning negative in that range, but returns positive in the far IR. This behavior was seen in stretched PAN–HCl samples parallel to the stretch direction [191]. For the best current materials, ε either returns negative or remains negative in the far IR, indicative of a small density of macroscopically delocalized electrons.

46.8.2 Optical Conductivity

For materials near the insulator–metal (localization–delocalization) transition the optical conductivity is suppressed at low frequencies relative to the usual Drude conductivity [115]. The suppression is usually strong for frequencies up to a critical-frequency $\omega_c \sim D/L^2$ where D is the diffusion coefficient and L is the localization length for the electron. This conductivity suppression occurs because the carriers would diffuse a distance greater than the localization length within the period of the AC wave for

FIGURE 46.27. Real part of the room temperature dielectric response (ε_1) versus frequency for PPY(PF$_6$) (A), PPY(TsO) (B), and PPY(S-PHE) (C) (from Refs. [74] and [192]).
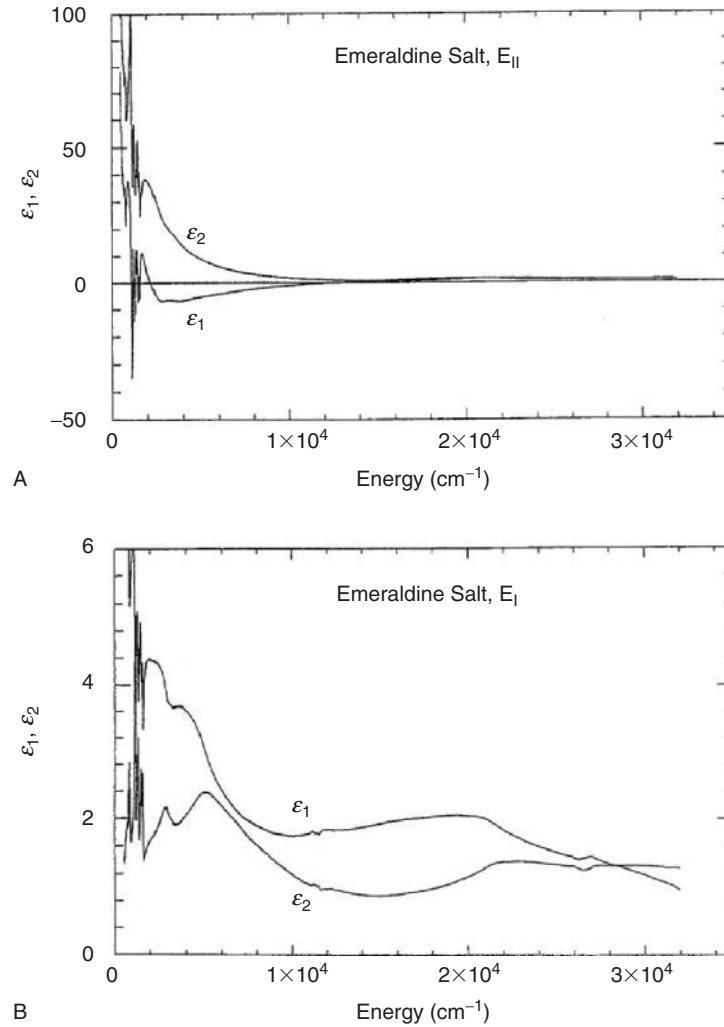
FIGURE 46.28. Real part of the dielectric constant versus frequency for light polarized (A) parallel and (B) perpendicular to the stretch direction in PAN doped with HCl (from Ref. [191]). The chain alignment is improved by stretching. ε_1 is negative in the mid IR for the parallel direction but not for the perpendicular direction, implying that the delocalization is much greater along the chain.

$\omega < \omega_c$. For frequencies greater than ω_c, the optical conductivity shows the normal Drude decrease with increasing frequency. For three-dimensional materials, localization corrections to the frequency dependent conductivity [115,194,200–202] yield

$$\sigma(\omega) = \sigma_{\text{Drude}} \left[1 - \frac{C}{(k_F v_F \tau)^2} + \frac{C(3\omega)^{1/2}}{(k_F v_F)^2 \tau^{3/2}} \right], \quad (46.10)$$

where C is an undetermined universal constant, k_F is the Fermi wavevector, v_F is the Fermi velocity, τ is the scattering time, and σ_{Drude} is the regular Drude conductivity given by

$$\sigma_{\text{Drude}} = \frac{\Omega_p^2 \tau}{4\pi(1 + \omega^2 \tau^2)}, \quad (46.11)$$

where Ω_p is the plasma frequency of the free electrons. Notice that as $k_F l$ (i.e., $k_F v_F \tau$) becomes large for more

ordered higher σ materials, the corrections to the Drude formula should become negligible and the three-dimensional conductor should obey the Drude formula.

The experimental optical conductivity of the doped polymers evolves from localized semiconducting behavior to metallic behavior with improved order. For $(CH)_x$ doped with perchlorate (ClO_4) [106,188,189], (Fig 46.30) or iodine [106,162,186] with different stretch ratios, the optical conductivity shows soliton features at midgap and a Drude plasma edge which develops with stretch alignment at $\sim 200 \text{ cm}^{-1}$ (0.02 eV) where the optical conductivity rises rapidly to its dc value with a very long scattering time. The full conduction electron plasma frequency for doped $(CH)_x$ is ~ 3 eV; therefore, the plasma edge at 0.02 eV is associated with only a small fraction of the conduction electrons [75]. Because a small fraction of the conduction electrons appear macroscopically delocalized with a long scattering time while the majority of conduction electrons are more
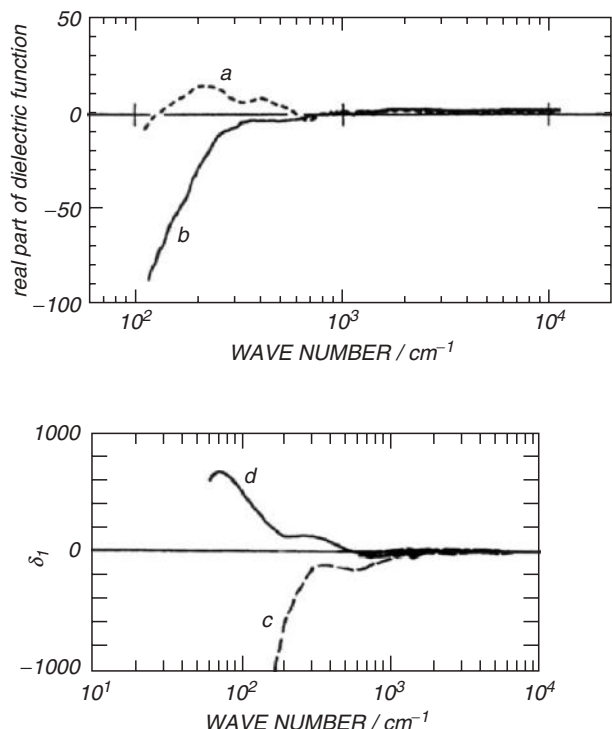
FIGURE 46.29. Top: real part of the dielectric constant versus frequency for light polarized perpendicular to the stretch direction in $(CH)_x$ doped with ClO_4 (from Ref. [188]). For sample (b), the chain alignment is improved over the sample (a) by stretching. ε_1 is negative at low frequencies indicating a three-dimensional metallic state. Bottom: real part of the dielectric constant vs. frequency for light polarized parallel to the stretch direction (from Ref. [187]). Samples (c) and (d) are both doped to the same level with iodine, but sample (c) was stretched before doping, resulting in greater ordering and a more metallic response.
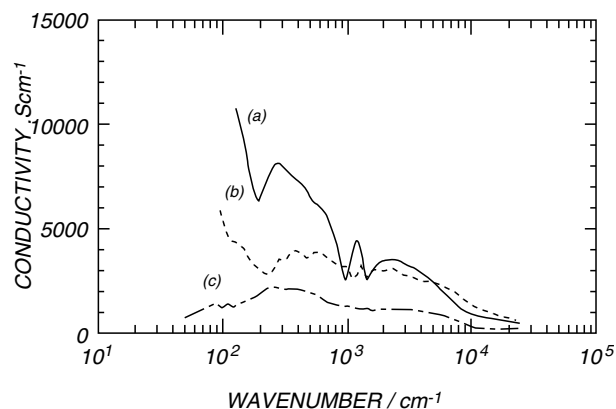
FIGURE 46.30. Optical conductivity versus frequency for $(CH)_x$ of different stretched ratios (a: stretched 8×; b: stretched 4×; c: unstretched) doped with perchlorate (ClO_4) (from Ref. [188]). There is a growth of a free carrier band (Drude response) around $\sim 200\,cm^{-1}$ with increased stretch ratio.

strongly localized, with a short scattering time, the localization modified Drude model [115,194,200–202] does not simultaneously fit well the frequency dependent dielectric function and conductivity of highly conducting $(CH)_x$. Models which take into account the inhomogeneous disorder of the systems provide a better representation as they allow for composite behavior (metallic islands which percolate in a semiconducting matrix).

Typical optical conductivity spectra for PAN and PPy films are shown in Figs. 46.31 and 46.32, respectively. For highly conducting PAN–CSA (m-cresol) [$\sigma_{DC} \sim 120\,S/cm$] [193], σ_1 begins to increase with decreasing wavenumber at $\sim 10,000\,cm^{-1}$ (~ 1.2 eV) to values as high as ~ 750 S/cm at ~ 0.1 eV and then decreases consistent with localization behavior. However, at ~ 0.02 eV, σ_1 begins to increase, qualitatively similar to the behavior of doped $(CH)_x$ though the increase in the far IR is not as rapid as for doped $(CH)_x$ as the dc conductivity is much lower for this PAN–CSA material. This type of frequency behavior for σ_1 is qualitatively similar to the composite behavior of metallic particles (islands) in a semiconducting matrix after percolation of the metallic particles [203]. $PPy(PF_6)$ [74,198] [$\sigma_{DC} \approx 300$ S/cm] has similar behavior, though σ begins to increase with decreasing wavenumber at a higher all-conduction-electron "plasma edge" of $\sim 17,000\,cm^{-1}$ (~ 2.1 eV).

In contrast to this behavior, σ for other doped PAN and PPy materials show more localized behavior. For example, the optical conductivity of PAN–CSA cast from a solution of chloroform and exposed to m-cresol [$\sigma_{DC} = 20\,S/cm$] [192], PAN–HCL ("intermediate cross linked (crystallinity)" IXL) [$\sigma_{DC} \sim 10\,S/cm$] [193], $PPy(TsO)$ [74.198] [$\sigma_{DC} \approx 100\,S/cm$], and PPy(S-PHE) [$\sigma_{DC} \approx 10\,S/cm$] [46,192] have maxima (in addition to phonon features) at higher energies in the IR than more highly conducting PAN and PPy. In the far IR, σ decreases with decreasing frequency more rapidly for these samples with increased disorder as expected for localized electrons. Similar behavior has been reported for perchlorate (ClO_4) doped PPy [166,187] and PF_6 doped poly(3-methylthiophene) [190] (Fig. 46.33). For the lower conductivity doped polymers, the localization modified Drude model [115,200–202] has the same frequency dependence as the experimental spectra. The low frequency conductivity peak shifts to lower energy with increasing dc conductivity in both PAN [197] (Fig. 46.31) and PPy [74] (Fig. 46.32) and likely results from the decrease of the critical frequency ω_c as the samples become more ordered. For the low conductivity PAN samples, most of the oscillator strength is shifted [146] into a peak at ~ 1.5 eV associated [54,146] with localized polarons. Thus with decreasing order the oscillator strength shifts to higher wavenumber and thus higher binding energies.

Qualitatively, the PAN and PPy materials with $\sigma_{DC} < 200\,S/cm$ show the behavior expected for both the good conductor/poor conductor composites as well as for the three-dimensional localization modified Drude model. The optical conductivity of highly conducting stretched
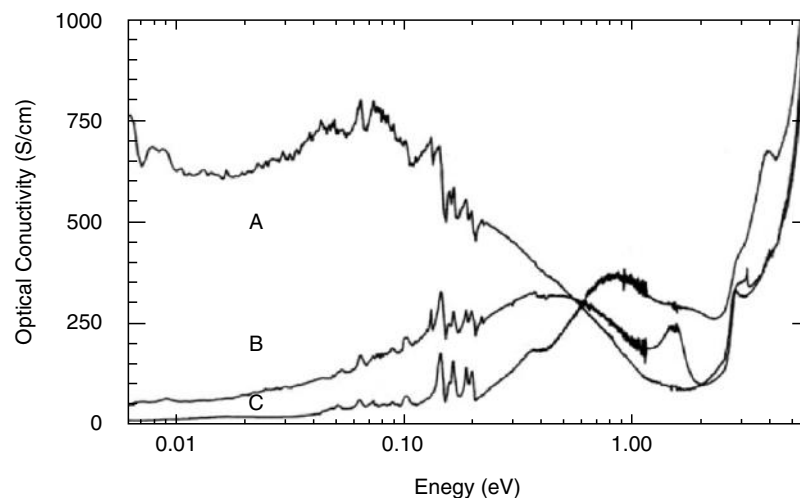
FIGURE 46.31. Room temperature optical conductivity vs. frequency for PAN–CSA(*m*-cresol) (A) PAN–CSA (chloroform/*m*-cresol) (B), and PAN–HCl IXL (C) (from Refs. [192, 193, and 224]).

polyacetylene and doped PAN and PPy with $\sigma_{DC} >$ 200 S/cm show Drude behavior for a small fraction of the conduction electrons which essentially percolate through the film while the remaining conduction electrons are more localized.

46.9 ULTIMATE CONDUCTIVITY

46.9.1 Drude Model Analysis

The intrinsic conductivity of conducting polymers is of interest for fundamental science and future materials applications. Though the materials currently have σ_{DC} less than common metals, the conducting polymers are not fully crystalline. Past progress suggests that as the synthesis,

doping routes, and processing are improved, further advances in materials properties can be expected. Estimates of the ultimate conductivity [122] of the quasi-one-dimensional polymer systems assuming the primary momentum relaxations are from $2k_F$ phonons which have modest population at room temperature suggests the ultimate conductivity for $(CH)_x$ is $\sim 2 \times 10^6$ S/cm (compared to 5.5×10^5 S/cm for copper).

From the experimental data which exist for current systems, estimates of the intrinsic conductivity also can be made [197]. The intrinsic Drude nature of metallic carriers has been identified using both microwave and optical techniques. Both of these techniques have identified the presence of a group of carriers which demonstrate Drude behavior with a long scattering time ($\tau \sim 10^{-11}$ s). The Drude conductivity for traditional metals is given by
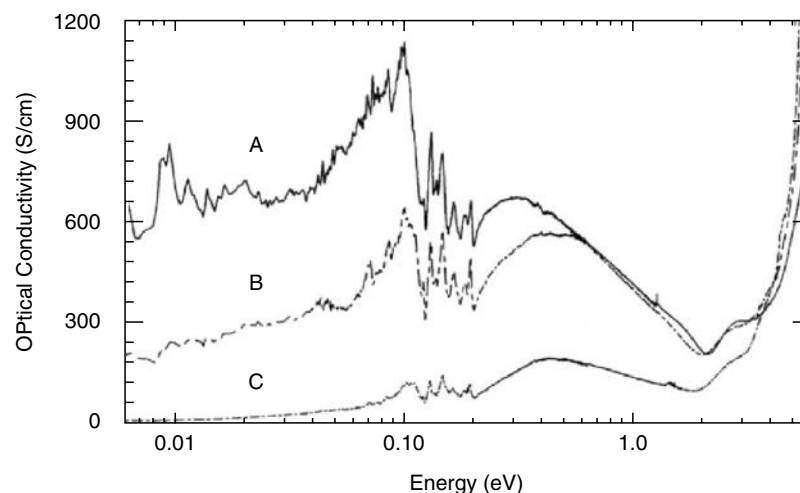
FIGURE 46.32. Room temperature optical conductivity versus frequency for PPy(PF$_6$) (A), PPy(TsO) (B), and PPy(S-PHE) (C) (from Refs. [74, 192, and 224]).
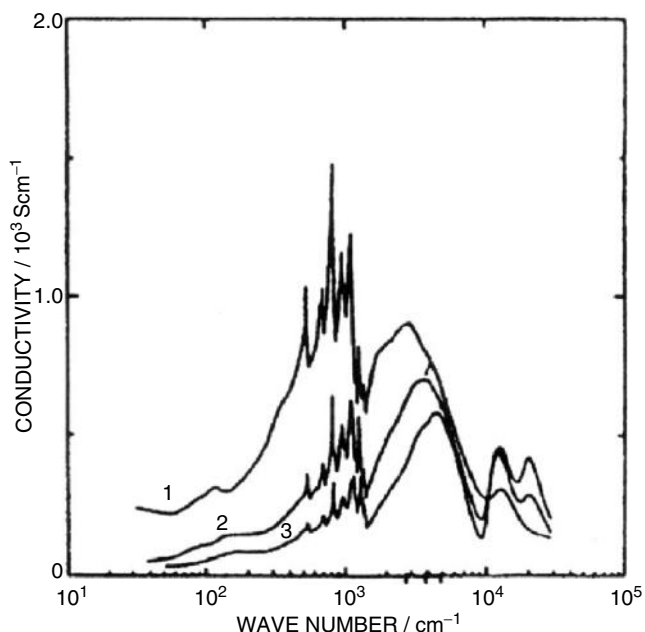
FIGURE 46.33. Optical conductivity versus frequency for poly-(methylthiophene) (PMT) doped with PF_6 as a function of doping level (from Ref. [190]). The spectra are for different doping levels [with (1) being highest and (3) the lowest doping level].

$\sigma = ne^2\tau/m^*$. In the present systems, only a small fraction ($\sim 0.1\%$) of the conduction electrons show this Drude behavior. If all of the conduction electrons (determined by doping percentage) have a scattering time equivalent to $\tau \sim 10^{-11}$ s, then $\sigma_{\text{ultimate}} \sim 10^7$ S/cm.

46.9.2 Resonance Quantum Transport in Doped Conducting Polymers

Metallic doped polymers (polyaniline and polypyrrole) have an electromagnetic response that, when analyzed within the standard theory of metals, is provided by an extremely small fraction of the total number of available electrons $\sim 0.1\%$ (in contrast to $\sim 100\%$ for common metals) but with anomalous long scattering time $\tau \geq 10^{-13}$ s (more then 100 times longer than for common metals). Prigodin and Epstein have shown [220] that a network of metallic grains (polymer's crystalline domains) connected by resonance quantum tunneling through localized states in surrounding disordered medium produces this behavior. The small fraction of electrons is assigned to the low density of resonance states and the long scattering time is related to the narrow width of energy levels in resonance. This differs from the general consensus [221–224] that the difference in doped conducting polymers between metal and insulator at low temperatures is caused by disorder driven localization of the conduction electrons (Anderson insulator–metal transition (IMT)) [153].

Figure 46.34 reviews the two conventional single particle transport mechanisms. For band transport (Drude theory) electrons behave as "free particles". They are accelerated by the applied electric field and loose their momentum through scattering by impurities and phonons. As a result, an electron's motion may be described as quantum diffusion. At low temperature the phonon scattering becomes weak and the conductivity increases with decreasing temperature to its residual value. For hopping the zero temperature electrical conductivity is zero because the charge carriers are localized. At finite temperatures electrons hop from one localized state to another by absorbing or emitting phonons. In contrast to band transport, hopping conductivity increases with temperature because of increased availability of phonons (see Fig. 46.34).

The dielectric constant ε can be used to identify the mechanism of charge transport [222,224]. For band transport, ε is negative because of inertia of "free electrons"; for hopping ε is positive and proportional to the square of the size of the localized state. Hopping often is expected to be the basic mechanism of transport for polymers because of their irregular structure and because even weak disorder localizes electrons in single isolated chains. This type of conductivity is observed in the dielectric polymers (doped polymers that become insulators at low temperatures) and their behavior qualitatively follows the above dependencies. However, the behavior of metallic polymers can be understood within neither the above hopping model nor the model of conventional metal with band electrons. The metallic conductivity of doped polymers decreases with decreasing temperature and a finite residual conductivity is within a decade of the room temperature value.

Though the decrease of the dc conductivity for metallic polymers with decreasing temperature can be accounted for within the band model by effects of localization caused by disorder, the experimental optical and low frequency conductivity and dielectric constant in the metallic state of doped polymers in principle cannot be accounted for by band models with homogeneous disorder. Experiments [221–224] show that the high frequency (≥ 0.1 eV) conductivity and dielectric constant generally follows a Drude law with the number of electrons $\sim 10^{21}$ cm^{-3} corresponding to the total density of conduction electrons and conventional scattering time $\sim 10^{-15}$ s in both the metallic and dielectric phases (Figs. 46.26–46.28). At decreasing frequency the polymers in the dielectric phase progressively display insulator properties and ε becomes positive for frequency ≤ 0.1 eV signaling that charge carriers are now localized. Microwave frequency (~ 6.6 GHz) ε experiments [222] yield localization lengths ~ 5 nm, depending on sample.

A surprising and remarkable feature of the metallic phase in polymers is that $\varepsilon(\omega)$ is similar to that of dielectric samples in magnitude and sign with decreasing frequency, also changing sign from negative to positive at approximately the same frequency ~ 0.1 eV. However, for metallic

Band Transport

1. Extended states: $\sigma(T{=}0) = \sigma_0$

2. Polarization is out-of-phase with an applied electric field due to electron inertia:

$\varepsilon(\omega{\sim}0) = -e^2\, N(\varepsilon_F)\, l^2 < 0$

l is the mean free path

3. Phonons resist electron's motion:

$\dfrac{d\sigma}{dT} < 0;$

$\sigma_{RT} \geq \sigma_{mm}$

4. Absorption decreases with frequency of an applied field because of less collisions :

Re $\sigma(\omega)$

Hopping Transport

1. Localized states: $\sigma(T{=}0) = 0$

2. Polarization is in-phase with an applied electric field because the electron is bound within ξ:

$\varepsilon(\omega{\sim}0) = -e^2\, N(\varepsilon_F)\, \xi^2 < 0$

ξ is the localization radius

3. Phonons initiate electron's hops:

$\dfrac{d\sigma}{dT} > 0;$

$\sigma_{RT} \geq \sigma_{mm}$

4. Absorption increases with frequency of an applied field due to polarization losses by clusters:

Re $\sigma(\omega)$

FIGURE 46.34. Comparison of band and hopping mechanisms of transport (after Ref. [220]).

samples ε changes again to negative at yet lower frequencies ≤ 0.01 eV indicating that "free electronic" motion is present, Fig. 46.35. The parameters of this low frequency coherent phase are quite anomalous. From the Drude model, the relaxation time is very long $\geq 10^{-13}$ s; also, the new plasma frequency below which ε is again negative is very small ~ 0.01 eV [3,5]. This second zero crossing of the dielectric constant at low frequency and the conclusion about a long relaxation time and a small plasma frequency were confirmed with radio frequency conductivity studies [225].
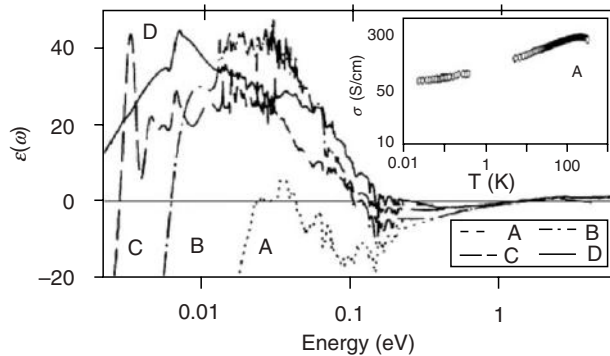
FIGURE 46.35. $\varepsilon(\omega)$ for camphor sulfonic acid doped polyaniline samples with room conductivities in the order of $\sigma_A > \sigma_B > \sigma_C > \sigma_D$ (Inset, σ_{DC} (T)). (after Ref. [222]).

These experimental data contrast with the Anderson IMT [153] in which electronic behavior is controlled by homogeneous disorder. In the dielectric phase electrons are bound by fluctuations of the random potential. On the metallic side of the transition, free carriers have short scattering times. In the metallic phase near the transition, ε is positive because the disorder causes dynamic polarization due to slowing diffusion by localization effects. When approaching the IMT the localization effects increase and ε diverges ("dielectric catastrophe" [200]).

The small plasma frequency and very long τ of the metallic state in doped polymers can be explained [222, 224,225] assuming that the conductivity is provided by a small fraction $\sim 0.1\%$ of the total carriers with long scattering time $> 10^{-13}$ s. However, it is difficult to reconcile this conclusion with the behavior for high frequencies which supports that the scattering time is usual $\sim 10^{-15}$ s and all available electrons participate in conduction. To account for these anomalies the possible presence of a collective mode, as in a charge density wave conductor, or superconductor, was suggested [199].

Prigodin and Epstein proposed [220] that in highly conducting polymers there is a new mechanism of charge transport, resonance quantum tunneling among metallic domains. These materials are strongly inhomogeneous [18,62,127,133] with "crystalline" regions within which polymer chains are well ordered (Fig. 46.36). Electrons are
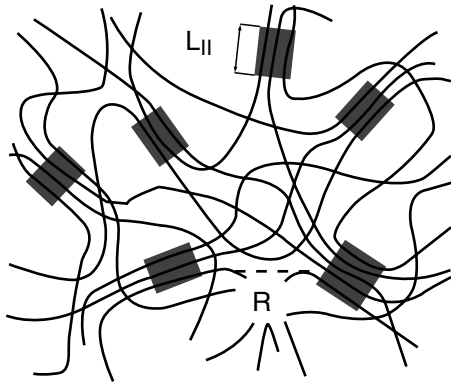
FIGURE 46.36. Schematic view of the structure of polyaniline and polypyrrole. The lines represent polymer chains. The dashed squares represent regions where polymer chains have crystalline order.

considered to be three-dimensionally delocalized over grains due to good overlap between chains within the grains. At least, when the IMT is approached, an electron's delocalization first occurs inside these regions. Outside the crystalline regions the chain order is poor and the electronic wave functions are strongly localized within single chains. Therefore, the crystalline domains can be considered as nanoscale metallic dots embedded in a disordered poorly conducting medium. The metallic grains remain always spatially separated by disordered regions, and, therefore, direct tunneling between grains is exponentially suppressed. The intergrain tunneling is possible through intermediate localized states in the disordered portion with strong contribution from resonance states whose energy is close to the Fermi level (Fig. 46.37). The dynamics of resonance tunneling can account for the frequency-dependent anomalies in the conductivity and dielectric constant of the metallic phase of these doped polymers. Reference [220] provides a detailed description and quantitative analysis of this model.

Within the Prigodin and Epstein model each grain is coupled to other grains by $2N_\perp$ independent chains. For simplicity one may assume that the two nearest grains are electrically connected by $\sim N_\perp/z$ chains, where z is the number of nearest neighboring grains. In the metallic phase the intergrain coupling leads to broadening of quantized levels in the grains, $\delta E = 2N_\perp g \Delta E$, where g is the transmission coefficient between grains through a single chain. The IMT occurs when $\delta E \sim \Delta E$ and the critical chain-link coupling g_c satisfies

$$2N_\perp g_c = 1. \tag{46.12}$$

For PAN(HCl) and similar PAN(CSA) this yields $g_c \sim 10^{-2}$.

If $g < g_c$ the system is a dielectric and the behavior (46.4) is retained for all $\omega \tau_T \ll 1$. However, on the metallic side $(g > g_c)$ electrons are delocalized and their low-frequency motion is a random walk among the grains. Introducing the mean transition rate, W, for hopping between the grains and the mean distance between the centers of neighboring grains, $R(b \sim (L_\parallel/R)^3)$, the corresponding diffusion coefficient D_3 and the macroscopic conductivity are

$$D_3 = R^2 W, \ \sigma(\omega \sim 0) = be^2 N(\varepsilon_F)D_3. \tag{46.13}$$

When approaching the IMT from the metallic side W tends to 0 as [12]: $W = (\Delta E/(2z)) \exp[-2\pi(g_c/(g-g_c))^{1/2}]$. In the metallic phase the hopping frequency W is related to the above model parameters as

$$W = \delta E/(2z) = (N_\perp/z)g\Delta E, \tag{46.14}$$

and the whole system can be represented as a network of random conductors. The nodes represent the grains where randomization of electronic motion happens. Further details of analysis and its application to specific polymers are in Ref. [220].

A principal difference between direct and resonance tunneling is the time for tunneling. Direct tunneling that occurs in a conventional granular metal is an almost instantaneous process, i.e., its characteristic time is the scattering time τ. Resonance tunneling that is anticipated to be in the metallic polymers shows a delay determined by the level width γ.
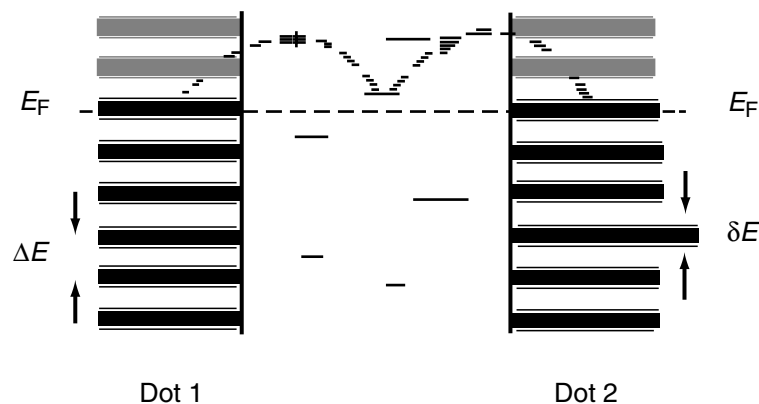
FIGURE 46.37. Schematic illustration of the electrical coupling of the metallic grains being provided by resonance tunneling of between the quantized states of the metallic grains through localized states in the amorphous region.

The temperature dependence of the dc conductivity in the metallic phase follows from that expected for resonant tunneling through the strongly localized states in the amorphous regions of the metallic polymer. With increasing temperature phonons increase the localization length of the states in the disordered regions thereby increasing the resonant transmission rate between grains and increasing the conductivity. As a result the low-frequency part of electromagnetic response is shifted with increasing temperature to a range of higher frequencies as it experimentally is observed [222].

46.10 APPLICATIONS

Intrinsically conducting polymers (ICPs) also are of interest for a wide range of applications [204]. The ICPs have been proposed for use as conducting wires, in batteries [205], as electromagnetic interference (EMI) shielding materials [206–209], joining (welding) of plastic materials [210], light emitting diodes (LEDs) [211], sensors [212], anticorrosive coatings [213], etc.

In LED studies, doped polyaniline and its blends have been used for the hole injecting layer [214], and undoped poly(p-phenylene vinylene) and other materials have been utilized for the light emitting layer [211]. More recently, a symmetrically configured alternating voltage light emitting (SCALE) device based on electronic polymers has been demonstrated [215,225,226,227]. The advantages of ICPs for light emitting devices include flexibility, mechanical strength, and relatively easy control of the color of light emission. Transparent conducting polymers may be incorporated as electrodes in efficient LEDs [216].

The use of plastics and their composites is rapidly increasing in numerous areas. However, the final assembly of products is often limited by the capability of existing joining techniques. The ability of ICPs, especially polyanilines, to absorb electromagnetic radiation and convert it into heat introduces another application in the welding of thermoplastics and thermosets [210].

With the rapid advances and broad implementation of computer and telecommunication technologies there is an increased need to shield EMI, especially in the radio and microwave frequency ranges. Intrinsically conducting polymers are promising materials for shielding of EMI because of their relatively high conductivity and dielectric constant and the ease of control of their conductivity and dielectric constant through chemical processing [207]. Also, they are relatively lightweight compared to standard metals, flexible, and do not corrode as common metals. The microwave conductivity and dielectric constant of polyanilines are controllable through chemical processing (e.g., stretch ratio, molecular weight, doping level, counter ion, solvent, etc.). Figure 46.38 compares the total shielding efficiency of PAN–CSA (m-cresol) materials with that of copper on the base of mass/area, while Fig. 46.39 compares the shielding efficiency of several different conducting polymer systems.

The ability to disperse conducting polymers into insulating hosts such as poly(3-octylthiophene) in polyethylene [217] and PAN–CSA in polymethylmethacrylate [218], or nylon [219], and achieve percolation at less than 1%, increases opportunities for applications.

Active electronic devices fabricated from semiconducting organic and polymer materials have become of increasing interest. In particularly, regioregular poly(3-hexylthiophene) (P3-HT) has been of interest because its relative
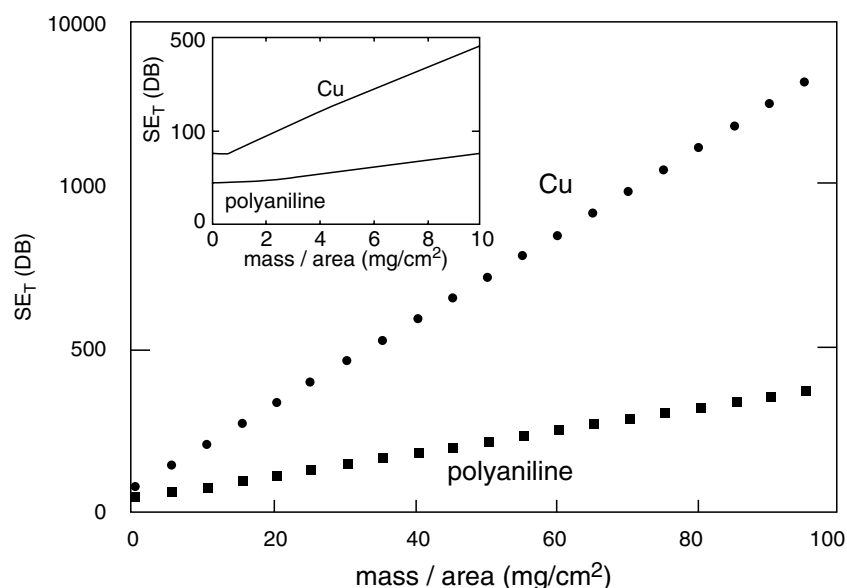
FIGURE 46.38. Comparison of total shielding efficiency (SE$_T$) of PAN–CSA (m-cresol) samples and copper (Cu) as a function of mass/area. Inset: magnification below 10 mg/cm^2 (from Ref. [207]).

sample	σ_{mw}(S/cm)	$10^{-5}\,\varepsilon_p$	$|\tan\delta|$
A	4700	−17	0.77
B	940	−3.9	0.67
C	560	−0.70	2.2
D	290	−1.0	0.80
E	110	0.32	0.99
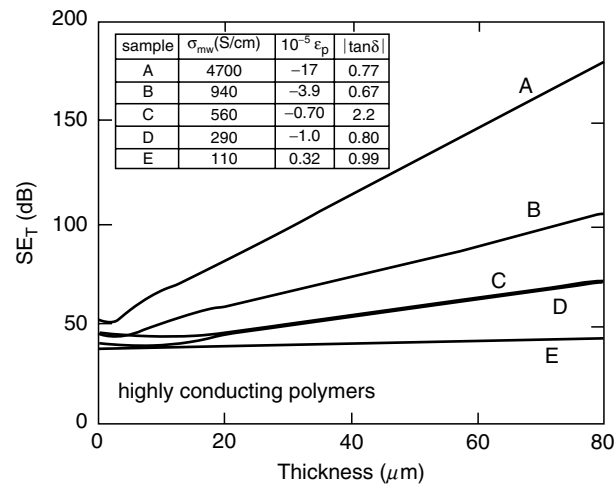
FIGURE 46.39. Comparison of total shielding efficiency (SE_T) of highly conducting polymers versus sample thickness. Sample A: stretched heavily iodine doped Tsukamoto polyacetylene; sample B: unstretched heavily iodine doped Tsukamoto polyacetylene; sample C: PAN–CSA (*m*-cresol); sample D: PPy(PF$_6$); sample E: PPy(TsO) (from Ref. [207]). The inset shows the microwave transport parameters σ_{mw}, ε_τ, and $\tan\delta$ for each of the materials.

structural order leads to a high mobility, in the range of 0.2 cm^2/(*Vs*) [228–231].

Recently a new interesting phenomenon, an electric field effect, was reported for the doped highly conducting polymers [232–235]. Figure 46.40 shows I–V characteristics of such a transistor [236] in which conducting polymer PEDOT:PSS [poly(ethylene dioxythiophene): poly(styrenesulfonic acid)] with $\sigma_{RT} \sim 30\,S/cm$ is used as active electronic element and PVP [poly(vinylphenol)] is used as a dielectric separating the gate and source–drain channel. As it is shown

on Fig. 46.40 the I_D current decreases with gate voltage V_G similarly to that normally observed for conventional semiconductors. The ratio I_{ON}/I_{OFF} reaches up to 10^4 in some devices [232–236].

Epstein *et al.* suggest [232,235] that the observed field effect in conducting polymers based "transistor" is closely related to the mesoscopic inhomogeneity of conducting polymers. They emphasize that the field effect cannot be observed if the conducting polymer is a conventional conductor. For conducting polymers with conductivity of $\sim$30 S/cm, the screening radius for an electric field produced by the FET gate electrode is expected to be less then 2 nm [232].

Epstein *et al.* propose that the field effect in conducting polymers is due to the ionic component of their charge conductivity. The inhomogeneous structure leaves enough free space for mobile ions. The ions inside the polymers produce the additional screening of the external field, but the crucial feature of ions is the ability of ions to migrate between the conducting polymer film and external dielectric layer interface. As a result the concentration of ions inside of the polymer is controlled by the gate potential. Due to electroneutrality the internal ionic density determines the concentration of primary charge carriers in the polymer and therefore it is anticipated that the polymer conductivity is governed by the gate potential. The critical concentration of ions for disrupting the conductivity along the polymer chains within the disordered regions was estimated within the following simple picture. If 50% crystallinity and size grain $\sim$10 nm were assumed, then intergrain hopping includes $\sim$ten intermediate sites along the chain linking two ordered regions. To interrupt this connection it is enough to introduce only one ion, i.e., approximately 5% "dedoping" would produce an appreciable effect. Figure 46.41 schematically illustrates the ability of a small concentration of excess ions to control the electrical conductivity of a doped polymers.
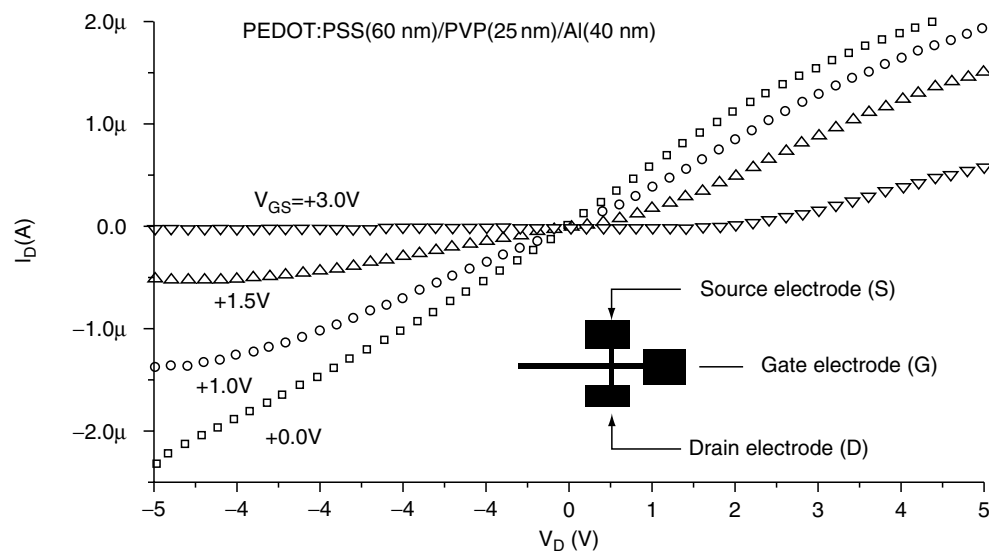
FIGURE 46.40. The drain–source current as the function of drain voltage of a thin PEDOT:PSS/PVP film. The insert shows the polymer-based transistor configuration (after Park *et al.* [236]).
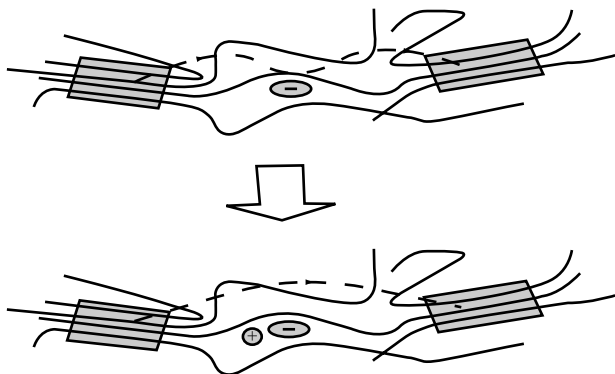
FIGURE 46.41. Schematic illustration of ionic suppression of intergrain hopping. Compensation by cations of charge of acceptors removes the nearby localized states on the polymer backbone that provide for holes easy hopping of electrons between grains. Reprinted from Ref. [235] © (2005) with permission from Elsevier.

46.11 NANOSTRUCTURING OF CONDUCTING POLYMERS

The conventional chemical polymerization of polyaniline only produces nonfibrous or irregular shaped morphologies [237,238]. In the past several years, a variety of chemical methods were reported that yield polyaniline nanofibers, such as use of hard templates [239,240], soft templates [241], electrospinning [242], interfacial polymerization [237], and seeding polymerization [238]. Recently, Chiou and Epstein discovered that polyaniline nanofibers can be directly synthesized in dilute chemical polymerization without aid of specific templates or techniques [243] (Fig. 46.42).

The nanofibrous structures prepared from dilute polymerization have no significant change when dedoped and redoped multiple times by base and acid solutions, respectively. The dispersion in deionized water of nanofibers is stable for several minutes without aggregation and precipitation [239]. Furthermore, a highly porous film of nanofibers is obtained as the dispersion is cast and dried on the glass or silicon wafer substrates. The UV/vis absorption patterns of polyaniline nanofibers obtained are consistent with previously reported results for conventionally synthesized polyaniline.

46.12 SUMMARY

The electrical transport properties of conducting polymers span the behaviors associated with semiconductors through to metals. Their properties depend critically upon the history of chemical synthesis, processing, and resulting structural order. Highly conducting doped polyacetylene, doped polypyrrole, and protonated polyaniline have similar dielectric responses, though on somewhat different scales. For each of these systems a positive dielectric constant is recorded at microwave frequencies for less conducting samples. A complex "metallic Drude response," involving both an all conduction band electron response and a delocalized electron response, is detected for well-processed, highly conducting samples. The ability to engineer the electrical and dielectric properties using chemistry opens the opportunity for a wide range of applications from electrostatic dissipation to sensors and field effect transistors.
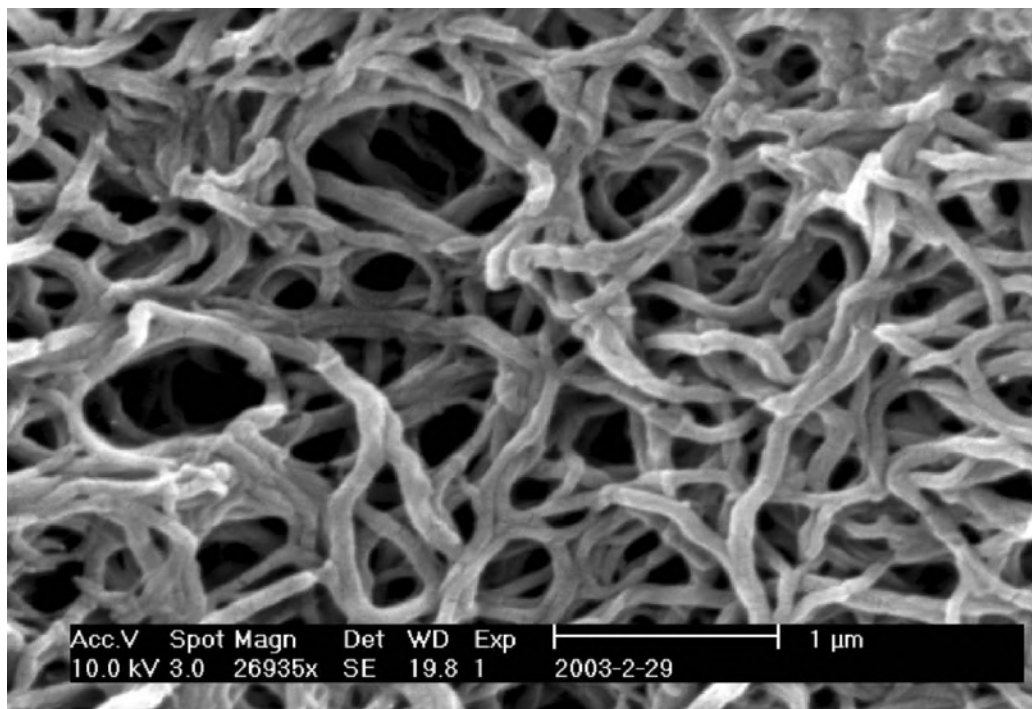
FIGURE 46.42. Nanofiber network of polyaniline prepared by dilute polymerization. Reprinted from [243] © (2005) with permission from Wiley-VCH.

Development of nanofibers and other morphologies will lead to new fundamental science and new opportunities for applications.

ACKNOWLEDGMENTS

GLOSSARY OF TERMS

Anderson Localization: spatial localization of electronic wavefunctions due to randomness of the electronic potential which causes a metal–insulator transition in sufficiently disordered materials.

Antisoliton: solitons are present in materials with two degenerate phases A and B. If a soliton is a kink between A and B phase, then an antisoliton is a kink between B and A phase.

Bipolaron: a bipolaron is similar to a polaron except that it is doubly charged, spinless, and both of its energy states in the band gap are totally filled or empty.

Bloch Waves: delocalized electronic wavefunctions which have the form $\psi_k(\vec{r}) = u_k(\vec{r}) \exp(i\vec{k} \cdot \vec{r})$, where $u_k(\vec{r})$ is a function with the periodicity of the lattice unit cell and $\exp(i\vec{k} \cdot \vec{r})$ is a wave of wavelength $\lambda = 2\pi/k$.

Commensurate Charge Density Wave: a static modulation of the charge density in the system with a periodicity equal to a rational number multiplied by the underlying periodicity of the lattice. Due to the charge density wave, a gap is opened at the Fermi level which lowers the total energy of the system.

Crosslinked Polymers: polymers with greater interaction between chains either through regions of greater crystallinity (physical crosslinks between the polymer chains), or through chemical bonding between chains.

Crystalline Coherence Length: a length which characterizes the spatial correlations for the polymer chain, indicating the length over which the local order randomizes. This length is determined from the width of x-ray scattering peaks from the Scherrer formula.

Curie Susceptibility: Paramagnetic susceptibility due to uncoupled spins free to align in a magnetic field and subject only to thermal fluctuations. The Curie susceptibility is given by $\chi_{\text{Curie}} = C/T$, where C is the Curie constant (0.375 emu K/mol) and T is the temperature.

Degenerate Ground State: for a degenerate ground state, the conjugation path is such that reversal of the single and double bonds results in a phase of the system with an equivalent energy.

Doping: a process whereby charges are removed or added to the polymer chain, altering the electronic structure and response.

Drüde Model: this model of the electrons in a conductor treats the electrons as free, subject only to dissipative, inertial, and electromagnetic forces. In this model, the conductivity $\sigma(\omega)$ and the dielectric function $\varepsilon(\omega)$ are given as $\sigma(\omega) = (\Omega_p^2 \tau/4\pi)/(1 - i\omega\tau)$ and $\varepsilon(\omega) = \varepsilon_B - \Omega_p^2/(\omega(\omega + i/\tau))$, where Ω_p is the plasma frequency and τ is the mean scattering for transport.

Electron–Electron Interactions: a broad term referring to the electromagnetic interaction between electrons as well as some of the effects of the Pauli exclusion principle.

Exciton: an electron–hole pair bound by Coulombic forces capable of transferring energy but not charge because it is electrically neutral.

Hole: a vacant orbital in an energy band which acts as a positive charge in an applied electric or magnetic field.

Hopping Transport: a form of charge transport which involves electron motion from one spatially localized state to another accompanied by the absorption or emission of a phonon.

Incommensurate Charge Density Wave: similar to a commensurate charge density wave except that the periodicity of the charge density modulation does not equal a rational number multiplied by the periodicity of the underlying lattice.

Inhomogeneous Disorder: Structural configuration for a polymer solid which consists of a mixture of ordered (crystalline) and disordered regions of the polymer.

Kramers–Kronig Analysis: a set of mathematical relations due to causality which relate the real (dispersive) and imaginary (absorptive) parts of a physical quantity. These relations can be used to determine the imaginary part of a quantity given information about the real part and vice versa.

Localization Modified Drude Model: a model for conduction electrons which includes suppression of the Drude conductivity at low frequencies due to finite localization lengths for the electrons.

Localized States: electronic states which are not extended over the entire solid as Bloch waves are localized states. The spatial dependence of the wavefunctions of a localized state is usually assumed to vary as $|\psi(\vec{r})| \sim \exp(-|\vec{r} - \vec{r}_0|/\xi)$, decaying exponentially in a characteristic length ξ, the localization length, away from $\vec{r}_0$. Charge transport by electrons in these states is due to hopping.

Lorentz Model: this model treats electrons as bound strongly to an atom, subject to dissipative, inertial, electromagnetic, as well as restoring forces. In this model, the dielectric function $\varepsilon(\omega)$ is given by $\varepsilon(\omega) = \varepsilon_B + \Omega_p^2/(\omega_0^2 - \omega^2 - i\omega/\tau)$, where ε_B is the background dielectric function due to everything else, Ω_p is the plasma frequency, ω_0 is the binding energy, and τ is the mean scattering time.

Mesoscopic Metallic State: a metallic state in an inhomogeneous system in which conduction electrons are delocalized over a number of crystalline regions (with disordered polymer regions between them). The size of the localization length is $\sim 10^2$–10^3 A, smaller than macroscopic dimensions (10^4 A or greater).

Mobility Edge: the critical energy which separates electronic states which are spatially localized due to disorder and thus have zero contribution to the electrical conductivity at very low temperature from those which are delocalized and therefore have nonzero contribution to the electrical conductivity at low temperature.

Mott Variable Range Hopping: a form of hopping transport which results when the electron may hop to a distant site instead of just a neighboring site if the energy difference between its current site and the distant site is smaller than the difference between its current site and the neighboring sites. Mott variable range conductivity has a form given by $\sigma(T) \cong \sigma_0 \exp[-(T_0/T)^{1/(d+1)}]$, where d is the dimensionality of the hops and T_0 is a reduced activation energy.

Nondegenerate Ground State: for a nondegenerate ground state, the conjugation path is such that reversal of the single and double bonds results in a distinctly different energy.

One-Dimensional Chain: a linear system for which the interactions along the chain direction are much stronger than the interactions perpendicular to the chain.

p_z Orbitals: electron wavefunctions with atomic principal quantum number p character which have a node in the x–y plane (the x–y plane is usually taken as the plane of the polymer sp^2 bonds.) Electrons in these orbitals usually pair to form double bonds and provide the conjugation responsible for the interesting electronic properties of conducting polymers.

π Conjugation: alternating single and double bonds in a single plane due to the overlap of atomic p_z orbitals along the polymer backbone. π conjugation leads to the electronic bands responsible for the interesting electronic properties of conducting polymers.

Pauli Susceptibility: paramagnetic, approximately temperature independent magnetic susceptibility due to conduction electrons. The Pauli susceptibility, $\chi_{Pauli} = 2\mu_B^2 N(E_F)$, where μ_B is a Bohr magneton and $N(E_F)$ is the density of states at the Fermi level.

Peierls Instability: an instability prominent in quasi-one-dimensional systems with strong electron–phonon interactions due to which the lattice spontaneously distorts with a $2k_F$ (k_F is the Fermi wavevector) periodicity, forming a gap at the Fermi level which lowers the total energy of the system.

Percolation: in a solid made up of more than one component (a composite system), the volume fraction of the different components can be varied. Percolation refers to the transitions which occur when the volume fraction of a component is such that there are connected paths of that component across the material. For example, in a composite of a metal and an insulator, the metal particles percolate when they form a connected path across the material and finite dc conductivity becomes possible.

Phonon: a quantum of lattice vibrational energy which reflects the normal vibrational modes of the lattice allowed by symmetry.

Phonon Induced Delocalization: in disordered solids, localization can result when a wavefunction interferes with itself due to elastic scattering and forms a standing wave. Phonon scattering can destroy this interference effect and cause the wavefunctions to be more extended.

Photoexcitation: the use of light (photons) to cause transitions of electrons from the ground state to excited states of the system.

Plasma Frequency: defined as $\Omega_p = 4\pi ne^2/m^*$, where n is the volume density of conduction electrons, e is the charge of an electron, and m^* is the effective mass renormalized from the free electron mass by lattice and interaction effects.

Plasma Response: an excitation of a solid for which the negative charge in the solid is displaced uniformly with respect to the ions. Plasma oscillations occur when the dielectric function is equal to zero.

Polaron: most generally a localized electronic state accompanied by a surrounding lattice distortion. In conduction polymers, it has been discussed as a bound state of a soliton and an antisoliton. This excitation can occur in degenerate and nondegenerate ground state polymers. A polaron possesses a single charge with normal spin–charge relations (i.e., with a single charge, it also has spin 1/2) and usually two states in the bandgap of the neutral polymer, one of which is half filled.

Polaron Lattice: a uniform periodic array of "polarons" assumed stabilized against a Peierls distortion by interchain interaction. The band structure for a polaron lattice is metallic.

Screened Plasma Frequency: the plasma frequency normalized or screened by a background dielectric constant. The screened plasma frequency, $\omega_p = \Omega_p/\sqrt{\varepsilon_B}$, where Ω_p is the plasma frequency and ε_B is the background dielectric constant due to all excitations except the conduction electrons.

Soliton: a low energy excitation of the electronic system which is localized in space and maintains its identity in the presence of other excitations. In conducting polymers, a soliton takes the form of a kink or misfit between two distinct energetically equivalent phases (in degenerate ground state systems). Its properties include a reversed spin–charge relation (i.e., when it is charge neutral, it has spin 1/2), the introduction of a single energy level within the band gap of the polymer, and a lattice distortion surrounding the soliton.

Time Reversal Symmetry: a symmetry of a system characterized by replacing t (time) with $-t$ without changing the physics of the system.

REFERENCES

For a more complete set of annotated references, see J. W. Blatchford and A. J. Epstein, Am. J. Phys. **64**, 120–135 (1996); for a compilation of original papers, see Yu Lu, *Solitons and Polarons in Conducting Polymers* (World Scientific, New Jersey, 1988).

1. See Chapters 47, 48, and 49 of this Handbook.
2. C. K. Chiang, C. R. Fincher, Jr., Y. W. Park, A. J. Heeger, H. Shirakawa, E. J. Louis, S. C. Gau, and A. G. MacDiarmid, Phys. Rev. Lett. **39**, 1098 (1977).
3. Proc. Int. Confs. on Science and Technology of Synthetic Metals. ICSM-'04, Wollongong, Australia, in Synth. Met. **152–154** (2005); ICSM-'02, Shanghai, P.R. China, in Synth. Met. **133–137** (2003); ICSM-'00, Gastein, Austria, in Synth. Met. **119–121** (2001); ICSM-'98, Montpellier, France, in Synth. Met. **101–103** (1999); ICSM-'96, Snowbird, UT, in Synth. Met. **84–86** (1997); ICSM-'94, Seoul, Korea, July 21–29, 1994, in Synth. Met. **69–71** (1995); ICSM '92, Goteborg, Sweden, Aug. 12–18, 1992, in Synth. Met. **55–57** (1993); ICSM '90, Tubingen, FRG, Sept. 2–9, 1990, in Synth. Met. **41–43** (1991); and ICSM '88, Sante Fe, NM, June 26–July 2, 1988, in Synth. Met. **27–29** (1988).
4. *Handbook of Conducting Polymers,* edited by T. A. Skotheim (Marcel Dekker, New York, 1986).
5. D. Baeriswyl, D. K. Campbell, and S. Mazumdar, in *Conjugated Conducting Polymers,* edited by H. G. Keiss (Springer-Verlag, Berlin, 1992), p. 7.
6. E. M. Conwell, IEEE Trans. Electri. Insul. **EI-22**, 591 (1987).
7. A. J. Heeger, S. A. Kivelson, J. R. Schrieffer, and W. P. Su, Rev. Mod. Phys. **60**, 781 (1988).
8. E. Jeckelmann and D. Baeriswyl, Synth. Met. **65**, 211 (1994).
9. J. E. Hirsch, Phys. Rev. Lett. **51**, 296 (1983).
10. S. N. Dixit and S. Mazumdar, Phys. Rev. B **29**, 1824 (1984).
11. W. K. Wu and S. Kivelson, Phys. Rev. B **33**, 8546 (1986).
12. C. Wu, X. Sun, and K. Nasu, Phys. Rev. Lett. **59** 831 (1987).
13. H. W. Gibson, F. C. Bailey, A. J. Epstein, H. Rommelmann, S. Kaplan, J. Harbour, X. -Q. Yang, D. B. Tanner, and J. M. Pochan, J. Am. Chem. Soc. **105**, 4417 (1983); K. Pakbaz, R. Wu, F. Wudl, and A. J. Heeger, J. Chem. Phys. **99**, 590 (1993).
14. M. C. dos Santos and J. L. Brédas, Phys. Rev. Lett. **62**, 2499 (1989).
15. J. M. Ginder and A. J. Epstein, Phys. Rev. Lett. **64**, 1184 (1990).
16. W. P. Su and A. J. Epstein, Phys. Rev. Lett. **70**, 1497 (1993).
17. J. C. Chiang and A. G. MacDiarmid, Synth. Met. **13**, 193 (1986).
18. J. P. Pouget, Z. Oblakowski, Y. Nogami, P. A. Albouy, M. Laridjani, E. J. Oh, Y. Min, A. G. MacDiarmid, J. Tsukamuto, T. Ishiguro, and A. J. Epstein, Synth. Met. **65**, 131 (1994).
19. M. Winokur, Y. B. Moon, A. J. Heeger, J. Barker, D. C. Bott, and H. Shirakawa, Phys. Rev. Lett. **58** 2329 (1987); R. H. Baughmann, S. L. Hsu, G. P. Pez, and A. J. Signorelli, J. Chem. Phys. **68**, 5405 (1978).
20. N. S. Murthy, G. G. Miller, and R. H. Baughmann, J. Chem. Phys. **89**, 2523 (1988).
21. W. P. Su, J. R. Schrieffer, and A. J. Heeger, Phys. Rev. Lett. **42,** 1698 (1979).
22. S. A. Brazovskii, Sov. Phys. JETP. Lett. **28**, 606 (1978).
23. M. J. Rice, Phys. Lett. **71A**, 152 (1979).
24. D. K. Campbell and A. R. Bishop, Phys. Rev. B **24**, 4859 (1981).
25. C. R. Wu, J. O. Nilsson, O. Inganäs, W. R. Salaneck, J. -E. Österholm, and J. L. Brédas, Synth. Met. **21**, 197 (1988).
26. C. X. Cui and M. Kertesz, Phys. Rev. B **40**, 9661 (1989).
27. F. Moraes, D. Davidov, M. Kobayashi, T. C. Chung, J. Chen, A. J. Heeger, and F. Wudl, Synth. Met. **10**, 169 (1985).
28. G. Harbeke, E. Meier, W. Kobel, M. Egli, H. Kiess, and E. Tosatti, Solid State Commun. **55**, 419 (1985).
29. G. S. Kanner, X. Wei, B. C. Hess, L. R. Chen, and Z. V. Vardeny, Phys. Rev. Lett. **69**, 538 (1992).
30. K. Kaneto, S. Hayashi, S. Ura, and K. Yoshino, J. Phys. Soc. Jpn **54** 1146 (1985).
31. J. L. Brédas, J. C. Scott, K. Yakushi, and G. B. Street, Phys. Rev. B **30**, 1023 (1984).
32. G. Zotti and G. Schiavon, Synth. Met. **41–43**, 445 (1991).
33. F. Genoud, M. Guglielmi, M. Nechtschein, E. Genies, and M. Salmon, Phys. Rev. Lett. **55**, 118 (1985).
34. O. Chauvet, S. Paschen, L. Forro, L. Zuppiroli, P. Bujard, K. Kai, and W. Wernet, Synth. Met. **63**, 115 (1994).
35. P. Gomes da Costa, R. G. Dandrea, and E. M. Conwell, Phys. Rev. B **47**, 1800 (1993).
36. M. Onoda, Y. Manda, T. Iwasa, H. Nakayama, K. Amakawa, and K. Yoshino, Phys. Rev. B **42**, 11826 (1990).
37. A. Sakamoto, Y. Furukawa, and M. Tasumi, J. Phys. Chem. **96**, 1490 (1992); A. Sakamoto, Y. Furukawa, and M. Tasumi, J. Phys. Chem. **96**, 3870 (1992); A. Sakamoto, Y. Furukawa, and M. Tasumi, Synth. Met. **55–57**, 593 (1993).
38. J. L. Brédas, R. R. Chance, and R. Sibley, Phys. Rev. B **26**, 5843 (1982).
39. G. Froyer, Y. Pelous, A. Siove, F. Genoud, M. Nechtschein, and B. Villeret, Synth. Met. **33**, 381 (1989).
40. Y. Furukawa, H. Ohtsuka, and M. Tasumi, Synth. Met. **55–57**, 516 (1993).
41. J. Libert, J. L. Brédas, and A. J. Epstein, Phys. Rev. B **51**, 5711 (1995).
42. J. M. Ginder and A. J. Epstein, Phys. Rev. B **41**, 10674 (1990).
43. S. Kivelson and W. K. Wu, Phys. Rev B. **34**, 5423 (1986).
44. X. Wei, B. C. Hess, Z. V. Vardeny, and F. Wudl, Phys. Rev. Lett. **68**, 666 (1992).
45. S. Abe, J. Yu, and W. P. Su, Phys. Rev. B **45**, 8264 (1992).
46. H. A. Mizes and E. M. Conwell, Phys. Rev. B **50**, 11243 (1994).
47. M. Chandross, S. Mazumdar, S. Jeglinski, X. Wei, and Z. V. Vardeny, Phys. Rev. B **50**, 14702 (1994).
48. M. J. Rice and Y. N. Gartstein, Phys. Rev. Lett. **73**, 2504 (1994).
49. N. F. Colaneri, D. D. C. Bradley, R. H. Friend, P. L. Burn, A. B. Holmes, and C. W. Spangler, Phys. Rev. B **42**, 11670 (1990).
50. M. Yan, L. J. Rothberg, F. Papadimitrakoupoulos, M. E. Galvin, and T. M. Miller, Phys. Rev. Lett. **72**, 1104 (1994).
51. J. M. Leng, S. Jeglinski, X. Wei, R. E. Benner, Z. V. Vardeny, F. Guo, and S. Mazumdar, Phys. Rev. Lett. **72**, 156 (1994).
52. E. M. Conwell, H. A. Mizes, and S. Javadez, Phys. Rev. B **40**, 1630 (1989).
53. S. Stafstrom, Phys. Rev. B **43**, 12437 (1993)
54. A. J. Epstein, J. M. Ginder, F. Zuo, R. W. Bigelow, H. -S. Woo, D. B. Tanner, A. F. Richtner, W.-S. Huang, and A. G. MacDiarmid, Synth. Met. **18**, 303 (1987).
55. S. Stafstrom, J. L. Brédas, A. J. Epstein, H. S. Woo, D. B. Tanner, W. S. Huang, and A. G. MacDiarmid, Phys. Rev. Lett. **59**, 1464 (1987).
56. J. L. Brédas, B. Thémans, J. G. Fripiat, J. M. André, and R. R. Chance, Phys. Rev. B **29**, 6761 (1984).
57. T. Ohsawa, O. Kimura, M. Onoda, and K. Yoshino, Synth. Met. **47**, 151 (1992).
58. M. Bartonek and H. Kuzmany, Synth. Met. **41–43**, 607 (1991).
59. K. Mizoguchi, T. Obana, S. Ueno, and K. Kume, Synth. Met. **55–57**, 601 (1993).
60. F. Genoud, M. Nechtschein, and C. Santier, Synth. Met. **55–57**, 642 (1993).
61. J. M. Ginder, A. F. Richter, A. G. MacDiarmid, and A. J. Epstein, Solid State Commun. **63**, 97 (1987).
62. M. E. Jozefowicz, R. Laversanne, H. H. S. Javadi, A. J. Epstein, J. P. Pouget, X. Tang, and A. G. MacDiarmid, Phys. Rev. B **39**, 12958 (1989).
63. J. Tsukamoto, Adv. Phys. **41**, 509 (1992); J. Tsukamoto, A. Takahashi, and K. Kawasaki, Jpn., J. Appl. Phys. **29**, 125 (1990).
64. H. Naarmann and N. Theophilou, Synth. Met. **22**, 1 (1987).
65. H. Shirakawa, Y. -X. Zhang, T. Okuda, K. Sakamaki, and K. Akagi, Synth. Met. **65**, 93 (1994).
66. T. Ito, H. Shirakawas, and S. Ikeda, J. Polym. Sci. Polym. Chem. Ed. **12**, 11 (1974).
67. K. Ito, Y. Tanabe, K. Akagi, and H. Shirakawa, Phys. Rev. B **45**, 1246 (1992).
68. J. H. Edwards and W. J. Feast, Polym. Commun. **21**, 595 (1980).
69. J. C. W. Chien, in *Polyacetylene: Chemistry, Physics, and Material Science* (Academic, New York, 1984), p. 24.
70. T. Ishiguro, H. Kaneko, Y. Nogami, H. Nishiyama, J. Tsukamoto, A. Takahashi, M. Yamaura, and J. Sato, Phys. Rev. Lett. **69**, 660 (1992); H. Kaneko, T. Ishiguro, J. Tsukamoto, and A. Takahashi, Solid State Commun. **90**, 83 (1994).
71. P. N. Adams, P. Laughlin, A. P. Monkman, and N. Bernhoeft, Solid State Commun. **91**, 895 (1994); the value of conductivity reported in Fig. 46.4 is for samples kindly provided by Monkman and coworkers, and measured at The Ohio State University.
72. R. D. McCullough, S. P Williams, S. Tristran-Nagle, M. Jayaraman, P. C. Ewbank, and L. Miller, Synth. Met. **69**, 279 (1995).

73. J. Joo, Z. Oblakowski, G. Du, J. P. Pouget, E. J. Oh, J. M. Weisinger, Y. Min, A. G. MacDiarmid, and A. J. Epstein, Phys. Rev. B **49**, 2977 (1994).

74. R. S. Kohlman, J. Joo, Y. Z. Wang, J. P. Pouget, H. Kaneko, T. Ishiguro, and A. J. Epstein, Phys. Rev. Lett. **74,** 773 (1995).

75. A. J. Epstein, J. Joo, R. S. Kohlman, G. Du, A. G. MacDiarmid, E. J. Oh, Y. Min, J. Tsukamoto, H. Kaneko, and J. P. Pouget, Synth. Met. **65**, 149 (1994).

76. A. J. Epstein, H. Rommelmann, M. A. Druy, A. J. Heeger, and A. G. MacDiarmid, Solid State Commun. **38**, 683 (1981).

77. P. K. Kahol, H. Guan, and B. J. McCormick, Phys. Rev. B **44**, 10393 (1991).

78. S. Ikehata, J. Kaufer, T. Woerner, A. Pron, M. A. Druy, A. Sivak, A. J. Heeger, and A. G. MacDiarmid, Phys. Rev. Lett. **45**, 1123 (1980).

79. N. S. Saricifti, A. J. Heeger, and Y. Cao, Phys. Rev. B **49**, 5988 (1994).

80. (a) Y. W. Park, Synth. Met. **45**, 173 (1991); (b) Y. W. Park, A. J. Heeger, M. A. Druy, and A. G. MacDiarmid, J. Chem. Phys. **73**, 946 (1980).

81. H. H. S. Javadi, A. Chakraborty, C. Li, N. Theophilou, D. B. Swanson, A. G. MacDiarmid, and A. J. Epstein, Phys. Rev. B **43**, 2183 (1991).

82. J. C. Clark, G. G. Ihas, A. J. Rafanello, M. W. Meisel, M. Reghu, C. O. Yoon, Y. Cao, and A. J. Heeger, Synth. Met. **69**, 215 (1995); R. S. Kohlman, A. J. Epstein, G. G. Ihas, and A. G. MacDiarmid, to be published.

83. A. J. Epstein, H. Rommelmann, R. Bigelow, H. W. Gibson, D. M. Hoffman, and D. B. Tanner, Phys. Rev. Lett. **50**, 1866 (1983).

84. Y. Cao, P. Smith, and A. J. Heeger, Synth. Met. **48**, 91 (1992).

85. Y. Z. Wang, J. Joo, C. -H. Hsu, J. P. Pouget, and A. J. Epstein, Phys. Rev. B **50**, 16811 (1994).

86. Z. H. Wang, H. H. S. Javadi, A. Ray, A. G. MacDiarmid, and A. J. Epstein, Phys. Rev. B **42**, 5411 (1990).

87. J. Yue, Z. H. Wang, K. R. Cromack, A. J. Epstein, and A. G. MacDiarmid, J. Am. Chem. Soc. **113**, 2655 (1991).

88. M. Yamaura, T. Hagiwara, and K. Iwata, Synth. Met. **26**, 209 (1988).

89. K. Sato, M. Yamaura, T. Hagiwara, K. Murata, and M. Tokumoto, Synth. Met. **40**, 35 (1991).

90. J. -E. Österholm, P. Passiniemi, H. Isotalo, and H. Stubb, Synth. Met. **18,** 213 (1987).

91. T. Ohnishi, T. Noguchi, T. Nakano, M. Hirooka, and I. Murase, Synth. Met. **41–43**, 309 (1991).

92. L. W Shacklette, R. R. Chance, D. M. Ivory, G. G. Miller, and R. H. Baughman, Synth. Met. **1**, 307 (1979).

93. G. Du, V. N. Prigodin, A. Burns, J. Joo, C. S. Wang, and A. J. Epstein, Phys. Rev. B **58**, 4485 (1998).

94. A. J. Epstein, H. Rommelmann, M. Abkowitz, and H. W. Gibson, Phys. Rev. Lett. **47**, 1549 (1981).

95. A. J. Epstein, H. Rommelmann, and H. W. Gibson, Phys. Rev. B **31**, 2502 (1985).

96. F. Zuo, M. Angelopoulos, A. G. MacDiarmid, and A. J. Epstein, Phys. Rev. B **39**, 3570 (1989).

97. J. C. Scott, P. Pfluger, M. T. Krounbi, and G. B. Street, Phys. Rev. B **28**, 2140 (1983).

98. G. E. Wnek, J. C. Chien, F. E. Karasz, and C. P Lillya, Polymer **20**, 1441 (1979).

99. R. E. Peierls, in *Quantum Theory of Solid* (Clarendon, Oxford, 1955), p. 108.

100. E. J. Mele and M. J. Rice, Phys. Rev. B **23**, 5397 (1981).

101. S. A. Kivelson and A. J. Heeger, Phys. Rev. Lett. **55**, 308 (1985).

102. H. -Y. Choi and E. J. Mele, Phys. Rev. B **34**, 8750 (1986).

103. D. B. Tanner, G. L. Doll, A. M. Rao, P. C. Eklund, G. A. Arbuckle, and A. G. MacDiarmid, Synth. Met. **28**, D141 (1989).

104. Y. H. Kim and A. J. Heeger, Phys. Rev. B **40**, 8393 (1989).

105. M. I. Salkola and S. A. Kivelson, Phys. Rev. B **50**, 13962 (1994); S. A. Kivelson and M. I. Salkola, Synth. Met. **44**, 281 (1991).

106. J. Tanaka, C. Tanaka, T. Miyamae, M. Shimizu, S. Hasegawa, K. Kamiya, and K. Seki, Synth. Met. **65**, 173 (1994).

107. A. Yamashiro, A. Ikawa, and H. Fukutome, Synth. Met. **65**, 233 (1994).

108. H. L. Wu and P. Phillips, Phys. Rev. Lett. **66**, 1366 (1991); P. Phillips and H. L. Wu, Science **252**, 1805 (1991).

109. F. C. Lavarda, M. C. dos Santos, D. S. Galvao, and B. Laks, Phys. Rev. Lett. **73**, 1267 (1994).

110. S. Stafstrom and J. L. Brédas, Phys. Rev. B **38**, 4180 (1988).

111. D. S. Galvao, D. A. dos Santos, B. Laks, C. P. de Melo, and M. J. Caldas, Phys. Rev. Lett. **63**, 786 (1989).

112. V. N. Prigodin and K. B. Efetov, Phys. Rev. Lett. **70**, 2932 (1993).

113. C. Kittel, in *Introduction to Solid State Physics* (John Wiley & Sons, Inc., New York, 1986), p. 157.

114. P. W Anderson, Phys. Rev. **109**, 1492 (1958).

115. N. F. Mott and E. Davis, in *Electronic Processes in Non-Crystalline Materials* (Clarendon Press, Oxford, 1979), p. 6.

116. M. Reghu, C. O. Yoon, D. Moses, A. J. Heeger, and Y. Cao, Phys. Rev. B **48**, 17685 (1993); M. Reghu, Y. Cao, D. Moses, and A. J. Heeger, Phys. Rev. B **47**, 1758 (1993).

117. C. O. Yoon, M. Reghu, D. Moses, A. J. Heeger, and Y. Cao, Phys. Rev. B **48**, 14080 (1993).

118. C. O. Yoon, M. Reghu, D. Moses, and A. J. Heeger, Phys. Rev. B **49**, 10851 (1994).

119. A. L. Efros and B. I. Shklovski, J. Phys. C**8**, L49 (1975); B. I. Shklovski and A. L. Efros, in *Electronic Properties of Doped Semiconductors* (Springer-Verlag, Heidelberg, 1984).

120. J. Joo, V. N. Prigodin, Y. G. Min, A. G. MacDiarmid, and A. J. Epstein, Phys. Rev. B **50**, 12226 (1994).

121. Z. H. Wang, A. Ray, A. G. MacDiarmid, and A. J. Epstein, Phys. Rev. B **43**, 4373 (1991).

122. S. Kivelson and A. J. Heeger, Synth. Met. **22**, 371 (1988).

123. P. Drüde, Ann. Phys. **1**, 566 (1900); **3**, 369 (1900).

124. G. Burns, in *Solid State Physics* (Academic, New York, 1985), p. 187.

125. R. H. Baughman, N. S. Murthy, and G. G. Miller, J. Chem. Phys. **79**, 515 (1983).

126. D. Chen, M. J. Winokur, M. A. Masse, and F. E. Karasz, Phys. Rev. B **41**, 6759 (1990).

127. J. P. Pouget, M. E. Jozefowicz, A. J. Epstein, X. Tang, and A. G. MacDiarmid, Macromolecules **24**, 779 (1991).

128. J. P. Pouget, C. -H. Hsu, A. G. MacDiarmid, and A. J. Epstein, Synth. Met. **69**, 119 (1995).

129. W. Fosong, T. Jinsong, W. Lixiang, Z. Hongfang, and M. Zhishen, Mol. Cryst. Liq. Cryst. **160**, 175 (1988).

130. Y. B. Moon, Y. Cao, P. Smith, and A. J. Heeger, Polym. Commun. **30**, 196 (1989).

131. M. E. Jozefowicz, A. J. Epstein, J. P. Pouget, J. G. Masters, A. Ray, and A. G. MacDiarmid, Macromolecules **25**, 5863 (1991).

132. J. Joo, Ph.D. Thesis, *Charge Localization and Delocalization Phenomena in Conducting Polymers,* The Ohio State University (1994); J. Joo, S. M. Long, J. P. Pouget, E. J. Oh, A. G. MacDiarmid, and A. J. Epstein, Phys. Rev. B **57**, 9567–9580 (1998).

133. M. Laridjani, J. P. Pouget, E. M. Scherr, A. G. MacDiarmid, M. E. Jozefowicz, and A. J. Epstein, Macromolecules **25**, 4106 (1992).

134. A. G. MacDiarmid and A. J. Epstein, Synth. Met. **65**, 103 (1994).

135. A. G. MacDiarmid, J. M. Weisinger, and A. J. Epstein, Bull. Am. Phys. Soc. **38**, 311 (1993); A. G. MacDiarmid and A. J. Epstein, Trans. 2nd Congresso Braziliero de Polimeros, Sao Paulo, Brazil, Oct. 5–8,1993, p. 544; Y. Min, A. G. MacDiarmid, and A. J. Epstein, Polym. Prepr. **35**, 231 (1994).

136. Y. Nagomi, J. P. Pouget, and T. Ishiguro, Synth. Met. **62**, 257 (1994).

137. P. A. Albouy, J. P. Pouget, J. Halim, V Enkelmann, and G. Wegner, Makromol. Chem. **193**, 853 (1992); P. Robin, J. P. Pouget, R. Comes, H. W. Gibson, and A. J. Epstein, Polymer **24**, 1558 (1983).

138. P. Pfluger, M. T. Krounbi, and G. B. Street, Phys. Rev. B **28**, 2140 (1983).

139. J. Chen and A. J. Heeger, Synth. Met. **24**, 311 (1988).

140. N. Theophilou, D. B. Swanson, A. G. MacDiarmid, A. Chakraborty, H. H. S. Javadi, R. P McCall, S. P. Treat, F. Zuo, and A. J. Epstein, Synth. Met. **28**, 35 (1988).

141. X. Q. Yang, D. B. Tanner, M. J. Rice, H. W Gibson, A. Feldblum, and A. J. Epstein, Solid State Commun. **61**, 335 (1987).

142. Y. Nogami, H. Kaneko, T. Ishiguro, A. Fakahashi, J. Tsukamoto, and N. Hosoito, Solid State Commun. **76**, 583 (1990).

143. Z. H. Wang, C. Li, E. M. Scherr, A. G. MacDiarmid, and A. J. Epstein, Phys. Rev. Lett. **66**, 1749 (1991); Z. H. Wang, E. M. Scherr, A. G. MacDiarmid, and A. J. Epstein, Phys. Rev. B **45**, 4190 (1992).

144. Y. Cao and A. J. Heeger, Synth. Met. **52**, 193 (1992).

145. P. Pfluger, U. M. Gubler, and G. B. Street, Solid State Commun. **49**, 911 (1984).

146. K. Mizoguchi, K. Misoo, K. Kume, K. Kaneto, T. Shiraishi, and K. Yoshino, Synth. Met. **18**, 195 (1987).

147. K. Kume, K. Mizuno, K. Mizoguchi, K. Nomura, Y Maniwa, J. Tanaka, M. Tanaka, and A. Watanabe, Mol. Cryst. Liq. Cryst. **83**, 285 (1982).

148. M. Onoda, Y Manda, T. Iwasa, S. Morita, T. Kawai, and K. Yoshino, Synth. Met. **41–43**, 1469 (1991).

149. H. Kaneko and T. Ishiguro, Synth. Met. **65**, 141 (1994).

150. M. Reghu, K. Vakiparta, Y. Cao, and D. Moses, Phys. Rev. B **49**, 16162 (1994).

151. A. G. Zabrodskii and K. N. Zeninova, Zh. Eksp. Teor. Fiz. **86**, 727 (1984) [Sov. Phys. JETP **59**, 425 (1984)].

152. A. I. Larkin and D. E. Khmelnitskii, Zh. Eskp. Teor. Fiz. **83**, 1140 (1982) [Sov. Phys. JETP **56**, 647 (1982)].

153. P. Lee and T. V. Ramakrishnan, Rev. Mod. Phys. **57**, 287 (1985); H. Fukuyama, in *Electron-Electron Interactions in Disordered Systems,* edited by A. L. Efros and M. Pollak (Elsevier Science Publishers, New York, 1985), p. 155.

154. D. E. Khmelnitskii and A. I. Larkin, Solid State Commun. **39**, 1069 (1981).

155. Y. Nogami, H. Kaneko, H. Ito, T. Ishiguro, T. Sasaki, N. Toyota, A. Takahashi, and J. Tsukamoto, Phys. Rev. B. **43**, 11829 (1991).

156. F. Zuo, M. Angelopoulos, A. G. MacDiarmid, and A. J. Epstein, Phys. Rev. B **36**, 3475 (1987).

157. A. B. Kaiser, C. K. Subramaniam, P. W. Gilberd, and B. Wessling, Synth. Met. **69**, 197 (1985); R. Pelster, G. Nimtz, and B. Wessling, Phys. Rev. B **49**, 12718 (1994).

158. J. Joo, S. M. Long, J. P. Pouget, E. J. Oh, A. G. MacDiarmid, and A. J. Epstein, Phys. Rev. B **57**, 9567 (1998).

159. H. Kaneko, T. Ishiguro, K. Sato, T. Hagiwara, M. Yamaura, H. Nishiyama, and H. Ishimoto, Synth. Met. **55–57**, 1102 (1993).

160. J. Joo, G. Du, A. J. Epstein, V. N. Prigodin, and J. Tsukamoto, Phys. Rev. B **52**, 8060 (1995).

161. C. R. Fincher, M. Ozaki, M. Tanaka, D. Peebles, L. Lauchlin, A. J. Heeger, and A. G. MacDiarmid, Phys. Rev. B **20**, 1589 (1979).

162. G. Leising, Phys. Rev. B **38**, 10313 (1988).

163. J. Tanaka and M. Tanaka, in *Handbook of Conducting Polymers,* edited by T. A. Skotheim (Marcel Dekkar, New York, 1986), p. 1269.

164. R. P. McCall, J. M. Ginder, J. M. Leng, H. J. Ye, S. K. Manohar, J. G. Masters, G. E. Asturias, A. G. MacDiarmid, and A. J. Epstein, Phys. Rev. B **41**, 5202 (1990).

165. J. M. Leng, R. P. McCall, K. R. Kromack, Y. Sun, S. K. Manohar, A. G. MacDiarmid, and A. J. Epstein, Phys. Rev. B **48**, 15719 (1993).

166. K. Yakushi, L. J. Lauchlan, T. C. Clarke, and G. B. Street, J. Chem. Phys. **79**, 4774 (1983).

167. G. B. Street, T. C. Clarke, M. Krounbi, K. K. Kanazawa, V. Y. Lee, P. Pfluger, J. C. Scott, and G. Weiser, Mol. Cryst. Liq. Cryst. **83**, 253 (1982); G. B. Street, T. C. Clarke, R. H. Geiss, V. Y. Lee, A. Nazzal, P. Pfluger, J. C. Scott, and G. Weiser, J. Phys. (Paris) **44**, C3-599 (1983).

168. S. Hotta, S. D. D. V Rughooputh, A. J. Heeger, and F. Wudl, Macromolecules **20**, 212 (1987).

169. M. Kobayashi, J. Chen, T. C. Chung, F. Moraes, A. J. Heeger, and F. Wudl, Synth. Met. **9**, 77 (1984).

170. K. Kaneto, K. Yoshino, and Y. Inuishi, Solid State Commun. **46**, 389 (1983).

171. T. -C. Chung, J. H. Kaufman, A. J. Heeger, and F. Wudl, Phys. Rev. B. **30**, 702 (1984).

172. M. Satoh, M. Tabata, F. Uesugi, K. Kaneto, and K. Yoshino, Synth. Met. **17**, 595 (1987).

173. D. L. Gin, J. K. Avlyanov, and A. G. MacDiarmid, Synth. Met. **66**, 169 (1994).

174. L. M. Goldenberg and P. C. Lacaze, Synth. Met. **58**, 271 (1993).

175. N. F. Colaneri, D. D. C. Bradley, R. H. Friend, P. L. Burn, A. B. Holmes, and C. W. Spangler, Phys. Rev. B **42**, 11670 (1990).

176. J. D. Stenger Smith, R. W. Lenz, and G. Wegner, Polymer **30**, 1048 (1989).

177. R. H. Friend, D. D. C. Bradley, and P. Townsend, J. Phys. D: Appl. Phys. **20**, 1367 (1987).

178. D. D. C. Bradley, A. R. Brown, P L. Burn, J. H. Burroughes, R. H. Friend, A. B. Holmes, K. D. Mackay, and R. N. Marks, Synth. Met. **41–43**, 3135 (1991).

179. K. Pichler, D. A. Halliday, D. D. C. Bradley, P. L. Burn, R. H. Friend, and A. B. Holmes, J. Phys. Condens. Matter **5**, 7155 (1993).

180. D. D. Gebler, Y. Z. Wang, J. W. Blatchford, S. W. Jessen, L. B. Lin, T. L. Gustafson, H. L. Wang, T. M. Swager, A. G. MacDiarmid, and A. J. Epstein, J. Appl. Phys. **78**, 4264 (1995).

181. S. W. Jessen, D. D. Gebler, Y. Z. Wang, J. W. Blatchford, L. B. Lin, T. L. Gustafson, H. L. Wang, T. M. Swager, A. G. MacDiarmid, and A. J. Epstein, Polym. Mater. Sci. Eng. **72**, 573 (1995).

182. M. Furukawa, K. Mizuno, A. Matsui, S. D. D. V. Rughooputh, and W. C. Walker, J. Phys. Soc. Jpn **58**, 2976 (1989).

183. U. Rauscher, H. Bassler, D. D. C. Bradley, and M. Hennecke, Phys. Rev. B **42**, 9830 (1990).

184. K. Pakbaz, C. H. Lee, A. J. Heeger, T. W. Hagler, and D. McBranch, Synth. Met. **64**, 295 (1994).

185. F. Wooten, in *Optical Properties of Solids* (Academic, New York, 1972), p. 173.

186. H. S. Woo, D. B. Tanner, N. Theophilou, and A. G. MacDiarmid, Synth. Met. **41–43**, 159 (1991).

187. S. Hasegawa, K. Kamiya, J. Tanaka, and M. Tanaka, Synth. Met. **14**, 97 (1986); J. Tanaka, S. Hasegawa, T. Miyamae, and M. Shimizu, Synth. Met. **41–43**, 1199 (1991).

188. T. Miyamae, M. Shimizu, and J. Tanaka, Bull. Chem. Soc. Jpn **67**, 40253 (1994).

189. X. Q. Yang, D. B. Tanner, A. Feldblum, H. W. Gibson, M. J. Rice, and A. J. Epstein, Mol. Cryst. Liq. Cryst. **117**, 267 (1985).

190. S. Hasegawa, K. Kamiya, J. Tanaka, and M. Tanaka, Synth. Met. **18**, 225 (1987).

191. R. P. McCall, E. M. Scherr, A. G. MacDiarmid, and A. J. Epstein, Phys. Rev. B **50**, 5094 (1994).

192. R. S. Kohlman, Ph.D. Thesis, *Optical Studies of the Metalie in Conducting Polymers*, The Ohio State University (1996).

193. R. S. Kohlman, J. Joo, Y. G. Min, A. G. MacDiarmid, and A. J. Epstein, Phys. Rev. Lett. **77**, 2766 (1996).

194. K. Lee, A. J. Heeger, and Y. Cao, Phys. Rev. B **48**, 14884 (1993).

195. Y. Xia, A. G. MacDiarmid, and A. J. Epstein, Macromolecules **27**, 7212 (1994).

196. Y. Xia, J. M. Weisinger, A. G. MacDiarmid, and A. J. Epstein, Chem. Mater. **7**, 443 (1995).

197. R. S. Kohlman, Y. Min, A. G. MacDiarmid, and A. J. Epstein, Synth. Met. **69**, 211 (1995).

198. R. S. Kohlman, T. Ishiguro, H. Kaneko, and A. J. Epstein, Synth. Met. **69**, 325 (1995).

199. K. Lee, M. Reghu, E. L. Yuh, N. S. Saricifti, and A. J. Heeger, Synth. Met. **68**, 287 (1995).

200. N. F. Mott and M. Kaveh, Adv. Phys. **34**, 329 (1985).

201. N. F. Mott, in *Localization and Interaction in Disordered Metals and Doped Semiconductors,* edited by D. M. Finlayson, Proceedings of the Thirty-First Scottish Universities Summer School in Physics of 1986 (Scottish Universities Summer School in Physics, 1986).

202. N. F. Mott, in *Localization 1990,* edited by K. A. Benedict and J. T. Chalker (Inst. of Phys. Conf. Ser. No. 108, Institute of Physics, Bristol, Philadelphia, New York, 1990). Paper presented at the Localization 1990 Conference held at the Imperial College, London.

203. D. J. Bergman and D. Stroud, in *Solid State Physics,* edited by H. Ehrenreich and D. Turnbull (Academic, New York, 1992), vol. 46, p. 148.

204. *Intrinsically Conducting Polymers: An Emerging Technology,* edited by M. Aldissi (Kluwer Academic Publishers, Boston, 1993); *Science and Applications of Conducting Polymers,* edited by W. R. Salaneck and D. T. Clark (IOP Publishing, Lofthus, Norway, 1990).

205. A. G. MacDiarmid and R. B. Kaner, *in Handbook of Conducting Polymers,* edited by T. A. Skotheim (New York, Marcel Dekker, 1986), vol. 1, p. 687; D. Naegele and R. Bittihn, Solid State Ionics **28–30**, 983 (1988); M. Maxfield, T. R. Jow, M. G. Sewchok, and L. W. Shacklette, J. Power Sources **26**, 93 (1989).

206. N. F. Colaneri and L. W. Shacklette, IEEE Trans. Instrum. Meas. **IM-41**, 291 (1992); T. Taka, Synth. Met. **41–43**, 1177 (1991).

207. J. Joo and A. J. Epstein, Appl. Phys. Lett. **65**, 2278 (1994).

208. T. Taka, Synth. Met. **41–43**, 1177 (1991).

209. J. Joo, A. G. MacDiarmid, and A. J. Epstein, Proc. Annual Technical Conf. of Plastic Engineers **2**, 1672 (1995).

210. A. J. Epstein, J. Joo, C. Y. Wu, A. Benatar, C. F. Faisst, Jr., J. Zegarski, and A. G. MacDiarmid, in *Intrinsically Conducting Polymers: An Emerging Technology,* edited by M. Aldissi (Kluwer Academic Publishers, Dordrecht, 1993), p. 165.

211. J. H. Burroughes, D. D. C. Bradley, A. R. Brown, R. N. Marks, K. Mackay, R. H. Friend, P. L. Burns, and A. B. Holmes, Nature **347**, 539 (1990); D. Braun and A. J. Heeger, Appl. Phys. Lett. **58**, 1982 (1991); P. L. Burns, A. B. Holmes, A. Kraft, D. D. C. Bradley,

A. R. Brown, R. H. Friend, and R. W. Gymer, Nature **357**, 47 (1992); D. D. C. Bradley, Synth. Met. **54**, 401 (1993); I. D. Parker, J. Appl. Phys. **75**, 1656 (1994).

212. J. Yue and A. J. Epstein, J. Chem. Soc., Chem. Commun. **21**, 1540 (1992); F. Selampinar, L. Toppare, U. Akbulut, T. Yalcin, and S. Suzer, Synth. Met. **68**, 109 (1995); and references therein.

213. S. Jasty and A. J. Epstein, Polym. Mater. Sci. Eng. **72**, 565 (1995); D. W. DeBerry, J. Electrochem. Soc. **132**, 1022 (1985); N. Ahmad and A. G. MacDiarmid, Bull. Am. Phys. Soc. **32**, 548 (1987); B. Wessling, Adv. Mater. **6**, 226 (1994); W. K. Lu, R. L. Elsenbaumer, and B. Wessling, Synth. Met. **71**, 2163 (1995).

214. G. Gustafsson, Y. Cao, G. M. Treacy, F. Klavetter, N. Colaneri, and A. J. Heeger, Nature **357**, 477 (1992).

215. Y. Z. Wang, D. D. Gebler, L. B. Lin, J. W Blatchford, S. W. Jessen, H. L. Wang, and A. J. Epstein, Appl. Phys. Lett. **68**, 894 (1996);

216. Y. Yang and A. J. Heeger, Appl. Phys. Lett. **64**, 1245 (1994); Y. Cao, G. M. Treacy, P. Smith, and A. J. Heeger, Appl. Phys. Lett. **60**, 2711 (1992).

217. A. Fizazi, J. Moulton, K. Pakbaz, S. D. D. V. Rughooputh, P. Smith, and A. J. Heeger, Phys. Rev. Lett. **64**, 2180 (1990).

218. C. O. Yoon, M. Reghu, D. Moses, A. J. Heeger, and Y. Cao, Synth. Met. **63**, 47 (1994).

219. G. Du, J. Avlyanov, C. Y. Wu, K. G. Reimer, A. Benatar, A. G. MacDiarmid, and A. J. Epstein, Synth. Met. **85**, 1339 (1997).

220. V. N. Prigodin and A. J. Epstein, Phys. B: Phys. Condens. Matter **338,** 310 (2003).

221. T. Ishiguro, H. Kaneko, Y. Nogami, H. Ishimoto, H. Nishiyama, A. Tsukamoto, A. Takahashi, M. Yamaura, T. Hagiwara, and K. Sato, Phys. Rev. Lett. **69**, 660 (1992).

222. R. S. Kohlman, A. Zibold, D. B. Tanner, G. G. Ihas, T. Ishuguro, Y. G. Min, A. G. MacDiarmid, and A. J. Epstein, Phys. Rev. Lett. **78**, 3915 (1997).

223. T. Menon, C. O. Yoon, D. Moses, and A. J. Heeger, in *Handbook of Conducting Polymers*, T. Skotheim, R. Elsenbaumer, and J. Reynolds (Eds.) (Marcel Dekker, New York, 2nd ed.) 1998, p. 27.

224. R. S. Kohlman and A. J. Epstein, in *Handbook of Conducting Polymers*, T. Skotheim, R. Elsenbaumer, and J. Reynolds (Eds.) (Marcel Dekker, New York, 2nd ed.) 1998, p. 85.

225. (a) H. H. S. Javadi, A. Chakraborty, C. Li, N. Theophilou, D. B. Swanson, A. G. MacDiarmid, and A. J. Epstein, Phys. Rev. B **43**, 2183 (1991); (b) J. Joo, Z. Oblakowski, G. Du, J. P. Pouget, E. J. Oh, J. M. Wiesinger, Y. Min, A. G. MacDiarmid, and A. J. Epstein, Phys. Rev. B **49**, 2977 (1994); (c) H. C. F. Martens, J. A. Reedijk, H. B. Brom, D. M. de Leuw, and R. Menon, Phys. Rev. B **63**, 073203 (2001).

226. Y. Z. Wang, D. D. Gebler, D. K. Fu, T. M. Swager, and A. J. Epstein, Appl. Phys. Lett. **70**, 3215 (1997).

227. Y. Z. Wang, R. G. Sun, D. K. Wang, T. M. Swager, and A. J. Epstein, Appl. Phys. Lett. **74**, 2593 (1999).

228. Z. Bao, A. Dodabalapur, and A. J. Lovinger, Appl. Phys. Lett. **69**, 4108 (1996).

229. H. E. Katz and Z. Bao, J. Phys. Chem. B **104**, 671 (2000).

230. S. Hoshino, M. Yoshida, S. Uemura, T. Kodzasa, N. Takada, T. Kamata, and K. Yase, J. Appl. Phys. **95**, 5088 (1994).

231. G. Wang, T. Hirasa, D. Moses, and A. J. Heeger, Synth. Met. **146**, 127 (2004).

232. J. Liu, N. J. Pinto, and A. G. MacDiarmid, J. Appl. Phys. **92**, 6033 (2002).

233. A. J. Epstein, F. -C. Hsu, N. -R. Chiou, and V. N. Prigodin, Curr. Appl. Phys. **2**, 339 (2002).

234. H. Okuzaki, M. Ishihara, and S. Ashizawa, Synth. Met. **137**, 947 (2003).

235. V. N. Prigodin, F. C. Hsu, Y. M. Kim, J. H. Park, O. Waldmann, and A. J. Epstein, Synth. Met. **153**, 157 (2005).

236. F. C. Hsu, V. N. Prigodin, and A. J. Epstein, Phys. Rev. B **74** (15 Nov. 2006).

237. J. Huang and R. B. Kaner, J. Am. Chem. Soc. **126**, 851 (2004).

238. X. Zhang, W. J. Goux, and S. K. Manohar, J. Am. Chem. Soc. **126**, 4502 (2004).

239. C. G. Wu and T. Bein, Science **264**, 1757 (1994).

240. C. R. Martin, Science **266**, 1961 (1994).

241. H. Qiu, M. Wan, B. Matthews, L. Dai, Macromolecules **34**, 675 (2001).

242. I. D. Norris, M. M. Shaker, F. -K. Ko, A. G. MacDiarmid, Synth. Met. **114**, 109 (2000).

243. N. R. Chiou and A. J. Epstein, Adv. Mater. **17**, 1679 (2005).

Electroluminescent Polymer Systems

Leni Akcelrud

Departamento de Quimica, Centro Politecnico da UFPR, Universidade Federal do Parana,
CP 19081, CEP 81531-990 Curitiba, Parana, Brazil

47.1 INTRODUCTION

Organic polymers that emit light on the imposition of an electric field have commanded increasing attention in the last decade both for their scientific interest and as potential materials for electrooptical and optoelectronic applications. A number of reviews on electroluminescent polymers focusing the basic physics [1–5], synthesis and properties [6,7], device operation and materials [8–11], design and synthesis [12] blue emitting structures [13] have been published. Some books are also out on the subject [14–18].

Apart from intrinsic electronic features, the color emitted by small organic molecules depends on microenvironment characteristics, such as their location in the device and medium polarity. When attached to a polymer chain, the mobility of the chromophore is restricted in all directions, and the emission becomes dependent on the structural features of the macromolecule (including the molecule's architecture, such as regioregularity, location and distribution of chromophores, etc.). This restriction opened a new avenue in the development of electroluminescent polymers: color tuning could be achieved by introducing variations in the polymeric structure, since in doing so the energy gap of the $\pi-\pi^*$ transition responsible for the color emitted is changed, and a broad range of colors can be achieved with one polymer. It may be noted that both low and high molecular weight organic EL materials are now under wide study. The perceived advantages of the former include the possibility of a definitive chemical structure, chemical purification at high purity levels by sublimation, and facile manufacture of complex 3D architectures, while polymers are favored for their mechanical properties, principally the ready formation of robust films and their processibility using easily accessible technology for simple device architectures. The two classes of materials are not infrequently used together in multicomponent chromophoric layers. A typical design of a polymer LED is shown in Fig. 47.1. More elaborate architectures may vary from this basic scheme, and may involve the use of a multicomponent chromophore and one or more transport layers (see below). Recent advances include microfabrication of diode-pixel arrays [19], patterned light emission with sizes of the order of 0.8 mm [20], polarized EL based on stretch or, rub aligned Langmuir-Blodgett deposited polymers, or specifically synthesized liquid crystal polymers [21–27]. The application of ultrathin and selfassembling films is an important development in LED technology. In this case the film in the device is not cast using a traditional processing technique such as spin coating, but using electrostatic layer-by-
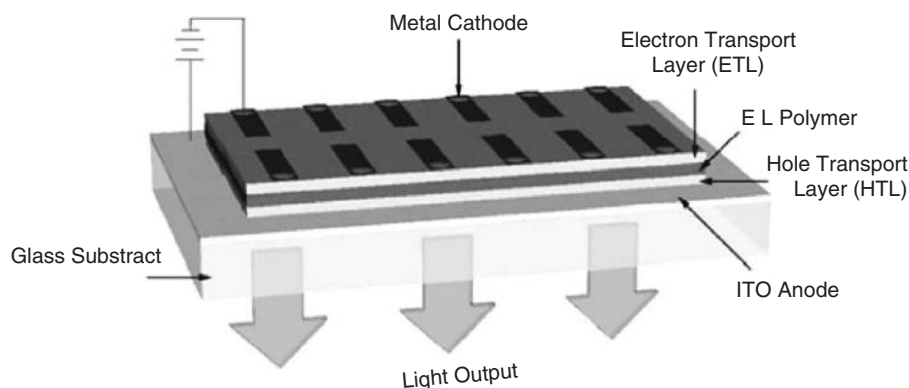
FIGURE 47.1. Design of a polymer LED showing optional HTL and ETL.

layer selfassembly methodologies [28–31]. This means that recent advances in the molecular level processing of conducting polymers have made it possible to fabricate thin film multilayer heterostructures with a high degree of control over the structural features and thickness of the deposited layers. As the dimensions of the individual layers approach molecular scales it may be possible to approach quantum effects in these multilayer contacts. Further progress is represented by the development of surface light-emitting devices (SLEDS), in which both anode and cathode lay underneath the electroluminescent layer, so that no transparent materials are required in the LED construction. These SLEDS were microfabricated using conventional silicon processing [32]. The patterning of light-emitting layers is the most important step in the manufacturing of multicolor organic electroluminescent devices, and should combine large area coatings with device patterning. One very promising methodology employs an ink jet patterning process [33–35]. Light emission of poly [3-(2-benzotriazolo)ethylthiophene] has been investigated by the cathodoluminescence (CL) spectroscopy. An electron beam was used to inject directly electrons and holes in the polymer. The introduction of benzotriazole, an electron-withdrawing moiety, to the thiophene was done to enhance electronic affinity [36].

47.2 LIGHT EMITTING DEVICES AND MECHANISM FOR LIGHT EMISSION

Light-emitting devices as shown in Fig. 47.1 can be operated in a continuous DC or AC mode. They behave like a rectifier, the forward bias corresponding to a positive voltage on the ITO electrode and are also called light-emitting diodes in analogy to p–n junction devices. Light emission is transmitted from the transparent side normal to the plane of the device. The polymer layer is usually deposited by spin coating, but dipping techniques can also be used. The cathode injects electrons in the conduction band of the polymer (π^* state), which corresponds to the lowest unoccupied molecular orbital (LUMO), and the anode injects holes in the valence band (π state), which corresponds to the highest occupied molecular orbital (HOMO). The injected charges (polarons) can travel from one electrode to the other, be

annihilated by any specific process such as multiphonon emission, Auger processes, or surface recombination. These concepts have been extensively studied in inorganic systems and may also apply to polymer systems. A simplified description involves the formation of a neutral species, called an exciton, through the combination of electrons and holes. The exciton can be in the singlet or triplet state according to spin statistics. Because only singlets can decay radiatively, and there is only one singlet for each three triplet states, the maximum quantum efficiency (photons emitted per electron injected) attainable with fluorescent polymers is theoretically 25%. This limit can be overcome by using phosphorescent materials that can generate emission from both singlet and triplet excitons [37]. As a result, the internal quantum efficiency can reach 100%. Forrest *et al.* [38] reported highly efficient phosphorescent LEDs by doping an organic matrix with heavy atoms containing phosphorus. Polymer devices were also fabricated by using polyfluorene [39] or poly(vinyl carbazole) [40] as the host for the phosphorescent dye. The singlet exciton decay time is typically in the ns timescale, whereas the triplet survives for up to 1 ms at low temperatures [41]. A major fact determining the internal quantum yield for luminescence (ratio of radiative to nonradiative processes) is the competition between radiative and nonradiative decays of the electron–hole pairs created within the polymer layer. These pairs can migrate along the chains and are therefore susceptible to trapping at quenching sites where nonradiative processes may occur. The sequence of charge processes leading to exciton formation is charge injection, transport, and recombination. These processes are difficult to separate on the basis of the device electrical characteristics, and the transport mechanism affects the other two. Two modes of injection mechanisms have been discussed for the operation of LEDs: thermoionic emission over a Schottky-like contact, and tunneling into the transport bands. Theoretical modeling of charge injection has been attempted by several approaches [42–48].

47.2.1 Interchain Excitons

In LEDs the polymers are thin films, leading to the possibility of electronic interactions between neighboring

chains and the creation of new excited state species. This topic has been the subject of many recent investigations [49–52] mainly related to PPV [53,54], PPV derivatives such as poly(2-methoxy-1,4-PPV), MEH-PPV [55–60], CN-PPV [51,55,61], poly(p-pyridyl vinylene) [59,62], acetoxy PPV [63], and other light-emitting polymers [49,64–68], showing good evidence to suggest that interchain excitations play a significant role. The importance of these interchain excitations continues to be one of debate: if they are nonemissive, then they are detrimental to device operation, but if they are emissive, they can be used effectively [69]. The final morphology has a direct effect on the performance of MEH-PPV based LEDs. Higher degrees of interchain interactions enhance the mobility of charge carriers at the expense of lower quantum efficiencies for EL. The reduction in efficiency in well-packed regions is attributed to rapid formation of nonemissive interchain species without the involvement of ground state dimers or aggregates [60,70].

47.2.2 Transport Layers

Single layer device architecture is typically employed and is appropriate for evaluation of new polymer chromophores and for measurements of their EL and PL spectra. In the simplest cases the two spectra are quantitatively identical, although in numerous cases their noncoincidence reveals a more complicated exciton formation and decay related to the differing modes of energy input. In devices which are intended to maximize photonic output and efficiency, however, it is established practice to employ additional layers of organic material (polymeric or low molecular weight) interspersed between chromophore film and the electrodes using materials chosen for their functional ability to facilitate charge transport and block (localize) carriers, avoiding their crossing the device without recombination. Usually the carriers do not form junctions with identical (or zero) barrier heights and therefore one carrier will be preferentially injected. If the two junction barriers are not identical, higher electric fields would be required near the junction with the greater barrier energy in order to equalize the injected current density from each contact [71]. The LED efficiency is also reduced if the excitons are formed at the interface of the polymer and the electrode, lowering the carrier injection. This location is also where the greatest number of defects is expected and can act as quenching sites [72,73]. The transport layer also decreases exciton quenching near the metal electrode by acting as spacer separating the metallic contact from the active luminescent layer. To confine holes in the emissive layer an electron-conducting-hole blocking layer should be used (electron transport layer, ETL). Its valence band should be lower in energy than the EL layer and its electron affinity should be equal to or greater than the EL layer. In this way holes are confined between the emissive layer and the ETL, and the space charge formed provides a higher electric field across

the interface with a more uniform distribution of charge, thus improving the balance between carriers. The same reasoning is valid for the use of hole transport layers (HTL). The use of transport materials represents an improvement in device stability since it makes it possible in certain cases to change from a lower work function ϕ_w metal electrode as calcium ($\phi_w = 2.9$ eV) which is unstable in atmospheric conditions to a higher work function material as aluminum ($\phi_w = 4.3$ eV), and adds it directly to the emitting polymer. Materials for ETL are electron deficient and the most used are oxadiazole compounds in the ''free'' form as PBD or grafted to a polymer main chain. Apart from PPV, a variety of electron-accepting polymers such as poly(vinyl carbazole) (PVK) [74,75], poly(pyridine-2,5-diyl), poly(1,10-phenanthroline-3-diyl), or poly(4,40-disubstituted-2,20-bithiazole-5,50-diyl) have been used as HTL materials. The incorporation of the transport/blocking material can also be made directly by blending them with the emissive material [76], as in the case of the green emitter poly(2-cholestanoxy-5-hexyldimethylsylyl-1,4-phenylene vinylene) (CCSPPV). With the combination of PVK as HTL and PBD as ETL it was possible to achieve internal quantum efficiency in excess of 4%. Several p-doped conjugated polymers have been used as hole injecting electrodes, like polypyrrole, polythiophene derivatives, and polyaniline [77–82], which have high work functions, providing low barriers for hole injection. There are reports of stable operation over long times for devices using polymeric dopants, which are expected to be relatively immobile. These include polystyrenesulfonic acid used to dope poly(dioxyethylene thienylene) (PEDOT) [3].

47.3 PPV AND PPV-TYPE STRUCTURES

47.3.1 Precursor Routes

47.3.1.1 The Wessling method

Like most highly conjugated materials, semiconducting polymers show poor solubility in organic solvents. Structural changes have been made to overcome this difficulty. The first highly structured electroluminescent polymer, PPV, a green-yellow emitter, was prepared via a precursor route because its insolubility in poly reactions resulted in only oligomeric materials. The precursor route involves the preparation of a soluble polymer intermediate that is cast in the appropriate substrate and after thermal treatment is converted to the final product *in situ*. This involves producing a polymer in which the arylene units are connected by ethylene units. The saturated units in the precursor contain a group which not only solubilizes the macromolecule and allows for processing, but also acts as a leaving group, thus affording the unsaturated vinylene units of a fully conjugated polymer. One of the most important soluble precursor routes to PPV was developed by Wessling and co-workers in the 1960s [83,84] based upon aqueous solvent synthesis
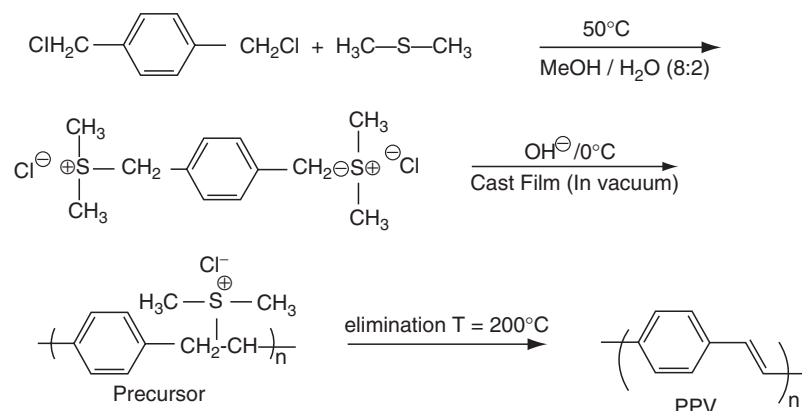
FIGURE 47.2. The sulfonium precursor route (Wessling) to PPV.

of poly(*p*-xylylene-a-dialkylsulfonium halides) from α-α'-bis(dialkylsulfonium salts), followed by thermolytic formation of the final conjugated polymer, as shown in Fig. 47.2. The charged sulfonium groups solubilize the polymer and are removed during the conversion step. The mechanism is believed to proceed according to a chain growth polymerization via the *in situ* generation of the monomer, a *p*-quinomethane-like intermediate [85,86], based on the facts that high molecular weight is formed very quickly, within the first minutes of the reaction and also that various radical inhibitors limit or prevent formation of long polyelectrolyte chains. However, the initiation process was not unequivocally identified [87–91]. Figure 47.3 depicts the radical chain mechanism for PPV synthesis [92]. A modified Wessling route where the solubilizing and leaving group is an alkoxy group has been developed and gives methoxyprecursor polymers, which are soluble in polar aprotic solvents such as chloroform, dichloromethane, and tetrahydrofurane [93,94]. The generation of precursor copolymers containing randomly placed methoxy and acetate groups (which are expected to be more labile to elimination) was an approach

used to prepare poly(2,5-dimethoxy-*p*-phenylene vinylene) (DMPPV) of controlled conjugation length [95,96]. A soluble PPV derivative which could be used directly without a second step treatment was a natural development since it would simplify device fabrication and at the same time allow for less imperfections in the final structure since the conversion process inevitably introduces defects (chemical, morphological, etc.) into the chain with the result that there is a distribution of effective conjugation lengths and these are far shorter than the nominal degree of polymerization. In fact, the different precursor polymers discussed above all give PPV, but the structural and hence electronic properties can vary quite dramatically depending on which precursor polymer was utilized [97]. Derivatization of PPV with long alkyl and/or alkoxy ramifications (RPPV, ROPPV) was the first approach for the obtainment of soluble electroluminescent polymers. The solubility by derivatization is due to the lowering of the interchain interactions, which should not in principle change the rigid rod-like character of the main chains. A variety of PPV derivatives can be obtained from *p*-xylylenes by analogous routes used to obtain PPV. A wide
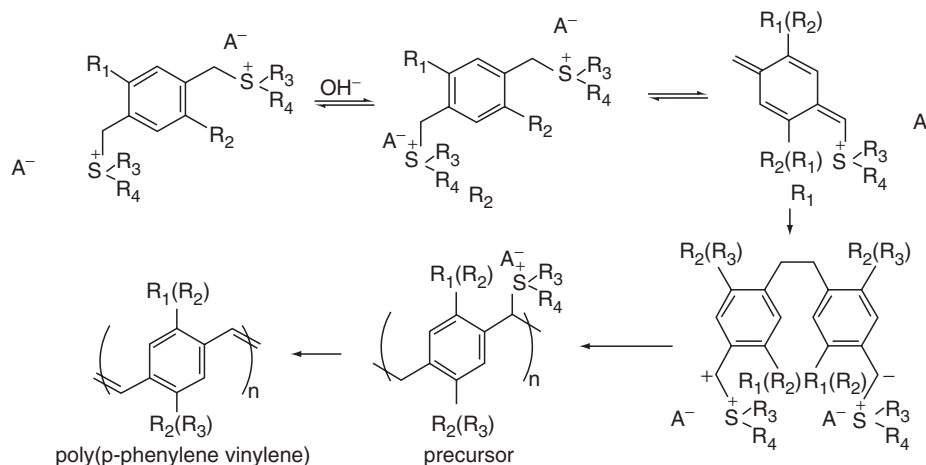
FIGURE 47.3. Mechanistic processes for the sulfonium precursor synthesis of poly(phenylene vinylene)s, showing the ylide, the xylylene, and the poly(*p*-xylylene-a-dialkylsulfonium halide) (PXD). Substituents X and Y can be alkyl, alkoxy, and aryl groups. Reprinted with permission from Synthesis, properties of poly(phenylene vinylene)s, related poly (arylene vinylene)s. 1998. p. 61. chapter 3. © 1998 Marcel Dekker, Inc.

variety of substituents are tolerated by the soluble sulfonium precursor route affording alkoxy [98–102], alkyl [103,104], alkyl and aryl [105] substituted PPVs. Attachment of alkoxy side chains to the polymer backbone lowers the optical bandgap of most polymers, thereby playing an important role in the color tuning of the polymeric materials. The solid-state properties (color, absorption, emission, fluorescence quantum yield, photoconductivity, etc.) of these polymers were found to be greatly dependent on the number, length position, and geometry of the grafted alkoxy side chains [106].

Substituted PPVs are soluble in organic solvents, which is a very useful feature in the preparation of polymer LEDs. One of the first PPV soluble derivatives, prepared by the Santa Barbara group in California via the precursor route, was methoxy-ethylhexyloxy PPV (MEH-PPV), which emitted a red-orange color [107,108]. Subsequently another PPV derivative with the bulky cholestanoxy group was prepared, namely the poly [2,5-bis(3a-5b cholestanoxy)-1,4-phenylene vinylene] (BCHAPPV). A blue shift was observed in relation to MEH-PPV; BCHA-PPV emitted in the yellow region [109,110].

47.3.1.2. The chlorine precursor route

An important soluble precursor route for PPV and related polymers involves the polymerization of 1,4-bis(chloromethyl or bromomethyl) arenes by treatment with potassium-*t*-butoxide in nonhydroxylic solvents like tetrahydrofuran. This methodology was first used by Gilch and Wheelright [111] as one of the most successful early PPV synthesis.

Hoerhold and co-workers elaborated fairly extensively on this method and recently applied it to synthesis of PPVs with large solubilizing groups on the aryl ring such as cholestanoxy (Fig. 47.4(a)), high molecular weight, highly phenylated PPVs [112–118] such as the diphenyl-4-biphenyl ring substituted PPV which showed green EL [119], poly(2,3-diphenyl-1,4-phenylene vinylene) (DP-PPV) [115, 120–122] (Fig. 47.4(b)). Without the presence of solubilizing side chains on the arene ring, premature precipitation can occur, but otherwise the method has the advantage of producing a precursor that is soluble in organic nonhydroxylic solvents, and therefore useful for electronic applications that require processing. The chlorine precursor route has been also applied to the synthesis of the extensively explored poly(2-methoxy 5-(2-ethyl hexyloxy polyphenylene vinylene) (MEH-PPV). A plausible source of defects in the precursor routes resides in the remaining saturated linkages between aromatic links, which can lead to localized traps via hydrogen abstraction, causing premature device decay. The regiochemical randomness associated with the Wessling based routes [123–126] is an important point, since it affects the solid-state morphology and electronic states connected with molecular architecture. In another variation of the Wessling route, nonionic sulfinyl groups in the ethylene moiety are the leaving groups [127,128]. In addition to the substituted aryl rings that can be incorporated in PPVs by the soluble precursor routes, it is also possible to use other aryl rings, like condensed ones, as long as they are derivable from *p*-xylylenes or their monocyclic analogs. The obtainment of PPVs with aryl or alkyl substituents at the phenylene or vinylene group of PPV can also be accomplished by the
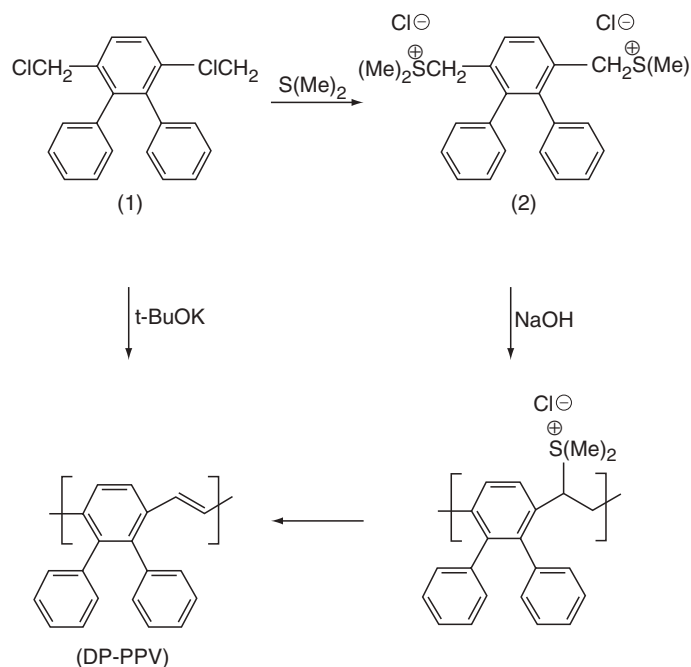
FIGURE 47.4. The dehydrohalogenation route to PPV derivatives illustrated in the synthesis of poly(2,3-diphenyl-1,4-phenylene vinylene) (DP-PPV) poly(1-methoxy-4-(2-ethylhexyloxy)-*p*-phenylene vinylene) (MEH-PPV).

palladium catalyzed coupling of dihalogenoarenes and ethylene [129]. It is a general trend that when electron donating alkoxy groups are attached to phenylene rings of PPV the bandgap is reduced and the wavelength of the emitted light shifts to red from the green region [104,107,110,130,131]. RO-PPVs where the alkoxy RO– length varied from C5 to C12 showed increasing EL intensity with increasing side chain length. This was attributed to the reductions of non-radiative decay processes due to preventing migration of excitons to traps. Apart from electronic effects, intermacro-molecular packing is a major factor in determining emission color and photoluminescence efficiency (PLeff). Since this quantity is a key factor in LED efficiency (along with balanced charge injection and carrier mobility as seen above), steric effects are important in the design of EL polymers. Figure 47.5 shows the influence of side groups on the emission characteristics of some important PPV derivatives [132]. As a general trend close packing as in BEH-PPV (due to its lateral symmetry) results in reduced PLeff, whereas polymers bearing bulky side groups show increased PLeff, as BCHA-PPV, despite the symmetry which gives higher order in the polymer films. Devices using poly(2,3-diphenyl-1,4-pheny-lenevinylene) derivatives containing long branched alkoxy chains or fluorenyl substituents with the configuration

of ITO/PEDOT/polymer /Ca/Al exhibited a low turn-on voltage (4.0 V), a very high external quantum efficiency (3.39 cd/A), and the highest brightness found in this survey (16,910 cd/m^2) [133].

Recently, a new synthetic route toward PPV and its derivatives has been reported in which the monomer is polymerized toward a dithiocarbamate precursor polymer by the addition of a strong base. The corresponding conjugated polymer is obtained via a heart treatment of the precursor polymer. This dithiocarbamate precursor route represents a compromise between several straightforward but sometimes troublesome precursor routes and the more complex sulfinyl precursor route [134].

A natural development was the introduction of hole and/or electron transporting groups in EL polymers aiming the improvement of injection/transporting properties as in the case of the incorporation of triphenyl amine and cyano groups in MEH-PPV [135,136]. Recent advances in PPV-related structures include soluble PPV derivatives containing pyrene [137] or perylene [138] dyes in the main and C60 grafted units [139].

Energy migration from a large bandgap polymer to another with lower bandgap is possible when the absorption of the latter overlaps with the emission of the former to a certain
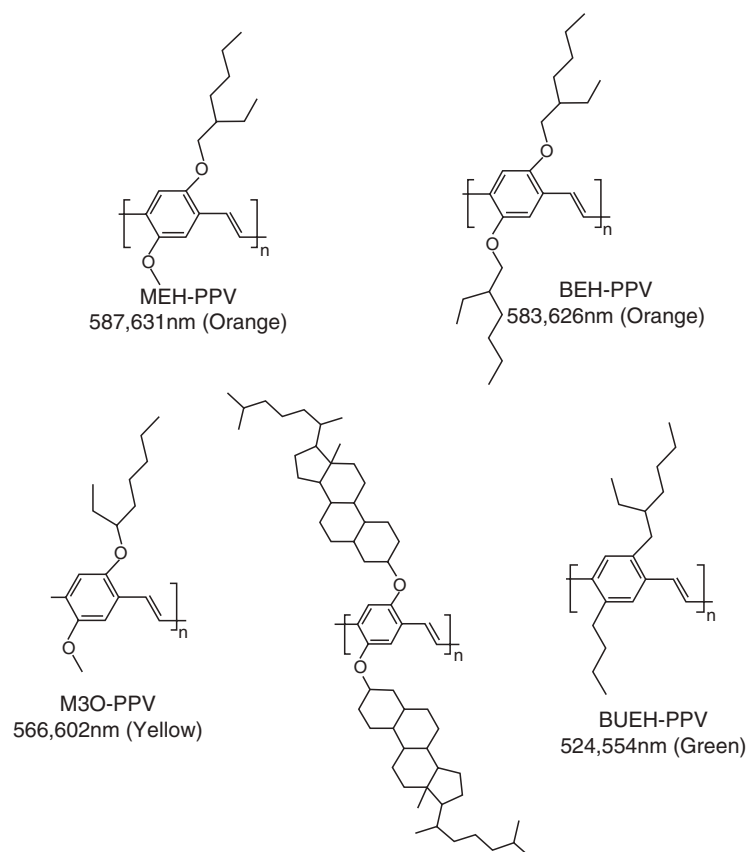
FIGURE 47.5. Influence of side groups on the emission properties of some important PPV derivatives. Reprinted with permission from Synth Met 1997;85(1–3):1275. © 1997 Elsevier Science.

extent, and the result is an enhancement of the lower bandgap emission. The dynamics of the excitation transfer process, measured in the ps timescale using an ultrafast Ti/sapphire laser, indicate that the energy transfer was completed in 10 ps when *m*-EHOP-PPV (poly [2-(*m*-2′-ethylhexoxyphenyl)-1,4-phenylene vinylene]) was used as the host with BCHA-PPV (poly[2,5-bis(cholestanoxy)-1,4-phenylene vinylene]) and BEH-PPV (poly[2,5-bis(2′-phenylene vinylene]) as the guests [140]. Mixtures of poly(2-methoxy-5-(2-ethylhexy-loxy-1,4-phenylenevinylene) (MEH-PPV) which emits at 600 nm (yellow-orange) with poly [1,3-propanedioxy-1,4-phenylene-1,2-ethenylene(2,5-bis(bimethylsylyl)-1, 4-phenylene)-1,2-ethenylene-1,4-phenylene]) a conjugated–nonconjugated block copolymer, DSiPV which emits at 450 nm (blue), yielded only the large wavelength emission. By varying the ratio DSiPV/MEH-PPV from 9:1 to 1:15 the relative quantum efficiency increased by a factor of 500. This was attributed not only to energy migration of the excitons from DSiPV to MEH-PPV but also to a dilution factor. As the EL active MEH-PPV is diluted by DSiPV, the intermolecular nonradiative decay is diminished by blocking of the charge carriers [141].

47.4 CONJUGATION CONFINEMENT

47.4.1 Conjugated–Nonconjugated Block Copolymers

So far we have seen that introducing substituents in the PPV molecule leads to various EL polymers, emitting in various regions of the visible spectrum according to their chemical structures. A theoretical study of the effects of derivatization can be found in reference [142]. From the red shift of the peaks in PL found with increasing chain length, the effective conjugation length for long chain precursor route samples of PPV are theoretically estimated to be 10–17 repeat units [143]. However, experimental work with oligomeric models led to the conclusion that the effective conjugation length of the solid polymer is not larger than 7–10 units [144]. Thus fully conjugated polymers may have chromophores with different energy gaps because the effective length of conjugation is statistically distributed. However, in the mixture, the chromophores with lower energy gaps will be the emitting species because of energy transfer. To solve this problem several approaches have been developed. The confinement of the conjugation into a well-defined length of the chain is one of the most successful strategies developed so far. Illustrative examples of EL structures exploring the concept of conjugation confinement are shown in Fig. 47.6 [145–147]. Copolymers in which a well-defined emitting unit is intercalated with nonemitting blocks have demonstrated that the emitted color was not affected by the length of the inert spacers but the EL efficiency of the single layer LEDs fabricated with the copolymers was a function of the length of the nonconjugated blocks; copolymers with longer spacers yielded higher efficiency devices [148]. Those conjugated–nonconjugated co-

polymers (CNCPs) are soluble, homogeneous in terms of conjugation length, and can be designed to emit in any of the visible spectrum [148–151]. In such structures energy transfer from high bandgap to lower bandgap sequences in which excitons may be partially confined will provide higher luminescence efficiency when compared to similar structures of uniform conjugation [152]. In soluble poly(dialkoxy-*p*-phenylene vinylene)s, the systematic variation on the degree of conjugation showed that PL and EL increased with the fraction of nonconjugated units. At the same time, confinement of the effective conjugation has proved to be an efficient means for blue shifting the spectrum because the conjugated emitters can allow charge carriers to form but not to diffuse along the chain, thus limiting the transport to quenching sites [153,154]. This electronic localization results in a large π–π* bandgap which decreases with conjugation length [155]. A widely used route to CNCPs involves the Wittig type coupling of dialdehydes with bis(phosphoranylidene)s [156,157]. A series of CNCPs was prepared, varying the $-O(CH2)_nO-$ spacer length, and chromophore's structure (PPV type) and length allowing to correlate conjugation length with emission color and device efficiency [148–151]. Changing the aromatic ring from a *p*-phenylene to a *p*-thienylene residue caused bandgap shifts in which the emission changed from blue to yellow [150,158, 159]. The introduction of nonconjugated segments not only confines the π electrons in the conjugated part but also imparts solubility and improves the homogeneity of the films. The Wittig route (as with other condensation routes) does not lead to high molecular weight polymers because these become insoluble after a certain degree of polymerization is reached. In CNCPs the solubility provided by the spacer permits the obtainment of high molecular weight materials. Conjugation confinement can also be achieved by tailoring the polymer structure in other ways, like inserting kink (*ortho* and *meta*) linkages or imposing steric distortions. Alkoxy substituted PPVs usually carry the alkoxy groups at the 2,5-positions in the ring and are red shifted in relation to unsubstituted PPV. By placing these substituents at the 2,3-positions and the ring in a *meta*-configuration it was possible to obtain blue emitting alkoxy PPVs [160]. Efficient blue-green polymer light-emitting diodes were prepared with block copolymers composed of the fluorescent segments, 1,4-di[2-(1-naphthyl)vinyl] benzene or 2, 5-dimethyloxy-1,4-di[2-(1-naphthyl)vinyl] benzene and the flexible segments, tri(ethylene oxide) [161]. A new type of cyclolinear polymer, poly(phenylene vinylene-*alt*-cyclotri-phosphazene), was synthesized through Heck-type coupling reaction. Apart from controlling the conjugation length and solubility, the nonemitting cyclophosphazene rings were capable of accommodating a wide variety of substituents with minimal effect on the electronic properties [162].

47.4.2 Chromophores as Side Groups

An extension of the concept of CNCPs is the attachment of the fluorofore as a pendant group to a nonemitting
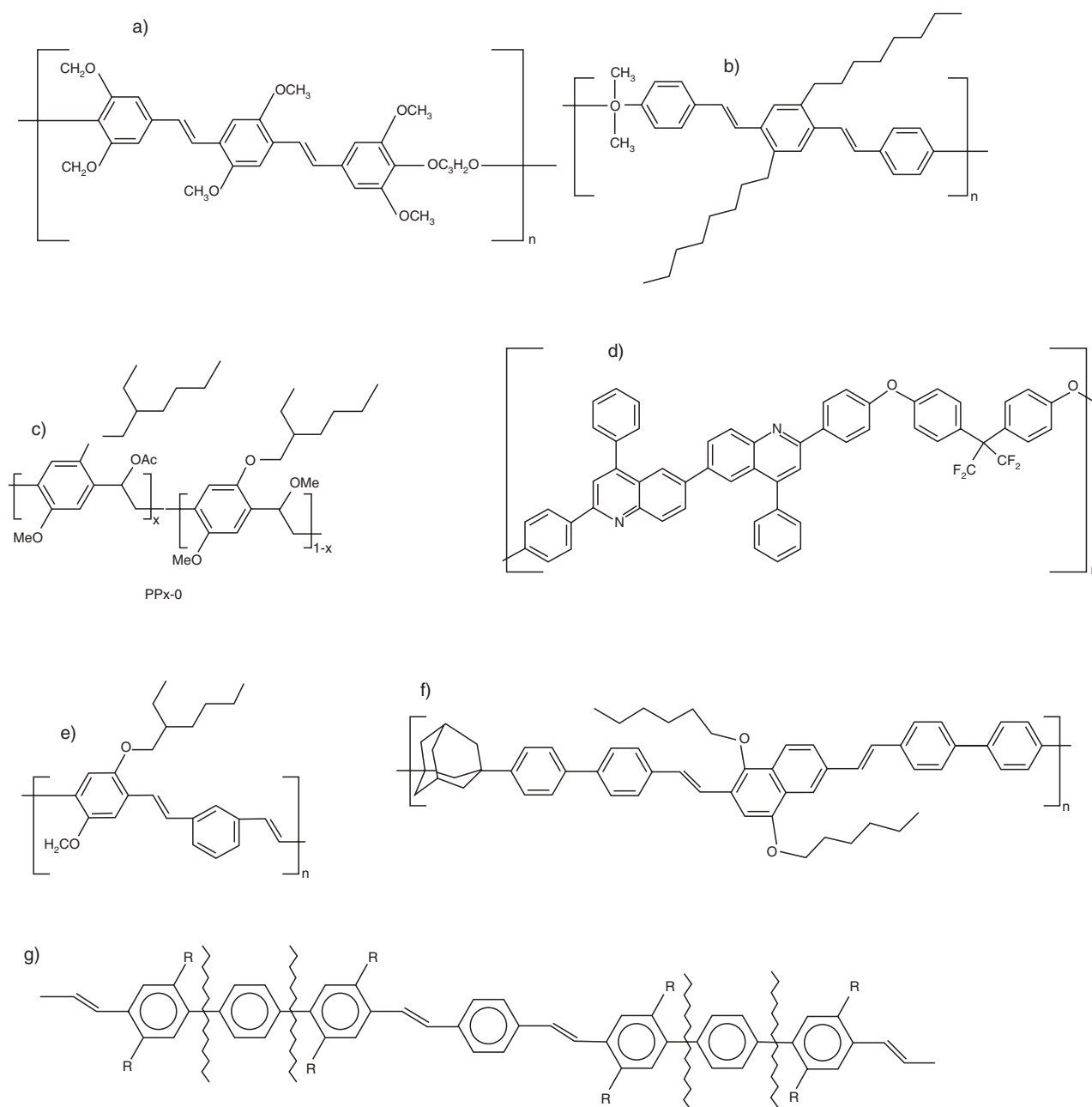
FIGURE 47.6. Examples of EL polymers exploring the concept of conjugation confinement. (a) An aliphatic spacer separating PPV type blocks; (b) dimethylsilane groups separating PPV type blocks; (c) partially eliminated MEH-PPV; (d) hexafluoroisopropylidene nonconjugated segment separating polyquinoline emitting units; (e) kink (*meta*-) linkages in MEH-PPV; (f) adamantane moiety as spacer; (g) the planarity is interrupted by the twisted *p*-phenylene groups, schematically illustrated with the wiggled lines.

random coil polymer. This idea should in principle present several advantages: the synthetic route would be simpler than that used for main-chain polymers, the solubility would be dominated by the nature of the backbone, the emission wavelength would be predetermined, and crystallization of the chromophore with concomitant degradation of the diode (in comparison with small molecular weight sublimable systems) would be prevented. In addition, an electroluminescent group could be placed on every repeat unit or in a controlled frequency along the backbone. Some

representative EL structures with emitting pendant groups are shown in Fig. 47.7. Using polystyrene as the main chain, stilbene groups were attached to every repeat unit, in every other repeating unit, or in every third repeat unit (Fig. 47.7(a)) [64,163,164], resulting in blue emitting polymers. Grafting anthracene derivatives (2,3,7,8-tetramethoxy-9,10-dibutyl anthracene) (Fig. 47.7(b)) and *N*-methyl naphthalimide (Fig. 47.7(c)) gave blue and green PMMA based light emitting materials. Charge transfer and emission from associated forms (ground state dimers or excimers) are common
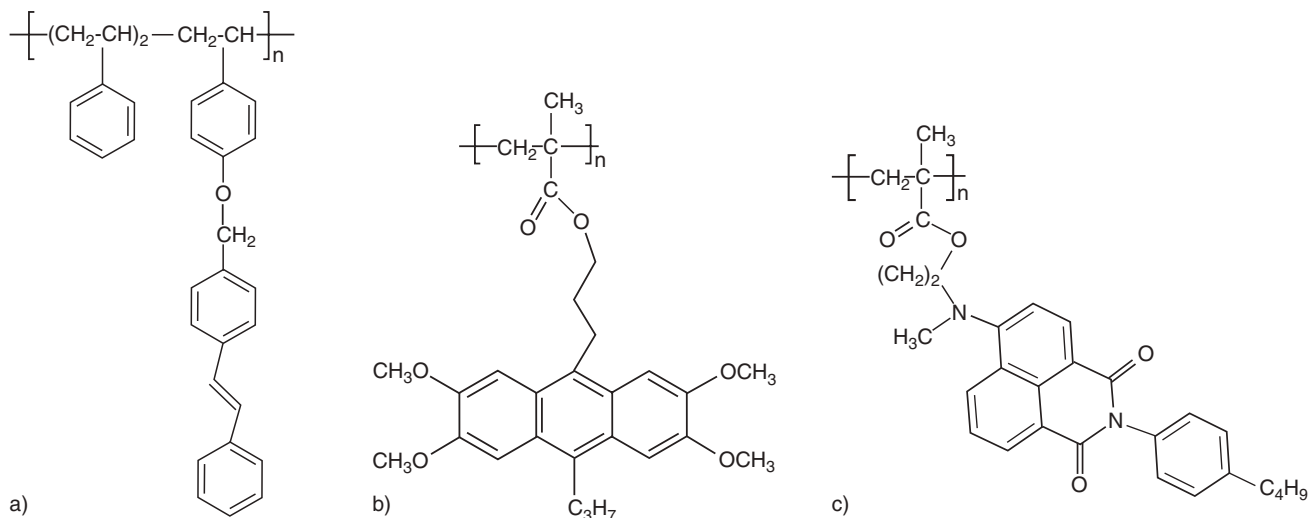
FIGURE 47.7. Examples of EL polymers with emitting pendant groups. (a) Stilbene chromophores linked to a polystyrene backbone; (b) anthracene derivatives linked to a poly(methyl methacrylate) backbone; (c) naphthalimide based chromophore as side chain in poly(methyl methacrylate).

events in pendant chromophore structures. Examples include the pyrene excimer emission only of polysiloxanes bearing a pyrene group in each mer and the suppression of carbazole emission of copolymers containing carbazole and pyrene attached to a polysiloxane backbone or carbazole and fluoranthene attached to a PMMA main chain [165]. PPV has also been used as a backbone for grafting of lumophores, giving rise to a structure with more than one simultaneously emitting center, like PPV containing the electron accepting trifluoromethyl stilbene moiety. This group emits in the violet, but the substituted PPV showed only the PPV characteristic emission, due to energy transfer [166]. The concept of pendant chromophores has been also explored to afford better transport properties, by covalently attaching charge transport groups to the emitting polymer. The hole transporting carbazole and the electron transporting 2-(4-biphenyl)-5-(4-*t*-butylphenyl)-1,3,4-oxadiazole) (PBD) were placed as side groups in each mer of PPV. A slight interaction between the π-electrons of the PPV backbone and those of the pendant groups was detected. Also, blue-shifted absorptions indicated that steric effects partially disrupted the conjugation in PPV; the copolymers showed overlapped emissions of the main chain and the side groups. The direct PBD attachment to PPV improved the EL efficiency to a great extent, but the carbazole insertion resulted in an increased imbalance in carrier transport, since PPV itself accepts and transports holes more readily than electrons [167,168]. Apart from designing a molecule capable of emitting light in a defined region of the visible spectrum, a very interesting approach is to design structures that can emit light over a broad spectral range so that the color emitted is white or close to it. With this objective polymers carrying more than one chromophore were prepared like a ring anthracenyl substituted PPV [169]. An

interesting blend was prepared using a side chain copolymer with pendant perylene groups and carrier transporting copolymers, in which hole and electron transporting units were incorporated in the same chain [170].

47.5 POLYTHIOPHENES

Among various polymers for LED fabrication poly(3-alkylthiophene) (PAT) [171] has stimulated much interest because it was the first soluble and even fusible conducting polymer, and it demonstrated novel characteristics such thermochromism [172] and solvatochromism [173]. EL in these materials was first reported by Ohmori [174,175] and it is now possible to tune the emission of substituted polythiophenes from ultraviolet to IR by changing the substituent [176]. LEDs made with PAT emitted a red orange color [177] peaking at 640 nm. For the series in which the side chain is an aliphatic branch of 12, 18, or 22 carbons the EL intensity increased linearly, the latter (22 carbons) being five times brighter than the former (12 carbons). This was explained in terms of confinement of carriers on the main chain where longer substitutions accounted for greater interchain distance decreasing the probability for quenching [165,178]. The emission intensity of PAT-based LEDs increases with increasing temperature (20–80°C) contrary to inorganic GaAs and InGaP semiconductor diodes [179]. This was explained in terms of changes in effective conjugation length with temperature due to changes in the main chain conformation which decreased the nonradiative recombination probability. Some representative polythiophene structures are shown in Fig. 47.8. Polythiophene and substituted polythiophenes can be prepared by chemical or electrochemical routes [180]. The eletrochemical method
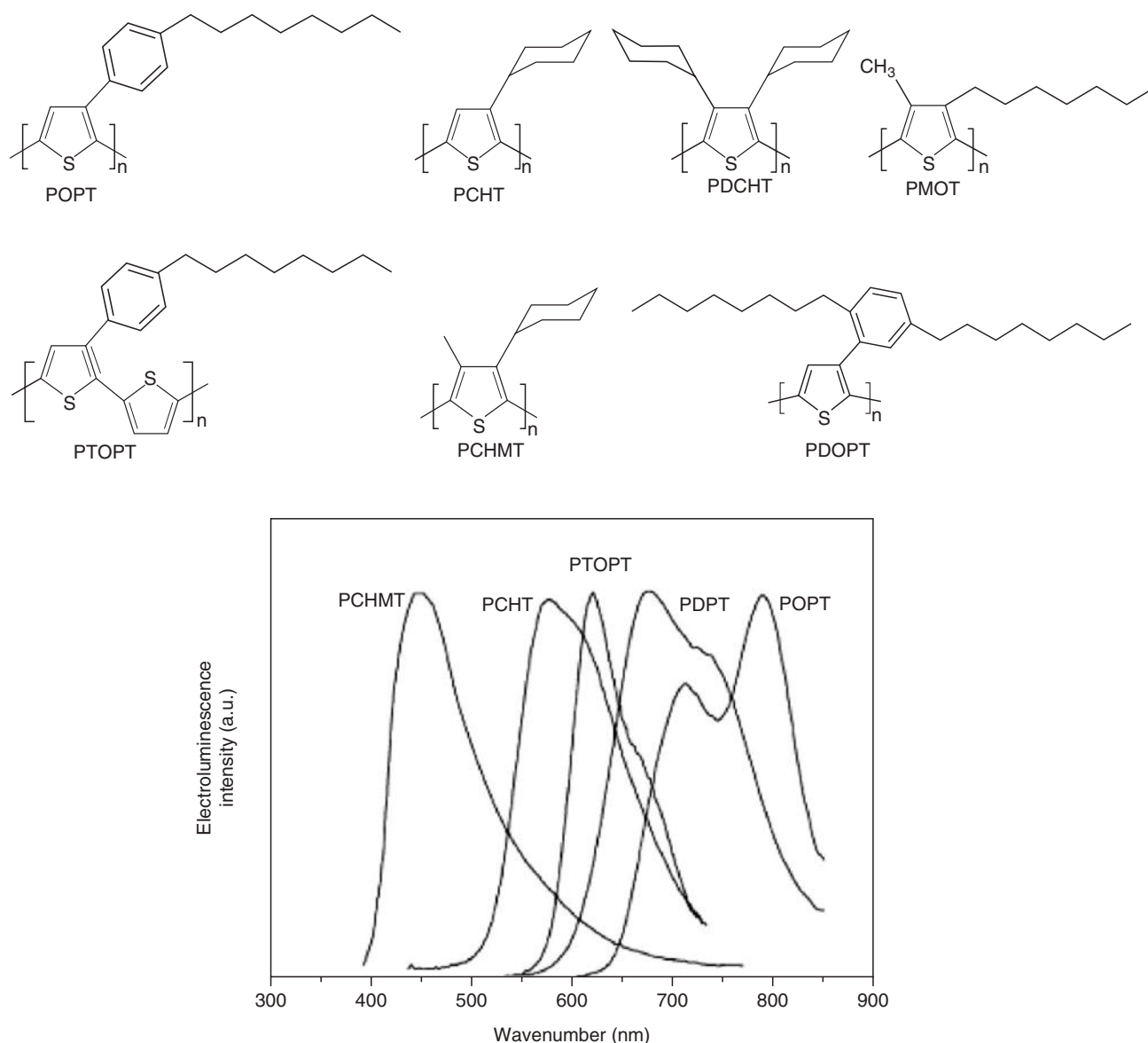
FIGURE 47.8. Effect of substitution on the emitting properties of polythiophenes. POPT* and POPT** are different forms of the same polymer, due to thermal treatment.

gives crosslinked materials, and chemical synthesis is most straightforward, in the iron chloride oxidative polymerization route. A particular point in this aspect is that of obtaining regioregular polymers, since regioregularity strongly influences the optical and transport properties of polythiophenes [181]. The dihedral angle and thus the p-orbital overlap between adjacent thiophene rings along the polymer backbone determine the conjugation length along the polymer chain. Short conjugation gives a blue-shifted emission and long conjugation gives a red-shifted emission. Three main strategies have been used for controlling the conjugation length and bandgap in polythiophenes. In the first the conjugation length is modified by adding different substituents on the repeating unit, imposing continuous steric torsions of the main chain [182]. In Fig. 47.8 polythiophenes bearing substituents at positions 3 and 4 in the ring are shown and illustrate the shifts in emission resulting from different degrees of torsion. The larger substituents give a large dihedral angle between the rings, and short conjugation along the polymer backbone is achieved, resulting in blue-shifted emission. This way emission from the blue (PCHMT), green (PCHT), orange (PTOPT) to red (and NIR) (POPT) were observed [32,183]. With mixtures of these polymers it was also possible to obtain voltage controlled EL and white light emitters. For poly(3-(2,5-octyldiphenyl)thiophene) (PDOPT) the bulky side chains efficiently separate the backbones giving the polymer a high PL yield (0.37 in. solution and 0.24 in. film). PTOPT

has a lower density of side chains, and the PL yield reduces from 0.27 to 0.05 going from solution to thin film. PMOT is twisted out of planarity by sterical hindrance and shows blue-shifted absorption and emission [184]. Substituted polythiophene-containing electron transporting groups such as benzotriazole, chlorobenzotriazole, and fluorene have also been reported [185,186]. Poly(3-octyl thiophene), which can be obtained as a 95% regioregular material, offers an example of how super structure can affect the electronic properties of an emissive polymer. Changing from poly(3-hexylthiophene) to poly(3-dodecylthiophene) increased the maximum efficiency from 0.05 to 0.2% with calcium electrodes [187]. The phase structure in blends of one or more polythiophenes with a PMMA matrix allowed the fabrication of nano-LEDs giving white light emission. The thiophene backbone has been functionalized with a wide variety of organic moieties including alkyl, fluoroalkyl, alkylthio, alkoxy, alcohol/thiol, amino, cyano, ester, carboxylic acid, and sulfonate side chains. Nitrogen-derivatized polythiophenes permit further modification of the polymers [188].

Other approaches to tune the emission color of polythiophene LEDs are the preparation of completely coplanar systems with controlled inclusion of head-to-tail dyads or the preparation of alternating block copolymer. The insertion of *p*-phenylene ring to head-to-head thiophene dyad linked [189], with different substituents on both thiophene and phenylene enhanced by 29% the PL efficiency, in comparison with other polythiophenes, and by changing the substitution on both the phenylene and thiophene rings, the electronic spectrum of the polymers could be tuned, emitting blue to green light. Photophysical and electrooptical properties of regioregular polythiophenes functionalized with tetrahydropyran moieties tethered to the main chain by alkyl spacers were prepared to access structure–property relationships of regioregular THP-bearing poly(3-alkylthiophene)s. In particular, aggregation phenomena were addressed by investigating the influence of the alkyl chain length with respect to their photophysical and electrooptical properties [190].

The emission of a series of p–n diblock copolymers with good electron transporting properties where oligothiophenes were linked with oxadiazolyl-dialkoxybenzene units could be tuned from blue to green to orange by increasing the number of thiophene rings from 1 to 3 [191,192]. In a recent study [193] of the transport properties of a polythiophene derivative, poly(3-(2′-methoxy-5′-octylphenyl)thiophene) (POMeOPT) the current–voltage characteristics of single layer devices were measured in two regimes: contact limited current and bulk-limited current. The passage from one regime to another was done upon insertion of a conducting polymer poly(3,4 ethylenedioxythiophene) doped with poly(4-styrenesulfonate) (PEDOT-PSS) between the metallic electrode and the POMeOPT. The measured mobility was seven times higher than that for MEH-PPV in the same conditions, illustrating the good transport properties and high mobility that can be attained with regioregular

substituted polythiophenes. An interesting property of polthiophenes is phosphorescence emission which can be obtained by doping the polymer with a phosphorescent heavy metal as iridium, platinum, and others as in the case of poly(3-methyl-4-octylthiophene) as host and the phosphorescent compounds bis(2-phenylbenzothiazole) iridium acetylacetonate (BTIr) or platinum(II) 2,8,12,17-tetraethyl-3,7,13,18-tramethyl porphyrin as guest [194,195].

Introduction of the electron withdrawing groups as bithithiophene, pyridinyl, dipyridyl, and phenanthroline can modify their optical and electrical properties. These structures are low bandgap conjugated polymers with higher conductivity (carrier mobility), and may be transparent in visible light. Therefore, they have a great potential application in transistor, transparent conductor, nonlinear optical devices, and smart windows [196,197].

An alternating structure in which an unsubstituted thiophene ring was linked to a 3-alkyl-substituted thiophene, the two repeating units being alternated and a bulky group in the side chain showed an interesting peculiarity of combining high conjugation length with large interchain distances. Differently from the regioregular PATs, the copolymer showed high PL efficiency both in the solid form and in partially aggregated solutions [198].

47.6 CYANO POLYMERS

Most of the electroluminescent polymers are suitable as hole-injecting and transporting materials. To set an adequate balance in the injection flows coming from each side of the device it has been necessary to use electron transporting layers and/or low work function metals at the cathode, like calcium, which are unstable at atmospheric conditions. The synthesis of polymers with high electron affinity as the solution processable poly(cyanoterephthalydene)s which are derivatives of PPV with cyano groups attached to the vinylic carbons has provided the material necessary to complement the existing hole transport PPVs [57,142,199–205]. Poly(arylene vinylene)s bearing electron withdrawing groups are not easily available by application of the Wessling and related procedures and thus these cyano derivatives of PPV were synthesized via a Knoevenagel condensation route between an aromatic diacetonitrile and the corresponding aromatic dialdehyde [206–208] as exemplified in Fig. 47.9(a) or by copolymerization of dibromoarenes in basic medium. This approach permits adjustment of the bandgap by varying the proportion of the two comonomers [209]. The synthesis of fully conjugated PPV type structures containing cyano groups attached to the ring afforded a more perfect structure when a Wittig type condensation was followed, as in Fig. 47.9(b) in relation to the Knoevenagel route, emitting orange light (3000 cd/m^2 at 20 V) in a double layer device with PPV as HTL [210]. A variety of monomers with different substituents in the ring as alkyl or alkoxy solubilizing groups (as hexyloxy or
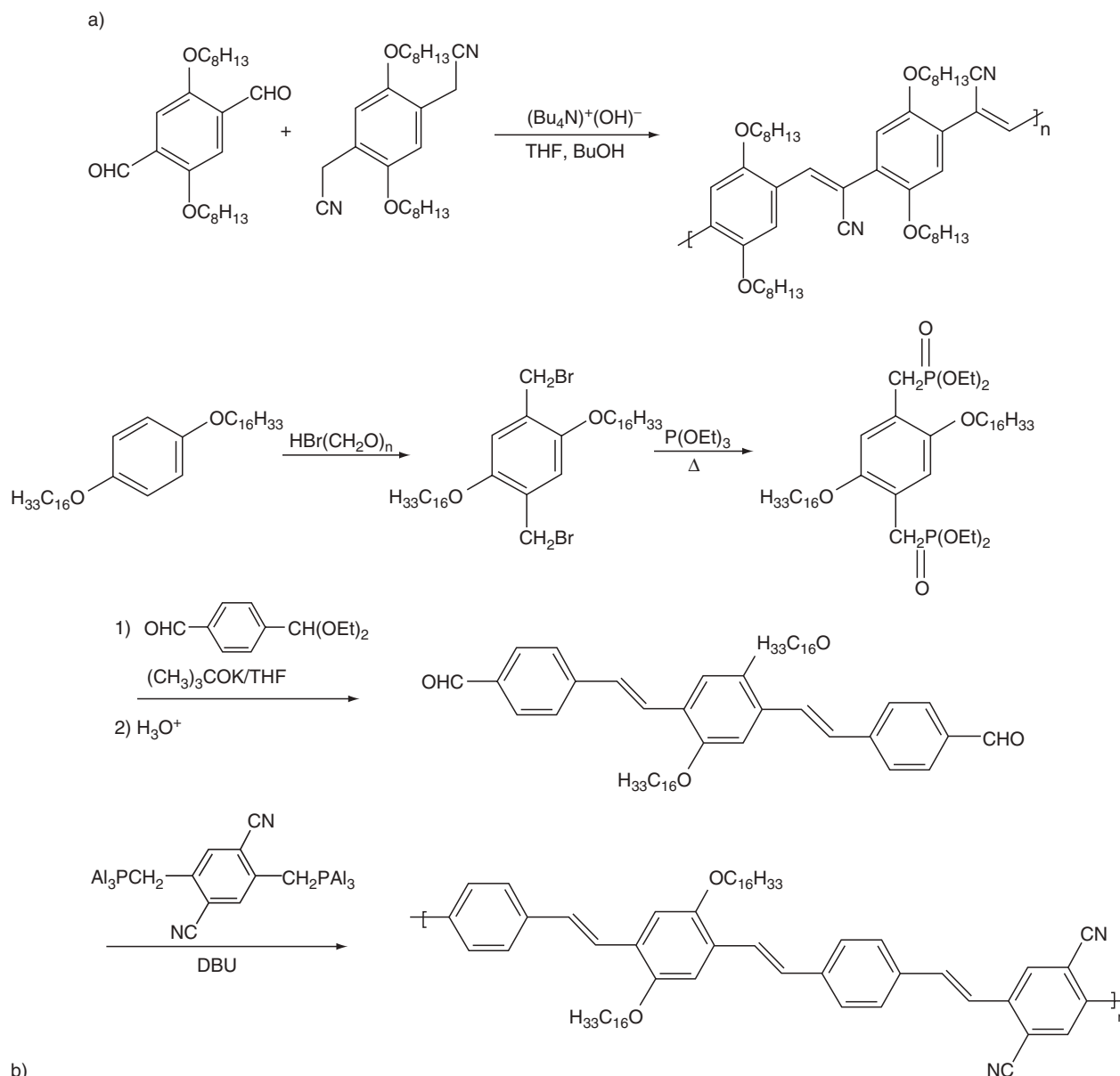
FIGURE 47.9. Synthetic routes to CN-substituted EL polymers. (a) Knoevenagel route leading to CN placement in the double bond; (b) Wittig route used to place the CN group in the aromatic ring in a conjugated–nonconjugated block copolymer.

methoxy-ethyl-hexyoxy as in MEH-PPV) were used to prepare cyano PPV like polymers emitting in the full-visible spectrum.

The inclusion of thiophene units in the main chain lowers the bandgap and shifts the emission to the infrared [211]. Examples EL polymers bearing cyano groups are given in Fig. 47.10. The electron withdrawing effect of the cyano group is calculated to increase the binding energies of both occupied π and unoccupied $\pi-\pi^*$ states, while at the same time keeping a similar $\pi-\pi^*$ gap [212]. The photophysical behavior of these polymers indicated that aggregates or excimers were probably the emitting associated form [213–216].

47.7 POLY(*P*-PHENYLENE)S (PPP) AND POLYFLUORENES

47.7.1 Polyphenylenes

Poly(*p*-phenylene) (PPP) is an interesting material for electrooptical applications as its bandgap is in the blue region of the visible spectrum and its thermal stability is combined with high PL. However, it is insoluble and infusible making it difficult to fabricate thin films. In the early stages of the search for PPP synthesis the limitations were related to the difficulties in the preparation of polymers possessing a defined architecture. Since only a few "classical"
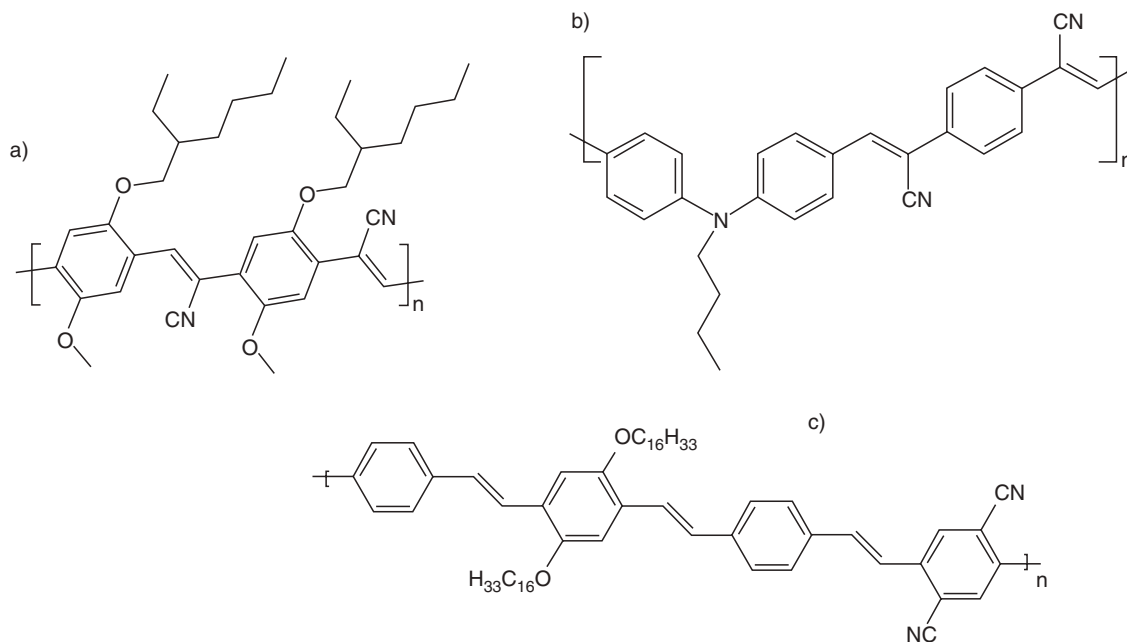
FIGURE 47.10. Examples of various EL polymers bearing the CN group in the double bond or in the aromatic ring.

organic reactions are known to generate a direct link between aromatic units, metal-catalyzed coupling reactions are commonly used for this purpose. The most successful routes are the Yamamoto route and the Suzuki crosscoupling reactions (SCC). The Yamamoto route involves the Ni mediated coupling of arenes by the reaction of the correspondent dibromo-substituted compounds [217]; the SCC involves the palladium-catalyzed crosscoupling reaction between organoboron compounds and organic halides. When applied to polymer synthesis, it proved to be a powerful tool to prepare poly(arylene)s and related polymers. In this case, SCC is a step-growth polymerization (Suzuki crosscoupling polymerization, SCP) of bifunctional aromatic monomers. The general method has been reviewed [218] and a wide variety of polymer structures prepared through this method [219]. In Fig. 47.11, a schematic representation of the step growth SCP is shown. Alkylated, soluble PPPs prepared via

coupling reactions using the Yamamoto [219] or Suzuki [220] routes yielded significant torsion angles. The interring twisting significantly changes the electronic structure as well as the conjugation length [221].

Copolymers consisting of oligo p-phenylene sequences linked by ethylene, vinylene, or units have been reported. By the combination of different AA/BB type monomers in various concentrations in a Suzuki coupling as polymerization route, a variety of well-defined structures were prepared with high quantum yields in solution [222] as shown in Fig. 47.12. Matrix-assisted laser desorption ionization time of flight mass spectrometry (MALDI-TOF-MS) and HPLC analyses of monodisperse-substituted PPP fractions indicated that the effective conjugation length was around 11 phenylene units [223]. One way of obtaining a planar conjugated backbone was to incorporate the phenyl rings into a ladder-type structure where four C-atoms of each phenyl
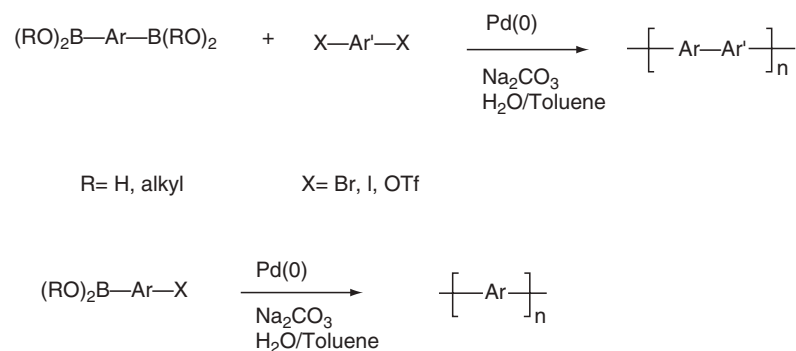
FIGURE 47.11. Schematic representation of the SCP —Ar— represent aromatic units, typically benzene derivatives.
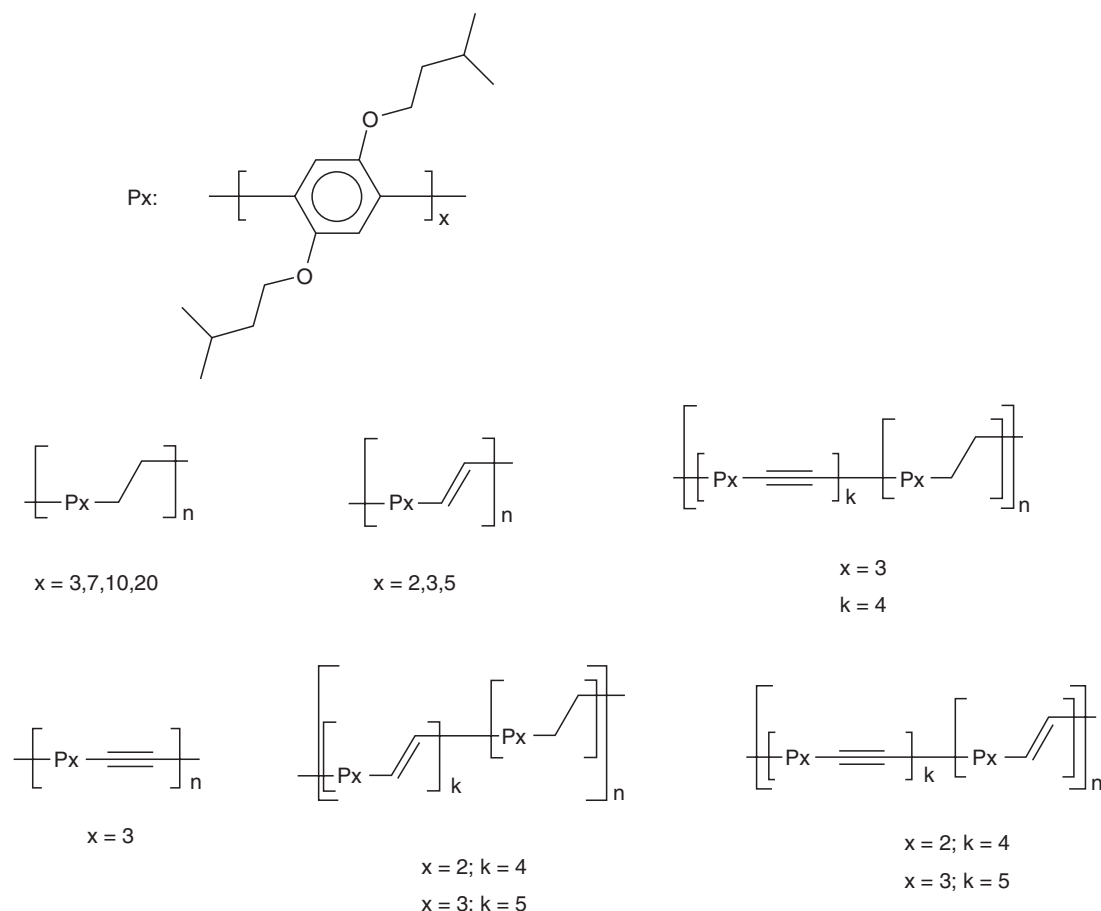
FIGURE 47.12. Polymers containing oligo-*p*-phenylene sequences linked by ethylene (E), vinylene (V) or ethynylene (A). The numbers correspond to the degree of polymerization of the phenylene sequences. The monomers were connected through the Suzuki coupling method.

ring are connected with neighboring rings (LPPP) in combination with an additional attachment of solubilizing side groups, thus creating a solution processable structure [224–229]. The forced planarity of the molecule led to a high degree of intrachain order, with a conjugation length of about eight phenyl rings [230,231]. The EL spectrum of the structures showed two emissions: a blue (461 nm) and a yellow (600 nm) which was attributed to the formation of excimers. A blue emitting PPP copolymer was reported in which tri-(*p*-phenylene) (LPP) and oligo(phenylene vinylene) segments were linked in an orthogonal arrangement to decrease quenching processes. Analogous structures with oligo (*p*-phenylene) units orthogonally and periodically tethered to a polyalkylene main chain have been prepared by the polymerization of oligomeric fluoreneacenes via an SN2 type of mechanism [232] Another class of PPP-type polymer is exemplified by the poly(benzoyl-1,4-phenylene) in a head-to-tail configuration [233]. The introduction of the carbazole unit in the ladder type tetraphenylene, blue emitting polymers brought about a slight bathochromic shift of the emission. The polymers exhibited good EL properties in initial PLED tests with high luminance values typically over

700–900 cd/m^2 at a bias of 10 but a definitive suppression of the excimer was not demonstrated [234].

47.7.2 Polyfluorenes

Recently, polyfluorenes were introduced as a prospective emitting layer for polymer LEDs. These materials are thermally stable and display high PL efficiencies both in solution and in solid films [235–239] with emission wavelengths primarily in the blue spectral region. Their photostability and thermal stability are also found to be better than those of the poly(phenylene vinylene)s. Polyfluorenes contain a rigidly planarized biphenyl structure in the fluorene repeating unit, while the remote substitution at C-9 produces less steric interaction in the conjugated backbone itself than in comparison with PPP, in which this interaction can lead to significant twisting of the main chain since the substituents used to control solubility are *ortho* to the aryl chain linkage, as is the case for the monocyclic monomers [240,241] discussed in Section 47.7.1. In this regard polyfluorenes can be considered as another version of PPP with pairs of phenylene

rings locked into a coplanar arrangement by the presence of the C-9 atom. Liquid crystallinity was observed in poly (dioctyl fluorene), which is important for the obtainment of polarized EL [26,242]. A representative number of poly-fluorenes and related structures are shown in Fig. 47.13. The nickel-mediated coupling of arylene dihalides, the Yamamoto route, has been used to prepare a variety of fluorene and substituted fluorene homo- and copolymers [235–244]. As with PPPs, the SCP has been recently applied

to the synthesis of a wide number of polyfluorenes and related structures. In the case of alternating copolymers obtained by SCP the optical and electronic properties of the polymers were tailored through selective incorporation of different aromatic units into the system. A variety of chromophores intercalated with fluorene has been reported, such as phenylene, naphthalene, anthracene, stilbene, cyanovinylene, thiophene, bithiophene [245] pyrazoline, quinoxaline, 1,2-cyanostilbene, pyridine, and carbazole [220, 246, 247].
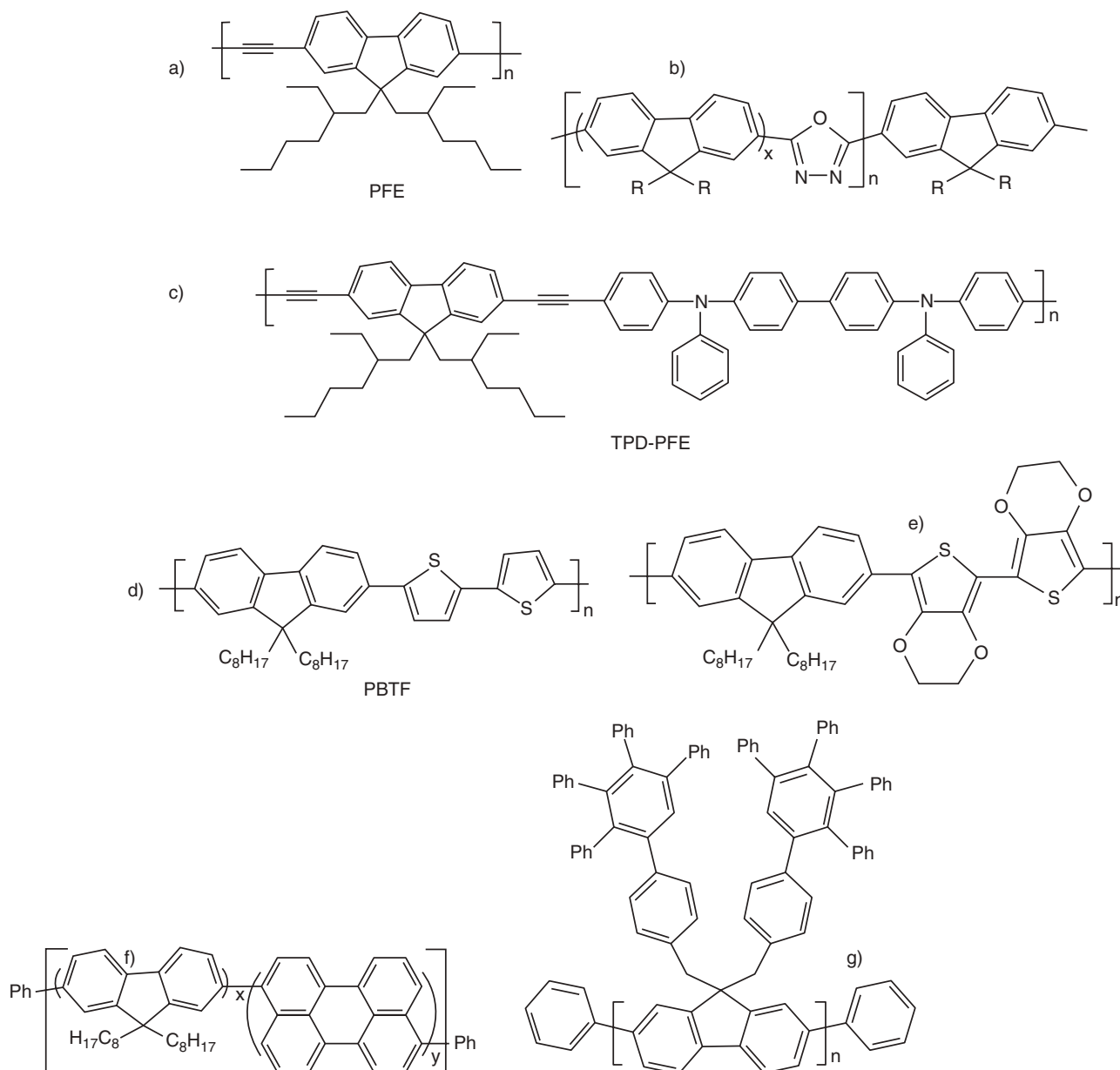
FIGURE 47.13. Examples of various fluorene based polymers. (a) Fluorene copolymer with triple bonds, poly(2,7-9,9-di-2-ethylhexylfluorenylene ethynylene); (b) alternating copolymers of 9,9-dioctylfluorene and oxadiazole; (c) copolymer containing the electron-accepting moiety 2,7-diethynylfluorene and the electron-donating moiety tetraphenyl diaminobiphenyl (TPD); (d) poly[2,20-(5,50-bithienylene)-2,7-(9,9-dioctylfluorene)] (PBTF); (e) poly[2,20-(5,50-di(3,4-ethylenedioxythienylene))-2,7-(9,9-dioctylfluorene)] (PdiEDOTF); (f) polyfluorenes with perylene groups in the main chain; (g) a dendronized polyfluorene.

Figures 47.14 and 15 show the Yamamoto and the SCP routes to synthesize fluorene-based copolymers, respectively. Well-defined monodisperse oligomers were prepared via SCP to access the effect of conjugation length on photoluminescent properties of polyfluorenes [248]. The Yamamoto route was also used to prepare 9-di-hexyl substituted oligofluorenes, containing 3–10 repeating units. The effective conjugation length was estimated to be 12 bonded fluorene units, by extrapolation of spectral data [249]. Substituted oligofluorenes in which the fluorene units alternate with triple bonds, namely oligo(9,9-dihexyl-2,7-fluorene ethyny-

lene)s, demonstrated strong EL, and their effective conjugation length was calculated to be around 10 fluorene units (Fig. 47.13(a)) [250]. Devices with fluorene polymers appear to have electrons as the majority carriers and their performance is notably improved when modified with an appropriate HTL. Hole transporting moieties such as tertiary amines and TPD [251] have been incorporated to polyfluorenes in attempts to optimize LED performance. The HOMO levels of fluorene-based poly(iminoarylene)s (~ -5.1 eV) were close to the work function of ITO, and their use as buffer layers has been suggested (buffer layers are inserted
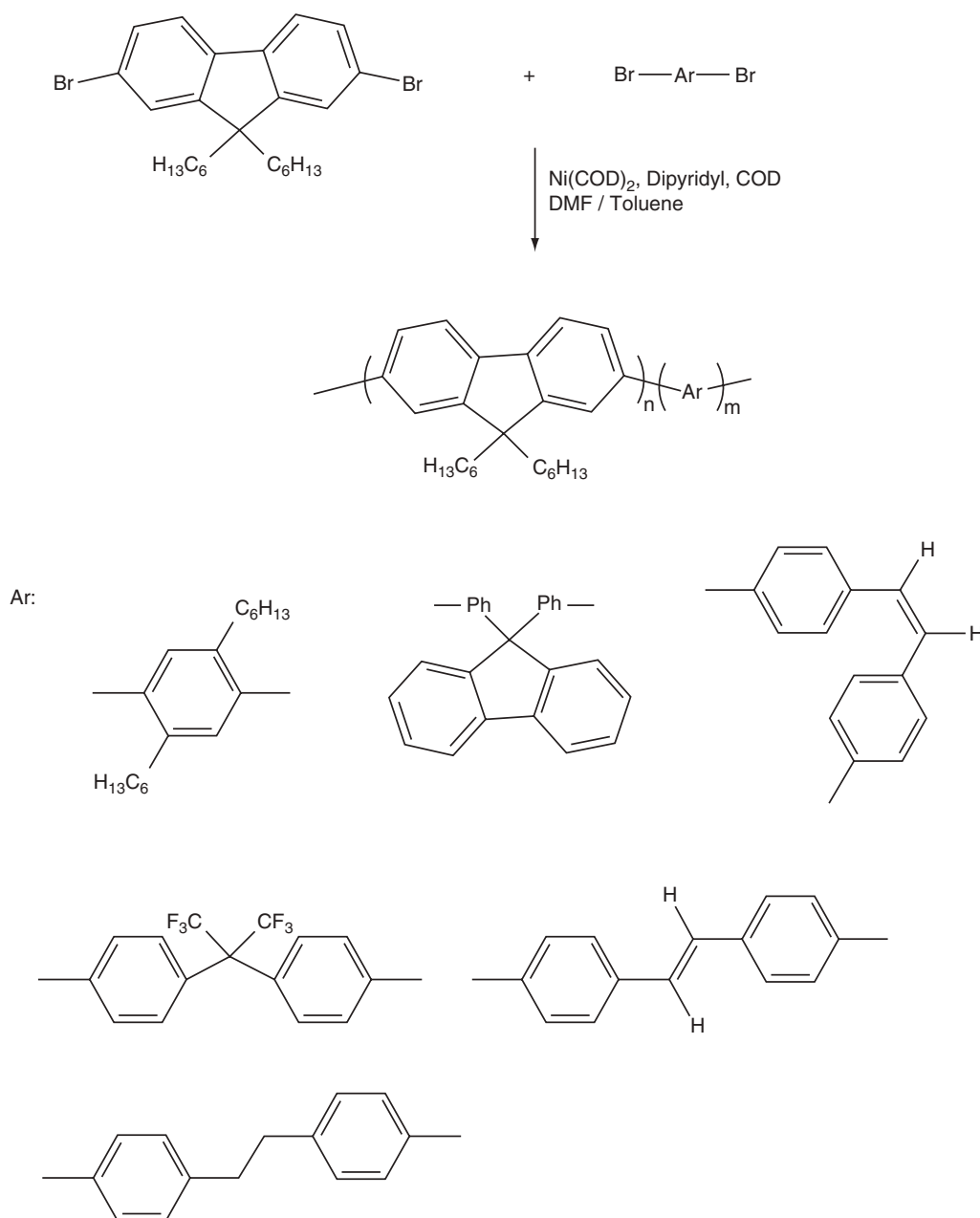
FIGURE 47.14. The Yamamoto route to polyfluorene based copolymers: nickel mediated coupling of 2,7-dibromo-9,9-dialkyl fluorene and various dibromoarenes.
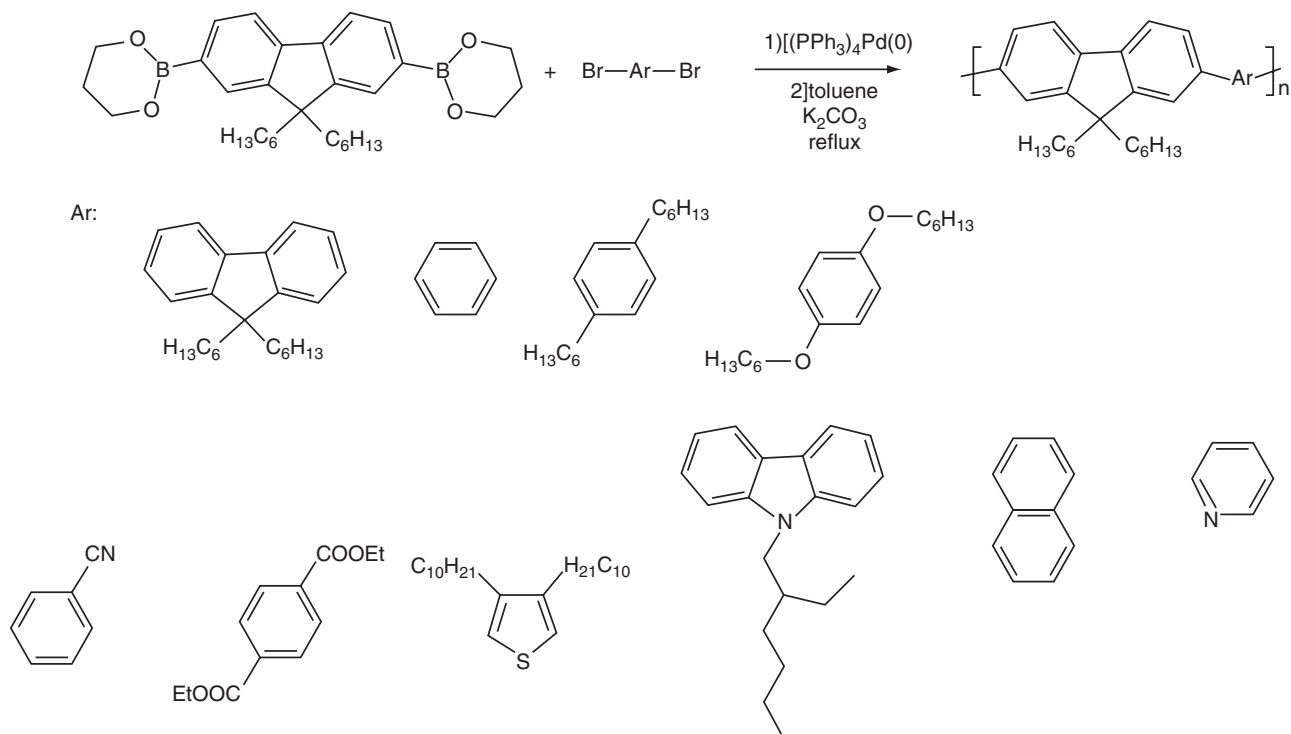
FIGURE 47.15. The SCP route to fluorene-based alternating copolymers: tetrakis(triphenylphosphine)palladium mediated condensation 9,9-dialkylfluorene-2,7-bis(trimethylene boronate) and various dibromoarenes.

between ITO anode and HTLs, as TPD). On the other hand, the incorporation of the electron withdrawing 1,3,4-oxadiazole units brought the electron affinity of the copolymers close to the work functions of Ca. These structures, shown in Fig. 47.13(b), prepared via the SCP, contained the oxadiazole evenly dispersed in the main chain, at every one, three, or four 9,9-dioctyl fluorene mers. All copolymers fluoresced in the blue range with quantum yields of about 70% in solution [252]. The combination of donor and accepting moieties in fluorene-based structures has been accomplished by alternating TPD (electron donating) with 2,7-diethylhexyl fluorene or diethynylfluorene units (electron donors), as shown in Fig. 47.13(c). A fluorinated copolymer formed by alternating mers of [2,3,5,6 tetrafluoro-1,4 phenylene] and [9,9′-dihexyl-2,7 fluorene] emitting blue light with low turn on voltages, showed a superior performance to that of the nonfluorinated analog copolymer and of the corresponding poly(9,9′dihexyl-2,7 polyfluorene) homopolymer [253]. An alternating polyfluorene with low bandgap segments has been designed and synthesized aiming to tune the emission. The low bandgap segment consists of an electron acceptor (thiophene, A), fenced by electron donors (benzodiathyazole, D). This D–A–D configuration lead to a partial charge transfer in the polymer backbone, and thereby a low bandgap (1.3 eV) [254]. The same approach was used by incorporating an analog of the red emitting dye DCM [(4-phenylamino)vinyl) pyran-4-ylidene-malononitrile] as a comonomer into the polyfluorene backbone. The emission was in the range 573–620 nm (greenish-yellow to red). DCM dye has

an electron-deficient 2-pyran-4-ylidene malononitrile (PM) group and an electron-rich aromatic amine group, so both the absorption and emission show a red region because of the effect of charge transfer from triphenylene (TPA) to the PM group [255].

Another fluorene copolymer containing the luminescent dye [4-dicyanomethylene-2-methyl-6-4H-pyran (DCM) as acceptor compound was irradiatiated with UV light in the presence of gaseous trialkylsilanes. This reagent selectively saturates the $C = C$ bonds in the DCM comonomer units while leaving the fluorene units essentially unaffected. As a result of the photochemical process, the red electroluminescence of the acceptor compound vanishes, and the blue-green electroluminescence from the polyfluorene units is recovered. Compared with previous processes based on polymer blends, this copolymer approach avoids problems associated with phase-separation phenomena in the active layer of OLEDs [256].

Orange-red emission was also seen in single layer devices of a series of conjugated copolymers of fluorene and 2- [2, 6-bis(2-arylvinyl)pyridine-4-ylidene]-malononitrile [257]. Another kind of red-emitting polyfluorenes with high electron affinity was reported, namely 9,9-dihexylfluorene and diketopyrrolopyrrole [258]. The Foerster-type energy transfer was efficiently used to tune the solid-state emission color of fluorene based copolymers bearing perylene dyes as end groups or side chains, as shown in Fig. 47.13(f). The emission coming almost exclusively from the perylene dyes could be tuned from yellow-green (558 nm) to red (675 nm)

[259]. Color tuning to the deep-red and NIR region was achieved by incorporating a selen-containing heterocycle, benzoselenadiazole, a selenium analog of benzothiadiazole in different compositions, resulting in a significant red shift in comparison with its sulfur analogue [260]. The abundant literature in polyfluorene and derivatives show that nowadays it is possible to tune the emission of polyfluorene derivatives from bluish-violet to deep red and near infrared [261].

One problem with polyfluorenes is the occurrence of an undesired low-energy band at 500–600 nm in the photo- and electroluminescence spectra of the pristine polymer or after annealing or the passage of current. The low-energy green band limits the emission efficiency and damages the blue color purity and stability as well. Two opposite points of view on the origin of this green emission have been reported. According to the first, the green emission is attributable to the interchain aggregates and/or excimers. Consequently, dendronization, introduction of spiro- or crosslinks, substitution with bulky side groups such as tetraphenylthiophene, blending, and the introduction of disorder units such as carbazole, pyridine, and thiophene have been applied to suppress intermolecular interaction [262]. The second point of view states that the green emission band is caused by keto defects of polyfluorenes, which are generated during the handling of the materials in air, or by a reaction with residual oxygen over the course of photophysical experimentation. Certain authors have proposed that the origin of the green-emission band stands on the fluorenone moiety and contradicted experimentally the assumption that intermolecular aggregates or excimers are involved. A series of well-defined 9,9′-dihexylfluorene-co-fluorenone copolymers with various fluorenone contents and a set of monodisperse oligofluorenes in the chain center have been prepared to elucidate the exact origin of the low-energy emission in polyfluorenes. On the basis of the steady-state photoluminescence (PL) and PL decay dynamics of the fluorenone-containing oligomers and copolymers both in dilute solutions and in thin films, the origin of the controversial low-energy emission band was attributed to the interaction between intrachain fluorenone moieties instead of the intermolecular aggregates or excimers. It was also proposed that a fluorene pentamer with a central fluorenone unit would be more appropriate to represent the actual chromophore responsible for the green emission in the copolymers [263]. Nevertheless the question remains still controversial. The introduction of 9-hexylcarbazole and 9-dimethylaminopropylcarbazole moieties into polyfluorene chain was claimed to effectively prevent excimer formation in the polymers [264], With the same idea 9,9-dihexylfluorenyl was inserted as a pendant group in a chain of poly(biphenylene vinylene). The insertion brought about steric interactions between adjacent rings, reducing conjugation length, but at the same time inhibited the formation of excimers. The polymer showed bright and stable blue emission [265].

Miller and co-workers at IBM have managed to overcome the low-energy emission by incorporating anthracene units which show stable blue emission even after annealing at 200°C for 3 days [266]. Mullen et al. [267] at the Max-Planck Institute in Germany produced nonaggregating polyfluorenes by the insertion of dendron side chains, as shown in Fig. 47.13(g) [268], giving a polymer with pure blue emission, as the bulky side chains do not cause distortion between the fluorene units. Recently, dendritic structures were attached to polyfluorenes with further addition of a low percentage of surface-modified semiconductor nanoparticles [269]. Starlike materials tethered to polyfluorene derivatives emitting blue, green, or red light were developed. Polyhedral oligomeric silsesquioxanes were incorporated into the center core of the derivatives to enhance thermal stability and reduce linear aggregation [270]. The optical properties of a series of light-emitting hyperbranched polyfluorenes through 1,3,5-substituted benzene crosspoints were investigated. With increase in crosspoint density, the emission color of the PEDOT-containing LEDs shift from green to violet and showed higher EL efficiency due to the effective exciton confinement and the reduction of intrachain or interchain exciton annihilation [271].

A series of electron-deficient, oxadiazole-, quinoline-, quinoxaline- and phenylenecyanovinylene-containing copolymers bearing ethyl hexyl in the fluorene unit was developed. These materials possess low-lying LUMO energy levels (-3.01 to -3.37 eV) and low-lying HOMO energy levels (-6.13 to -6.38 eV), with sharp blue emission, and may be promising candidates for electron transport-hole-blocking materials in LED fabrication. The film emissions were only 7–11 nm red shifted in comparison with the solution emissions, indicating that excimer formation was suppressed. This was explained in terms of the prevention of molecular stacking by the presence of sterically demanding ethyl-hexyl substitutions at the fluorene unit [272]. The formation of a network is a useful strategy in the obtainment of various performance improvements in polyfluorenes. For example, the attachment of styryl end groups, via reaction of the bromo-terminated polymer with bromostyrene in a Yamamoto coupling, allowed the deposition of a crosslinkable layer through the thermal polymerization of the terminal styrene groups. Apart from the added advantage of further casting other layers, the immobilization of the chains leads to suppression of intermolecular excited state interactions, hampering the ability to π stack [273,274]. Another kind of fluorene-containing structure consisted of conjugated polyfluorene/poly(p-phenylenevinylene) copolymer containing the pendant bis(4-alkoxyphenyl) groups in the C-9 position of every alternating fluorene unit. The main advantage of the use of an extended 9,9-bis(4-hydroxyphenyl)fluorenyl core in the polymerization reaction is that the insertion of a rigid phenylene spacer between the large side chain and the polymer backbone may lead to a more efficient shielding effect on the polyfluorene main chain, which would suppress the formation of aggregates/excimers while

not blocking the reaction sites of the macromonomer from the palladium catalyzed polymerization reaction. The chain stacking, however, was not completely avoided, and a green electroluminescence was observed [275].

Energy migration has been explored in polyfluorenes to enhance emission intensity. For example, devices of poly (9,9-dioctylfluorene) mixed with the amine-substituted *co*-polyfluorene poly(9,9-dioctyl-fluorene-*co*-bis-*N*,*N'*-phenyl-1,4-phenylenediamine), showed a blue emission with a luminance of 1550 cd/m^2 and a maximum external quantum efficiency of 0.4%, much larger than the original homopolymer. White-light-emitting devices have been demonstrated with new single-component fluorene-acceptor copolymers with three emitting units: blue-emitting 9,9-dihexyl-fluorene, green emitting quinoxaline (or yellow-emitting 2,1,3-benzothiadiazole), and red-emitting (thieno [3,4-b]-pyrazine) units in the same chain. The energy-transfer between the emitting moieties suggests the white-light emission could be obtained by a relatively small fraction of the acceptor moieties. The EL devices typically had a luminance of 1,870 cd/m^2 at 10 V. The CIE coordinates of this device are (0.33, 0.34), which are almost identical to the standard white emission, and they exhibit insignificant changes in driving voltages. The results suggest that very bright and highly stable white-emission devices could be achieved by single-component fluorene-acceptor copolymers with three emitting moieties as an emissive layer [276].

A recent aspect of the research in polyfluorenes is related to supramolecular ordering of these conjugated polymers by making rod-coil block copolymers. The rod-like conjugated polyfluorene was end capped on one or both ends with poly-ethylene oxide, forming di- or triblock copolymers. The solid-state fluorescence spectra of these materials had better resolution than the homopolymer, indicating an enhanced number of well-ordered rods in the films and an additional increase in long wave emission. Multilayer fluorene-based LEDs were reported by a Japanese group [277] where a three layer device having the structure ITO/*N*,*N'*-bis (2,5-di-tertbutylphenyl)-3,4,9,10-perylene dicarboxamide (BPPC)/*N*,*N'*-diphenyl-*N*,*N'*-(3-methylphenyl)-1,10-biphenyl-4,40-diamine (TPD)/poly(9,9-dihexylfluorene) (PDHF) was able to emit either red or blue by changing the polarity of the applied voltage. TPD is a material mainly used for hole transport, BPPC is a red emitter, and the polymer emits in the blue region. The particular set of gap conditions in this system allowed the emission of blue light under positive bias conditions (ITO anode, AI cathode) and emission of red light under negative conditions. Furthermore, the device can be driven with an AC field and the emission color can be gradually modulated by changing the frequency of the applied AC field. Placing a small amount of surface-tailored CdS nanoparticles into the dendritic structure of copolyfluorene substantially improves the efficiency of the polymer's light emission, as well as the purity of the emitted light. One possible explanation for the enhancements in PL and EL may be the reduction in the concentration of interpolymer

excimers, i.e., the CdS nanoparticles caused an increase in the interpolymer chain distance.

An intermediate structure between PPP and polyfluorene has been developed, the poly(2,8-indenofluorene). This blue emitting polymer is stable up to 380°C, and shows thermotropic LC behavior at high temperatures (250–300°C) making it a good candidate as the active material in polarized LEDs [278].

Models of spin statistics predict that the electron–hole recombination event should produce three times as many triplets as singlets, and this has been confirmed experimentally for electroluminescent devices. Considerable effort has been devoted nowadays to attach phosphors covalently to a conjugated polymer backbone so as to allow efficient energy transfer between polymer and phosphor. Electrofosforencesce seems to be the new trend to maximize LED performance. One exemple is the red Electrofosforescent Light Emiiting Diode based on iridium complexes with the [lr(btp)2(acac)] fragment (where btp is 2-(2'-benzo [*b*]thienyl)pyridinato and acac is acetylacetonate). The fragment was attached directly or through a –(CH2)$_8$–spacer chain at the 9-position of a 9-octylfluorene host. The dibromo-functionalized spacerless or octamethylene-tethered fluorene monomers were chain extended by Suzuki polycondensations using the bis(boronate)-terminated fluorene macromonomers in the presence of end-capping chlorobenzene solvent to produce the statistical spacerless and octamethylene-tethered copolymers containing an even dispersion of the pendant phosphorescent fragments [279].

47.8 SILICON-CONTAINING POLYMERS

The interest in silicon-based polymers resides in the delocalization of the σ electrons over a Si backbone providing electronically analogous properties to the π-conjugated polymers. Polysilanes are σ-conjugated polymers with a one-dimensional (1D) Si chain backbone and organic side chain substituents. Progress in understanding their electronic structure derived from both theoretical and experimental studies has revealed that they are quasi-1D semiconductors with a direct and wide bandgap (∼4 eV), and that the σ-conjugated electronic structure typically observed in silane high polymers appears in Si chains with more than 20–25 Si units [280]. Polysilanes exhibit photoconductivity, intense near-UV absorption, and strong PL of small Stokes shift and high hole mobility (on the order of 10^{-4} cm^{-2} s^{-1}) [281]. Near-UV or UV emitting LEDs of diaryl, dialkyl, mono-alkyl-aryl polysilanes have been reported [282–285], and the bandgap energies tend to shift to lower values based on the size of substituents with aromatic side groups [286]. The emissions in polysilanes have been attributed to the σ−σ* transitions of 1D excitons in the Si backbone. Nevertheless, PL studies of poly(methylphenylsilane) demonstrated the existence of another emission due to a charge transfer state from the intrachain σ to pendant π* groups which appear in

larger wavelengths (400–500 nm) [287]. Being typical p-type semiconductors, polysilanes cannot transport electrons, and for this reason the incorporation of electron transporting groups with emitting properties seemed to be an interesting way of combining good properties [288].

Polymethyl phenyl silane (PMPS), poly [bis(*p-n*-butyl-phenylphenyl)silane] (PBPS), and poly(2-naphthyl phenyl silane (PNPS) are examples of polysilanes, shown in Fig. 47.16(a). A blue emission (480 nm) with a PL of 87% was achieved with a poly(methylphenylsilane) containing anthracene units in the polymer backbone [289].

Silicon-containing PPV derivatives have been developed in which the silicon unit acts a spacer to improve solubility, film forming characteristics, and confine conjugation, in analogy of the conjugated–nonconjugated block copolymers with an aliphatic spacer. While the aliphatic segments as spacers can act as a barrier to injection and mobility of the charge carriers, resulting in higher threshold voltages, the silicon units with an aromatic or flexible group are able to produce the same spacer effects with low operating voltages [290]. It has been argued that the participation of the d-orbital of the Si atom could be assisting to increase the
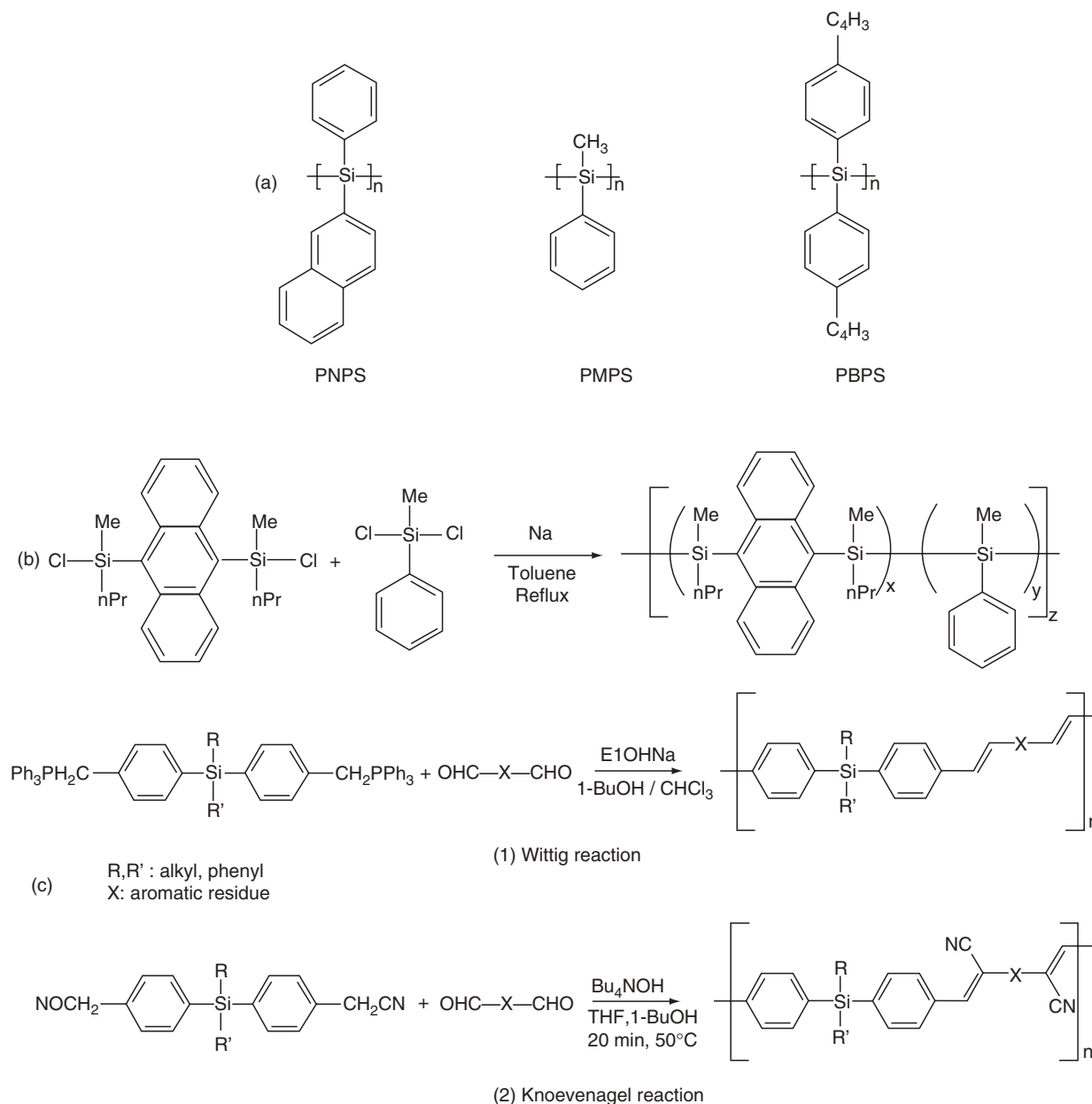
FIGURE 47.16. Examples of (a) polysilanes, where the main chain is made up of Si–Si bonds: poly(phenyl methyl silane) (PMPS), poly(naphthylmethyl silane) (PNPS), poly[bis(*p-n*-butylphenyl)silane] (PBPS); (b) synthetic route to poly(methyl phenyl silane) containing anthracene units; (c) copolymers with Si inserted between *p*-conjugated blocks: Wittig (top) and Knoevenagel (bottom) routes.

effective conjugation length, thus facilitating charge mobility [291], although previous theoretical work has demonstrated that Si bonds break effectively the π-conjugation [292]. A variety of PPV-related structures such as copolymers of diphenyl/dibutylsilane [293], dibutyl, butyl/methyl, diphenyl silanes [294] with PPV and alkoxy PPV [295] have been reported, in which the organosilicon groups are used as spacers [296]. Some representative examples are shown in Fig. 47.16(b). The EL spectrum of the diphenyl-substituted copolymer (SiPhPPV) gave the highest peak (450 nm) when the operating voltage of 9 V was applied. With 12 V applied bias a strong white color was emitted due to additional emissive bands. This threshold voltage was further decreased to 7 V by the introduction of a CN group into the double bond of PPV (Fig. 47.16(c)) [291]. Similar results were obtained in alternating copolymers of silane and carbazolyl or fluorenyl derivatives, peaking around 440–476 nm with operating voltages of 6–12 [297]V. In contrast to alkoxy groups, the lack of electron donor capacity (and consequent red shifting of the emission) of alkylsilicon groups has suggested the introduction of these groups as ramifications in EL polymers, improving processing characteristics [298,299].

One of the unique properties of polysilanes is the SiSi bond scission of the backbone chain under UV radiation. In the presence of oxygen it is accompanied by a SiOSi bond formation that leads to the conversion into an insulator, with no hole transport ability. Using this property, a patterning-image-display electroluminescent device was built. Before turning on the voltage, the anthracene-containing polysilane LED was irradiated in order to pattern an image onto the emission area, from the glass substrate side. Blue patterned light was obtained, corresponding to the negative photomask used [289,300].

47.9 NITROGEN-CONTAINING CONJUGATED POLYMERS

47.9.1 Pyridine-Containing Conjugated Polymers

Due to their strong electron-acceptor character, nitrogen-containing groups of various kinds have been incorporated to conjugated polymeric structures. The most extensively studied structures carry the pyridine moiety, in homopolymers (poly(2,5-pyridine), poly(3,5 pyridine)) [301,302], in PPV-type structures (poly(p-pyridylene vinylene))s [302,303], in copolymers with PPV (poly(phenylene vinylene pyridylene vinylene)s) or in p-phenylene derivatives [304,305]. Alternating pyridine-based backbone copolymers with substituted phenylene and fluorene units have been reported for tunability of electronic properties with enhanced stability [306].

As compared to phenylene-based analogues, one of the most important features of pyridine-based polymers is the higher electronic affinity. As a consequence, the polymer is more resistant to oxidation and shows better electron transport properties. The higher electron affinity enables the use of relatively stable metals such as Al, Cu or Au, or doped polyaniline as electrodes [302,307]. The pyridine-containing conjugated polymers are highly luminescent, especially the copolymers with phenylene vinylene. The solubility of polypyridines in organic solvents represents another advantage as compared to PPV for device fabrication. The ability to protonate and quaternize the nitrogen makes it possible to manipulate the electronic structure and thereby the emission wavelength [305,308]. The synthesis of poly(2,5-pyridine) and poly(3,5-pyridine) is straightforward: one step coupling polymerization of the 2,5 (or 3,5) dibromopyridine using a metal catalyst [309]. It was proposed that two blue electroluminescent devices emitting at 420 and 520 nm can be constructed by varying the degree of protonation. Another example illustrating the possibility of tuning spectroscopic properties by protonation of the lone pair of electrons of the pyridine ring is the red shift observed in the fluorescence and EL emission of poly(2,5-pyridylene-co-1,4-(2,5-bis(ethylhexyloxy)phenylene)[310]. Excitation profiles show that emission arises from both protonated and non-protonated sites in the polymer chain. Protonation is also accompanied by intramolecular hydrogen bonding to the oxygen of the adjacent solubilizing alkoxy group, providing a new mechanism for driving the polymer into a near planar conformation, extending the conjugation and tuning the emission profiles. The PL and EL spectra of copolymers of 1,4-phenylene vinylene and 2,6-pyridylene vinylene(co(2,6-PyV–PV)) could be tuned, respectively, in function of the excitation wavelength of the light and the external voltage applied in LED devices. The incorporation of the pyridine moiety increased the EL efficiency of the devices by a factor of 5 in relation to PPV [302,308,311]. A series of poly(2,5-dialkoxy-1,4-phenylene-alt-2,5-pyridine)s in which the [alkoxy phenylenepyridyilene] structural unit acts as donor–acceptor pair was synthesized via a SCP [304]. The electron affinity of these polymers is ca. 2.5 eV, comparable to that of copolymers containing oxadiazole moieties. The electron-withdrawing pyridinylene groups were able to lower the LUMO energy in such a way that these polymers may have similar electron injection properties as typical oxadiazole-containing electron transport polymers, when they are used as active materials in LEDs. The Wittig and Wittig–Horner reactions have been employed to prepare copolymers containing bipyridine and silicon units. The organosilicon moiety improves the solubility and limits the conjugation length [312]. Recently, the bipyridine moiety linked to metals as iridium was used to fabricate blue phosphorescent LEDs with high emission intensity [313].

47.9.2 Oxadiazole-Containing Conjugated Polymers

One of the best electron transport structures is the oxadiazole group, as noted above. The covalent attachment of the PBD moiety to an emitting polymer (Fig. 47.4(b)), was a natural development in LED technology, avoiding the
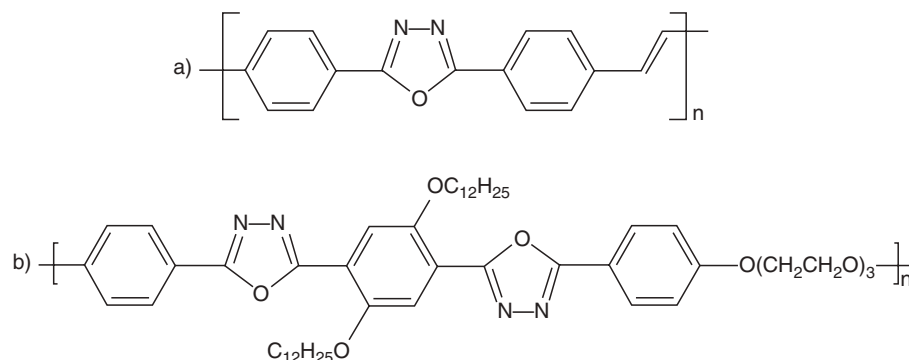
FIGURE 47.17. Oxadiazole-containing EL polymers. (a) Poly(2,5-diphenylene-1,3,4-oxadiazole)-4,40-vinylene; (b) alternating oxadiazole-*alt*-alkoxyphenylene and a aliphatic spacer.

problems with the deposition of an additional layer in diode construction and the anticipated phase separation after film preparation or under operating conditions. Some examples of oxadiazole-containing EL polymers are given in Fig. 47.17. Among the various examples found in the literature one can cite the use of oxadiazole incorporated in the main chain [168,314–316] or as a pendant group [168,214,317–320].

In the first case the oxadiazole moiety was used as a comonomer in chromophoric imides [168,321], copolymers containing thiophene sequences [322], or in a PPV type main chain [168,267,323]. Synthetic approaches for the oxadiazole-containing polymers were the Heck reaction or via the formation of a polyhydrazide precursor [324]. Oxadiazole moieties linked to PPV [168,325], alkyl-PPV, and polythiophene chains as pendant groups with improved EL efficiencies due to higher electron affinity, better injection, and transport properties have also been reported [326]. The insertion of electron-transporting groups in p-type polymers brings about bipolar carrier transport ability. The combination of donor–acceptor groups in the same chain in attempts to achieve balanced electron–hole injection and transport avoiding the use of intermediate transport layers has been widely explored, such as the combination in the same chain. Due to their strong electron-acceptor character, oxadiazole and PPV [158,326] or oxadiazole and oligothiophenes [327] have been reported, for example for PPV type chains [169,326,328] or other chromophores like naphthalimide [329], fluorene [330], anthracene, triphenyl amine.

47.9.3 Polyquinolines and Polyquinoxalines

Polyquinolines and polyquinoxalines are n-type (electron transporting) polymers and therefore offer alternative EL device engineering in conjunction with the extensively studied p-type (hole transporting) polymers such as poly(*p*-phenylene vinylene)s, polyphenylenes, and polythiophenes. A variety of polyquinolines [331,332] and polyquinoxalines [333] has been reported in the literature, acting as the active

emitting layer [331,334,335] or as the transport layer [336–338] in LEDs. Figure 47.18 shows some representative examples of these emitting and electron-transporting polymers. The increased electron deficiency of the quinoxaline ring due to additional imine nitrogen, compared to the quinoline ring, enhances the electron-accepting ability of conjugated polyquinoxalines, thus improving electron transport protonated by means of acidic solvents, intense blue emission was observed at 450 nm. When the positive charge on the nitrogen atom of the quinolines reached a critical value, intermolecular electrostatic repulsion prevented the aggregation, and the emission spectra were those of the isolated chain. The nonprotonated forms formed LC structures, which formed excimers with emissions in the 550–600 nm range. pH-Tunable PL was also demonstrated in poly(vinyl diphenylquinoline) with emission maxima varying from 486 to 529 nm (blue to green). Intramolecular excimer emission was observed in acidic solutions but not in neutral solutions or thin films of the polymer. The polymer, which was obtained from a modification of polystyrene, was introduced as a prospective high T_g, electron transporting counterpart of the hole transporting side chain PVK. The electron transporting properties of copolymers bearing fluorene and quinoline units with conjugation confinement varied with the chain rigidity and conjugation length and proved to be useful in double and triple layer devices [339]. A series of polyquinolines containing 9,9′-spirobifluorene was recently reported. The two fluorene rings were orthogonally arranged and were connected via a common tetracoordinated carbon. The incorporation of the piro moiety provided good solubility due to a decrease in the degree of molecular packing and crystallinity while imparting a significant increase in both Tg and thermal stability, by restricting segmental mobility. Polymers incorporating bis(phenylquinoline) and regioregular dialkylbithiophene in the backbone showed substantial enhancement in device performance under ambient air conditions (1.4% external quantum efficiency, $2,170 \, cd/m^2$) in bilayer MEH-PPV LEDs [340] properties [334,335]. Polyquinolines are
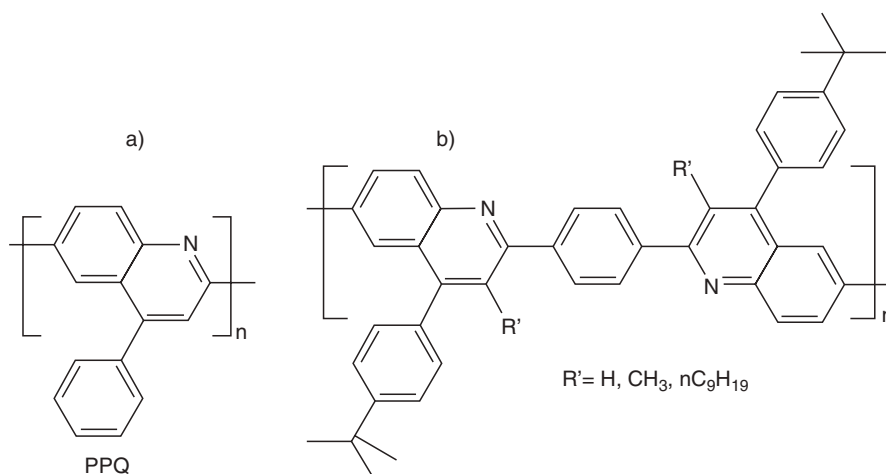
FIGURE 47.18. Examples of EL polyquinolines.

usually prepared by the acid-catalyzed Friedlandler conden-sation of bis(*o*-aminoketone)s and bis(ketomethylene) monomers, have good mechanical properties and high ther-mal stability, and can be processed into high quality thin films. A new synthetic route to organic solvent-soluble conjugated polyquinolines incorporating bis(4-alkylquino-line) units through a new A–A monomer was used to prepare 3,3′-dinonanoylbenzidine copolymers, poly(2,2¢-arylene-4,4′-bis(4-alkylquinoline)) [341].

Variations in the polyquinoline backbone linkage (R) and pendant side groups provided a means to regulate the intra-molecular and supramolecular structures which in turn en-abled tuning of the light emission from blue to red.

Studies of supramolecular photophysics of selfassembled block copolymers bearing styrene–polyquinoline sequences demonstrated evidence of J-aggregation in well-defined, ordered structures such as micelles and vesicles. The poly-mers represent a novel class of functional luminescent ma-terials [342]. In a recent contribution, Jenekhe reported a detailed study on voltage-tunable multicolor emission-bilayer LEDs combining PPV (as typical p-type layer) with a series of polyquinolines, polyanthrazolines, polyben-zothiazoles, and a poly(benzimidazobenzophenanthroline) ladder, addressing the influence of the polymer–polymer interface in the diode efficiency and luminance and showing that its electronic structure plays a more important role than the injection barrier at the cathode/polymer interface [343].

47.9.4 Carbazole-Containing Conjugated Polymers

Due to its electro- and photoproperties, the carbazole molecule has been used in various technological applica-tions [344,345]. Polymers based on this compound have been used to enhance LED emission and also for color tuning. In Partridge's study of EL of dye doped PVK sys-tems [346–348], the hole transport properties of this poly-mer were demonstrated. Devices in which the emitting layer was formed by PVK blended with other polymeric systems have shown remarkable increases in luminescence effi-ciency, as compared to those in which PVK was not incorp-orated. As an example, the blue emitting device with the ITO/polymer blend/Ca configuration made of poly(*p*-phenyl phenylene vinylene) (PPPV) blended with PVK showed a quantum efficiency of 0.16% which is a good result for a blue emitter [349]. As in all cases of PVK blends, it was observed that there is an optimum molar ratio be-tween the emitting polymer and PVK for the increase in EL intensity. If the diode is doped excessively with PVK the conductivity can be reduced, when the other polymer is more conductive than PVK itself. Apart from the homopo-lymer, the carbazole moiety can be incorporated in polymer chains as part of the main chain, like poly(2,5-dihexylphe-nylene-*alt*-N-ethyl-3,6-carbazolevinylene), which was com-bined with an electron transporting oxadiazole-containing structure [350]. Alternating structures containing units of 2,5-bis-trimethylsilyl-*p*-phenylene vinylene, or 2-methoxy-5-(2-ethylhexyloxy)-*p*-phenylene vinylene with *N*-ethyl hexyl-3,6-carbazolevinylene or 9,9-*n*-hexyl fluorenevinyl-lene were prepared via Wittig polycondensation. Among the four combinations the silyl-substituted carbazole co-polymers presented the most interesting properties, for ex-ample, its EL quantum efficiency was 32 times higher than the MEH-PPV analog (film quantum efficiency was 0.81, one of the highest reported). The participation of the silyl group in the PL enhancement and also to the blue shift observed was attributed to its sterical hindrance and lack of electron donating ability as compared to alkoxy substitu-ents [350]. Well defined carbazol-3,9-diyl based oligomer homologues were prepared by the Ullmann condensation and used for multilayer LEDs [351].

The hole conduction of the carbazole unit was studied by comparing polydiphenylacetylene derivatives without and with a carrier transport moiety as poly[1-(*p*-*n*-butylphenyl)2-phenylacetylene] and poly[1(*p*-*n*-carbazolylphenyl)-2-phenylacetylene], respectively. It was shown that hole mobility enhancement by the attachment of the carbazolyl side groups brings about a remarkable improvement in the EL devices. Recently carbazole-imide moieties combined with fluorene were used to prepare LEDs with a brightness of 14,228 cd/m^2, maximum luminous efficiency of 4.53 cd/A and maximum power efficiency of 1.57 lm/W [352]. A write-once read-many-times (WORM) memory device based on an acrylate polymer containing electron donating carbazole pendant groups, or poly(2-(9H-carbazol-9-yl)ethyl methacrylate) (PCz), was demonstrated [353]. Carbazole–pyrene-based compounds when blended to PVK afforded EL devices with green emission with luminance up to 1,000 cd/m^2 [354]. Semiladder poly(*p*-phenylene)s containing carbazole and fluorene moieties exhibited maximum luminescence of 5,500 cd/m^2 and maximum luminance efficiency of 0.556 cd/A in single-layer light emitting devices with pure-blue emission (λ_{max} 447 nm) [355].

A new type of electron-transporting polymer was reported as the first stereoregular polymerization of (*N*-*n*-octyl-3-carbazoyl)acetylene, initiated with a Rh norbornadiene catalyst. The resulting polymers were composed of amorphous *cis*-transoid isomers, called a columnar, with wide range of emitting colors [356].

Light-emitting alternating copolymers of 9,9-dialkylfluorene and *N*-hexylcarbazole with conjugated and δ-Si interrupted structures have been synthesized as an approach or the synthesis of nonaggregating optoelectronic polymers [357].

47.9.5 Other Nitrogen-Containing Conjugated Polymers

Other electron affinity enhancer nitrogen-containing heterocyclic groups include the triazole [358], bithiazole [359] and nonconjugated amino groups as substituents, such as =N(CH3,C6H13) attached to the ring in (poly(2,5-bis(*N*-methyl-*N*-alkylamino)phenylene vinylenes) [360]. In this case the nitrogen atom does not participate in the conjugation system, and its electron donor character provides a stronger donor effect to the amino substituent than the corresponding alkoxy substituents. As mentioned earlier (under transport layers), triamines have been used as hole transport materials. In a recent report, this class of compounds have shown emissive capacity as well, when inserted as pendant groups in conjugated backbones. Single layer devices fabricated from these copolymers can emit light ranging from yellow to bright red, depending on the aromatic units incorporated [361]. The attachment of carbazolyl groups as pendant groups grafted to a backbone

as PMMA, which was blended with MEH-PPV, enhanced the emission four times when compared to that of the pure polymer [362]. Apart from hole transport ability, PVK can interact with low molecular weight compounds or polymers to form new emitting species as exciplexes [363], and consequently bring about a shift in the emission wavelength. In the case of PPPV/PVK [364] mentioned above, where PVK was used both as matrix and hole transport material, the EL spectra of the system tended to blue shift as compared to the respective pure PPP. It was speculated that this was caused by a change in molecular conformation or aggregation of the PPP in the PVK matrix. In blends of the conjugated–nonconjugated multiblock copolymer PPV derivative (CNMBC) with PVK, the EL blue shifted according to PVK increments in the blend. The new emission was attributed to an exciplex formed by the two polymers. As the composition of the blend changed from a PVK-poor to a PVK-rich ratio the emitted light changed from green to blue. Further blends of composition 97/3 (wt%) PVK/block copolymer yielded an EL spectrum with a single emission peak in the blue region different in location from either single component, whereas for a certain range of composition the new peak coexisted with those of the pure components. An exciplex where an excited PVK combines with ground state copolymer was proposed.

47.10 POLYACETYLENES AND POLYMERS WITH TRIPLE BONDS IN THE MAIN CHAIN

47.10.1 Polyacetylenes

Polyacetylene is the first conjugated polymer to exhibit a metallic conductivity. However, polyacetylene shows a very low PL efficiency [365]. Recently, in contrast, a number of good light emitting polyacetylene derivatives have been produced, covering the visible spectrum. The poor solubility of these rod-like structures with concomitant color tuning was addressed in three ways: by substituting the hydrogen atoms with alkyl or aryl groups as done in PPV, by means of copolymerization, or by a combination of both methods. In the first approach many of substituents were tried [366,367]. Monosubstituted polyacetylenes were often referred to as nonluminescent polymers, but the insertion of mesogenic pendants afforded intense blue emitting materials [368] as shown in Fig. 47.19(a). The emission observed from a series of alkyl and phenyl disubstituted polyacetylenes changed from blue-green to pure blue and the luminescence intensity was enhanced when the length of the alkyl side chain increased [369]. This effect was also observed in poly(3-alkylthiophene) and in PPV derivatives [370], indicating that the π–π^* interband transition increases with the length of the side chain, and at the same time the diffusion rate of the excitons to quenching sites is reduced by the longer interchain distances. Examples of EL disubstituted polyace-
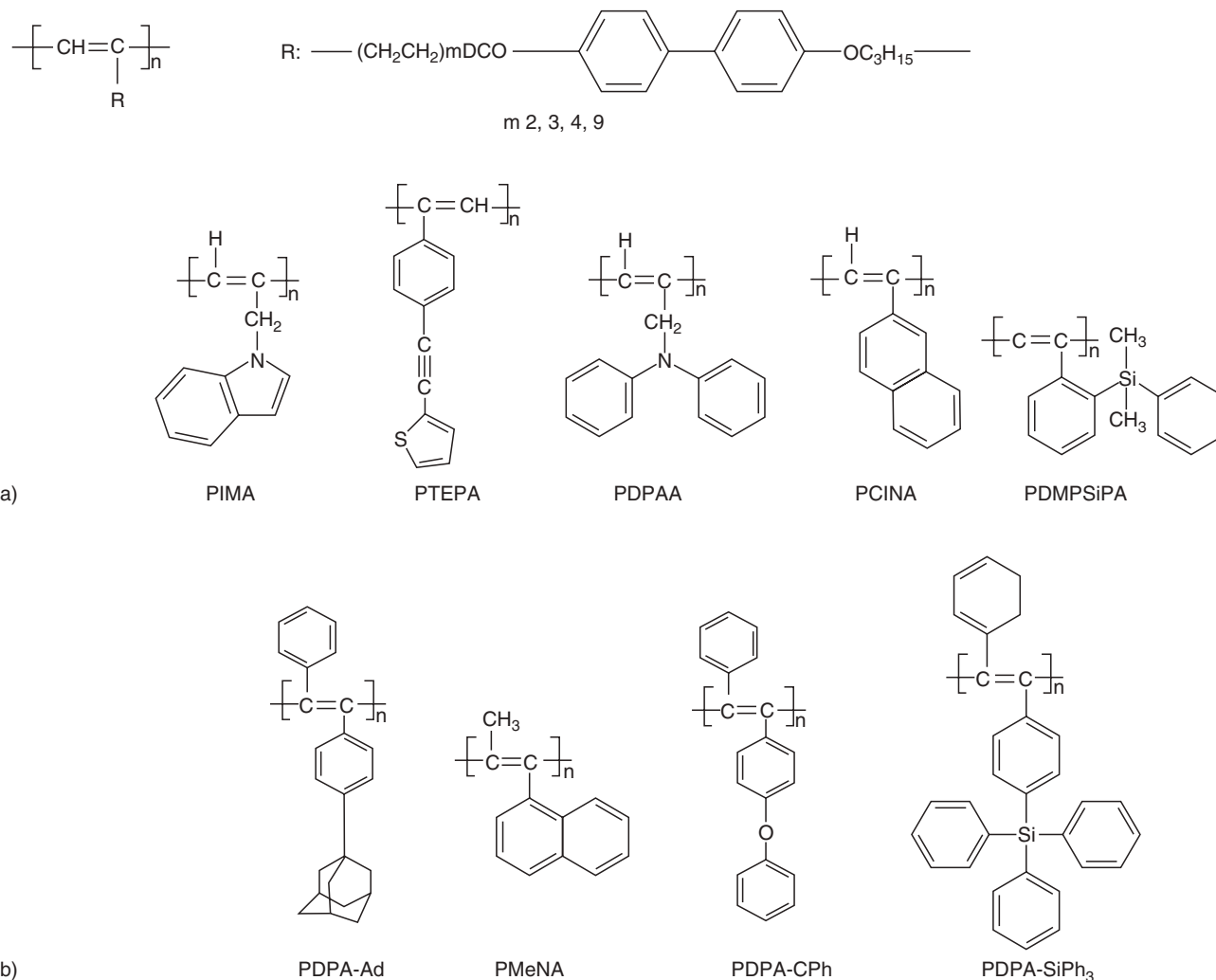
FIGURE 47.19. Examples of EL polyacetylenes. (a) Monosubstituted; (b) disubstituted. Reprinted with permission from Synth Met 1997;91:283. © 1997 Elsevier Science.

tylenes are given in Fig. 47.19(b). Aryl-substituted poly-acetylenes were stable to 200°C in either air or nitrogen, according to thermogravimetric analysis. With the interest in combining the electrooptical properties of PPA and PCz in a CPN film, we have synthesized a series of substituted poly(phenylacetylene)s containing carbazole unit as side groups, which subsequently through. Electropolymerization or chemical oxidation resulted in a conjugated polymer network having both *inter-* and *intra*molecular crosslin-kages between the pendant monomer units [371].

47.10.2 Poly(phenylene ethynylene)s

The HOMO–LUMO energy gap of some alkoxy substi-tuted poly(phenylene ethynylene)s (ROPPE) is higher than that of the corresponding ROPPVs, indicating that introdu-

cing triple bonds in the main chain shortens the effective conjugation length. For example, poly(3,4-dialkyl-1,6-phe-nylene ethynylene) has a bandgap of 3.1 eV [372]. Poly(*p*-phenylene ethynylene)s showed a lower energy barrier for electron injection than for hole injection, in contrast with the PPV analogs. This is an important feature for cathode sta-bility, since more stable metals can be used [373]. A high quantum efficiency was obtained with poly(2,5 dialkoxy-1,4-phenylene ethynylene) (ROPPE) in which the triple bond is equivalent to the double bond in poly(2,5-dialkoxy-1,4-phenylene vinylene) (ROPPV) [374]. Bright blue-green EL was observed from an LED made with the copolymer ROPPE and pyridine (Py) with Al/ROPPE–Py/ITO. In com-parison with PPV it was suggested that the triple bonds in the chain were responsible for the blue shift and enhance-ment of the EL, due to the shortening of the effective conjugation length and effective confinement of the

excitons. However, the effects of the triple bonds were suppressed by the introduction of electron-rich moieties in the chain, such as in poly(2,5-dialkoxy-1,4-phenylene-diethylene-*co*-9,10-anthracenylene) (ROPPE–An). In this case the insertion of the 9,10-anthracenyl group caused a delocalization of the π-electrons and enhancement of inter-chain interactions [372,375].

Linear copolymers containing phenylene ethynylene link-ages have been synthesized using precursor routes [376], inserting *m*-linkages [377] or aliphatic spacers [378,379]. In the precursor route, regular building blocks of *p*-phenylene, norbonadiene, and diethynyl benzene made up the soluble precursor, which was converted to a polymer with enyne units upon the release of cyclopentadiene through a retro-Diels–Alder pathway. The copolymer with phenylene with *m*-linkages made through a Heck-type route, using Pd as catalyst, displayed a PL four times stronger than that of the corresponding *p*-substituted analog. This synthetic method is very often employed in a general way in poly(arylene ethynylene)s chemistry [380]. PPE analogs obtained by copolymerization with di(2-octyldecyl)anthracene yielded stable blue and green emission without chain stacking [381].

REFERENCES

1. Bradley DDC. Synth Met 1993;54(1–3):401–15.
2. Kalinowski J. Electronic processes in organic electroluminescence. In: Miyata S, Nalwa S, editors. Organic Electroluminescent Materials and Devices. Japan: Gordon & Breach; 1997. p. 1.
3. Friend RH, Gymer RW, Holmes AB, Burroughes JH, Marks RN, Taliani C, Bradley DDC, dos Santos DA, Brë das JL, Lö glund M, Salaneck WR. Nature 1999;397:121–8.
4. Cacialli F. Phil Trans R Soc Lond Ser A— Math Phys Eng Sci 2000; 358(1765):173–92.
5. Cacialli F. Curr Opin Colloid Interf Sci 1999;4(2):159–64.
6. Segura JL. Acta Polym 1998;49(7):319–44.
7. Kraft A, Grimsdale A, Holmes AB. Angew Chem Int 1998;37(4):402–28.
8. Mori Y. Single layer organic electroluminescent devices. In: Miyata S, Nalwa S, editors. Organic Electroluminescent Materials and Devices. Japan: Gordon & Breach; 1997. p. 391.
9. Leventis N, Huang L-Y. Polym News 1995;20(10):307–13.
10. Rothberg LJ, Lovinger AJ. J Mater Res 1996;11(12):3174–87.
11. Sheats JR, Chang YL, Roitman DB, Socking A. Acc Chem Res 1999;32(3):193–200.
12. Greiner A. Polym Adv Technol 1998;9(7):371–89.
13. Kim DY, Cho HN, Kim CY. Prog Polym Sci 2000;25(8):1089–139.
14. Conwell EM, Stolka M, Miller MR. Electroluminescent materials, devices and large- screen displays. International Society for Optical Engineering (SPIE) Proceedings, San Jose, CA, 1993.
15. Miyata S, Nalwa HS. Organic Electroluminescent Materials and Devices. Amsterdam: Gordon & Breach; 1997.
16. Hsieh BR, Wei Y. Semiconducting polymers: properties and synthesis. ACS Symp Series 735, American Chemical Society; 1999.
17. Kippelen B, Bradley D. Polymer photonic devices. IV. International Society for Optical Engineering (SPIE) Proceedings, *vol.* 3281, San Jose, CA, 1998.
18. Akcelrud L. Prog Polym Sci 2003;28:875–962.
19. Faraggi EZ, Davidov D, Cohen G, Noah S, Golosovsky M, Avny Y, Neumann R, Lewis A. Synth Met 1997;85(1–3):1187–90.
20. Rogers JA, Bao Z, Dhar L. Appl Phys Lett 1998;73(3):294–6.
21. Li AK, Yang SS, Jean WY, Hsu CS, Hsieh BR. Chem Mater 2000;12(9):2741–4.
22. Clauswitz KUW, Geffarth F, Greiner A, Lüssen G, Wendorff JH. Synth Met 2000;111/ 112:169–71.
23. Miteva T, Meisel A, Grell M, Nothofer HG, Lupo D, Yasuda A, Knoll W, Kloppenburg L, Bunz UHF, Sherf U, Neher D. Synth Met 2000;111/ 112:173–6.
24. Jandke M, Strohriegl P, Gmeiner J, Brütting W, Schwoerer M. Synth Met 2000;111/ 112:177–80.
25. Contoret AEA, Farrar SR, Jackson PO, Khan SM, May L, O' Neill M, Nicholls JES, Kelly M. Richards G. Adv Mater 2000;12(13):971–4.
26. Grell M, Bradley DDC, Inbasekaran M, Woo EP. Adv Mater 1997;9(10):798.
27. Peeters E, Christiaans MPT, Janssen RAJ, Scoo HFM, Dekkers HP JM, Meijer EW. J Am Chem Soc 1997;119(41):9909–10.
28. Das S, Pal AJ. Langmuir 2002;18:458–61.
29. Tsukruk VV, Bliznyuk VN, Visser D, Campbell AL, Bunning TJ, Visser WW. Macromolecules 1997;30:6615–25.
30. Yang SY, Rubner MF. J Am Chem Soc 2002;124(10):2100–1.
31. Tang J, Li WJ, Wang Y, Wang B, Sun J, Yang B. J Photochem Photobiol A: Chem 2001;141:179–82.
32. Kaminorz Y, Smela E, Johansson T, Brehmer L, Anderson MR, Inganä s O. Synth Met 2000;113(1/ 2):103–14.
33. Speakman SP, Rozenberg GG, Clay KJ, Milne WI, Ille A, Gardner IA, Bresler E, Steinke JHG. Org Electron 2001;2:65–73.
34. Kobayashi H, Kanbe S, Seki S, Kigchi H, Kimura M, Yudasaka I, Miyashita S, Shimoda T, Towns CR, Burroughes JH, Friend RH. Synth Met 2000;111/ 112:125–8.
35. Pede D, Serra G, Rossi DD. Mater Sci Eng 1998;C5:289–91.
36. Panin GN, Kang TW, Lee H. Physica E 2004;21:1074–8.
37. Dreuth H, Heiden C. Mater Sci Eng 1998;C5:227–31.
38. Adachi C, Kwong R, Forrest SR. Org Electron 2001;2:37–43.
39. Guo TF, Chang SC, Yang Y, Kwong RC, Thompson ME. Org Electron 2000;1:15–20.
40. Lee CL, Lee KB, Kim JJ. Mater Sci Eng 2001;B85:228–31.
41. Samuel IDW, Crystall B, Rumbles G, Burn PL, Holmes AB, Friend RH. Chem Phys Lett 1993;213(5/ 6):472–8.
42. Malliaras GG, Scott JC. J Appl Phys 1998;83(10):5399–403.
43. Vestweber H, Pohmerehne J, Sander R, Mahrt RF, Greiner A, Heitz W, Bä ssler H. Synth Met 1995;68(3):263–8.
44. Blom PWM, Jong MJM. IEEE J Sel Top Quant Electron 988; 4(1):105–12.
45. Barth S, Bassler H, Hertel D, Nikitenko VI, Wolf U. Pure Appl Chem 1999;71(11):2067–77.
46. Davids PS, Kogn SM, Parker ID, Smith DL. Appl Phys Lett 1996;69(15):2270–2.
47. Conwell EM, Wu MW. Appl Phys Lett 1997;70(14):1867–9.
48. Bassler H. Polym Adv Technol 1998;9(7):402–18.
49. Jenekhe AS, Osaheni JA. Science 1994;265(5173):765–8.
50. Conwell E. Trends Polym Sci 1997;5(7):218–22.
51. Conwell E. Phys Rev B 1998;57(22):14200–2.
52. Beljonne D, Shuai Z, Cornil J, Calbert JP, Bré das JL. J Photochem Photobiol A: Chem 2001;144:57–62.
53. Hsu JWP, Yan M, Jedju TM, Rothberg LJ, Hsieh BR. Phys Rev B 1994;49(1):712–5.
54. Rothberg LJ, Yan M, Papadimitrakopoulos F, Galvin ME, Kwock EW, Miller TM. Synth Met 1996;80(1):41–58.
55. Wu MW, Conwell E. Phys Rev B 1997;56(16):R10060–2.
56. Yan M, Rothberg LJ, Kwock EW, Miller M. Phys Rev Lett 1995;75(10):1992–5.
57. Samuel ID, Rumbles G, Collison CJ, Friend RH, Moratti SC, Holmes AB. Synth Met 1997;84(1):497–500.
58. Shi Y, Liu J, Yang Y. J Appl Phys 2000;87(9):4254–63.
59. Jakubiak R, Rothberg LJ, Wan W, Hsieh BR. Synth Met 1999;101(1):230–3.
60. Nguyen TQ, Martini IB, Liu J, Schwartz BJ. J Phys Chem B 2000;104(2):237–55.
61. Samuel ID, Rumbles G, Collison CJ. Phys Rev B 1995;52(16): R11573–6.
62. Blatchford JW, Gustafson TL, Epstein AJ, Vandenbout D, Kerimo A, Higgins DA, Barbara PF, Fu DK, Swager TM, MacDiarmid AG. Phys Rev B 1996;54(6):R3683–6.
63. Aguiar M, Fugihara MC, Hummelgen IA, Peres LO, Garcia JR, Gruber J, Akcelrud L. J Lumin 2002;96:219–25.

64. Aguiar M, Karasz FE, Akcelrud L. Macromolecules 1995;28(13):4598–602.
65. Aguiar M, Hu B, Karasz FE, Akcelrud L. Macromolecules 1996;29(9):3161–6.
66. Aguiar M, Hu B, Karasz FE, Akcelrud L. Macromol Chem Phys 1998;199(7):1255–61.
67. Gruner JF, Friend RH, Scherf U, Huber J, Holmes AB. Adv Mater 1994;6(10):748–52.
68. Martin SJ, Cadby AJ, Lane PA, Bradley DDC. Synth Met 1999;101(1):665–6.
69. Rumbles G, Samuel IDW, Collison CJ, Miller PF, Moratti SC, Holmes AB. Synth Met 1997;101(1–3):158–61.
70. Collison CJ, Rothberg LJ, Treemaneekarn V, Li Y. Macromolecules 2001;34(7):2346–52.
71. Brown AR, Bradley DDC, Burroughs JH, Friend RH, Greenham NC, Burn PL, Holmes AB, Kraft A. Appl Phys Lett 1992;61(23):2793–5.
72. Bradley DDC, Friend RH. J Phys Condens Matter 1989; 1(23): 3671–8.
73. Ziemelis KE, Hussain AT, Bradley DDC, Friend RH, Ruhe J, Wegner G. Phys Rev Lett 1991;66(17):2231–4.
74. Romero DB, Schaer M, Leclerc M, Ad' es D, Siove A, Zuppiroli L. Synth Met 1996;80(3):271–7.
75. Kido J, Shinoya H, Nagai K. Appl Phys Lett 1995;67(16):2281–3.
76. Yamamoto T, Suganuma H, Saitoh Y, Maruyama T, Inoue T. Jpn J Appl Phys, Part 2: Lett 1996;35(9A):L1142–4.
77. Cao Y, Treacy GM, Smith P, Heeger AJ. Appl Phys Lett 1992;60(22):2711–3.
78. Yang Y, Heeger AJ. Appl Phys Lett 1994;64(10):1245–7.
79. Scott JC, Carter SA, Karg S, Angelopoulos M. Synth Met 1997;85(1–3):1197–200.
80. Yang Y, Westerweele E, Zhang C, Smith P, Heeger AJ. J Appl Phys 1995;77(2):694–8.
81. Yan M, Rothberg LJ, Papadimitrakopoulos F, Galvin ME, Miller TM. Phys Rev Lett 1994;72(7):1104–7.
82. Hayashi S, Etoh H, Saito S. Jpn J Appl Phys, Part 2: Lett 1986; 25(9):L773–5.
83. Wessling RA. J Polym Sci, Polym Symp 1985; 72:55–66.
84. Wessling RA, Zimmerman RG. US Patent 3,401, 152; 1968.
85. Machado JM, Karasz FE, Kovar RF, Burnett JM, Druy MA. New Polym Mater 1989; 1(3):189–207.
86. Karasz FE, Capistran JD, Gagnon DR, Lenz RW. Mol Cryst Liq Cryst 1985; 118(1–4):327–32.
87. Denton FR, Lahti PM, Karasz FE. J Polym Sci, Part A: Polym Chem 1992;30(10):2223–31.
88. Montaudo G, Vitalini D, Lenz RW. Polymer 1987; 28(5):837–42.
89. Murase I, Ohnishi T, Noguchi T, Hirooka M. Polym Commun 1984; 25(11):327–9.
90. Capistran JD, Gagnon DR, Antoun S, Lenz RW, Karasz FE. ACS Polym Prepr 1984; 25(2):282–3.
91. Gagnon DR, Capistran JD, Karasz FE, Lenz RW. Polym Bull 1984; 12(4):293–8.
92. Denton FR, Lahti PM. Synthesis and properties of poly (phenylene vinylene)s and related poly(arylene vinylene)s. In: Wise DL, Wnech GE, Trantolo DJ, Cooper TM, Gresser JD, editors. Photonic Polymer Systems: Fundamentals, Methods and Applications; 1998, p. 61–102, chapter 3; see also page 9.
93. Tokito S, Momii T, Murata H, Tetsui T, Saito S. Polymer 1990; 31(6):1137–41.
94. Burn PL, Bradley DDC, Brown AR, Friend RH, Holmes AB. Synth Met 1991;41(1/ 2):261–4.
95. Gowri R, Padmanaban G, Ramakrishnan S. Synth Met 1999;101:166.
96. Padmanaban G, Ramakrishnan S. J Am Chem Soc 2000;122(10):2244–51.
97. Colaneri NF, Bradley DDC, Friend RH, Burn PL, Holmes AB, Spangler CW. Phys Rev B: Condens Matter 1990; 42(18):11670–81.
98. Askari SH, Rughooputh SD, Wudl F. Polym Mater Sci Eng Proc 988; 59:1068–70.
99. Patil AO, Rughooputh SD, Heeger AJ, Wudl F. ACS Polym Mater Sci Eng Proc 1988; 59:1071–3.
100. Machado JM, Denton FR, Shlenoff JB, Karasz FE, Lahti PM. J Polym Sci, Phys Ed 989; 27(1):199–203.
101. Burn PL, Bradley DDC, Friend RH, Halliday DA, Holmes AB, Jackson RW, Kraft A. J Chem Soc, Perkin Trans 1992;23:3225–31.
102. Rughooputh HSD, Wudl F, Heeger AJ. ACS Polym Prepr 1989; 30(1):157–60.
103. Sonoda Y, Kaeriyama K. Bull Chem Soc Jpn 1992;65(3):853–7.
104. Doi S, Kuwabara M, Noguchi T, Ohnishi T. Synth Met 1993;57(1):4174–9.
105. Paulvannan K, Feld WA. ACS Polym Prepr 1991;32(1):192–3.
106. Egbe DAM, Ulbricht C, Orgis T, Carbonnier B, Kietzke T, Peip M, Metzner M, Gericke M, Birckner E, Pakula T, Neher D, Grummt U-W. Chem Mater 2005;17:6022–32.
107. Braun D, Heeger AJ. Visible Appl Phys Lett 1991;58(18):1982–4.
108. Braun D, Heeger AJ, Kroemer H. J Eletron Mater 1991;20:945.
109. Aratani S, Zhang C, Pakbaz K, Hoger S, Wudl F, Heeger AJ. Electron Mater 1993;22(7):745–9.
110. Wudl F, Hoger S, Zhang C, Pabkaz K. ACS Polym Prepr 1993;34(1):197–8.
111. Gilch HG, Wheelright WL. J Polym Sci, Part A 1996;4:1337.
112. Hoerhold HH, Raabe D. Acta Polym 1979; 30(2):86–92.
113. Hoerhold HH, Ozegowski JH, J Prakt Chem 1977; 319(4):622–6.
114. Swatos WJ, Gordon B. ACS Polym Prepr 1990; 31(1):505–6.
115. Hsieh BR, Feld WA. ACS Polym Prepr 1993;34(2):410–1.
116. Hsieh BR, Razafitrimo H, Gao Y, Nijakowski TR, Feld WA. ACS Polym Prepr 1995;36(2):85–6.
117. Wan WC, Gao Y, Goodwin TE, Gonzalez SA, Feld WA, Hsieh BR. Macromol Symp 1997;125:205.
118. Hsieh BR, Yu Y, Forsythe EW, Schaaf GM, Feld WA. J Am Chem Soc 1998;120(1):231–2.
119. Wan WC, Cao Y, Salomone JC. Polymeric Materials Encyclopedia. Boca Raton, FL: CRC Press, Inc.; 1996, chapter 6; p. 6537.
120. Hsieh BR, Antoniadis H, Bland DC, Feld WA. Adv Mater 1995;7(1):36–8.
121. Westveber H, Greiner A, Lemmer U, Richert R, Heitz W, Bassler H. Adv Mater 1992;4(2):661–2.
122. Johansson DM, Srdanov G, Yu G, Theander M, Inganäs O, Andersson M. Macromolecules 2000;33(7):2525–9.
123. Gurge RM, Sarker A, Lahti PM, Hu B, Karasz FE. Macromolecules 1996;29(12):4287–92.
124. Kim JJ, Kang SW, Hwang DH, Shim HK. Synth Met 1993;57(1):4024–8.
125. Sarker A, Lahti PM, Garay RO, Lenz RW, Karasz FE. Polymer 1994;35(6):1312–6.
126. Höger S, McNamara JJ, Schricker S, Wudl F. Chem Mater 1994;6(2):171–3.
127. Vanderzande DJ, Isaaris AC, Van der Borght MJ, Van Breemen A, Kokk M, Gelan JM. Macromol Symp 1997;125:189–203.
128. Van der Borght M, Adriaensens P, Vanderzande D, Gelan J. Polymer 2000;41(8):2743–53.
129. Martelock H, Greiner A, Heitz W. Makromol Chem 1991;192(4):967–79.
130. Bradley DDC. Adv Mater 1992;4(11):756–9.
131. Greenham NC, Samuel LDW, Hayes GR, Phillips RT, Kessener YARR, Moratti SC, Holmes AB, Friend RH. Chem Phys Lett 1995;241(1/2):89–96.
132. Anderson MR, Yu G, Heeger AJ. Synth Met 1997;85(1–3):1275–6.
133. Chen K-B, Li H-C, Chen C-K, Yang S-H, Hsieh BR, Hsu C-S. Macromolecules 2005;38:861724.
134. Henckens A, Duyssens I, Lutsen L, Vanderzande D, Cleij TJ. Polymer 2006;47:123–31.
135. Liang F, Pu Y- J, Kurata T, Kido J, Nishide H. Polymer 2005;46:3767–75.
136. Zhang Q, Yang M, Wu P, Ye H, Liu X. Mater Sci Eng, B 2004;113:130–35.
137. Mikroyannidis JA. Synth Met 2005;155:125–29.
138. Hu J, Meng F, Li J, Ding F, Fan X, Tian H. Eur Polym J 2006; 42:2686–2694.
139. Chen Y, Midorikawa T, Bai J, Liu Y, Araki Y, Itob O. Polymer 2005;46:9803–9.
140. Gupta R, Stevenson M, Dogariu A, McGehee MD, Park JY, Srdanov V, Heeger AJ. Appl Phys Lett 1998;73(24):3492–4.
141. Kang IN, Hwang DH, Shim HK, Zyung T, Kim JJ. Macromolecules 1996;29:165–9.
142. Cornil J, Beljonne D, Santos DA, Bredas JL. Synth Met 1996;76(1–3):101–4.
143. Woo HS, Lhost O, Graham SC, Brédas JL, Schenk R, Mullen K. Synth Met 1993;59(1):13–28.

144. Tian B, Zerbi G, Schenk R, Mullen K. J Chem Phys 1991;95(5):3191–207.
145. Ohnishi T, Doi S, Tsuchida Y, Noguchi T. IEEE Trans Electron Devices 1997;44(8):1253–7.
146. von Seggern H, Wnkel PS, Zhang C, Schimdt HW. Macromol J Chem Phys 1994;195(1–3):2023–37.
147. Zheng S, Shi J, Mateu R. Chem Mater 2000;12(7):1814–7.
148. Yang Z, Hu B, Karasz FE. J Macromol Sci, Pure Appl Chem 1998;A35(2):233–47.
149. Hu B, Yang Z, Karasz FE. J Appl Phys 1994;76(4):2419–22.
150. Sokolik I, Yang Z, Morton DC, Karasz FE. J Appl Phys 1993;74(5):3584–6.
151. Hu B, Morton DC, Sokolik I, Yang Z, Karasz FE. J Lumin 1994;60/61:919–22.
152. Zhang C, Braun D, Heeger AJ. J Appl Phys 1993;73(10):5177–80.
153. Sun RG, Wang YZ, Wang DK, Zheng QB, Kyllo EM, Gustafson TL, Wang F, Epstein AJ. Synth Met 2000;111/112(1):595–602.
154. Kyllo EM, Gustafson TL, Wang DK, Sun RG, Epstein AJ. Synth Met 2001;116(1–3):189–92.
155. Burn PL, Holmes AB, Kraft A, Bradley DDC, Brown AR, Friend RH, Gymer RW. Nature 1992;356(6364):47–9.
156. Hay M, Klavetter FL. J Am Chem Soc 1995;117(27):7112–8.
157. Ahn T, Jang MS, Shim H- K, Hwang D- H, Zyung T. Macromolecules 1999;32(10):3279–85.
158. Yang Z, Sokolik I, Karasz FE. Macromolecules 1993;26(5):1188–90.
159. Hu B, Karasz FE. Synth Met 1998;92(2):157–60.
160. Cacialli F, Chuah BS, Friend RH, Moratti SC, Holmes AB. Synth Met 2000;111/ 112(1):155–8.
161. Wang H, Li QSY, Li X. Thin Solid Films 2003;426:40–46.
162. Stone DA, Chang YK, Allcock HR. J Polym Sci, Part A: Polym Chem 2006;44(1):69–76.
163. Aguiar M, Karasz FE, Hu B, Akcelrud L. Macromol Chem Phys 1998;199(7):1255–61.
164. Aguiar M, Karasz FE, Hu B, Akcelrud L. Synth Met 1995;71(1–3):2189–90.
165. Bisberg J, Cumming WJ, Gaudiana RA, Hutchison KD, Ingwall RT, Kolb ES, Mehta PG, Minns RA, Petersen CP. Macromolecules 1995;28:386–9.
166. Yoon CB, Shim HK. Synth Met 2000;111/ 112:469.
167. Chung SJ, Kwon KY, Lee SK, Jin J- II, Lee CH, Lee CE, Park Y. Adv Mater 1998;10(14):1112–6.
168. Jang JW, Oh DK, Lee CH, Lee CE, Lee DW, Jin J- II. J Appl Phys 2000;87(6):3183–5.
169. Chung SJ, Jin J, Kim KK. Adv Mater 1997;9(7):551–4.
170. Lee CH, Ryyu SH, Jang HD, Oha SY. Mater Sci Eng, C 2004;24:87–90.
171. Garten F, Vrijmoeth J, Schatmann AR, Gill RE, Klapwijk TM, Hadziiiannou G. Synth Met 1996;76(1–3):85–9.
172. Yoshino K, Nakajima S, Park DH, Sugimoto R. Jpn J Appl Phys: Part 2 1988; 27(4):L716–8.
173. Yoshino K, Love P, Onoda M, Sujimoto R. Jpn J Appl Phys: Part 2 1988; 27(12):L2388–91.
174. Ohmori Y, Uchida M, Muro K, Yoshino K. Jpn J Appl Phys 1991;30:L1938.
175. Ohmori Y, Uchida M, Muro K, Yoshino K. Solid State Commun 1991;80:605.
176. Granströ m M, Inganä s O. Appl Phys Lett 1996;68(2):147–9.
177. Braun D, Gustafsson G, McBranch D, Heeger AJ. J Appl Phys 1992;72(2):564–8.
178. Uchida M, Ohmori Y, Morishima C, Yoshino K. Synth Met 1993;55–57:4168.
179. Ohmori Y, Morishima C, Uchida M, Yoshino K. Jpn J Appl Phys 1992;31(Pt 2(5A)):L568.
180. Inganäs O. Making polymer light emitting diodes with polythiophenes. In: Miyata S, Nalwa HS, editors. Organic Electroluminescent Materials and Devices. Amsterdam: Gordon & Breach; 1997.
181. McCullough RD, Tritsram-Nagle S, Williams SP, Lowe RD, Jayaraman M. J Am Chem Soc 1993;115(11):4910–1.
182. Anderson MR, Beggren M, Inganas O, Gustafsson G. Macromolecules 1995;28(22):7525–9.
183. Berggren M, Inganäs O, Gustaffson G, Anderson MR, Hjertberg T, Wennerström O. Synth Met 1995;71:2185.
184. Theander M, Anderson MR, Inganä s O. Synth Met 1999;101:331.
185. Ahn SH, Czae MZ, Kim ER, Lee H, Han SH, Noh J, Hara M. Macromolecules 2000;34:2522.
186. Skabara PJ, Serebryakov I, Perepichka IF, Sariciftci NS, Neugebauer H, Cravino A. Macromolecules 2001;34:2232.
187. Greenham NC, Brown AR, Bradley DDC, Friend RH. Synth Met 1993;55–57:4134.
188. Ogawa K, Sttaford JA, Rothstein SD, Tallman DE, Rassmunsen S. Synth Met 2005;152:137–40.
189. Pei J, Yu W-L, Huang W, Heeger AJ. Macromolecules 2000; 33:2462.
190. Vamvounis G, Yu J, Holdcroft S. Eur Polym J 2004;40:2659–64.
191. Huang W, Yu WL, Meng H, Pei J, Li SFY. Chem Mater 1998;10:3340.
192. Huang W, Meng H, Yu WL, Pei J, Chen ZK, Lai YH. Macromolecules 1999;32:118.
193. Roman LS, Inganäs O. Synth Met 2002;125:419–22.
194. Wanga X, Anderssn MR, Thompson ME, Inganäs O. Thin Solid Films 2004;468:226–33.
195. Wang XJ, Andersson MR, Thompson ME, Ingana O. Synth Met 2003;137:1019–20.
196. Wu C-G, Hsieh C-W, Chen D-C, Chang S-J, Chen K-Y. Synth Met 2005;155:618–22.
197. Wu C-G, Lin Y-C, Wu C-E, Huang P-H. Polymer 2005;46:3748–57.
198. Bolognesi A, Schieroni AG, Botta C, Marinelli M, Mendichi R, Rolandi R, Relini A, Inganäs O, Theandher M. Synth Met 2003;139:303–10.
199. Greenham NC, Moratti SC, Bradley DDC, Friend RH, Holmes HB. Nature 1993;365(6447):628–30.
200. Holoch M, Segura JL, Dottinger SE, Hohnholz D, Steinhuber E, Spreitzersand H, Hanack M. Synth Met 1997;84:319.
201. Staring EGL, Demandt RCJE, Braun D, Rikken GLJ, Kessener YARR, Ven Huizen AHJ, Van Knippenberg MMF, Bowmans M. Synth Met 1995;71:2179.
202. Baigent DR, Holmes AB, Moratti SC, Friend RH. Synth Met 1996;80:119.
203. Grem G, Leditzky G, Ulrich B, Leising G. Adv Mater 1992;4(1): 36–7.
204. Moratti SC, Bradley DDC, Friend RH, Greenham NC, Holmes AB. Mater Res Soc Symp Proc 1994;328:371–6.
205. Moratti SC, Bradley DDC, Friend RH, Greenham NC, Holmes AB, Cervini R. Proc SPIE 1994;2144:108–14.
206. Ryu H, Subramanian LR, Hanack M. Tetrahedron 2006;62:6236–47.
207. Moratti SC, Bradley DDC, Friend RH, Greenham NC, Holmes AB. Polym Prepr ACS 1994;35:214.
208. Peng ZH, Galvin ME. Chem Mater 1998;10(7):1785–8.
209. Xiao Y, Yu WL, Pei J, Chen Z, Huang W, Heeger AJ. Synth Met 1999;106:165.
210. Pinto MR, Hu B, Karasz FE, Akcelrud L. Polymer 2000;41: 8095–102.
211. Moratti SC, Cervini R, Holmes AB, Baigent DR, Friend RH, Greenham NC, Gruner J, Hamer PL. Synth Met 1995;71:2117.
212. Brë das JL, Heeger AJ. Chem Phys Lett 1994;217(6/ 5):507–12.
213. Pucci A, Biver T, Ruggeri G, Meza LI, Pang Y. Polymer 2005;46:11198–205.
214. Miller PF, de Souza MM, Moratti SC, Holmes AB, Samuel IDW, Rumbles G. Polym Int 2006;55(7):784–92.
215. Chasteen SV, Carter SA, Rumbles G. J Chem Phys 2006;124:214704–5.
216. Kim Y-H, Shin D-C, Kwon S-K. Polymer 2005;46:4647–53.
217. Yamamoto T, Morita A, Muyazaki Y, Maruyama T, Wakayama H, Zhou Z-H, Nakamura Y, Kanbara T, Sasaki S, Kubota K. Macromolecules 1992;25(4):1214–23.
218. Suzuki A. J Organomet Chem 1999;576(1/ 2):147–68.
219. Schlüter AD. J Polym Sci, Part A: Polym Sci 2001;39(10):1533–56.
220. Liu C, Yu WL, Lai YH, Huang W. Chem Mater 2001;13(6):1984–91.
221. Lögdlund M, Salaneck WR, Meyers F, Brédas JL, Arbuckle GA, Friend RH, Holmes AB, Froyer G. Macromolecules 1993;26(15): 3815–20.
222. Remmers M, Schulze M, Wegner G. Macromol Rapid Commun 1996;17:239–52.
223. Remmers M, Müller B, Martin K, Räder HJ, Köhler W. Macromolecules 1999;23(4):1073–9.
224. Scherf U, Mullen K. ACS Symposium 1997, chapter 4; p. 358.

225. Grem G, Leditzky G, Ulrich B, Leising G. Synth Met 1992;51 (1–3):383–9.
226. Chmil K, Scherf U. Makromol Chem Rapid Commun 1993;14(4):217–22.
227. Fahnenstich U, Koch KH, Pollmann M, Scherf U, Wagner M, Wegener S, Mullen K. Makromol Chem Makromol Symp 1992;54/55:465–76.
228. Scherf U, Mullen K. Makromol Chem Rapid Commun 1991;12:489–97.
229. Stampfl J, Graupner W, Leising G, Scherf U. J Lumin 1995;63:117–23.
230. Graupner W, Mauri M, Stampfl J, Leising G, Scherf U, Mullen K. Solid State Commun 1994;91(1):7–12.
231. Grem G, Leising G. Synth Met 1993;57(1):4105–10.
232. Xia C, Advincula R. Macromolecules 2001;34:6922.
233. Edwards A, Blumstengel S, Sokolik I, Yun H, Okamoto Y, Dornsinville R. Synth Met 1997;84:639.
234. Mishra AK, Graf M, Grasse F, Jacob J, List EJW, Müllen K. Chem Mater 2006;18:2879–85.
235. Yang Y, Pei Q. Appl Phys Lett 1997;81(7):3294–8.
236. Klaerner G, Miller RD. Macromolecules 1998;31(6):2007–9.
237. Kreyenschimdt M, Klaerner G, Fuhrer T, Ashenhurst J, Karg S, Chen W, Lee VY, Scott JC, Miller RD. Macromolecules 1998;31(4):1099–103.
238. Klärner G, Davey MH, Chen WD, Scott JC, Miller RD. Adv Mater 1998;10(13):993–7.
239. Bliznyuk VN, Carter SA, Scott JC, Klärner G, Miller RD. Macromolecules 1999;32(2):361–9.
240. Rehahn M, Schlüter AD, Wegner G. Macromol Chem 1990;191(9):1991–2003.
241. Rehahn M, Schlüter AD, Wegner G, Feast WJ. Polymer 1989;30(6):1054–9.
242. Bradley DDC, Grell M, Grice A, Tajbakhsh AR, O' Brien DF, Bleyer A. Opt Mater 1998;9:1–11.
243. Inbasekaran M, Wu W, Woo EP. US Patent 5,777,070 to Dow Company; 1998.
244. Inbasekaran M, Shiang WR, Woo EP, Roof GR. US Patent 5,962,631 to Dow Company; 1999.
245. Lin H-C, Sung H- H, Tsai C-M, Li K-C. Polymer 2005;46:9810–20.
246. Inbasekaran M, Woo EP, Wu W, Bernius M, Wujkowski L. Synth Met 2000;111/ 112:397.
247. Wong W-Y, Liu L, Cui D, Leung LM, Kwong C-F, Lee T-H, Ng H-F. Macromolecules 2005;38:4970–6.
248. Wang ZJ, Yang XH, Chen XH, Xu Z, Xu XR. Thin Solid Films 2000;363(1/ 2):94–7
249. Meng H, Huang W. J Organomet Chem 2000;65(13):3894–901.
250. Lee SH, Nakamura T, Tsutsui T. Org Lett 2001;3(13):2005–7.
251. Zhan X, Liu Y, Zhu D, Huang W, Gong Q. Chem Mater 2001;13:1540–4.
252. Ding J, Day M, Robertson G, Roovers Macromolecules 2002;35:3474–83.
253. Assaka AM, Rodrigues PC, de Oliveira ARM, Ding L, Hu B, Karasz FE, Akcelrud L. Polymer 2004;45:7071–81.
254. Perzon E, Wang X, Admassie S, Inganäs O, Andersson MR. Polymer 2006;47:4261–68.
255. Kim JH, You N-H, Lee H. J Polym Sci Part A: Polym Chem 2006;44:3729–37.
256. Buchgraber C, Pogantsch A, Kappaun S, Spanring J, Kern W. J Polym Sci, Part A: Polym Chem 2006;44:4317–27.
257. Peng Q, Kang ET, Neoh KG, Xiaob D, Zou D. J Mater Chem 2006;16:376–83
258. Cao DD, Liu Q, Zeng W, Han S, Peng J, Liu S. J Polym Sci, Part A: Polym Chem 2006;44:2395–405.
259. Yang G- Z, Wu M, Lu S, Wang M, Liu T, Huan W. Polymer 2006;47:4816–23.
260. Yang R, Tian R, Yan J, Zhang Y, Yang J, Hou Q, Yang W, Zhang C, Cao Y. Deep- Red Macromolecules 2005;38:244–53.
261. Cho NS, Hwang D-H, Jung B-J, Lim E, Lee J, Shim H-K. Macromolecules 2004;37:5265–73.
262. Mikroyannidis JA. J Polym Sci, Part A: Polym Chem 2006;44:4015–26.
263. Zhou X- H, Zhang Y, Xie Y- Q, Cao Y, Pei J. Macromolecules 2006;39:3830–40.
264. Liu C- H, Chen S- H, Chen Y. J Polym Sci, Part A: Polym Chem 2006;44:3882–95.
265. An BK, Kim YH, Shin DC, Park SY, Yu HS, Kwon SK. Macromolecules 2001;34:3993–7.
266. Song SY, Jang MS, Shim HK, Song IS, Kim WH. Synth Met 1999;102:1116.
267. Becker S, Ego C, Grimsdale AC, List EJW, Marsitzky D, Pogantsch A, Setayesh S, Leising G, Mullen K. Synth Met 2002;125:73–80.
268. Setayesh S, Grimsdale AC, Weil T, Enkelmann V, Müllen K, Meghdadi F, List EJW, Leising G. J Am Chem Soc 2001;123: 946–53.
269. Chou C- H, Wang H- S, Wei K- H, Huang JY. Adv Funct Mater 2006;16:909–16.
270. Chen K- B, Chen H- Y, Yang S- H, Hsu C- S. J Polym Res 2006;13:237–45
271. Ding L, Bo Z, Chu Q, Li J, Dai L, Pang Y, Karasz FE, Durstock MF. Macromol Chem Phys 2006;207:870–78.
272. Zhan X, Liu Y, Wu X, Wang S, Zhu D. Macromolecules 2002;35:2529–37.
273. Klaerner G, Lee JI, Lee VY, Chan E, Chen JP, Nelson A, Markiewicz D, Siemens R, Scott JC, Miller RD. Chem Mater 1999;11:1800–5.
274. Chen JP, Klaerner G, Lee JI, Markiewicz D, Lee VY, Miller RD, Scott JC. Synth Met 1999;107:129–35.
275. Chen Y, Araki Y, Doyle J, Strevens A, Ito O, Blau WJ. Chem Mater 2005;17:1661–6.
276. Wu W- C, Lee W- Y, Chen W- C. Macromol Chem Phys 2006;207:1131–38.
277. Yoshida M, Fujii A, Ohmori Y, Yoshino K. J Appl Phys Lett 1996;69(6):734–6.
278. Setayesh S, Marsitzky D, Müllen K. 2000;33:2016–20.
279. Sandee AJ, Williams CK, Evans NR, Davies JE, Boothby CE, Köhler A, Friend RH, Holmes AB. J Am Chem Soc 2004;126:7041–8.
280. Hoshino S, Furukawa K, Ebata K, Yuan C- H, Suzuki H. J Appl Phys 2000;88(5):2892–7.
281. Stolka M, Yuh HJ, McGrane K, Pai DM. J Polym Sci: Part A 1987;25(3):823–7.
282. Xu YH, Fujino T, Naito H, Oka K, Dohmaru T. Chem Phys Lett 1998;4:299–300.
283. Suzuki H, Hoshino S, Yuan CH, Fujiki M, Toyoda S. IEEE J Sel Top Quant Electron 1998;4(1):129–36.
284. Suzuki H, Hoshino S, Yuan CH, Fujiki M, Toyoda S, Thin Solid Films 1998;331(1/ 2):64–70.
285. Kamata N, Aihara S, Umeda M, Kanezaki S, Nagumo K, Terunuma D, Yamada JK. Luminescence 2000;87(9):1186–8.
286. Fujii A, Yoshida M, Yoshimoto K, Ohmori Y, Yoshino K, Ueno H, Kakimoto M, Kojima H. Synth Met 1997;85:1261.
287. Ito O, Terzima T, Azumi T, Matsumoto N, Takeda K, Fujino M. Macromolecules 1989; 22(4):1718–22.
288. Tonzola CJ, Alam MM, Jenekhe SA. Opt Mater 2002;21:135–142.
289. Satoh S, Suzuki H, Kimata Y, Kuriyama A. Synth Met 1996;79:97.
290. Paik KL, Baek NS, Kim HK, Lee J- H, Lee Y. Opt Mater 2002:21135–42.
291. Park JS, Kim KD, Jung SH, Kim HK, Jeoung SC, Kim YH, Kim D. Synth Met 1999;102:106.
292. Pohl A, Bredas JL. Int J Quant Chem 1997;63(2):437–40.
293. Gill RE, Malliaras GG, Wilderman J, Hadziioanou G. Adv Mater 1994;6:132–6.
294. Kim HK, Ryu MK, Cho SW, Park JW. Macromolecules 1998;31:1114.
295. Garten F, Hilberer A, Cacialli F, Essenlink FJ, Van Dam Y, Schlatmann AR, Friend RW, Klapwijk TM, Hadziioannou G. Synth Met 1997;85:1253–4.
296. Ryu MK, Lee JH, Lee SM, Zyung T, Kim HK. ACS Polym Mater Sci Eng Proc 1996;75(2):408–12.
297. Jung SH, Kim HK. J Lumin 2000;87(9):51–5.
298. Rost H, Chuah BS, Hwang DH, Moratti SC, Holmes AB, Wilson J, Morgado J, Halls JJM, DeMello JC, Friend RH. Synth Met 1999;102:937–42.
299. Zhang Q, Yanga M, Wu P, Ye H, Liu X. Mat Sci Eng, B 2004;113:130–5.
300. Lee T, Jung II, Song KH, Lee H, Choi J, Lee K, Lee BJ, Pak JY, Lee C, Kang SO, Ko J. Organometallics 2004;23:5280–5.
301. Wang YZ, Epstein AJ. Acc Chem Res 1999;32:217–24.
302. Fua YJ, Wonga TKS, Wangb GM, Hub X, Zhang HX. J Lumin 2003;10135–43.
303. Wang YZ, Gebler DD, Fu DK, Swager TM, Mac Diarmid AG, Epstein AJ. Synth Met 1997;85:1179–82.

304. Ng SC, Lu HF, Chan HSO, Fujii A, Laga T, Yoshino K. Macromolecules 2001;34:6895–903

305. Monkman AP, Palsson LO, Higgins RWT, Wang C, Bryce MR, Batsanov AS, Howard JAK. J Am Chem Soc 2002;124(21):6049–55.

306. Yang W, Huang J, Liu C, Niu Y, Hou Q, Yang R, Cao Y. Polymer 2004;45:865–72.

307. Balasubramaniam E, Tao YT, Danel A, Tomasik P. Chem Mater 2000;12:2788–93.

308. Hong H, Sfez R, Vaganova E, Yitzchaik S, Davidov D. Thin Solid Films 2000;366:260–4.

309. Yun H, Kwei TK, Okamoto Y. Macromolecules 1997;30:4633–8.

310. Meghdali F, Leising G, Wang YZ, Gebler DD, Swager TM, Epstein AJ. Synth Met 1999;102:1085.

311. Koga T, Takase A, Yasuda S, Yamashita S, Gorohmaru H, Thiemann T, Mataka S, Takahashi K. Chem Phys Lett 2002;354:173–8.

312. Yu SY, Chen ZK, Hang LH, Kang ET, Chua SJ, Huang W. Synth Met 2000;114:101.

313. Zhang X, Jiang C, Mo Y, Xu Y, Shi H, Caoa Y. Appl Phys Lett 2006;88–99.

314. Wu F- I, Reddy DS, Shu C- F. Chem Mater 2003;15:269–74.

315. Pösch P, Thelakkat M, Schmidt HW. Synth Met 1999;102:1110–2.

316. Zhu W, Hu Y, Tian H. Synth Met 2000;111/ 112:477–9.

317. Bao Z, Rogers JA, Dodabalapur A, Lovinger AJ, Katz HE, Raju VR, Peng Z, Galvin ME. Opt Mater 1999;12(2/ 3):177–82.

318. Jin S- H, Kim M- Y, Kim JY, Lee K, Gal Y- S. J Am Chem Soc 2004;126:2474–80.

319. Sung H- H, Lin H- C. Macromolecules 2004;37:7945–54.

320. Mochizuki H, Hasui T, Kawamoto M, Ikeda T, Adachi C, Taniguchi Y, Shirota Y. Macromolecules 2003;36:3457–64.

321. Peng ZH, Bao ZN, Galvin ME. Chem Mater 1998;10:2086–99.

322. Pei Q, Yang Y. Adv Mater 1995;7(6):559–61.

323. Yang X, Hua Y, Yin S, Wang Z, Hou Y, Xu Z, Xu X, Peng J, Li W. Synth Met 2000;111/ 112:455–7.

324. Zhu W, Hu Y, Tian H. Synth Met 2000;111/ 112:477–9.

325. Chung SJ, Kwon KY, Lee SW, Jin JI, Lee CH, Lee CE, Park Y. Adv Mater 1998;10(14):1112–6.

326. Yu WL, Meng H, Pei J, Huang W. J Am Chem Soc 1980; 120:1108–9.

327. Kim JL, Kim JK, Cho HN, Kim DY, Hong SI. Macromolecules 2000;33(16):5880–5.

328. Jiang X, Register RA, Killen KA, Thompson M, Pschenitza F, Sturm JC. Chem Mater 2000;12:2542–47.

329. Peng ZH, Bao ZN, Galvin ME. Chem Mater 1998;10:2086–92.

330. Yang Y, Westerweele E, Zhang C, Smith P, Heeger AJ. J Appl Phys 1995;77(2):694–8.

331. Lee JI, Klaerner G, Miller RD. Chem Mater 1999;11:1083–8.

332. Cui Y, Zhang X, Jenekhe SA. Macromolecules 1999;32:3824–6.

333. Zhang X, Kale DM, Jenekhe SA. Macromolecules 2002;35:382–93.

334. Yamamoto T, Sugiyama K, Kushida T, Inoue T, Kanbara T. J Am Chem Soc 1996;118:3930–7.

335. Zhang X, Shetty AS, Jenekhe SA. Macromolecules 1999;32:7422–9.

336. Dai Y, Katz TJ. J Organomet Chem 1997;62:1274–85.

337. Jenekhe SA, Chen XL. J Phys Chem B 2000;104(27):6332–5.

338. Lu L, Jenekhe SA. Macromolecules 2001;34:6249–354.

339. Chiang CL, Shu CF. Chem Mater 2002;14:682–7.

340. Tonzola CJ, Alam MM, Bean BA, Jenekhe SA. Macromolecules 2004;37:3554–63.

341. Tonzola CJ, Alam MM, Bean BA, Jenekhe SA. Macromolecules 2005;38:9539–47.

342. Huang WY, Yun H, Lin HS, Kwei TK, Okamoto Y. Macromolecules 1999;32:8089–93.

343. Zhang X, Jenekhe SA. Macromolecules 2000;33:2069.

344. Nespurek S. Synth Met 1993;61(1/ 2):55–60.

345. Zhang C, Von Seggern H, Kraabel B, Schimdt WH, Heeger AJ. Synth Met 1995;72:185–8.

346. Partridge RH. Polymer 1983; 24(6):739–47.

347. Partridge RH. Polymer 1983; 24(6):748–54.

348. Partridge RH. Polymer 1983; 24(6):755–62.

349. Zhang A, Von Seggern H, Pakbaz K, Kraabel B, Schmidt KHW, Heeger AJ. Synth Met 1994;62:35–40.

350. Ajn T, Song SY, Ku H. Macromolecules 2000;33:6764.

351. Grigalevicius S, Tsai M- H, Grazulevicius JV, Wu C- C. J Photochem Photobiol A: Chem 2005;174:125–9.

352. Mei C, Tu G, Zhou Q, Cheng Y, Xie Z, Ma D, Geng Y, Wang L. Polymer 2006;47:4976–84.

353. Teo EYH, Ling QD, Song Y, Tan YP, Wang W, Kang ET, Chan DSH, Zhu C. Org Electron 2006;7:173–80.

354. Xing Y, Xu X, Zhang P, Tian W, Yu G, Lu P, Liu Y, Zhu D. Chem Phys Lett 2005;408:169–73.

355. Qiu S, Liu L, Wang B, Shen F, Zhang W, Li M, Ma Y. Macromolecules 2005;38:6782–8.

356. Tabata M, Fukushima T, Sadahiro Y. Macromolecules 2004;37:4342–50.

357. Liu X- M, Xu J, Lu X, He C. Macromolecules 2006;39:1397–1402.

358. Long X, Grell M, Malinovski A, Bradley DDC, Inbasekaran M, Woo EP. Opt Mater 1998;9:70–6.

359. Politis JK, Curtis MD, Gonzalez L, Martin DC, He Y, Kanicki J. Chem Mater 1998;10(6):1713–9.

360. Stenger-Smith JD, Zarras P, Merwin LH. Macromolecules 1998;31(21):7566–9.

361. Shi J, Zheng S. Macromolecules 2001;34:6571–7.

362. Shim HK, Kim HJ, Ahn T, Kang IN, Zyung T. Synth Met 1997;91:289–99.

363. Chung SJ, Jin J, Kim KK. Adv Mater 1997;9(7):551–4.

364. Zhang A, Von Seggern H, Pakbaz K, Kraabel B, Schmidt KHW, Heeger AJ. Synth Met 1994;62:35–40.

365. Yoshino K, Hirohata M, Hidayat R, Kim DW, Tada K, Ozaki M, Teraguchi M, Matsuda T. Synth Met 1999;102:1159.

366. Yoshino K, Hirohata M, Hidayat R, Tada K, Ozaki M, Teraguchi M, Matsuda T, Sada T, Frolov SV, Shkunov M, Vardeny ZV, Hamaguchi M. Synth Met 1997;91:283–8.

367. Sun R, Masuda T, Kobayashi T. Synth Met 1997;91:301–7.

368. Yuang YM, Ge W, Lam JWY, Tang BZ. Appl Phys Lett 1999;75(26):4094–6.

369. Sun R, Masuda T, Kobayashi T. Jpn J Appl Phys: Part 2 1996;35(12B):L1673–5.

370. Chuah BS, Cacialli F, Santos DA, Feeder N, Davies JE, Moratti SC, Homes AB, Friend RH, Brédas JL. Synth Met 1999;102(1–3):935–6.

371. Fulghum T, Karim SMA, Baba A, Taranekar P, Nakai T, Masuda T, Advincula RC. Macromolecules 2006;39:1467–73.

372. Montali A, Smith P, Weder C. Synth Met 1998;97:123–8.

373. Yoshino K, Tada K, Onoda M. Jpn J Appl Phys 1994;33(12B):L1785–8.

374. Tada K, Onoda M, Hirohata M, Kawai T, Yoshino K. Jpn J Appl Phys: Part A 1996;35(2B):L251–3.

375. Choi CK, Tomita I, Endo T. Macromolecules 2000;33:1487–92.

376. Pang Y, Li J, Hu B, Karasz FE. Macromolecules 1998;31:6730–8.

377. Dellsperger S, Dotz F, Smith P, Weder C. Macromol Chem Phys 2000;201(2):192–8.

378. Yamamoto T, Honda K. J Polym Sci: Part A 1998;36(1B):2201–7.

379. Lucht BL, Mao SSH, Tilley TD. J Am Chem Soc 1998;120:4354.

380. Chen Y, Dujardin R, Elschner A, Jonas F, Quintens D, Wehrmann R. ACS Polym Prepr Proc San Francisco Meet 1997;38:345.

381. Yang C, Jacob J, Müllen K. Macromol Chem Phys 2006;207: 1107–15.

<div align="center">CHAPTER 48</div>

Magnetic, Piezoelectric, Pyroelectric, and Ferroelectric Properties of Synthetic and Biological Polymers

<div align="center">Andrzej Kloczkowski* and Taner Z. Sen*,†</div>

*L .H. Baker Center for Bioinformatics and Biological Statistics, Iowa State University, Ames, IA 50011, USA;
†Department of Biochemistry, Biophysics, and Molecular Biology, Iowa State University, Ames, IA 50011, USA

48.1 MAGNETIC POLYMERS

Depending on the behavior in the presence of the external magnetic field all materials may be classified as diamagnetic, paramagnetic, ferromagnetic (or antiferromagnetic).

Diamagnetism is exhibited by materials with a negative magnetic susceptibility, i.e., they magnetize in a direction opposite to the direction of the applied magnetic field, and are repelled by a magnet. All materials with zero net electronic orbital moment and zero net spin magnetic moment are diamagnetics. Most of the organic molecules and polymers have a closed shell electronic structure with a singlet ground state with all electron spins paired, and therefore have diamagnetic properties. The diamagnetism follows from the Lenz's law, that the induced field opposes the applied magnetic field. All substances including paramagnets (or ferromagnets) have diamagnetic susceptibility components, but these components are very small, usually much smaller in comparison to paramagnetic susceptibilities. Substances with nonzero net electronic orbital moments or with unpaired electron spins are paramagnetics. Paramagnetic materials have open-shell electronic structure, with some unpaired electrons. Organic molecules with one unpaired electron in doublet ground state show paramagnetic properties and are called free radicals. The magnetic moments of molecules of paramagnetic substances are randomly distrib-

uted throughout the volume of the material, and the total magnetic moment of the material is zero. Paramagnetics magnetize parallel to the direction of the external magnetic field, the magnetization of the paramagnetic material vanishes when the external magnetic field is switched off.

Ferromagnetism is a property exhibited by compounds of certain metals: iron group or rare-earth elements. The atomic magnetic moments of these materials, below the so called Currie temperature, orient in one direction. The resulting magnetic susceptibility is very high and shows a saturation effect. The large magnetization of the material is preserved when the external field is switched off, i.e., ferromagnetics may have spontaneous magnetization below the Curie point. Above the Curie temperature ferromagnetics behave as ordinary paramagnetics. Ferromagnetic materials are composed of small, spontaneously magnetized regions, so called domains. The directions of magnetization of different domains do not coincide and the net magnetic moment of the substance in the absence of the external magnetic field may be zero. The application of even weak external magnetic field aligns magnetic moments of domains of the ferromagnet and gives rise to the high magnetic moment of the sample. Antiferromagnetism is a property of certain crystals containing transition elements which show spontaneous antiparallel magnetic ordering below Néel temperature. Above the Néel temperature the antiferromagnetic

ordering vanishes. The quantum theory of ferromagnetism was developed by Heisenberg. According to the Heisenberg theory there is an effective interaction between the electron spins, which arises from to the interplay between electrostatic Coulomb forces and the effect of the Pauli exclusion principle. The exchange energy of this interaction is

$$E_{ij} = -2J_{ij}\boldsymbol{\sigma}_i \cdot \boldsymbol{\sigma}_j, \qquad (48.1)$$

where σ_i and σ_j are spin angular momenta for electrons i and j, and the coupling constant J_{ij} is called the exchange integral. If the coupling constant J is positive and large enough the ferromagnetic ordering in the system is favorable. For large negative values of J the antiparallel antiferromagnetic alignment of spins is favored. If the exchange integral is small, the ferromagnetic (or antiferromagnetic) state is not possible.

Ferromagnetism of the transition and rare-earth metal salts and complexes is due to high-spin states of those atoms. The electronic structure of these metal atoms is open-shell, with d-orbitals and f-orbitals containing several unpaired electrons [1–3].

Until recently the only known ferromagnetic polymers were metallo-polymers containing transition metals or rare-earth elements. The presence of the metal, particularly Fe, Ni, Co may lead to ferromagnetic behavior due to the formation of extrinsic separate magnetic phase of the metal. Another possible mechanism of ferromagnetism in metallo-polymers, of the intrinsic nature, is the strong coupling of the spins of metal ions with organic polymeric ligand. The problem if the ferromagnetic behavior of the metallo-polymer has intrinsic or extrinsic origin is very complicated [4]. There are several known polymers containing iron atoms which show ferromagnetic properties. An example is complex of the PPH polymer with $FeSO_4 \cdot 7H_2O$ shown below, containing each iron ion surrounded by six nitrogen atoms
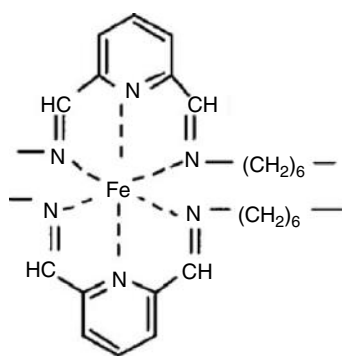
The observed ferromagnetic behavior of this polymer was first attributed to the intrinsic mechanism, but later studies have shown that the ferromagnetism is of the extrinsic nature, due to the formation of the ferromagnetic phase containing Fe_2O_3 [4].

Discoveries of purely-organic ferromagnetic materials, i.e., materials which do not contain transition metals or rare-earth elements, have been reported. The possibility of existence of organic ferromagnetic compounds has been theoretically postulated in 1963 by McConnell for high spin charge transfer complexes [5]. The proposed systems contained alternating linear sequences of donor–acceptor pairs in triplet and singlet ground states. A parallel ordering of all spins in those systems was predicted [6]. In 1968 Mataga proposed theoretically several magnetic polymer structures containing high spin blocks, as shown below with dots above carbon atoms denoting free radicals [7].
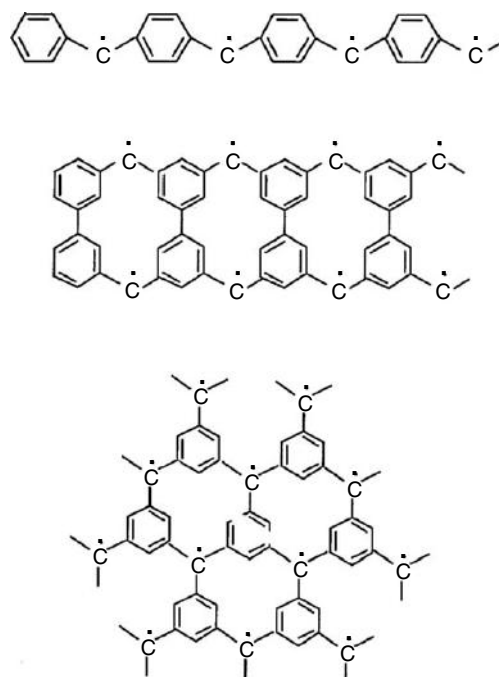
Mataga predicted that according to Hund's rule unpaired electrons in these polymers may have parallel spins, leading to ferromagnetic behavior.

In 1987 Ovchinnikov et al. announced the discovery of the first ferromagnetic organic polymer based on polydiacetylene chain with dangling nitroxyl radicals [8,9]. The compound was obtained by bulk polymerization of stable paramagnetic biradical BIPO initiated by light. The chemical structure of this compound is shown below.
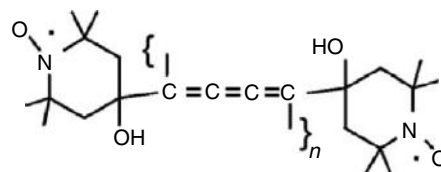
The saturation magnetization of this material was very low (0.1% of the theoretical prediction), and the fraction of crystallites showing ferromagnetic properties was also extremely small. The Curie temperature was reported to be $440 \pm 20\,\mathrm{K}$. Those results, however, were unverified by other laboratories. Also Torrance reported the synthesis of

an organic ferromagnet by iodine oxidation of 1,3,5-triami-nobenzene [10]. Iwamura obtained fully characterized ferromagnetically coupled oligomers of polycarbenes [11,12]. These announcements have been followed by many other reports on discoveries of ferromagnetic polymers, by various authors [4]. However, all those results were unconvincing because of the poor characterization of those polymers and problems with reproducibility of the results. There is a growing list of well-characterized high spin polymers, mostly based on polyacetylene chain with pendant groups containing radical centers, but the only observed magnetic behavior of these compounds is a weak antiferromagnetism. Generally, the fraction of the bulk of the polymers exhibiting ferromagnetic behavior is very small, usually less than 5%. It is very probable that the reported ferromagnetic properties of organic polymers are due to such accidental factors, as ferrometalic impurities [4]. Several liquid–crystalline ferromagnets have also been reported [13].

Another approach to magnetic polymers are so-called polaronic ferromagnets, with spins introduced to the polymer molecules by doping, which form radical ions named polarons. With proper molecular topology ferromagnetic coupling among polarons may be possible [2]. The field of magnetic polymers are reviewed by Miller and Epstein [14] and by Kamachi [15].

48.2 PIEZOELECTRIC POLYMERS

Piezoelectricity is an effect of the generation of electric polarity in certain dielectric materials (i.e., electric insulators) in response to the applied mechanical pressure. The effect was discovered by Pierre and Jacques Curie in 1880. The polarization of the material is proportional to the applied stress. The piezoelectric effect has very important practical applications in transducers, i.e., devices which convert electric signals to mechanical signals, or the mechanical signals to electric signals, such as microphones, loudspeakers, gramophone needles, ultrasound generators, quartz clocks, etc [16,17].

The most known piezoelectric materials are some inorganic crystals, such as: quartz, barium titanate $BaTiO_3$, ammonium dihydrogen phosphate $NH_4H_2PO_4$, Rochelle salt (potassium sodium tartrate tetrahydrate $NaKC_4H_4O_6 \cdot 4H_2O$), or zinc blende ZnS. The electric polarization generates the electric potential between opposite surfaces of the crystal, and gives rise to the electric current if these two sides of the crystal are connected by a wire. The converse piezoelectric effect, i.e., the generation of the mechanical stress in the piezoelectric material by applying the electric voltage to opposite sides of the crystal is also observed. The generated piezoelectric strain is proportional to the applied electric field. (There is an important difference between converse piezoelectric effect and electrostriction, where the deformation is proportional to the square of the field). On the molecular level, piezoelectricity occurs

when elastic deformations of the body are accompanied by unequal vectorial displacements of centers of gravity of positive and negative charges (ions) leading to the net polarization of the sample. The unequal vectorial displacements in the crystal require the lack of the crystallographic center of symmetry. There is a correlation between the symmetry of the crystal and the type of stresses which generate the piezoelectric polarization. The lower the symmetry of the crystal, the more different types of stresses produce piezoelectric polarization.

Generally, each of the three components of the polarization ΔP_i is linearly related to each of the nine components of the stress tensor σ_{jk}

$$\Delta P_i = d_{ijk}\, \sigma_{jk}, \qquad (48.2)$$

where d_{ijk} is the third-rank tensor having 27 components called piezoelectric coefficients. In the absence of body torques the stress tensor is symmetric, i.e., $\sigma_{jk} = \sigma_{kj}$ and has only 6 components so the maximum number of piezoelectric coefficients is 18 [18]. It is therefore convenient to represent the stress tensor as a six component vector σ_m, and the piezoelectric coefficients as a second-rank tensor d_{im}, where $m = 1\text{–}6$, so that

$$\Delta P_i = d_{im}\, \sigma_m. \qquad (48.3)$$

Similarly in the converse piezoelectric phenomena each of the 6 components of the strain tensor ε_m is related to each of the 3 components of the electric field

$$\varepsilon_m = d_{im}^c\, E_i, \qquad (48.4)$$

where d_{im}^c are converse piezoelectric coefficients.

The stress and strain tensors are related through the relations

$$\varepsilon_m = s_{mn}\, \sigma_n \qquad (48.5)$$

and

$$\sigma_m = c_{mn}\, \varepsilon_n, \qquad (48.6)$$

where s_{mn} and c_{mn} (with $m, n = 1\text{–}6$) are the elastic compliance tensor and the elastic stiffness tensor, respectively [17].

The most known polymer exhibiting piezoelectric behavior is poly(vinylidene fluoride) (PVF_2) which has the structure $(CF_2CH_2)_n$ [19]. The piezoelectric polymer sample is obtained by orienting dipole moments in the polymer by poling. The symmetry of the highly oriented poled polymer film reduces the number of possible piezoelectric coefficients from 18 to 5. Using the convention where 1 is the direction of drawing, 2 is in the direction of the film, and 3 is normal to the film surface the only nonzero piezoelectric coefficients for uniaxially oriented film are $d_{31}, d_{32}, d_{33}, d_{15}$, and d_{24} [18]. For biaxially oriented films $d_{31} = d_{32}$ and $d_{15} = d_{24}$. The coefficient d_{33} is very difficult to measure, so sometimes it is calculated from the hydrostatic piezoelectric coefficient

$$d_h = d_{31} + d_{32} + d_{33}. \qquad (48.7)$$

Table 48.1 shows some piezoelectric coefficients for thin PVF$_2$ films obtained by Kepler and Anderson from static measurements [18].

It should be noted that piezoelectric coefficients, especially d$_{33}$ are very difficult to measure and stress-induced changes in polymer crystallinity contribute significantly to the piezoelectric coefficients [20]. Because of the viscoelastic properties of polymers the piezoelectric charge signal is not in phase with the stress or strain. Piezoelectric coefficients obtained from dynamic measurements depend on the frequency. It has been found that experimental values of the piezoelectric coefficients also depend on the method of processing of polymer films. For example, Wang found that in drawn and rolled films, d$_{31}$ is about 25% higher than in films only drawn [21]. It has been shown that annealing has a large effect on the magnitude of the piezoelectric coefficients. For example Takase *et al.* found that annealing the stretched PVF$_2$ films in temperatures between 160 and 180 °C increased d$_{31}$ from 20 to 28 pCN^{-1} [22]. Piezoelectric coefficients depend also on temperature. It has been found that piezoelectric coefficients increase with increasing temperature, especially rapidly above the glass transition temperature (-50 °C for PVF$_2$) [23].

Table 48.2 shows piezoelectric coefficients of PVF$_2$ obtained from dynamic measurements at frequencies 10 Hz and 25 Hz [20].

Other most known piezoelectric polymers are: poly(vinylchloride) (PVC), poly(vinylfluoride) (PVF), and Nylon 11. The piezoelectric coefficients of these polymers are much lower than piezoelectric coefficient of PVF$_2$. Table 48.4 shows piezoelectric coefficients of these polymers and compares them with those of some piezoelectric inorganic crystals.

TABLE 48.1. *Piezoelectric coefficients of thin* PVF$_2$ *films (in* pCN^{-1}*) [18].*

Coefficient	Biaxially oriented film	Uniaxially oriented film
d$_{31}$	4.34	21.4
d$_{32}$	4.36	2.3
d$_{33}$	−12.4	−31.5
d$_h$	−4.8	−9.6
d$_{33}$ (calculated from d$_h$)	−13.5	−33.3

TABLE 48.2. *Piezoelectric coefficients of* PVF$_2$ *(in* pCN^{-1}*) obtained from dynamic measurements [20].*

Coefficient	Frequency 10 Hz	Frequency 25 Hz
d$_{31}$	28	17.5
d$_{32}$	4	3.2
d$_{33}$	−35	
d$_h$	−3	

48.3 PYROELECTRIC POLYMERS

Pyroelectricity is the effect of the generation of electric polarization in certain dielectrics by the change of temperature. The change of the electric polarization ΔP_i (for each component of the polarization vector) in the pyroelectric material is proportional to the change of the temperature ΔT

$$\Delta P_i = p_i \, \Delta T, \qquad (48.8)$$

where p_i (with $i = 1$–3) are pyroelectric coefficients. Pyroelectricity is related to piezoelectricity, since it also occurs in crystals with crystallographic cells without a center of symmetry. Additional requirement for pyroelectric crystal is the occurrence of a polar axis, which reduces the number of possible crystal classes in comparison with piezoelectrics. Out of the total 32 possible crystallographic point groups, 20 groups fulfill requirements for piezoelectricity, but only 10 groups exhibit pyroelectricity. The most known pyroelectric crystals are: barium titanate BaTiO$_3$, cane sugar, and tourmaline. Because pyroelectric materials have polar axis they have permanent electric polarization, which is usually compensated by free charges on the surface of the material. The change in temperature alters the electric polarization, and leads to the pyroelectricity. The converse pyroelectric effect, the so called electrocalorimetric effect in pyroelectrics is also observed. The external electric field applied to a pyroelectric material changes its temperature. In order to eliminate the effect of the thermal expansion, measurements of the pyroelectric effect are often performed for mechanically constrained (e.g., by clamps) materials. We may also define two types of pyroelectricity: the primary pyroelectricity, which is measured when the dimensions of the sample are fixed (by clamps), and secondary pyroelectricity containing additional contribution to the polarization resulting from the thermal expansion. The secondary pyroelectricity coefficients p_i^s are related to piezoelectric coefficients d$_{im}$, elastic stiffness tensor c$_{mn}$, and thermal expansion coefficients α_n [18].

$$p_i^s = d_{im} \, c_{mn} \, \alpha_n. \qquad (48.9)$$

The pyroelectric effect is widely used for the detection of infrared radiation, and for very precise measurements of the temperature [16,17].

The most known polymer showing the pyroelectric effect is poly(vinylidene fluoride) $(CF_2CH_2)_n$ (PVF$_2$) [19]. Polymer samples exhibiting pyroelectric properties are prepared by poling. Pyroelectric coefficients for polymers depend on the electric poling field. With the increasing poling field pyroelectric coefficients increase.

Table 48.3 shows primary and calculated secondary pyroelectric coefficients of PVF$_2$ films, together with thermal expansion coefficients, and elastic stiffness coefficients, obtained by Kepler and Anderson [18]. The corresponding piezoelectric coefficients were earlier shown in Table 48.1.

Other popular pyroelectric polymers are: poly(vinylchloride) (PVC), poly(vinylfluoride) (PVF), and Nylon 11, but their pyroelectric coefficients are smaller than pyroelectric coefficient of PVF_2. On the other hand the pyroelectric coefficient of PVF_2 is much smaller than pyroelectric coefficients of inorganic crystals. Table 48.4 shows the comparison of piezoelectric and pyroelectric coefficients of some inorganic crystals and polymers [24]. An extensive review of pyroelectric materials including single crystals, ceramics, liquid crystals, and composites has been recently published by Lang and Das-Gupta [25].

48.4 FERROELECTRIC POLYMERS

Ferroelectrics are materials with built-in spontaneous, permanent electric polarization. Similarly as ferromagnetics possess the spontaneous, permanent magnetization, ferroelectrics have spontaneous polarization, which can be reversed by applying external electric field. The most known ferroelectrics are inorganic monocrystals, such as Rochelle salt (potassium sodium tartrate tetrahydrate

TABLE 48.3. *Pyroelectric coefficients p_i and p_i^s, thermal expansion coefficients α_n, and elastic stiffness coefficients c_{mn} of PVF_2 films [18].*

Coefficient	Biaxially ordered film	Uniaxially ordered film
$p_3(10^{-5}\,Cm^{-2}K^{-1})$	-1.25	-2.74
$p_3^s(10^{-5}\,Cm^{-2}K^{-1})$	-0.44	-1.48
$\alpha_1(10^{-4}\,K^{-1})$	1.24	0.13
$\alpha_2(10^{-4}\,K^{-1})$	1.00	1.45
$c_{11}(10^9\,Pa)$	5.04	5.04
$c_{12}(10^9\,Pa)$	3.25	3.25

TABLE 48.4. *Piezoelectric coeffiecients d and pyroelectric coefficients p of several inorganic crystals and several polymers with references to original papers.*

Material	d(in pCN^{-1})	Ref.	p(in 10^{-5} $Cm^{-2}K^{-1}$)	Ref.
Quartz	2.3 (d_{11})	[26]		
PZT-4 (lead zirconate titanate)	289 (d_{33})	[27]	27	[28]
$BaTiO_3$	190 (d_{33})	[27]	20	[28]
Rochelle Salt	53 (d_{25})	[26]		
Triglycine sulfate	50	[29]	30	[28]
$Sr_{0.5}Ba_{0.5}Nb_2O_6$	95	[29]	60	[29]
PVC	0.7	[30]	0.1	[30]
PVF	1	[19]	1.0	[31]
Nylon 11	0.26	[30]	0.5	[28]
PVF_2	28 (d_{31})	[23]	4	[32]

$NaKC_4H_4O_6 \cdot 4H_2O$), monopotassium dihydrophosphate (KH_2PO_4), or barium titanate ($BaTiO_3$). At sufficiently high temperatures ferroelectrics show normal dielectric behavior. However, below a certain critical temperature (so called, Curie temperature), even a small electric field causes a large polarization, which is preserved even if the external field is switched off. This means that below the Curie point ferroelectric materials show spontaneous polarization. The phase transition at the Curie temperature is related to the change of the lattice symmetry of the sample.

The spontaneously polarized crystal is anisotropic and has lower symmetry than the nonpolarized one. Ferroelectric materials below the Curie temperature are also always piezoelectric, because the polarized sample has no center of symmetry. If the nonpolarized crystal has the center of symmetry, the piezoelectricity of the sample vanishes above the Curie temperature. All ferroelectrics below the Curie temperature also always show pyroelectric behavior.

Until the late sixties the only known ferroelectrics, piezoelectrics, and pyroelectrics were certain inorganic monocrystals, or polycrystalline ceramics like lead titanate zirconate perovskites. Other known materials with macroscopic polarization were electrets, (for example mixtures of beeswax and rosin) in which the polarization was produced by application of the electric field in the melted state and then by cooling and the solidification of the polarized material.

In 1969 Kawai discovered that the poly(vinylidene fluoride) polymer (known as PVF_2 or PVDF) is ferroelectric [19]. PVF_2 has a simple molecular structure $(CF_2CH_2)_n$ with the degree of polarization n usually greater than 10,000. PVF_2 is a crystalline polymer, with about the half of the polymer molecules in the amorphous noncrystalline state and another half in crystalline lamella state [33]. The crystallographic studies have shown that PVF_2 may form four different phases. One of the phases called the α-phase (or phase II) obtained by quenching from the melt is nonpolar, while other three phases called the β, γ, and the δ-phase (or phases I, III and IV), respectively, are ferroelectric [18]. The most important is the β-phase, in which the polymer has the all-*trans* conformation (and the largest dipole moment) and two chains in the unit cell are aligned in the same direction. The phases γ and δ have the electric polarization per unit cell smaller then the β-phase. The phase transformations between different phases of PVF_2 are possible by means of annealing, drawing, or poling. The ferroelectric phase of PVF_2 was discovered by poling PVF_2 film, i.e., by heating a film above temperature $100\,^{\circ}C$ and applying high electric field (above $50\,MVm^{-1}$) and then cooling the sample to the room temperature. The resulting material had very large piezoelectric coefficient ($6.7\,pCN^{-1}$), about ten times larger than for any other polymer, and possessed also pyroelectric properties, at temperatures well above the glass transition temperature ($-40\,^{\circ}C$) of the polymer [16]. The magnitude of the piezoelectric coefficient and the induced polarization increase with the increasing

voltage and the increasing poling temperature. Poling can take place even at room temperature and below, if sufficiently high electric field is applied. The $PVF_2\beta$-phase melts in temperature range 175–180 °C and no ferroelectric phase transition below the melting temperature is observed. The ferroelectric phase transition is observed in copolymers of PVF_2 with poly(trifluoroethylene) (PF_3E) or with poly (tetrafluoroethylene) (PF_4E). For example the study of the 51%mol PVF_2 – 49%mol PF_3E copolymer shows the ferroelectric-to-paraelectric first order phase transition at the temperature 65 °C. The addition of PF_4E or PF_3E to PVF_2 increases the number of defects in the PVF_2 chains and lowers the Curie temperature of the copolymer in comparison to the pure PVF_2. The extrapolation of the plot of the Curie temperature as a function of the PVF_2 content in the copolymer to the pure PVF_2 gives the estimation of the Curie point of PVF_2 at 190 °C. This temperature is above the melting point temperature of PVF_2 and therefore the Curie point for pure PVF_2 is not observed [18].

Ferroelectric properties (much weaker than PVF_2) are shown also by other polymers like poly(vinylchloride) (PVC) or poly(vinylfluoride) (PVF). (See Table 48.3 for comparison of piezoelectric and pyroelectric coefficients of PVC and PVF with those for PVF_2 and for some ferroelectric inorganic crystals).

In the mid-seventies it was shown that because of the symmetry requirements, chiral smectic C liquid crystals are ferroelectric [34]. Liquid crystals are formed by anisotropic rod-like molecules. The most known liquid crystals are nematics, with orientational ordering of molecular axis of mesogenic molecules around the preferred direction, but no spatial ordering. The smectic A liquid crystals have (in addition to the orientational ordering) spatial alignment of molecules in layers, with the preferred direction perpendicular to the plane of the layers. In the smectic C phase the direction of orientational ordering is tilted relative to the normal to the plane of the layers. Chiral molecules have no center of symmetry, i.e., the mirror image of the molecule differs from the molecule itself. If a chiral mesogenic molecule has permanent dipole moment, then the unit cell of the smectic C phase has no center of symmetry and the material should be ferroelectric. The first ferroelectric liquid crystalline polymer synthesized by Shibaev and Plate [35] is shown below

The molecule is a liquid crystalline polymer with chiral smectic C phase forming parts attached as side chains. The field required to switch the direction of polarization of the polymer is very low (0.3 MVm^{-1}). There is a lot of interest in liquid crystalline ferroelectric polymers, because of their possible use for fast-switching electro-optical devices. More information about ferroelectric liquid crystals can be found in references [36,37].

Another group of ferroelectric polymers are odd nylons. The most known is Nylon 11
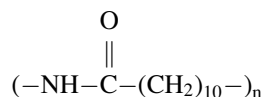
In crystal phase Nylon 11 molecules are packed in sheets with hydrogen bonds between oxygen atoms and NH groups of neighboring chains, and dipole moments of Nylon 11 chains are aligned. The piezoelectric and pyroelectric coefficients of Nylon 11 are smaller than those for PVF_2 (see Table 48.4 for comparison).

A comprehensive bibliography for ferroelectric materials (including polymers) has been recently published by Toyoda [38].

48.5 PIEZOELECTRIC, PYROELECTRIC, AND FERROELECTRIC PROPERTIES OF BIOPOLYMERS

Piezoelectricity, pyroelectricity, and ferroelectricity is hardly confined to synthetic polymers. Some biopolymers also possess these properties, and scientists study them to understand how nature exploits these properties. The earliest studies of biopolymer piezoelectricity, for example, go back to 1960s when Morris Shamos and Leroy Lavine (with Michael Morris) studied bone piezoelectricity [39] and later postulated piezoelectricity as a "fundamental property" of tissues of biological origins [40]. In 1968, RNA ferroelectricity was demonstrated by Stanford and Lorey [41]. However, the scientific interest in these properties of biological molecules was dwarfed by the interest in other materials. In 1999 Sidney Lang [42] indicated that compared to "thousands" of publications on piezoelectric, pyroelectric, and ferroelectric materials, only less than 100 of them were biologically related.

Piezoelectricity in biological molecules can be found both in soft and hard tissues as shown in Table 48.5. In this table, d_{ij} represent piezoelectric coefficient components, which

TABLE 48.5. *Piezoelectric coefficients (in 10^{-12} m/V) in biomaterials (taken from Lemanov [43]).*

Material	d_{14}	d_{15}	d_{31}	d_{33}
Bovine achiles tendon	−2.7	1.4	0.09	0.07
Horse femur	−0.2	0.04	0.003	0.003
Silk	−1.1	0.25	0.02	0.023

TABLE 48.6. *Pyroelectric coefficients (in 10^{-5}Cm^{-2}K) in biomaterials (taken from Lemanov [43]).*

Material	Coefficient
Hoof tendon	0.00004
Insect thorax	0.35
Wheat	0.46
Plant leaves	0.015

TABLE 48.7. *Piezoelectricity and symmetry groups of amino acids [45] (L and D denote left-sided and right-sided enantiomers, and DL is the equimolar mixture of enantiomers).*

Amino acid	Piezoelectricity	Symmetry
α-glycene	+	C_{2h}
γ-glycene	+	C_3
L-alanine	+	D_2
L-valine	+	C_2
L-isoleucine	−	C_2,D_2
L-glutamic acid	+	C_2,D_2
L-cysteine	−	C_4,D_6
DL-alanine	+	C_{2v}
DL-valine	−	C_1
DL-serine	−	C_{2h}
DL-aspartic acid	−	C_{2h}
DL-lysine	−	D_2
DL-tyrosine	+	C_{2v}
DL-trptophan	−	C_1

are previously explained under piezoelectric polymers section. Pyroelectric coefficients for some biological materials are similarly given in Table 48.6. As explained under pyroelectric polymers section, pyroelectric coefficients are related to piezoelectric coefficients. Compared to those of PVF$_2$ films in Table 48.3, piezoelectric coefficients of biopolymers shown in Table 48.6 are very small and have positive signs.

Piezoelectricity and pyroelectricity in biopolymers originate from their building blocks: biopolymers are copolymers with 20 different monomers. These monomers are called amino acids and consist of a chiral carbon (except glycine) surrounded by an amino group, hydrogen atom, carboxyl group, and a side chain R as shown below.

$$
\begin{array}{c}
H \\
| \\
NH_2 - C - COOH \\
| \\
R
\end{array}
$$
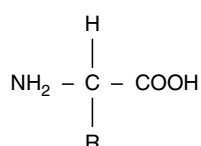
Different side chain groups determine the type of a given amino acid. These side chains can be classified as neutral, acidic, or basic; aliphatic or aromatic; hydrophobic or polar, etc. As discussed previously, the piezoelectricity and pyroelectricity requires restrictions on crystal symmetry (e.g., 20 crystallographic groups can be piezoelectric, and only 10 groups demonstrates pyroelectricity). The piezoelectric response of amino acids to the high-frequency electric pulses is shown in Table 48.7; the pyroelectric properties of amino acids were also measured, but found not significant [44].

Ferroelectricity is a requirement for some biopolymers for their biological function. Microtubules which hold the cell structurally intact are a good example. These biostructures consist of identical α and β tubulin proteins which have permanent dipole moments. Since cells utilize microtubules in cell division and to transport motor proteins, the orientation of tubulin proteins becomes crucial for cell fitness. This orientation may be controlled by electric fields [46]. Microtubules alignment was reviewed by Cyr [47].

Another interesting biological example that shows ferroelectric properties is voltage-dependent ion channels. These channels are glycoproteins located in the cell membrane, and they are found in either open or closed conformations. In the open conformation, these proteins are ion conductors. In the closed conformation, they become non-conducting, yet they still retain their ferroelectricity, even showing liquid crystalline properties [36,48].

There is a growing interest in studying the piezoelectricity, pyroelectricity, and ferroelectricity in biological systems to understand what roles they play in cellular functions, and this interest is expected to increase in the future.

REFERENCES

1. Kahn O. Molecular magnetism, New York: VCH publishers, 1993.
2. CJ O'Connor, editor, Research frontiers in magnetochemistry, Singapore: World scientific, 1993.
3. D. Gatteschi et al., editors, Magnetic molecular materials, Dordrecht: Kluwer, 1991.
4. Miller JS. Adv. Mater. 1992; 4:298.
5. McConnell HM. J. Chem. Phys. 1963;39:1910.
6. Miller JS, Epstein AJ, Rief WM. Chem.Rev. 1988; 88:201.
7. Mataga N. Theor. Chim. Acta 1968; 10:372.
8. Korshak YV, Medvedeva TV, Ovchinnikov AA. Nature 1987;326:370.
9. Ovchinnikov AA, Spector VN. Synth. Met. 1988;27:B615.
10. Torrance JB, Oostra S, Nazzal A. Synth. Met. 1987;19:709.
11. Iwamura H. Pure Appl.Chem. 1986;58:187.
12. Iwamura H. Adv. Phys. Org. Chem. 1990;26:179.
13. Palacio F, Ramos J, Castro C. Mol. Cryst. Liq. Cryst. Technol. Sect. A 1993;232:173.
14. Miller JS, Epstein AJ. Chem. Eng. News 1995;(October 2):30.
15. Kamachi M. J. Macromol. Sci. Part C Polym. Rev. 2002;42(4):541–561.

16. Wang TT, Herbert JM, Glass AM. editors, The application of ferro-electric polymers, Glasgow: Blackie and Son, 1988.
17. Wong CP, editor, Polymers for electronic and photonic applications, San Diego: Academic Press, 1993.
18. Kepler RG, Anderson RA. J. Appl. Phys. 1978;49:4490.
19. Kawai H. Jpn. J. Appl. Phys. 1969;8:975.
20. Schewe H, McAroy BR, editors. Ultrasonics Symposium Proceedings. New York:IEEE, 1982. pp. 519.
21. Wang TT. J. Appl. Phys. 1979;50:6091.
22. Takase Y, Scheinbeim JI, Newman BA. J. Polym. Sci., Part B: Polym. Phys. 1989;27:2347.
23. Ohigashi H. J. Appl. Phys. 1976;47:949.
24. GM Sessler, editor, Electrets, 2nd. ed. Berlin: Springer-Verlag, 1987.
25. Lang SB, Das-Gupta DK. Ferroelectrics Rev. 2000;2:217–354.
26. W.G. Caddy, Piezoelectricity, New York: McGraw-Hill, 1946.
27. Berlincourt DA, Curran DR, Jaffe H. Physical Acoustics. New York: Academic Press, 1964. pp. 1.
28. Garn LE, Sharp EJ. IEEE Trans. PHP 1974;10:28.
29. Liu ST, Long D. Proc. IEEE 1978;66:14.
30. Litt MH, Hsu C, Basu P. 2005;No: 5 on Office of Naval Research Contract No. N00014–75-c-0842
31. Phelan RJ Jr., Mahler RJ, Cook AR. Appl. Phys. Lett. 1971;19:337.
32. Day GW, Hamilton RL, Phelan RJ Jr., Mullen LO. Appl. Phys. Lett. 1974;24:456.
33. Lovinger AJ. Science 1983;220:1115.
34. Meyer RB, Liebert L, Strzelecki L, Keller P. J. Phys. Lett. 1975;36:L69.
35. Shibaev V, Plate N. Pure Appl. Chem. 1985;57:1589.
36. JW Goodby et al., Ferroelectric liquid crystals: principles, properties, and applications, Philadelphia: Gordon and Breach, 1991.
37. Barny PL, Dubois JC, McArdle CB, editors. Side chain liquid crystal polymers. Glaskow:Blackie and Son, 1989.
38. Toyoda K. Ferroelectrics 2003;282:57–216.
39. Shamos MH, Shamos MI, Lavine LS. Nature 1963;197:81.
40. Shamos MH, Lavine LS. Nature 1967;213:267–269.
41. Stanford AL, Lorey RA. Nature 1968;219:1250–1251.
42. Lang SB. 10th Inter. Symp. Electrets 1999.
43. Lemanov VV. Piezo-, Pyro-, and Ferroelectricity in biological mater-ials. In:Galassi C, Dinescu M, Uchino K, Sayer M, editors. Piezoelec-tric materials: advances in science, technology and applications. Kluwer, 2000.
44. Lemanov VV, Popov SN, Pankova GA. Ferroelectrics 2003;285: 581–590.
45. Lemanov VV. Ferroelectrics 2000;238:211–218.
46. White RG, Hyde GJ, Overall RL. Protoplasma 1990;158:73–85.
47. Cyr RJ. Annu. Rev. Cell Biol. 1994;10:153–180.
48. Helluin O, Beyermann M, Leuchtag HR, Duclohier H. IEEE Trans. Diec. Electr. Insul. 2001;8(4):637–643.

CHAPTER 49

Nonlinear Optical Properties of Polymers

W. M. K. P. Wijekoon, K.-S. Lee, and P. N. Prasad

The Institute for Lasers, Photonics and Biophotonics, Department of Chemistry,
The State University of New York at Buffalo, Buffalo, NY 14260-3000

49.1 INTRODUCTION

Nonlinear optical (NLO) properties of organic polymers can be viewed as dielectric phenomena, and their origins can conveniently be explained by considering a planar wave propagation through a nonlinear dielectric medium [1–4]. In a dielectric medium the polarization P induced by the incident field E can be written as a power series of the field strength as follows:

$$P = \chi^{(1)} \cdot E + \chi^{(2)} \vdots EE + \chi^{(3)} \vdots EEE + \cdots, \qquad (49.1)$$

where P and E are vectors and $\chi^{(1)}$, $\chi^{(2)}$, and $\chi^{(3)}$, which relate P and E, are tensors. The linear polarizability tensor $\chi^{(1)}$ is a second-rank tensor. $\chi^{(2)}$ is the hyperpolarizability tensor and is a third-rank tensor and $\chi^{(3)}$, the second hyperpolarizability tensor, is a fourth-rank tensor. The first-order term $\chi^{(1)}$ describes linear processes such as absorption, refraction, and scattering while the higher-order terms $\chi^{(2)}$ and $\chi^{(3)}$ describe the second- and third-order NLO processes, respectively.

In general, the polarization induced in an optical medium by incident radiation can be written as [2,3]

$$P_I(\omega) = \chi^{(1)}_{IJ}(-\omega) \cdot E^\omega_J + \chi^{(2)}_{IJK}(-\omega;\omega_1,\omega_2) \vdots E^{\omega_1}_J E^{\omega_2}_K$$

$$+ \chi^{(3)}_{IJKL}(-\omega;\omega_1,\omega_2\omega_3) \vdots E^{\omega_1}_J E^{\omega_2}_K E^{\omega_3}_L + \cdots. \quad (49.2)$$

Obviously the larger the values of $\chi^{(2)}_{IJK}$ and $\chi^{(3)}_{IJKL}$, the higher the second- and third-order polarization created in the sample, respectively. In polymeric materials, the origin of the optical nonlinearity can be traced to the molecular constituents, and therefore, one can identify polarization due to molecular units. Accordingly, the interaction of radiation with materials can be expressed in terms of the induced molecular polarization (induced dipole moment) as follows [3]:

$$p_i(\omega) = \alpha_{ij}(-\omega) \cdot F^\omega_j + \beta_{ijk}(-\omega;\omega_1,\omega_2): F^{\omega_1}_j F^{\omega_2}_k$$

$$+ \gamma_{ijkl}(-\omega;\omega_1,\omega_2,\omega_3) \vdots F^{\omega_1}_j F^{\omega_2}_k F^{\omega_3}_l + \cdots, \quad (49.3)$$

where the molecular susceptibilities β and γ are analogous to the bulk susceptibilities $\chi^{(2)}$ and $\chi^{(3)}$ given in Eq. (49.2)

and the local fields $F_p^{q\omega}$ take into account the difference between the actual field seen by the molecules and the applied field $E_p^{q\omega}$. There are several experimental techniques that can be employed to evaluate NLO coefficients β, γ, $\chi^{(2)}$, and $\chi^{(3)}$ of polymeric materials.

At present, polymers that exhibit large nonresonant optical nonlinearities are of considerable interest in scientific and industrial circles. Organic polymers offer significant tailoring flexibility in that their chemical structures can be modified to optimize the microscopic NLO response at the molecular level. Furthermore, at the bulk and microstructure level polymers can be processed as fibers, thin films in oriented or unoriented forms, glasses, and gels. NLO processes provide important functions of frequency conversion (for example, frequency doubling to increase the density of data storage), light controlled by electric field and even optical processes such as light controlled by light, the manifestation of which can be utilized to build photonic devices. A photonic device utilizes photons instead of electrons to acquire, process, transmit, and store information [3]. In order to be successfully applied in light-wave technology and optical circuitry a material should satisfy many criteria: easy processing, high transparency, high physical, mechanical, thermal, electrical, and chemical stability, compatibility with the other materials used for microelectronics, high optical power damage threshold, high optical nonlinearity, and reasonably low cost. Polymeric materials may be, perhaps, the first to combine most of these properties, avoiding stringent tradeoffs.

Concepts of optical computing and optical signal and image processing have been developed utilizing NLO processes to perform the functions of frequency conversions, light modulation, optical switching, optical logic, optical memory storage, and optical limiter functions. Devices performing these functions utilize two important manifestations: frequency conversion and refractive-index modulation. In the case of the second-order NLO effects refractive-index modulation is produced by application of an external electric field. Using second-order effects polymeric materials may find applications such as in second-harmonic generation, high-density data storage, and electro-optic spatial light modulation in the near future. As far as the third-order NLO effects are concerned, the refractive index is modulated by controlling the intensity of the optical field, and it provides the mechanism for optical switching and optical bistability. The main advantage of using all-optical processing is the gain of speed and gain in connectivity. Polymeric materials posses fast NLO response and also can be fabricated in the form of fibers and channel waveguides to satisfy the necessary requirements. In addition, an important third-order NLO phenomenon is two-photon absorption (TPA) in which a molecule can simultaneously absorb two photons, when irradiated by intense laser pulses. Since the availability of femtosecond (fs) laser in the 1990s, a great deal of work has been done for developing the efficient two-photon absorbing materials. Such TPA materials can be

employed for various photonic applications including 3-D optical data storage, 3-D microfabrication, photodynamic therapy, and optical power limiting. In this chapter, we discuss the topics related to certain theoretical aspects, concepts of material design, and evaluation techniques for second- and third-order NLO polymers as well as for two-photon absorbing organic and polymeric materials.

49.2 MEASUREMENTS OF β OF POLYMERS

Organic polymers, being amorphous, do not exhibit any second-order NLO effect, even though the molecules themselves are acentric. Therefore, in order to observe any second-order NLO effect, the isotropy of the medium has to be perturbed. This is usually accomplished by application of a strong dc electric filed. In the liquid phase, measurements are made by the technique known as electric-field-induced second-harmonic (EFISH) generation [5]. In this technique the solution is contained in a wedge-shape fused silica cell. The cell is sandwiched between two electrodes. A large dc voltage pulse is applied to the electrodes to disturb the average molecular orientation. At the same time the probing laser beam also is incident on the cell. The emerging second-harmonic generation (SHG) signal at 2ω from the cell is recorded, as the cell is translated across the laser beam (Fig. 49.1). The NLO polarization responsible for the EFISH process can be expressed as [3]

$$P_i(2\omega) = \chi_{ijkl}^{(3)}(-2\omega;\omega,\omega,0)E_j^\omega E_k^\omega E_l^0. \qquad (49.4)$$

As the cell is moved across the incident laser beam, the optical path inside the cell varies linearly with the translated distance, so the resulting SHG signal exhibits an oscillatory behavior. The intensity of the EFISH signal can be approximated by

$$I_{2\omega} = \left(\frac{8\pi(2\omega)^2}{n_\omega^2 n_{2\omega}^2 c^2 \varepsilon_0^2}\right)\frac{\sin^2\left[\Delta k(l/2)\right]}{\left[\Delta k(l/2)\right]^2}|\chi^{(3)}|^2 l^2 I_\omega^2, \qquad (49.5)$$
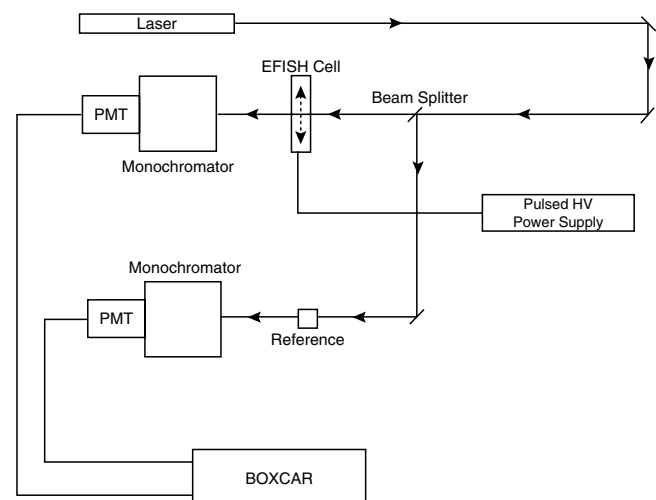
FIGURE 49.1. Schematics of experimental arrangement of electric-field-induced second-harmonic generation.

where n_i^ω are the refractive indices at corresponding frequencies, c is the velocity of light in vacuum, l is the thickness of the cell, ε_0 is the permittivity of free space, and Δk is the phase mismatch. Because of the dispersion of the refractive index, the fundamental and the SHG waves propagate with two different phase velocities (ω_i/K_i). Therefore, in general there exists a phase mismatch between the fundamental and the SHG waves. As shown in Eq. (49.5) when the cell is moved across the incident laser beam optical path inside the cell varies, so the emerging SHG signal generates fringes. These fringes are numerically analyzed to obtain coherence length and amplitude, which contain the necessary information to deduce β. In fact, in an EFISH experiment what one measures is an effective third-order nonlinearity $\chi_{\text{EFISH}}^{(3)}$, which can be given by

$$\chi_{\text{EFISH}}^{(3)} = f^{(0)}f^{(\omega)}f^{(\omega)}f^{(2\omega)} \sum_c N\left(\frac{\mu\beta}{5KT} + \gamma_{\text{el}}\right), \quad (49.6)$$

where N is the number density, kT is the thermal energy, and the summation is over all components of the solution (the solute and the solvent). γ_{el} is the effective third-order hyperpolarizability for the pure four-wave mixing process ($2\omega = \omega + \omega + 0$) and it can be determined by examining the temperature behavior of $\chi_{\text{EFISH}}^{(3)}$ or can be approximated from results of a third-harmonic generation or degenerate four-wave mixing experiment. However, the magnitude of γ_{el} is generally an order of magnitude smaller than the $\mu\beta/5kT$ contribution and, therefore, can be neglected. In a centrosymmetric medium ($\mu=0$) the EFISH signal is generated only by the third-order polarizability. The terms f describe the local field factor, which relates the applied field $E(\omega)$ to the local field $F(\omega)$.

49.3 MEASUREMENTS OF $\chi^{(2)}$ OF POLYMERS

In polymeric materials the second-order bulk susceptibility $\chi^{(2)}$ can be related to the hyperpolarizability β through the relationship [3]

$$\chi_{IJK}^{(2)}(-2\omega;\omega,\omega) = N\beta_{IJK}f_I^{2\omega}f_J^\omega f_K^\omega \langle O(\theta,\phi)\rangle, \quad (49.7)$$

where N is the molecular number density, $f_p^{q\omega}$ is the local-field factor, and $\langle O(\theta,\phi)\rangle$ is the orientation factor that projects β_{ijk} on to macroscopic coordinates IJK. It should be noted that in the past the majority of the SHG data have been presented in terms of a d_{ijk} coefficient, which is related to $\chi^{(2)}$ by $\chi_{ijk}^{(2)} = 2d_{ijk}$. The number of nonzero components in the $\chi_{ijk}^{(2)}$ tensor depends on the point-group symmetry of the material.

There are several techniques, both absolute and relative, which can be used to evaluate $\chi_{ijk}^{(2)}$ components of a material [3]. However, in the case of polymeric materials the most useful method is Maker fringe method [6–8]. The general form of the second-order polarization created in a sample by the incoming fundamental beam can be approximated as [3]

$$P_i(2\omega) = \chi_{ijk}^{(2)}(-2\omega;\omega,\omega)E_J^\omega E_k^\omega. \quad (49.8)$$

In the Maker fringe method the sample is rotated in a plane perpendicular to the plane of the probing laser beam (Fig. 49.2), giving rise to a fringe pattern. The magnitude of the second-order polarization created in the sample depends on a number of parameters as shown in Eq. (49.9), where $\chi^{(2)}$ is the NLO coefficient, l is the thickness of the sample, $n_{i\omega}$ is the refractive index at the relevant frequency, P_ω is the intensity of the fundamental beam, and Δk is the phase mismatch between the fundamental and the SHG beams:

$$P_{2\omega} \propto \left(\frac{1}{n_\omega^2 n_{2\omega}}\right)\frac{\sin^2[\Delta k(l/2)]}{[\Delta k(l/2)]^2}|\chi^{(2)}|^2 l^2 |p_\omega|^2. \quad (49.9)$$

As shown in Eq. (49.9) the SHG polarization generated in the sample shows an oscillatory behavior as a function of the sample thickness. Therefore, if the sample is rotated the SHG intensity shows a fringe pattern as a function of the angle of rotation. These fringes under the condition $\Delta k \neq 0$ are known as Maker fringes and their period is related to the coherent length l_c. The fringes are originated due to the phase mismatch (Δk) between the forced and harmonic waves. The SHG intensity oscillates with the angle as shown in Eq. (49.10), where l is the sample thickness, $I_m(\theta)$ is the envelope function, and $l_c(\theta)$ is the coherence length. Experimentally, the coherent length is determined by fitting the Maker fringes to the appropriate theoretical expression. Once the coherent length is determined by a fitting procedure, with the proper choice of input and output polarization combinations, one can evaluate the NLO coefficients with respect to a known reference (for example, quartz) by using the simplified ($n_\omega \approx n_{2\omega} \approx n$) relationship given in Eq (49.11) [2]:
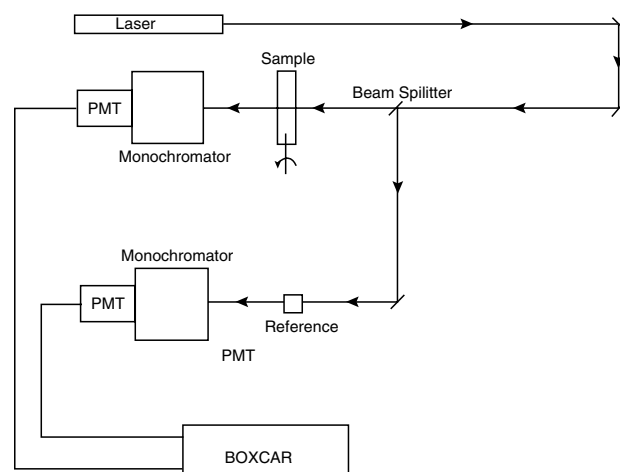
FIGURE 49.2. Schematics of experimental arrangement for measuring $\chi^{(2)}$ values of oriented polymers by the second-harmonic generation. The same arrangement can be used for the measurements ox $\chi^{(3)}$ via third-harmonic generation. In the case of the third-harmonic generation the measurement is usually carried out in a vacuum.

$$I_\omega = I_m^2(\theta) \left[\sin^2 \left(\frac{\pi l}{2 l_c(\theta)} \right) \right]^2, \qquad (49.10)$$

$$\chi_s^{(2)} \approx \frac{\pi}{2} \left(\frac{n_s^3}{l_s^2} \right)^{1/2} \left(\frac{l_c^2}{n_r^3} \right)^{1/2} \frac{I_{2\omega, S}}{I_{2\omega, r}} \chi_r^{(2)}. \qquad (49.11)$$

However, organic polymers, being amorphous, do not show second-order NLO effects. In order to employ them in second-order NLO measurements a polar order is induced by an external means such as electric field poling process or the Langmuir–Blodgett (LB) technique. Poled polymers and the majority of the LB films possess $C_{\infty v}$ symmetry. Therefore, the second-order optical susceptibility tensor for SHG has only three independent nonzero elements, namely, $\chi_{zzz}^{(2)}$, $\chi_{zxx}^{(2)}$ and $\chi_{xxz}^{(2)}$. Under Klienman symmetry [9] conjecture this reduces to two independent elements $\chi_{zzz}^{(2)}$ and $\chi_{zxx}^{(2)}$. These two elements can be evaluated by measuring the p-polarized SHG intensity emerging from the sample by incident p- and s-polarized fundamental beams, respectively.

49.4 β AND $\chi^{(2)}$ VALUES OF POLYMERS

The β and $\chi^{(2)}$ values have been measured for a large number of chromophores in solution and in polymeric films in attempts to identify efficient second-order NLO polymers. Table 49.1 shows $\mu\beta$ values that were derived from EFISH measurements of several organic polymers. All polymers in Table 49.1 have basically the same hyperpolarizability as their analogous monomers [10]. Also the copolymer and the homopolymers exhibit the same $\mu\beta$ values in solution, indicating no enhancement of NLO properties due to cooperative effects. In the case of 4-methoxy-4′-carbomethoxy-α-amino-α'-cyanostilbene polymers, again the $\mu\beta$ values are approximately the same [11]. However, in the case of NSPMA$_n$,NSV$_n$, and NBSBMA$_n$ polymers, NSPMA$_n$ has a noticeably larger hyperpolarizability

which can be attributed to the electron donating strength of the amino group [10].

The early studies on electric field poling were performed mainly on the guest-host systems, for instance, DANS dissolved in thermotropic nematic liquid-crystalline polymers [12]. In this guest-host system polar order decays rapidly. The $\chi_{zzz}^{(2)}$ value was about 1 pm/V. Therefore, the later investigations on guest-host systems were focused on both increasing the temporal stability as well as the $\chi_{zzz}^{(2)}$ value.

Among guest-host systems, the most studied system is Disperse Red-doped polymethylmethacrylate (PMMA) (Fig. 49.3) [13]. The early poling experiments on this system were accomplished by using parallel-plate electrodes and different doping levels. The maximum $\chi_{zzz}^{(2)}$ value obtained with parallel-plate poling was 5 pm/V. Subsequent experiments employed corona poling, and it was possible to achieve a $\chi_{zzz}^{(2)}$ value of 13.4 pm/V in thus poled samples [14]. Table 49.2 shows $d_{33}(= 0.5\chi_{zzz}^{(2)})$ values of various NLO chromophores in a PMMA polymer host [13–17].

One efficient way to increase the number density of NLO chromophores in a polymeric host, without crystallization, phase separation, and any concentration gradient, is to attach them as side chains of a polymer [15,18]. Also, the temporal stability of the poled structures of side-chain NLO polymers has been proven to be much better than that of the same guest–host system due to the higher glass transition temperature of the polymer. A number of poled side-chain NLO polymers (Fig 49.4) have employed for SHG measurements. Table 49.3 exhibits d_{33} values of some side-chain NLO polymers [16–28].

Many of the side-chain NLO polymers, both copolymers and homopolymers, have been designed using a PMMA polymer skeleton as the backbone. This includes novel methacrylate polymers which contain a molecular-ionic NLO chromophore, N-akkylpyridinium salt, in the side chain [25,26]. The corona-poled polymer films of such polymers showed a larger $\chi^{(2)}$ value of the homopolymer

TABLE 49.1. *The product ($\mu\beta$) obtained from EFISH measurements of several second-order NLO polymers.*

Polymer	$\mu\beta(10^{-48}$ esu)	$\lambda\mu$	References
NSPMA$_n$	93.1	1.9074	[9]
NSV$_n$	315	1.064	[9]
NSME-BP6-5	305	1.907	[9]
	561	1.064	
NBSBMA$_n$	93	1.907	[9]
	265	1.064	
4-Methoxy-4′-carbomethoxy-α-amino-α'-cyanostilbene: R $= 4 - CH_2CH_2O-$	74	1.907	[10]
4-Methoxy-4′-carbomethoxy-α-amino-α'-cyanostilbene: R $= 4 - CH_2O-$	61	1.907	[10]
4-Methoxy-4′-carbomethoxy-α-amino-α'-cyanostilbene: R $= 4 - O-$	63	1.907	[10]
4-Methoxy-4′-carbomethoxy-α-amino-α'-cyanostilbene: copolymer	79	1.907	[10]

NSPMA$_n$ NSV$_n$ NBSBMAn NSME-BP6-5

4-methoxy-4'-carbomethoxy-α-amino-α'-cyanostilbene

4-methoxy-4'-carbomethoxy-α-amino-α'-cyanostilbene: copolymer
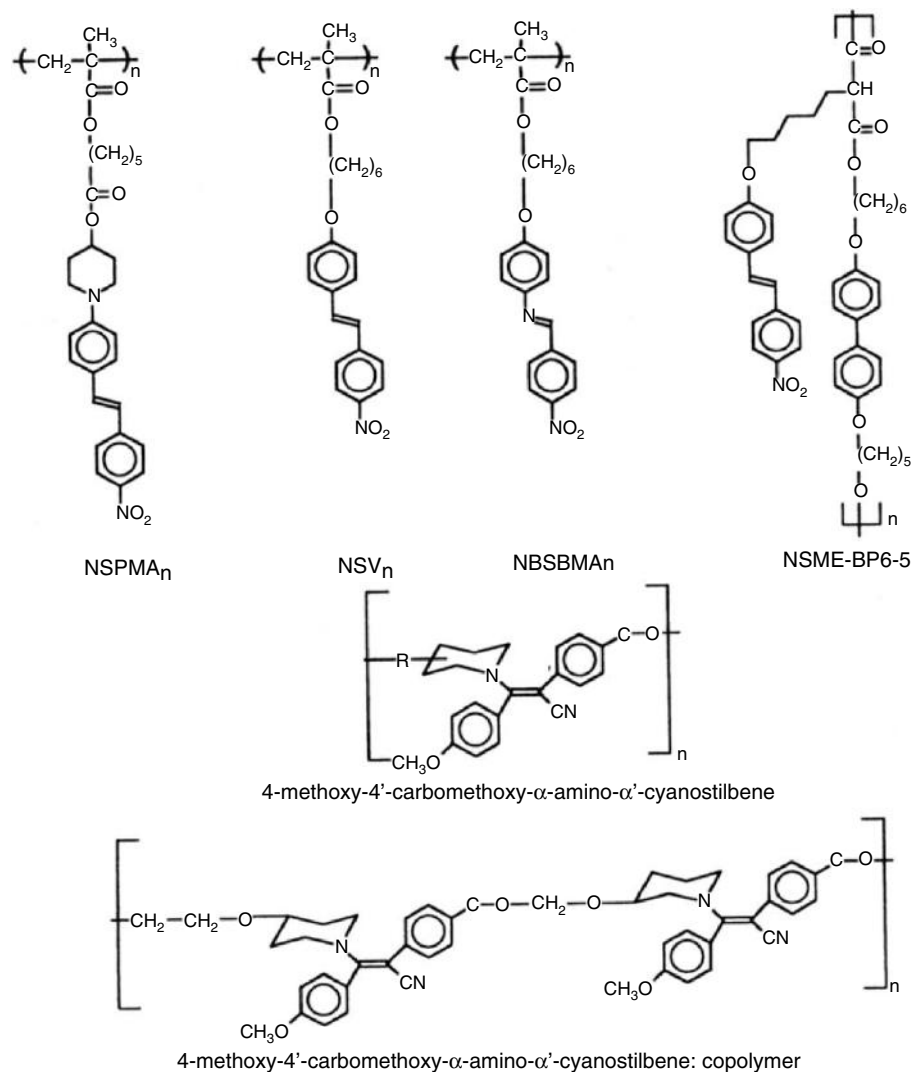
FIGURE 49.3. Molecular structures of the NLO polymers described in Table 49.1.

TABLE 49.2. *The NLO coefficient $d_{33}(=0.5\chi_{333}^{(2)})$ of various NLO chromophores doped in a PMMA polymer matrix. NLO chromophores have been oriented by the poling process.*

Polymer	d_{33} (pm/V)	$\lambda(\mu m)$	References
PMMA:Disperse Red (plate poling)	2.5	1.58	[12]
PMMA:Disperse Red (corona poling)	6.7	1.58	[13]
PMMA:4-(dicyanovinyl)-4-(dialkylamino) azobenzene	74	1.58	[14]
PMMA:Disperse Orange 3	5.8	1.064	[15]
PMMA:4-(tricyanovinyl)-N, N'-dimethylaniline	16	1.064	
PMMA:Disperse Red	5.8	1.064	
PMMA:3-(dicanomethylene)-5,5dimethyl-1-[[5-(dimethylamino)-2-thienyl]vinyl]cyclohexene	38	1.3	[16]
PMMA:3-(dicyanomethylene)-5,5-dimethyl-1-[p-(dimethylamino)styryl]cyclohexene	26	1.3	[16]
PMMA:2-[[4-[-(dimethylamino)styryl]phenyl] methylene]propanediritrile	27	1.3	[16]
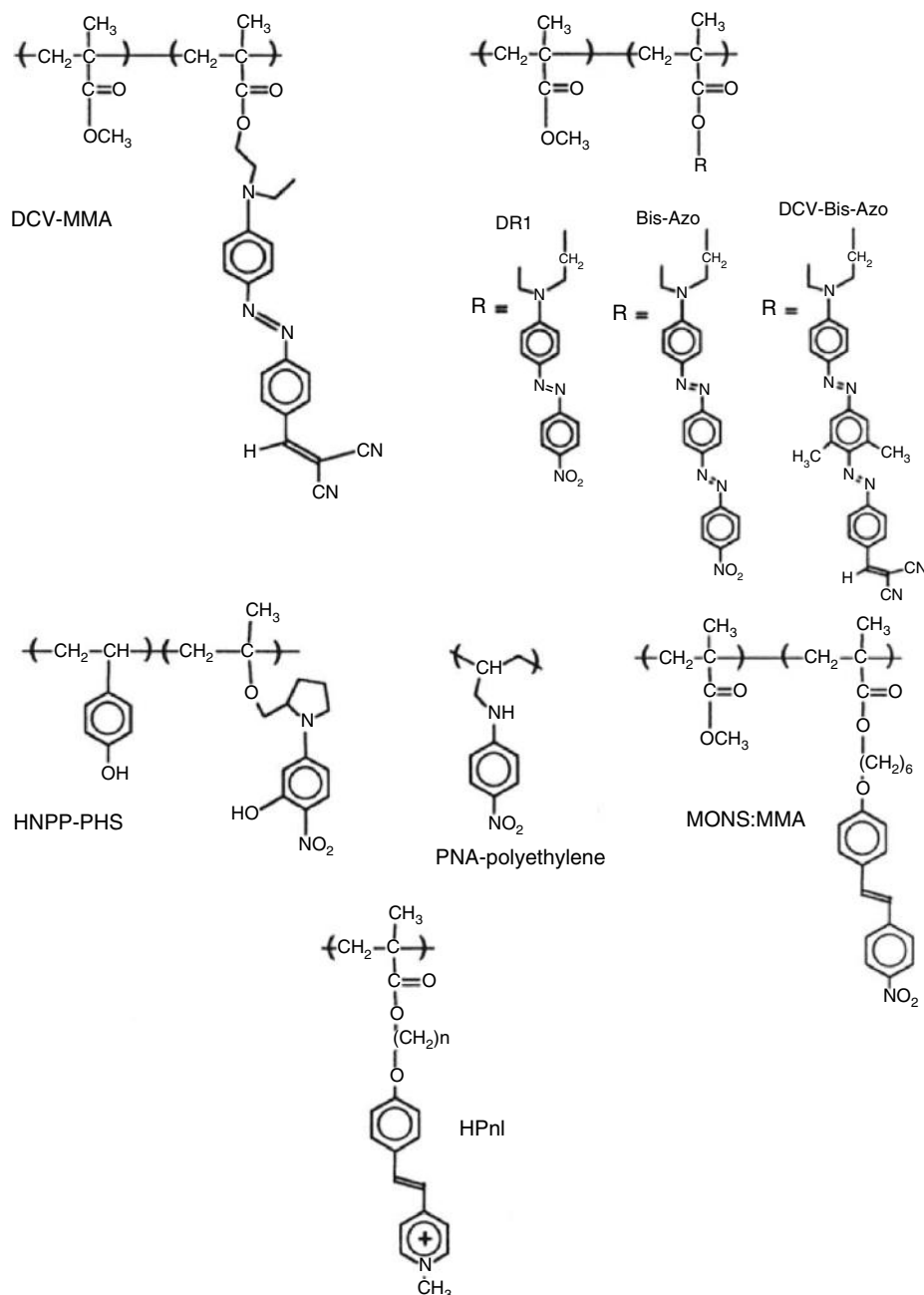
FIGURE 49.4. Molecular structures of the NLO polymers described in Table 49.3.

($\chi^{(2)}_{zzz} = 15.9\,\text{pm/V}$) compared to that of the copolymer ($\chi^{(2)}_{zzz} = 10.0\,\text{pm/V}$). The lower $\chi^{(2)}_{zzz}$ value of the homopolymer has been attributed to the lower chromophore concentration in the copolymer. The temporal stability as well as the poling-induced alignment of these side-chain molecular-ionic polymers can be largely improved by incorporation of bulky counterions. For example, the SHG intensity in a bulky counterion, tetraphenylborate, -containing polymer is about five times larger than that of the analogous iodide-containing polymer [25].

Somewhat larger d_{33} values (40 pm/V at $1.064\,\mu\text{m}$) have been obtained in several poly(styrene-co-acrylic acid esters)

side-chain copolymers that were synthesized by attaching hydroxy-functionalized azobenzene, benzylidene aniline, and coumarin chromophores. The stability of the poled structures of these polymers was found to be better than that of NLO guest-loaded PMMA films [29]. Temporal stability of poled structures can be improved if NLO chromophores are attached to the polymer backbone forming a main-chain polymer (Fig. 49.5) (Table 49.4). One such example is poly(urea) [30]. This polymer can be prepared from vapor deposition polymerization. Some main-chain NLO polymers in which the dipole moment of the NLO chromophore is perpendicular to the polymer backbone

TABLE 49.3. *The NLO coefficient $d_{33}(= 0.5\chi^{(2)}_{333})$ of poled side-chain NLO polymers.*

Polymer	d_{33} (pm/V)	$\lambda(\mu m)$	References
DCV-MMA	>50	1.58	[15]
DR1-tethered PMMA	43	1.064	[18]
bis-Azoanalog of DR1-tethered PMMA	69	1.064	[18]
Dicyanovinyl bis-Azoanalog of DR1-tethered PMMA	150	1.064	[18]
PNA attached polyethylene	>30	1.064	[19]
HNPP-PHS	7.5	1.064	[20]
Poly(N-MNA acrylamide)	3	1.064	[21]
NPP-PPO	27	1.064	[22,23]
HPOB	15.6 (10^{-8} esu)	1.064	[24]
HP6B	36.2 (10^{-8} esu)	1.064	[24]
HP6I	7.6 (10^{-8} esu)	1.064	[24]
HP10B	21.8 (10^{-8} esu)	1.064	[24]
HPBR15	11.8	1.064	[25]
HPBR21	10.8	1.064	[25]
CP6I-HEMA	20	1.064	[25]
NSPMA$_n$	7.3 (10^{-8} esu)	1.064	[9]
NBSBMA$_n$	7.0 (10^{-8} esu)	1.064	[9]
NSME-BP6-5	1 (10^{-8} esu)	1.064	[9]
MONS:MMA	20 (10^{-8} esu)	1.064	[26]
EPO-TEK 310-2 and DANS	0.04–0.4	1.064	[27]

BISA-NAT

BISA-NA

BISA-NPDA

Polyurea
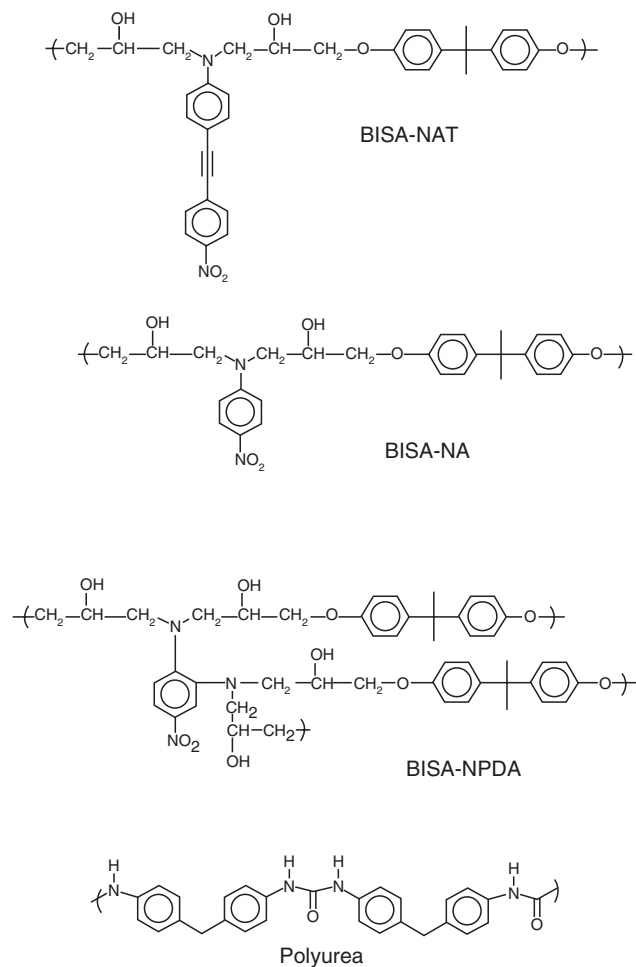
FIGURE 49.5. Molecular structures of the NLO polymers described in Table 49.4.

FIGURE 49.5. Continued

have also been used for NLO measurements. An example of such a polymer is bisA-ANT [31]. This type of main-chain polymer is expected to be easier to pole than the head-to-tail main-chain polymers due to their enhanced flexibility. The bulky tolane unit in bisA-ANT is supposed to improve the temporal stability of the poled films. In fact, the decay of polar order of bisA-ANT was found to be much better than that of the analogous pNA polymer.

The temporal stability of poled NLO materials is considerably improved by incorporating them in cross-linked systems (Fig. 49.6). Interesting results have also been obtained recently by Dalton and co-workers in cross-linked poly(urethanes). In their study the NLO chromophore was polymerized with bifunctional isocyanate to obtain the corresponding urethane polymer [32,33]. Both cross-linked and non-cross-linked polymers show no thermal transitions below 270°C. Although cross-linking can remarkably improve the temporal stability of poled structures, thermal and chemical cross-linking require processing of materials at elevated temperatures. These temperatures sometimes tend to degrade NLO chromophores. Therefore, an alternative cross-linking procedure such as photochemical cross-linking has been studied [34,35]. One such system is poly-

Chromophore density: 33 wt %
Mw: 4664
r_{33} = 60 pm/V at 1.55 μm

FIGURE 49.6. Chemical structure of a multiarm cross-linkable Nlo dendrimer.

(vinylcinnamate) doped with a NLO chromophore. In this guest–host system it was possible to achieve a 20% loading level of guest molecules without phase separation. Although the T_g of the system is found to be dependent on the chromophore concentration, plasticization of the chromophore was remarkably small. Absorption measurements indicate that the polar order in the poled film persists for a long period of time (many months) without any change [35]. Table 49.4 shows d_{33} values obtained from poled films of some side-chain polymers [36–43].

Also, the Langmuir–Blodgett (LB) technique has been employed to prepare oriented thin films of organic polymers for NLO investigations. An LB film containing 20 bilayers of alternating monolayer of two different polymers yield a thickness of 60 nm and a $\chi^{(2)}_{zzz}$ of 11.2×10^{-16} esu cm per bilayer at 1.047 μm [44]. Molecular nonlinearity in this LB film is supposed be arising from charge-transfer excitation in the polymer with the sulfonyl group as the acceptor and amino group as the donor. Optical waveguides capable of guiding blue light with low loss (2–6 dB cm^{-1}) over several centimeters have been fabricated from NLO polymers using the LB technique. However, it was necessary to use another NLO inactive polymer (t-butyl methacrylate polymer) as buffer layer in order to prevent the formation of inversion center in the film [45–48]. An LB film containing 168 bilayers (thickness $\sim 0.44\,\mu$m) showed waveguide attenuation at 457.9 nm of 5.8 dB/cm for TE polarization and 2.6 dB/cm for TM polarization. The SHG measurements on a 0.88-μm-thick LB film results in a $\chi^{(2)}_{zzz}$ value of 8×10^{-9} esu. Similar $\chi^{(2)}_{zzz}$ values ($d_{33} = 5.3 \times 10^{-9}$ esu) have been obtained for Langmuir–Schaefer films of mesogenic moieties containing polysilane copolymers [49].

Current strategies for developing highly $\chi^{(2)}$ activities of NLO polymers basically involve molecular design concepts, same as presented in the previous sections. The key steps are: (i) design of high $\mu\beta$ chromophores; (ii) improvement of temporal stability of NLO response in polymer matrices; and (iii) poling efficiency of the polymeric systems [50]. Among these, the most important factor might be to design highly efficient NLO chromophores. Therefore, to under-

stand the structure–property relationship of chromophores with high $\chi^{(2)}$ values, quantum mechanical analysis based on a simple two-level model description and bond-order alternation principle have been investigated [51,52]. Table 49.5 shows values of $\mu\beta$ at the off-resonance wavelength of 1907 nm for some representative chromophores, with improved optical nonlinearity [53,54]. A large enhancement of optical nonlinearity can be obtained by extending the length of π-bridged chains with strong electron acceptor such as the cyano group. It was shown that very large electro-optic (E-O) coefficients could be achieved by introducing highly efficient chromophores into amorphous polymer matrix such as poly(methyl methaacrylate)(PMMA), polycarbonate, polyquinoline, etc. [55–59]. In the case of PMMA added with 17.5% of chromophore 10, the E-O coefficient was reported to be $r_{33} = 105\,\mathrm{pmV}^{-1}$ at 1.33 μm [60]. This is more than three times higher than that of lithium niobate (LiNbO$_3$; $r_{33} = 31\,\mathrm{pmV}^{-1}$), which has been used as a material for E-O modulators.
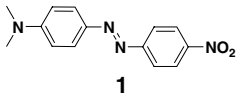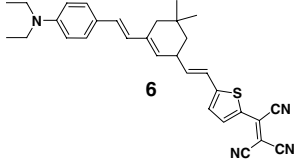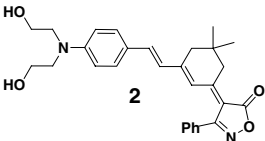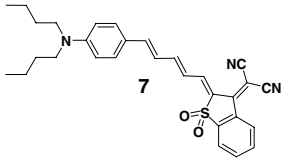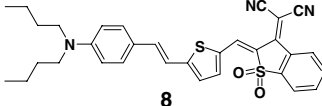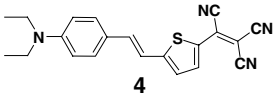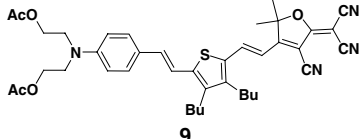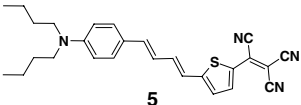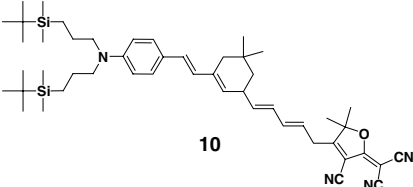
To improve the temporal and the thermal stabilities of poled NLO dipoles, polyurethanes can be considered as one of the best matrix materials, because of their extensive formation of H-bonding between the urethane linkages which would increase the rigidity of the polymer chain. Several researchers succeeded in making greatly enhanced NLO polymeric systems by using polyurethane backbone [61–68]. Also, polyimides [69–80], polyetherimides [81,82], polyamides [83–89], and polyesters [90–94] as matrix polymers can also provide an enhanced thermal stability of aligned dipoles due to high glass transition temperature (T_g) characteristics which also result in the chain stiffness. By incorporating the NLO chromophores into these polymer backbones, much improved long-term thermal stability of NLO activity were obtained.

Another promising approach for making efficient NLO systems is the employment of dendritic polymers [95–111]. Compared to common polymers, dendritic NLO polymers can provide many advantages from the viewpoint of structural variation, optimization of E-O values, thermal stability, optical loss, etc. Jen's group prepared a multiarm

TABLE 49.4. *The NLO coefficient $d_{33}(= 0.5\chi^{(2)}_{333})$ of poled main-chain NLO polymers.*

Polymer	d_{33} (pm/V)	$\lambda(\mu m)$	References
Polyurea	6.6	1.064	[29]
BisA-NAT	90	1.064	[35]
BisA-NAT	$\sim$30	1.064	[35]
BisA-NPDA	13.5	1.064	[36]
	$d_{31} = 3$		
Polyurethane	40	1.064	[37]
NLO chromophore tethered	120	1.064	[38]
Polyimide (NLO chromophore tethered)	4.6–5.5	1.064	[39]
NLO-chromophore-tethered acrylate	60		[40]
Polycinnamate: photocross-linked with NLO chromophore	<11.5–21.5	1.54	[41,42]

TABLE 49.5. *The $\mu\beta$ values of NLO chromophores with the extended π-chain length and strong acceptor at the end of molecules.*

NLO Chromophores	$\mu\beta$ (10^{-48} esu)	NLO Chromophores	$\mu\beta$ (10^{-48} esu)
1	580	**6**	13,000
2	926	**7**	13,500
3	3,300	**8**	15,000
4	6,200	**9**	18,000
5	9,800	**10**	35,000

cross-linkable NLO dendrimer which consists of phenyl-tetracyanobutadienyl thiophene-stilbene-based NLO chromophore as the core and cross-linkable trifluorovinyl ether-containing dendrons as the exterior unit (Fig. 49.6) [99]. The maximum r_{33} value of this system was found to be $60\,\mathrm{pmV^{-1}}$ at 1.55 μm and long-term alignment stability was achieved for the poled dendrimer after thermal curing. It retained over 90% of its original r_{33} value at 85 °C for more than 1,000 hours.

49.5 THIRD-ORDER NLO PHENOMENA

Third-order NLO effects are described by the macroscopic term $\chi^{(3)}_{IJKL}$ in Eq. (49.2). As in the case of second-order NLO susceptibility, the third-order NLO susceptibility $\chi^{(3)}_{IJKL}$ can be related to the microscopic third-order NLO coefficient γ_{IJKL} via the following relationship [2,3]:

$$\chi^{(3)}_{IJKL} = N f_I^{\omega_1} f_J^{\omega_2} f_K^{\omega_3} f_L^{\omega_4} \gamma_{IJKL}, \qquad (49.12)$$

where N is the molecular number density and f_p^{ω} is the appropriate local field factor. The γ_{IJKL} in the laboratory fixed frame can be related to the molecular frame as

$$\gamma_{IJKL} = \sum_{ijkl} a_{Ii} a_{Jj} a_{Kk} a_{Ll} \gamma_{ijkl}, \qquad (49.13)$$

where a_{Ii} is the directional cosine between I and i of the laboratory and molecular frame, respectively. Being a fourth-rank tensor, $\chi^{(3)}_{IJKL}$ contains 81 elements [112]. However, the nonzero components of $\chi^{(3)}_{IJKL}$ depend on the symmetry of the molecule. Third-order NLO measurements can conveniently be made on solution or in thin films of polymers. In solution measurements an average over all directions (orientations) has to be taken into account. For example, if the solute molecules belongs to the orthorhombic point group there are 21 nonzero components in the γ_{ijkl} tensor. If one assumes Klienman symmetry [9] ($\gamma_{xxyy} = \gamma_{xyxy} = \gamma_{xyyx} = \gamma_{yyxx} = \gamma_{yxxy} = \gamma_{yxyx}$ the number of independent elements reduces to six, i.e., γ_{xxxx}, γ_{yyyy}, γ_{zzzz}, γ_{yyzz}, γ_{xxzz}, and γ_{xxyy}. What is measured in experiments is the macroscopic third-order NLO susceptibility $\chi^{(3)}_{IJKL}$. For example, in the degenerate four-wave mixing experiment, when all the beams possess the same polarization, one measures $\chi^{(3)}_{xxxx}(-\omega;\omega,\omega,-\omega)$. The third-order polarizability calculated from this measurement is an orientationally averaged quantity, $\langle\gamma\rangle$, which can be expressed as [113]

$$\langle \gamma \rangle = \frac{1}{5}(\gamma_{xxxx} + \gamma_{yyyy} + \gamma_{zzzz} + 2\gamma_{xxyy} + 2\gamma_{xxzz}$$
$$+ 2\gamma_{yyzz}). \qquad (49.14)$$

There are several four-wave mixing techniques that can be used to evaluate $\chi_{IJKL}^{(3)}$ components of a material [3]. It should be noted that there are numerous third-order processes that are described by different $\chi_{IJKL}^{(3)}$ terms. Hence, a comparison of $\chi_{IJKL}^{(3)}$ derived from one technique with $\chi_{IJKL}^{(3)}$ evaluated with another technique should be made cautiously.

49.6 THIRD-HARMONIC GENERATION

In general, the NLO polarization responsible for third-harmonic generation (THG) can be given by [2,3]

$$P_I(3\omega) = \chi_{IJKL}^{(3)}(-3\omega;\omega,\omega,\omega)E_J^\omega E_K^\omega E_K^\omega. \qquad (49.15)$$

THG is a coherent process and arises due to purely electronic contributions and does not depend on the population of the excited state. However, the process can be resonantly enhanced in the vicinity of one- or multiphoton absorption bands. The THG intensity created in a sample can be expressed as [2]

$$I_{3\omega} = \left(\frac{(3\omega)^2}{n_{3\omega}n_\omega^3 c^4 \varepsilon_0^2}\right)\frac{\sin^2[\Delta k(l/2)]}{[\Delta k(l/2)]^2}|\chi^{(3)}|^2 l^2 I_\omega^3. \qquad (49.16)$$

As shown in Eq. (49.16) the THG intensity shows symmetrically damped oscillatory behavior near $\Delta k = 0$. Unlike SHG, phase matching is very difficult to achieve in THG due to dispersion of the refractive indices. In the THG experiment, the intensity of the sample is measured with respect to a standard sample under identical experimental conditions. Under the conditions $\Delta k \neq 0$, the sample is rotated around an axis perpendicular to the plane of incidence, and the THG signal is recorded as a function of the angle of rotation. The resulting THG fringes are analyzed to obtain the coherent length of the material. Then the

$\chi_{IJKL}^{(3)}(-3\omega;\omega,\omega,\omega)$ of the sample is evaluated using the following relationship [3]

$$\frac{I_{3\omega,\,s}}{I_{3\omega,\,r}} = \left(\frac{\chi_s^{(3)}}{\chi_r^{(3)}}\right)^2 \left(\frac{l_{c,\,r}}{l_{c,\,s}}\right)^2 \qquad (49.17)$$

49.7 DEGENERATE FOUR-WAVE MIXING

In a degenerate four-wave mixing (DFWM) process, three optical beams of the same frequency interact with the material to create a fourth beam of the same frequency. The NLO polarization responsible for this process can be given by [2,3]

$$P_I(\omega) = \chi_{IJKL}^{(3)}(-\omega;\omega,\omega,-\omega)E_J^\omega E_K^\omega E_L^{*\omega}. \qquad (49.18)$$

Measurements of DFWM contain both real and imaginary parts of $\chi_{IJKL}^{(3)}$. This method is convenient and versatile in measuring both electronic and dynamic nonlinearities and their response times. The experiment can be performed either in a forward (boxcar) geometry or in a backward-wave geometry. In the case of the backward-wave geometry the condition $\Delta k = 0$ is automatically satisfied. In this geometry two pump beams counterpropagate in the sample (Fig. 49.7). The probe beam is incident on the sample. The probe beam is incident on the sample at a small angle with the two pump beams. The signal beam is obtained as a phase conjugate beam (counterpropagating to the probe beam), and it corrects every distortion of the probe beam when it retraces it. The intensity of the signal beam for this process is given by

$$I_s = \left(\frac{\omega^2}{4n^2c^2}\right)|\chi^{(3)}|^2 l^2 I_f I_b I_p. \qquad (49.19)$$

Both pump beams are synchronized in time with their cross-correlation, and the DFWM signal is studied as a function of the time delay of the probe beam. For nonabsorbing materials the $\chi^{(3)}$ value is calculated using the relationship [3]
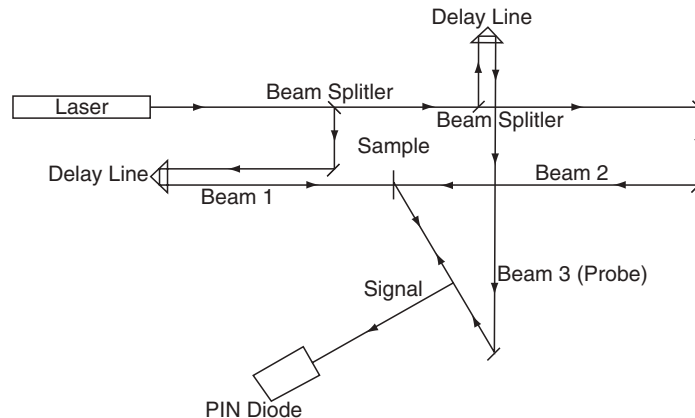
FIGURE 49.7. Schematics of experimental arrangement of the degenerate four-wave mixing (backward geometry) experiment.

$$\frac{\chi_s^{(3)}}{\chi_r^{(3)}} = \left(\frac{n_s}{n_r}\right)^2 \left(\frac{l_r}{l_s}\right)\left(\frac{I_s}{I_r}\right)^{1/2} \qquad (49.20)$$

For absorbing samples a correction should be made to compensate the absorption losses; consequently, $\chi^{(3)}$ can be calculated by the following relationship [3]:

$$\frac{\chi_s^{(3)}}{\chi_r^{(3)}} = \left(\frac{n_s}{n_r}\right)^2 \left(\frac{l_r}{l_s}\right)\left(\frac{I_s}{I_r}\right)^{1/2} \frac{\alpha l_s}{e^{(-\alpha l_s/2)}(1 - e^{(-\alpha l_s)})}, \quad (49.21)$$

where α is the linear absorption coefficient. In Eqs. (49.20) and (49.21), I_s and I_r refer to intensities at zero time delay.

49.8 OPTICAL KERR GATE

The optical Kerr gate (OKG) is a process that arises due to optically induced birefringence caused by a nonlinear phase shift. The NLO polarization for the OKG can be expressed as [2,3]

$$P_I(\omega) = \chi_{IJKL}^{(3)}(-\omega;\omega,\omega,-\omega)E_J^\omega E_K^\omega E_L^\omega. \qquad (49.22)$$

There are several different mechanisms such as electronic deformation, molecular reorientation, electrostriction, molecular redistribution, and thermal change that are responsible for the OKG process. Each of these mechanisms has its own strength and response time, which generally differ from each other. OKG measurements are usually performed by the incidence of a strong pump beam (orienting beam) on the sample. Then propagation characteristics of a weak probe beam is studied as a function of the delay time (Fig. 49.8). Initially both beams are linearly polarized. To retrieve the optical birefringence information the probe beam is passed through an analyzer.

The optical birefringence created in the sample due to penetration of strong pump beam can be expressed as
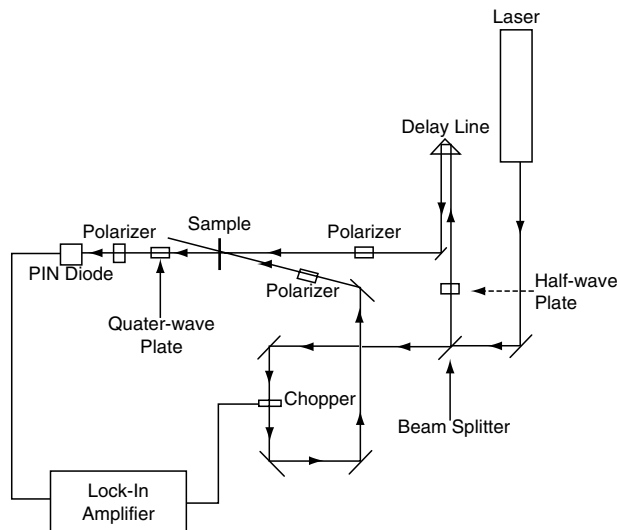
FIGURE 49.8. Schematics of experimental arrangement of the optical Kerr gate measurement.

$$\delta n = (\delta n_\parallel - \delta n_\perp) \propto \frac{\pi}{n_0}(\chi_{xxxx}^{(3)} - \chi_{xxyy}^{(3)}). \qquad (49.23)$$

This birefringence is probed by the weak probe beam. By delaying the probe beam, the time evolution of the process can be studied. The intensity of the signal of the probe beam through the Kerr gate as a function of the delay time can be written as [3]

$$I_t(\tau) = \int_{-\infty}^{+\infty} \langle E_{probe}^2(t - \tau) \rangle \sin^2\left(\delta n \frac{\pi l}{2}\right)dt \qquad (49.24)$$

Away from electronic resonances $\delta n = n_2 I_{pump}$. The quantity n_2 can be obtained from the measurement at $t = 0$ (peak value). Therefore, $\chi_{xxxx}^{(3)}$ can be obtained assuming that $\chi_{xxyy}^{(3)}$ is very small. However, away from resonances, in an isotropic medium a purely electronic nonlinearity leads to $\chi_{xxxx}^{(3)} = 3\chi_{xxyy}^{(3)}$. In such a situation $\chi_{xxxx}^{(3)}$ can be directly evaluated.

49.9 SELF-FOCUSING AND DEFOCUSING

Self-focusing and defocusing (SFD) also arise from the intensity dependence of the refractive index of the medium [114,115]. It is referred as self-action because the NLO polarization created by the input beam changes its own propagation characteristics. SFD does not provide any information on response time. In general the intensity-dependent refractive index responsible for SFD can be written as

$$n(\lambda) = n_0(\lambda) + n_2(\lambda)I, \qquad (49.25)$$

where I is the intensity of the input beam and n_0 is the linear refractive index. The NLO refractive index n_2 is related to $\chi^{(3)}$ as shown in Eq. (49.26). The self-focusing occurs as a combined effect of a positive n_2 and spatial variation of the laser-beam intensity. If the laser-beam intensity at the center of the beam is higher than that at the beam edges, a relatively larger refractive index is resulted at the center. So the sample acts as a positive lens and focuses the beam. Similarly, self-defocusing occurs when n_2 is negative. The relationship between n_2 and $\chi^{(3)}$ is shown below:

$$n_2(\lambda) = \frac{8\pi^2}{cn_0(\lambda)} \frac{\chi^{(3)}(\lambda)}{6}. \qquad (49.26)$$

There are two different $\chi^{(3)}$ measurement techniques that are based on self-action: (i) optical power limiter and (ii) the z scan. In the case of the optical power limiter the laser beam is focused in the sample with high n_2. For low input powers the transmitted beam is focused through a pinhole on the detector. As the power increases the self-focusing starts so that the focused beam is no longer focused through the pinhole and the power after pinhole decreases. Beyond a certain critical input power P_c, transmitted power levels off due to many other NLO processes. The critical power P_c is directly related to n_2 through the relation (for spatial Gaussian beam) [116]
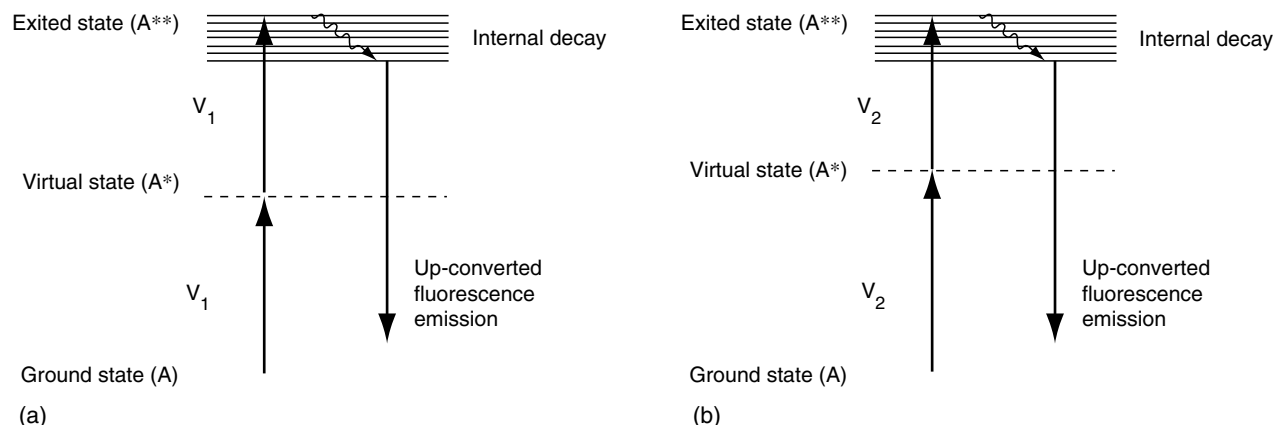
FIGURE 49.9 Two-photon absorption schemes. (a) Degenerate TPA process and (b) nondegenerate TPA process by simultaneous excitation of two-photons.

$$n_2 = \left(\frac{3.72c\lambda^2}{32\pi^2}\right)\frac{1}{P_c}. \qquad (49.27)$$

Therefore, $\chi^{(3)}$ can be evaluated.

The z-scan method allows determination of both the magnitude and the sign of n_2 [117]. In this technique a gaussian beam is focused on the sample, and the transmitted power is measured with a detector after passing the beam through a pinhole kept at the far field. The sample is then moved through the focus of the beam. Near the vicinity of beam focus self-action may occur due to strong intensity. The resultant plot of the intensity of the transmitted beam through the pinhole yields a dispersionlike behavior from which n_2 can be evaluated. The z-scan method is very sensitive to the beam quality so that beam should be a pure gaussian TEM$_{00}$. Because of the high-power and long-interaction- length requirements, the z scan is more suitable for the $\chi^{(3)}$ measurements of polymer solutions.

49.10 TWO-PHOTON ABSORPTION

The two-photon absorption (TPA) phenomenon was proposed by Göeppert-Mayer in 1931 [118] and experimentally first observed by Kaiser and Garrett [119]. TPA is one of the important third-order NLO features. When a molecule is exposed to an intense optical field such as from a pulse laser, it can absorb two photons simultaneously by involving a virtual intermediate state. Figure 49.9 schematically represent this process. If the two photons are of the same frequency, the process is called degenerate TPA; if they are of different frequency, the process is a nondegenerate TPA [120].

For a degenerate TPA process, the transfer rate of absorbed energy can be expressed as [121]:

$$\frac{dW}{dt} = \frac{8\pi^2\omega}{n^2c^2}I^2\chi^{(3)\text{imag}}, \qquad (49.28)$$

where I is the intensity of light, c is light velocity, n is refractive index, ω is optical frequency, and $\chi^{(3)}_{\text{imag}}$ is the imaginary part of $\chi^{(3)}$. Third-order NLO coefficient $\chi^{(3)}$

consists of a real part, $\chi^{(3)}_{\text{real}}$, and an imaginary part, $\chi^{(3)}_{\text{imag}}$, i.e., $\chi^{(3)} = \chi^{(3)}_{\text{real}} + \chi^{(3)}_{\text{imag}}$.

From the above equation, the following theoretical expression for TPA coefficient (center dot) can be derived because dW/dt is defined by multiplying the number of photons absorbed per unit time with the energy of light source, i.e., $dW/dt = (dn_{\text{photon}}/dt)h\nu$.

$$\sigma = \frac{8\pi^2h\nu^2}{n^2c^2N}\chi^{(3)\text{imag}} \quad \text{(unit: cm}^4\text{GW}^{-1}\text{)}, \qquad (49.29)$$

where N is the number of absorbing molecules per unit volume. Also, σ can be transformed into the following equation for the use of common unit.

$$\sigma_2 = \sigma h\nu^2 \quad \text{(unit: cm}^4 \text{ sec photon}^{-1}\text{)}. \qquad (49.30)$$

In addition, TPA cross-section σ_2 value is also expressed in Göeppert-Mayer (GM) unit; 1 GM is defined as 1×10^{-50} cm^4 sec photon^{-1}.

The evaluation of TPA activity of the materials can be made by various techniques such as up-converted fluorescence emission, nonlinear transmission, transient absorption, Z-scan, and four-wave mixing [122]. Among them, the up-converted fluorescence emission method is a simpler technique and the setup is shown in Fig. 49.10. In this method, the TPA cross-section value, σ_2 can be estimated according to the following equation [123]:

$$\sigma_2 = \frac{S_s\eta_r\phi_rC_r}{S_r\eta_s\phi_sC_s}\sigma_r, \qquad (49.31)$$

where the subscripts s and r denote the sample and reference compounds, respectively. The intensity of the two-photon excited fluorescence emission signal collected by a PMT detector is referred as S. The η and ϕ are the overall fluorescence efficiency and the fluorescence quantum yield, respectively. The number density of the molecules in solution is denoted as C. The σ_r is the TPA cross section value of the reference. As a reference material, fluorescein or Rodamine B is generally used [124]. The observed TPA cross-sections of a large variety of organic and polymeric materials are in
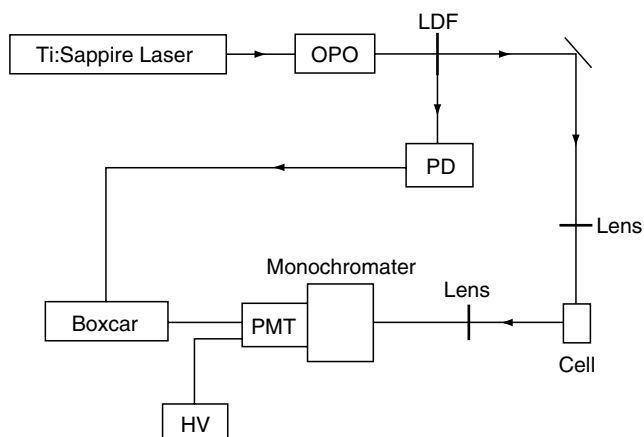
FIGURE 49.10. Schematics of experimental arrangement for measuring σ_2 values by the up-converted fluorescence emission method.

the range of several tens GM ($1GM = 1.0 \times 10^{-50} \, cm^4$ sec photon^{-1}) to the order of $\sim 10^4$ GM. The detailed TPA cross section values of various materials are presented in Section 49.12.

By virtue of quadratic power dependence of the TPA process, a tightly focused excitation beam can be used to induce photochemical reactions such as photopolymerization and photoisomerization in three-dimensions with high spatial resolution. As a result, various photonic devices including photonic crystals [125–128], optical data storage systems [129–135], 3-D micro-waveguides [136–138], and micro-electromechanical systems (MEMS) [139–142] have been fabricated. In addition to this, the two-photon approach can

contribute to novel photonic and biophotonic applications like two-photon upconverted lasing [143–150], optical power limiting for the protection of human eyes and efficient sensors against intense light [151–158], two-photon fluorescence bioimaging [159–163], photodynamic therapy [164–170], etc. A detailed general description of these potential applications using TPA techniques exists in the literature [122].

49.11 γ AND $\chi^{(3)}$ VALUES OF POLYMERS

Electronic structural requirements for third-order NLO polymers are different from those for second-order polymers [3,4]. The third-order NLO properties are very sensitive to the length of the π-electron conjugation. An interesting third-order NLO polymer is polydiacetylene, which can be prepared by solid-state polymerization (Fig. 49.11). The backbone of polydiacetylene is derived from a diacetylene skeleton, $R_1C \equiv CC \equiv CR_2$, therefore, depending on the nature of substituents a variety of derivatives can
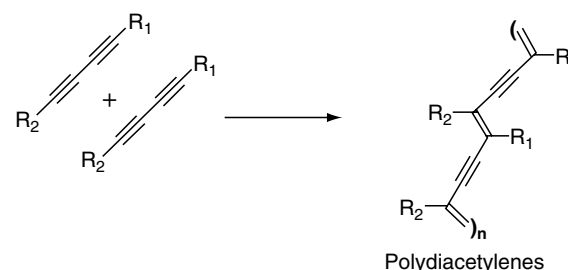
FIGURE 49.11. Molecular structures of the NLO polymers described in Table 49.5.

TABLE 49.6. $\chi^{(3)}$ values of different forms and different derivatives of polydiacetylenes.

R_1, R_2	$\chi^{(3)}(10^{-10}$ esu)	Method	References
R_1, $R_2 = CH_2OSO_2C_6H_4CH_3$ (single crystal)	8.5	THG	[56]
R_1, $R_2 = (CH_2)_4OCONHC_6H_5$ (single crystal)	1.6	THG	[56]
R_1, $R_2 = CH_2OSO_2C_6H_4CH_3$	90.0	DFWM	[57]
R_1, $R_2 = CH_2OSO_2C_6H_4CH_3$	2×10^5	SA	[58]
$R_1 = C_6H_3CF_3CF_3$; $R_2 = C_{13}H_{10}N$	1.1	THG	[59]
R_1, $R_2 = C_6F_4H_2(CH_2)_3CH_3$	1.2	THG	[59]
$R_1 = C_6H_3CF_3CF_3$; $R_2 = C_{13}H_{10}N$ (film)	4.3	EFISH	[60]
R_1, $R_2 = (CH_2)_3OCONHCH_2COOC_4H_9$ (film)	1.5	EFISH	[61]
R_1, $R_2 = (CH_2)_3OCONHCH_2COOC_4H_9$ (film)	0.13	DFWM	[62]
R_1, $R_2 = (CH_2)_3OCONHCH_2COOC_4H_9$ (film)	1.0	THG	[63]
R_1, $R_2 = (CH_2)_3OCONHCH_2COOC_4H_9$	2	DFWM	[64]
R_1, $R_2 = (CH_2)_3OCONHCH_2COOC_4H_9$	2.5	DFWM	[64]
R_1, $R_2 = (CH_2)_3OCONHCH_2COOC_3H_7$	9.0	DFWM	[62]
R_1, $R_2 = (CH_2)_3OCONHCH_2COOC_5H_{11}$	2.4	THG	[63]
R_1, $R_2 = C_{13}H_{10}N$ (film)	0.7	THG	[65]
R_1, $R_2 = C_{13}H_{10}N$ (oriented film)	6.0	THG	[66]
R_1, $R_2 = (CH_2)_4OCONH(CH_2)_{n-1}CH_3$	17.0	THG	[67]
R_1, $R_2 = CH_3(CH_2)_{15} - C - C = C - C(CH_2)_8COO$	0.56	THG	[68]
R_1, $R_2 = CH_3(CH_2)_{15} - C - C = C - C(CH_2)_8COO$	0.08	THG	[69]
R_1, $R_2 = C_6H_3CF_3CF_3$ (film)	0.4	THG	[59]
$R_1 = C_6H_3CF_3CF_3$; $R_2 = C_6H_4NHCH_3$ (film)	8.0	THG	[70]

be obtained. Table 49.6 shows $\chi^{(3)}$ values of a series of polydiacetylenes measured with different techniques at different wavelengths [171–185]. As seen in Table 49.6 the resonantly enhanced $\chi^{(3)}$ of polydiacetylene can be as high as 10^{-5}esu, the largest third-order nonlinearity for an organic observed to date.

Another interesting conjugated polymer is polythiophene, which has good environment stability compared to polyacetylenes (Fig. 49.12) (Table 49.7). Polythiophene has a $\chi^{(3)}$ value of 3×10^{-11} at a wavelength of $1.06 \, \mu$m. The resonantly enhanced value is about 2 orders of magnitude larger than the nonresonant value. Table 49.7 shows $\chi^{(3)}$ values of a polythiophene derivatives. Polythiophenes are colored materials [186–193]. The $\chi^{(3)}$ behavior of polythiophene has been studied in several forms. Electrochemically polymerized films of polythiophene results a $\chi^{(3)}$ value of 4×10^{-10}esu as measured by DFWM at 602 nm [194]. A monolayer prepared by the LB technique (thickness ~22 Å) yields a $\chi^{(3)}$ value of ~ 10^{-9}esu at 602 nm as measured with femtosecond DWFM technique [195].

Polyacetylene is another interesting π-conjugated one-dimensional polymer that exists in two geometrical forms: *cis* and *trans* [196]. In polyacetylene the $\chi^{(3)}$ value of the *cis* form is found to be 15–20 times smaller than that of *trans* form. The difference in $\chi^{(3)}$ for the two forms results from the fundamental difference in the polymer symmetry. Also, oriented films of polyacetylene exhibit larger $\chi^{(3)}$ values than unoriented films [197]. Polyketene, in which acetylene hydrogens are substituted with hydroxy groups, shows a $\chi^{(3)}$ value of 1.15×10^{-12}esu at 532 nm [198]. In polyphenylacetylene substitution at the phenyl ring increases $\chi^{(3)}$ significantly [199]. An *ortho*-trimethylsilyl-substituted polyphenylacetylene has a $\chi^{(3)}$ value, which is an order of magnitude larger than the $\chi^{(3)}$ value of polypphenylacetylene.

The $\chi^{(3)}$ values of polyphenylacetylene and several other polymers such as poly-*p*-phenylenevinylene (PPV), PBT, PBO, LARC-TPI, polyketene, polyaniline, polyazine, and polypyrrole are shown in Table 49.8 (Fig. 49.13). Also, included in Table 49.8 are $\chi^{(3)}$ of several heterocyclic ladder
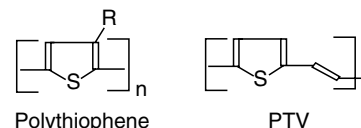
FIGURE 49.12. Molecular structures of the NLO polymers described in Table 49.6.

polymers. Polyazine is an NLO polymer that is isoelectronic with polyacetylene. Both polyazine and polyacetylene have a simple one-dimensional chain of alternating single and double bonds. In the case of polyazine, pairs of N are substituted for pairs of C in the backbone. Even though the optical nonlinearity of polyazine is moderate, its optical transparency and environmental stability are great advantages.

Good-optical-quality polymers of PPV and poly-*p*-thienylene vinylene (PTV) can be prepared from soluble sulfonium precursors. This feature allows one to fabricate a device structure with the precursor and then convert it to the polymer by heat treatment. Good-optical-quality, stretchoriented, free-standing films of PPV can be obtained with good mechanical strength and high optical damage thresholds. In stretched films, doping produces high electrical conductivity along the draw direction, indicating a high effective π-conjugation in polymer. Singh, Prasad, and Karasz [201] studied the anisotropy of $\chi^{(3)}$ in a stretched PPV film by measuring the DFWM signal as a function of the angle of rotation (Fig. 49.14).[7] The highest $\chi^{(3)}$ value is obtained when electric fields of all the four waves are polarized along the draw direction, while the minimum value is obtained when all the beams are polarized in a direction perpendicular to the draw direction. The ratio of $\chi^{(3)}_{\parallel} : \chi^{(3)}_{\perp}$ was 39 obtained by fitting the experimental data to the following expression:

$$\chi^{(3)}_{1111,L} = \chi^{(3)}_{1111,F} \cos^4 \theta + \chi^{(3)}_{2222,F} \sin^4 \theta + (\chi^{(3)}_{1122,F}$$
$$+ \chi^{(3)}_{1221,F} + \chi^{(3)}_{2122} + \chi^{(3)}_{1212,F} + \chi^{(3)}_{2211,F}$$
$$+ \cdots) \cos^2 \theta \sin^2 \theta. \qquad (49.32)$$

TABLE 49.7. $\chi^{(3)}$ *values of different forms and different derivatives of polythiophenes.*

Polymer	$\lambda(\mu$m)	$\chi^{(3)}(10^{-10}$ esu)	Method	References
Polythiophene	0.532	10	DFWM	[71]
R = H	1.907	3.52	THG	[72]
R = $C_{12}H_{25}$	0.602	0.55	DFWM	[73]
R = $C_{12}H_{25}$	0.602	5.0	DFWM	[74]
R = $C_{12}H_{25}$	0.602	5.0	DFWM	[75]
R = CH_3	1.50	0.48	THG	[76]
R = C_4H_9	1.50	0.2	THG	[77]
R = C_6H_5	1.50	0.81	THG	[76]
PTV	1.85	0.32	THG	[78]
Polythiophene (electrochemical)	0.602	0.07	DFWM	[79]
Polythiophene (LB film)	0.532	2700	DFWM	[80]

TABLE 49.8. $\chi^{(3)}$ values of a number of third-order NLO polymers.

Polymer	$\chi^{(3)}(10^{-12}$ esu)	$\lambda(\mu m)$	Method	References
PBT	−100.0	0.602	DFWM	[200]
	9.0			
PBO	−100.0	0.602	DFWM	[179]
PPV (stretch-oriented)	400.0	0.620	DFWM	[201]
PPV (R = H)	75	1.064	THG	[202]
PPV (R = OCH$_3$)	2900	1.064	THG	[203]
PPV (sol–gel)	45	0.620	DFWM	[204]
PPV (sol–gel)	6.6	0.620	OKG	[204]
MOPPV (stretch-oriented)	91	0.608	DFWM	[205]
PPV (sol–gel)	300	0.602	DFWM	[206]
MOPPV (LB film)	2900	1.064	THG	[207]
Polyphenyl acetylene	50.0	0.602	DFWM	[179]
LARC-TPI	−2	0.602	DFWM	[179]
Poly-4-BCMU, yellow	25.0	0.602	DFWM	[179]
Poly-4-BCMU, red	300.0	0.602	DFWM	[179]
Polyketene	1150	0.532	THG	[198]
Polyaniline	800	0.620	DFWM	[208]
Polypyrrole	2	0.602	DFWM	[209]
BBL	7	0.602	DFWM	[210]
	150	0.620		
BBB	4500	1.064	DFWM	[210]
Polyazomethine	2.4	0.602	DFWM	[211]
Polyquinoline	2.2	2.38	THG	[212]
Polyquinoxaline	4500	0.532	DFWM	[213]
Polyazine	8	1.5	THG	[214]
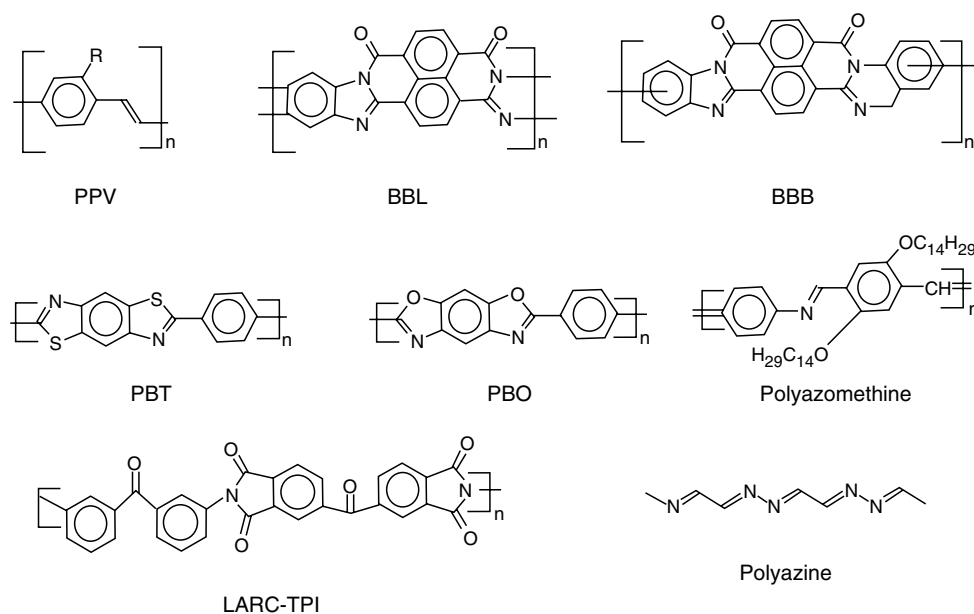
FIGURE 49.13. Molecular structures of the NLO polymers described in Table 49.8.

Similar results also has been obtained by Swiatkiewicz and co-workers [205] in stretch-oriented films of poly-(2,5-dimethoxy-p-phenylenevinylene) thin films. Also, oriented films of PPV have been fabricated with the LB technique [201]. The $\chi^{(3)}$ value (at $\lambda = 1.064\,\mu m$) of an LB film of poly-(2,5-dimethoxy-p-phenylenevinylene) is 2.9×10^{-9} and 7.5×10^{-11} esu along the orientation axis and perpendicular to the orientation axis, respectively. The above investigations show that, as in polydiacetylenes, the chain orientation is an effective way of enhancing $\chi^{(3)}$ of PPV and its derivatives.
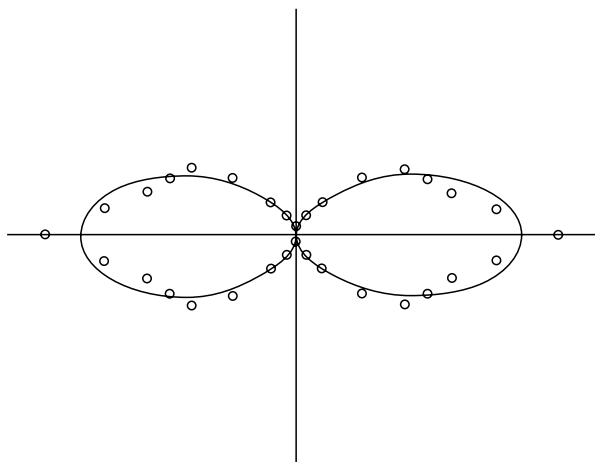
FIGURE 49.14. Polar plot (orientational anisotropy) of the square root of the DFWM signal intensity for the 10:1 stretch-oriented PPV film. Scattered are the experimental data points; continuous line is the theoretical fit [201].

Another interesting feature of PPV is that it can be incorporated into sol–gel glasses (up to 50 wt %) without phase separation. Sol–gel composites of PPV have been prepared using SiO_2 and V_2O_5 gels [206]. A light beam at 1.064 μm can be guided in a sol–gel processed PPV film (thickness $\sim 1\,\mu$m) up to 2 cm with a loss of $\sim$4 dB/cm. The refractive indices ($n_{TE} = 1.72$ and $n_{TM} = 1.60$ at 1.064 μm) indicate the presence of birefringence even in as cast film [215,216].

Another important class of photonic materials is polysilanes (Fig. 49.15) [217–222]. In polysilanes the delocalization of σ orbitals of the Si atom along the polymer backbone plays a significant role in their NLO properties. Their physical and chemical properties can be tailored by the choice of an appropriate substituent, which also determines the conformation of the polymer and its solubility. What is of more interest is their transparency in their NLO properties. $\chi^{(3)}$ values of a series of polysilanes are given in Table 49.9. Tables 49.10–49.13 contain γ and $\chi^{(3)}$ values of some other third-order materials, namely metallophthalocyanine, bis-metallophthalocyanine, metallonaphthalocyanines, fullerenes, and β-carotenes. Although these molecules are not considered as polymers, they are macromolecules that have drawn a considerable amount of attention as third-order NLO materials. For example, the highly stable icosa-

PEPS :	$R_1 = C_2H_5$	$R_2 = C_5H_{11}$
PDHS :	$R_1 = R_2 = C_6H_{11}$	
PPMS :	$R_1 = CH_3$	$R_2 = C_6H_5$
POMS :	$R_1 = CH_3$	$R_2 = C_6H_{17}$
PHPnS :	$R_1 = C_6H_{13}$	$R_2 = C_5H_{11}$
PHPS :	$R_1 = C_6H_{13}$	$R_2 = C_6H_5$
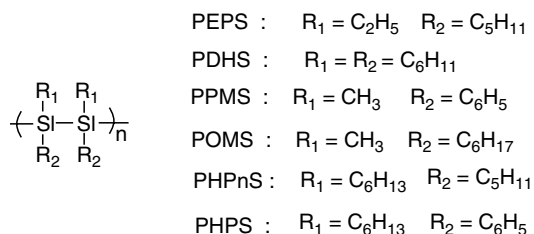
FIGURE 49.15. Molecular structures of the NLO ploymers described in Tables 49.9.

hedral-cage C_{60} molecule (fullerene) has been studied by a large number of research groups as a third-order NLO material. Fullerene is considered to be a new form of carbon in that it possesses a soccer ball structure. All the carbon atoms in fullerene are connected with sp^2 bonds and 60 π electrons are distributed in a manner giving the molecule a highly aromatic character. The interesting π conjugation in fullerenes has made it an important candidate for thirdorder NLO optics. Table 49.10 reports the NLO properties of fullerenes measured by different research groups. Other highly conjugated molecules can be considered as one-dimensional (β-carotene) and two-dimensional (phthalocyanines and naphthalocyanines) for NLO purposes.

49.12 TPA CROSS-SECTION VALUES OF ORGANICS AND POLYMERS

The basic structural requirement as a TPA material is π-conjugation of the molecule, because the TPA process originates from third-order NLO activity. At the initial stage of TPA research, only commercial chromophores such as fluorescein, coumarin 307, Rodamine B, etc., were reported to exhibit TPA activities, but they all exhibited relatively low TPA cross-section σ values (< 200 GM) which is expressed in Göeppert-Mayer (GM) units ($1GM = 1 \times 10^{-50}$ cm^4 sec photon^{-1}) [124]. To address this problem, several research groups focused attention on synthesizing materials with high TPA cross-section. This entailed an improved understanding of the structure–property relationship. In particular, there have been intense efforts to identify contributions from different structural models of a molecule on the TPA cross-section. Systems with symmetrical donors (donor–π–bridge–donor; D–π–D) and acceptors (acceptor–π–bridge–acceptor; A–π–A) as well as asymmetrical structure having both donor and acceptor (donor–π–bridge–ac-

TABLE 49.9. $\chi^{(3)}$ values of polysilane derivatives.

Polymer	$\chi^{(3)}$ (10^{-12}esu)	$\lambda(\mu m)$	Method	References
PEPS	5.3	1.064	THG	[217]
PDHS	11.3	1.064	THG	[221]
	1.3	1.907		
PDIHS	1.8	1.064	THG	[217]
PPMS	1.5	1.064	THG	[220]
	7.2	1.064	THG	[219]
	4.2	1.907	THG	[219]
POMS	2.9	0.532	THG	[218]
PtBuPS	4.9	1.064	THG	[217]
PSM-MSM	3.6	1.064	THG	[221]
PSM-n-HSM	3.1	1.064	THG	[221]
Polycarbosilane	0.34	1.064	THG	[221]
PHPnS	2.3	1.064	THG	[217]
PHPS	6.2	1.064	THG	[217]
PDES	3000	0.620	DFWM	[222]

TABLE 49.10. $\chi^{(3)}$ values of fullerenes and β-carotene.

	Method	$\chi^{(3)}(10^{-12}$ esu)	$\gamma(10^{-33}$ esu)	$\lambda(\mu m)$	References
C_{60} (solution)	DFWM	60 000	11 000	1.064	[223]
C_{60}/DEA	EFISH	. . .	67 000	1.064	[224]
C_{60} (solution)	z scan	33 200	. . .	0.532	[225]
C_{60} (solution)	EFISH	. . .	0.75	1.064	[226]
C_{60} (solution)	DFWM	0.12	. . .	1.064	[227]
C_{60} (film)	DFWM	200	. . .	0.633	[228]
C_{60} (film)	THG	200	. . .	1.064	[229]
C_{60} (film)	THG	20	. . .	1.064	[226]
C_{60} (film)	THG	30	0.43	1.32	[237]
C_{60} (film)	DFWM	7	0.3	1.064	[229]
C_{60} (solution)	DFWM	220	. . .	0.602	[230]
	OKG	. . .	$\gamma_{real} = -5$	0.620	
		. . .	$\gamma_{im} = 9$		
C_{70} (solution)	EFISH	. . .	1.3	1.064	[224]
C_{70} (solution)	z scan	12000	. . .	0.520	[225]
C_{70} (film)	DFWM	300	. . .	0.633	[228]
C_{70} (film)	DFWM	5.6	1200	1.064	[231]
$C_{60} + C_{70}$	DFWM	2.6	160	1.064	[232]
$C_{60} + C_{70}$	DFWM	3300	. . .	1.064	[232]
β-carotene	THG	. . .	4.8	1.89	[233]
β-carotene	DFWM	. . .	720	1.064	[234]
β-carotene	THG	. . .	11	1.908	[235]
β-carotene	OKG	. . .	$\gamma_{real} = -110$		[236]
			$\gamma_{im} = 160$		

ceptor; D–π–A) groups have been intensively investigated [123,247–262]. Schematics of these structures are shown in Fig. 49.16.

TABLE 49.11. $\chi^{(3)}$ values of metallophthalocyanines and metallonaphthalocyanines.

Compound	$\chi^{(3)}(10^{-12}$esu)	$\lambda(\mu m)$	Method	References
F-AIPc	50	1.064	THG	[238]
Cl-GaPc	25	1.064	THG	[238]
H_2Pc	3.0	1.907	THG	[239]
CoPc	7.5	1.907	THG	[239]
NiPc	2.3	1.907	THG	[239]
SnPc	40.0	1.907	THG	[239]
VOPc	93.0	1.907	THG	[239]
H_2PcCP$_4$	4.0	1.064	DFWM	[240]
PbPcCP$_4$	20.0	1.064	DFWM	[240]
PtPcCP$_4$	200.0	1.064	DFWM	[240]
Cl-InPc	130.0	1.907	THG	[241]
Cl-AIPc	15.0	1.907	THG	[241]
VOPc	40.0	2.1	THG	[241]
TiOPc	53.0	2.1	THG	[241]
CuPc	1.5	1.907	THG	[241]
PtPc	0.76	1.5	THG	[241]
TBH$_2$PC	1.9	1.907	THG	[239]
TBVOPC	6.0	1.907	THG	[239]
TBNiPc	2.0	1.907	THG	[239]
Sb(Pc)$_2$	1700.0	1.064	DFWM	[242]
SiPc (LB film)	20.0	00602	DFWM	[243]

For the π- bridges, phenylenevinylene, flourine, fused aromatics based on benzene, thiophene, or phenyleneethynylene, etc., showing high co-planarity have been used. It has been inferred that TPA activities of above-mentioned structures could be enhanced by increasing co-planarity of the π-center, donor strength, the conjugation length, and intramolecular charge redistribution. As shown in Fig. 49.17, the bis(styryl)-

TABLE 49.12. $\chi^{(3)}$ values of several metallophthalocyanine metallonaphthalocyanine derivatives as measured by the harmonic generation technique.

Compound	$\chi^{(3)}$ $(10^{-12}$esu)	λ (μm)	Method	References
VoNc(CO$_2$C$_5$H$_{11}$)$_4$	86.0	2.1	THG	[244, 245]
CuNc(CO$_2$C$_5$H$_{11}$)$_4$	2.0	2.1	THG	[244, 245]
ZnNc(CO$_2$C$_5$H$_{11}$)$_4$	1.88	2.1	THG	[244, 245]
PdNc(CO$_2$C$_5$H$_{11}$)$_4$	1.28	2.1	THG	[244, 245]
NiNc(CO$_2$C$_5$H$_{11}$)$_4$	1.59	2.1	THG	[244, 245]
CuPc(C$_6$H$_{13}$S)$_4$	20.0	1.907	THG	[241]
CuPc(C$_7$H$_{15}$S)$_4$	12.0	2.1	THG	[241]
CuPc(C$_8$H$_{17}$S)$_4$	50.0	2.1	THG	[241]
CuPc(C$_{10}$H$_{21}$S)$_4$	26.0	2.1	THG	[241]
CuPc(C$_{12}$H$_{25}$S)$_4$	1.30	2.1	THG	[241]
VOPc(C$_6$H$_{13}$S)$_4$	31.0	2.1	THG	[241]
ClInNc{(CH$_3$)$_3$}$_4$	4.21	2.1	THG	[244, 245]
IrNc{(CH$_3$)$_3$}$_4$	1.05	2.1	THG	[244, 245]
RuNc{(CH$_3$)$_3$}$_4$	1.0	2.1	THG	[244, 245]
RhNc{(CH$_3$)$_3$}$_4$	1.16	2.1	THG	[244, 245]

TABLE 49.13. γ values of a series of metallophthalocyanine metallonaphthalocyanine as measured by the degenerate four wave mixing technique. All measurements were made at 1.064 μm [131].

Compound	$\gamma(10^{-32}$ esu$)$	Method
$H_2Pc(CP)_4$	0.1	DFWM
$PbPc(CP)_4$	2	DFWM
$ZnPc(CP)_4$	0.5	DFWM
$CuPc(CP)_4$	2	DFWM
$NiPc(CP)_4$	4	DFWM
$CoPc(CP)_4$	5	DFWM
$PdPc(CP)_4$	1	DFWM
$PtPc(CP)_4$	10	DFWM
bis-Phthalocyanines		
$ScPc_2$	48	DFWM
$LuPc_2$	34	DFWM
$YbPc_2$	41	DFWM
$YPPc_2$	26	DFWM
$GdPc_2$	22	DFWM
$EuPc_2$	22	DFWM
$NdPc_2$	15	DFWM

FIGURE 49.16. Various design strategies for highly efficient TPA chromophores.

TPA cross section for SM-1 give a maximum σ_2 of 210 GM at an excitation wavelength of 605 nm, which is much smaller value than that of SM-2 ($\sigma_2 = 995$ GM at 730 nm) due to the shortness of the π-conjugated chain length. The large increase in the TPA activity of SM-4, compared with SM-3, is also related to the extension of π-chain length. One of the most interesting phenomena in the TPA tendency of bis(styryl)-benzene derivatives is the role of electron acceptor in the π-center of the molecules. In the case of SM-6 with a D–A–D structure, TPA cross-section exhibits an exceptionally high value of 1,940 GM at 835 nm. This is due to the increase of the extent of charge transfer from the end of molecule to the π-center, and this indicates that symmetric charge transfer and a change in quadrupole moment greatly contribute to the enhancement of the σ_2 value. The detailed photophysical data of the above-mentioned bis(styryl)benzene derivatives are listed in Table 49.14.

benzene derivatives with symmetrical donors (D–π–D) structures and some modified structures of donor–acceptor–donor (D–A–D) and acceptor–donor–acceptor (A–D–A) types exhibit high TPA activity [123,263]. Measurement of the
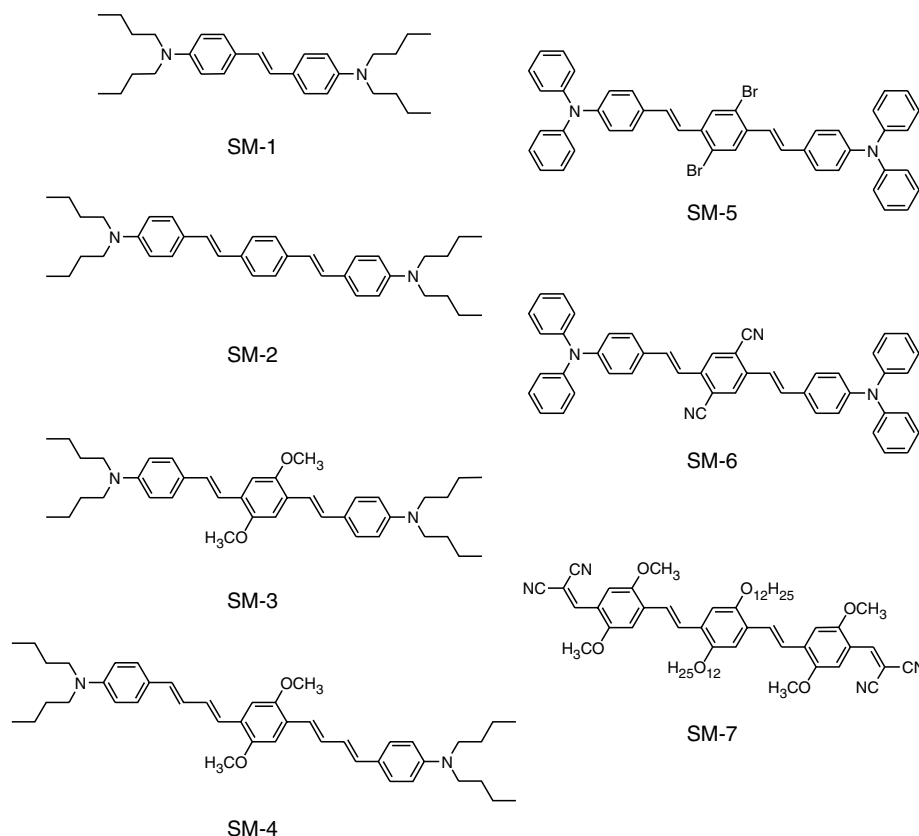
FIGURE 49.17. Molecular structures of two-photon absorbing bis(styryl)benzene derivatives.

TABLE 49.14. *The detailed photophysical date of bis(styryl)benzene derivatives depicted in Fig. 49.17.*

Chromophore	λ_{max}(UV) nm	λ_{mas}(PL) nm	λ_{max}(TPA) nm	$\sigma_2{}^a$ GM[b]	Φ^b
SM-1	374	410	605 (620)	210 (100)	0.90
SM-2	408	455	730 (~725)	995 (635)	0.88
SM-3	428	480	730 (~725)	900 (680)	0.88
SM-4	456	509	775 (~750)	1,250 (1,270)	0.12
SM-5	424	490	~800 (–)	450 (–)	0.41
SM-6	472	525	835 (810)	1,940 (3,670)	0.86
SM-7	513	580	825 (815)	480 (650)	0.82

[a]σ_2 values were determined by two-photon-excited fluorescence measurements with 5-ns laser pulses. Data given in parentheses are determined with fs laser pulses.
[b]Φ is fluorescence quantum yield.

It is also helpful to understand the role of π-center in a TPA materials on its σ_2 value. Figure 49.18 shows chemical structures of TPA chromophores with four different π-center types such as fluorene [264,265], dithienothiophene (DTT) [248], phenylenevinylene (PV) [128,266,267] and phenyleneethynylene (PE) [268,269]. Among them, DTT-based molecules exhibit the highest TPA activity, considering the π-conjugated length of molecules. The maximum σ_2 of KS-3 based on DTT at the excitation wavelength of 785 nm is 1,140 GM which is a larger value compared to that of fluorene-based KS-2 ($\sigma_2 = 954$ GM at 740 nm) and PV-based KS-5 ($\sigma_2 = 470$ GM at 780 nm). This result indicates that planarity of the π-center might be a crucial mo-

lecular factor, together with the electron-donor strength at the end of molecules. Due to the longer π-conjugated length of KS-6 and KS-7, a direct comparison on PE unit with flourine, DTT, and PV as a π-bridge is difficult, but it is reasonable to surmise that PE may also be a good candidate for making efficient TPA materials (Table 49.15).

More recently, several researchers have also reported octupolar [270–272] and multibranched [273–279] type chromophores as well as dendritic molecules [280–284] showing highly efficient TPA cross-sections. Some representatives are presented in Fig. 49.19. They correlated the activity with the intramolecular charge transfer between the donor moiety and the π-center, and the increase the number density
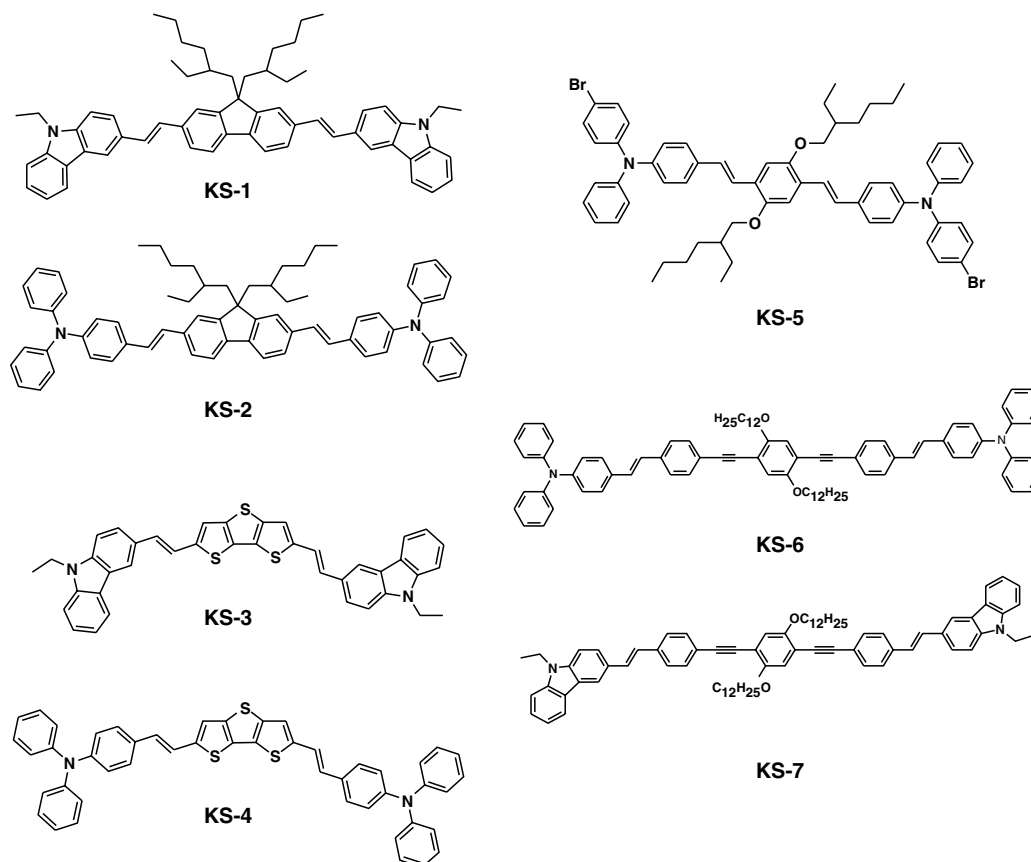
FIGURE 49.18. Molecular structures of various two-photon absorbing chromophores with different π-bridges.

TABLE 49.15. *The detailed photophysical data of various two-photon absorbing chromophores with different π-bridges depicted in Fig. 49.18.*

Chromophore	$\lambda_{max}(UV)$ [a] nm	$\lambda_{mas}(PL)$[a] nm	$\lambda_{max}(TPA)$ nm	σ_2[b] GM	Φ[c]
KS-1	398	434	≤ 735	290	0.80
KS-2	411	452	740	954	0.78
KS-3	441	486	740	740	0.69
KS-4	453	503	785	1,140	0.70
KS-5	424	507	780	470	0.81
KS-6	403	446	704	960	0.81
KS-7	412	464	704	1,184	0.89

[a]UV and PL data obtained in THF solution.
[b]TPA cross-section; 1 GM = 10^{-50} cm^4 sec photon^{-1} measured in two-photon fluorescence method with 80 fs pulse laser.
[c]Fluorescence quantum yield determined relative to fluorescin in 0.1 N NaOH.

of chromophore. It has been observed that the σ_2 value increases with increasing the number of octupolar units in the octupolar oligomers [271] and also with increasing the number of branches in the multibranched chromophores [273]. Moreover, the TPA activity in dendritic macromolecules can gain strong cooperative enhancement by increasing the number of constituent identical chromophore-building units [281]. As shown in Fig. 49.20, the σ_2 value increases by a factor of 2.1 and 3.8, when going from CS-2 (In the name of CS-2, 2 means the number of constituent identical chromophore unit, i.e., triphenylamine) to CS-4 and CS-6, respectively. In the case of CS-14 and CS-30, the σ_2 values were enhanced to 4,500 GM and 11,000 GM, respectively.

In addition, most TPA compounds based on π-conjugated double bond experience a reduction in TPA activities due to the quenching of fluorescence resulting from the formation of π-complex by the chromophore aggregation. This occurs both in the solid state and in solutions of high chromophore concentrations. To prevent the interaction with other chromophores in the vicinity, TPA chromophore center can be attached with dendrons (KS-9) so as to restrict a free conformation motion (Fig. 49.20). As a result, the hindered molecular twisting motion of the center TPA chromophore for a dendrimer results in about 5–16 times increase in fluorescence emission, along with increased emission lifetime [278]. For these reasons, octupolar, multibranched, and dendritic chromophores can be promising candidates for TPA science and technology.

Polymers as TPA materials provide several advantages. These are: (i) photochemical and photophysical stability against organic solvents and intense light, (ii) prevention of aggregation between chromophores, and (iii) ease of processing toward a thin film. Considering these merits, several conjugated polymers based on poly(1,4-phenyleneethynylene) (PPE), polyfluorene (PF), and poly(1,4-phenylenevinylene) (PPV) backbones have been investigated as prospective TPA materials (Fig. 49.21) [285–289].

In the case of PPE, electron-donating long alkoxy chains on each phenyleneethynylene moieties are introduced which improve its solubility and also electron density of the poly-

mer chains. Moreover, alkoxy branches can also play an important role to restrict the $\pi-\pi$ interaction between conjugated polymer chains which cause fluorescence quenching. The σ_2 value of PPE was 80×10^{-20} cm^{4}GW^{-1} observed by nanosecond laser pulses. Due to its high TPA activity this polymer showed efficient optical power limiting performance [286]. Also, polyfluorene was investigated for its TPA activity in chloroform (2×10^{-3} M) at wavelengths ranging from 550 to 680 nm. The TPA dispersion curve displays a peak at 625 nm with $\sigma_2 = 20,000$ GM, utilizing 2.6 ns pulses [288].

Poly(1,4-phenylenevinylene) derivatives also constitute another set of interesting TPA materials, and even they are well-known as third-order NLO polymers as well as efficient electroluminescence materials. According to a study of excitation dynamics and TPA properties in PPV derivatives having phenylanthracene and branched alkoxy pendants, a complete energy transfer from the pendant phenyanthracene unit to the PPV backbone in PPV-1 and PPV-2 was observed [289]. From ns and fs measurements, their TPA cross sections at around 800 nm were found to be 11.9 for PPV-1, 66.6 for PPV-2, and 44.0×10^{-20} cm^{4}GW^{-1} for PPV-3 in ns laser pulses and 0.074 for PPV-1, 0.196 for PPV-2, and 0.168×10^{-20} cm^{4}GW^{-1} for PPV-3 in fs pulses, respectively. The observation of higher TPA values obtained in ns pulses compared with that of fs pulses is due to contribution from excited-state absorption in the ns regime. PPV-2, carrying both the phenylanthracene and alkoxy branches exhibited the highest TPA performance in both of ns and fs measurements.

49.13 VARIATION IN THE $\chi^{(2)}$, $\chi^{(3)}$, AND σ_2 VALUE

It is important to note that the $\chi^{(2)}$ and $\chi^{(3)}$ values reported in this chapter has been estimated in different experimental laboratories. The main source of the error in these values is due to the inadequacy of the local-field factors. Very often the local fields are calculated from the refractive-index measurements that are made at a particular wavelength, without considering the dispersion. Also, the numerical

	X	Y	σ_2(180 fs)
BR-1	NHex$_2$	N(Me)EtOH	3125 GM (at 990 nm)
BR-2	N(Me)EtOH	NHex$_2$	3010 GM (at 990 nm)
BR-3	NPh$_2$	NHex$_2$	5395 GM (at 990 nm)

BR-4 σ_2 = 840 GM (at 780 nm; 180 fs)

X = H (2), CN (3)

Y = t-Bu (a), CN (b)

CH$_3$ (c)

BD

BD-2a:	950 GM at 780 nm
BD-2b:	870 GM at 780 nm
BD-3b:	740 GM at 890 nm
BD-3c:	1,360 GM at 800 nm

KS-8

σ_2= 5,210 GM (at 700 nm, 80 fs)

BD-4

σ_2= 1,080 GM (at 740 nm, 80 fs)
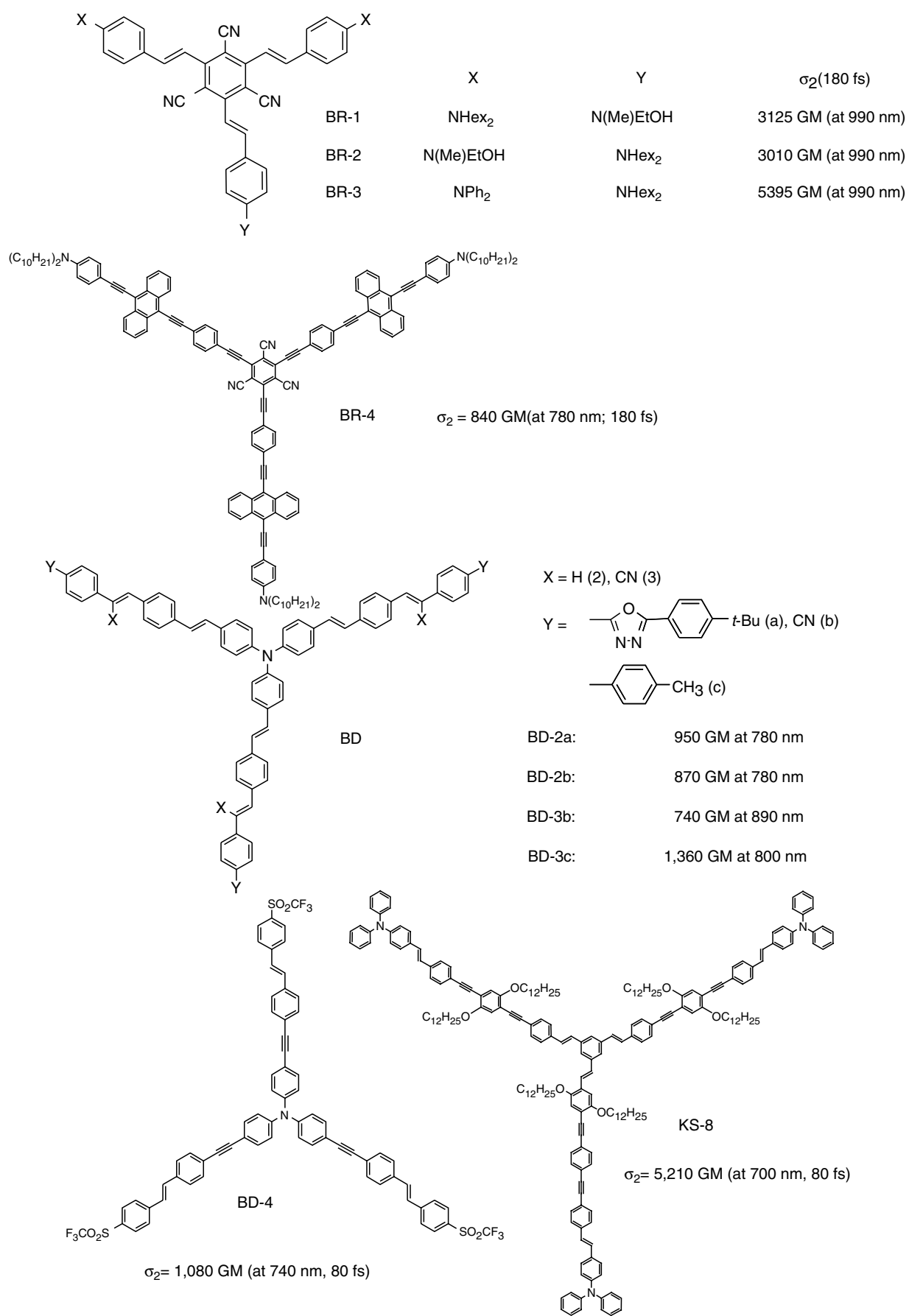
FIGURE 49.19. Chemical structures of two-photon absorbing octupolar and multibranched type chromophores.

CS-2: σ_2= 320 GM (150 fs)

CS-6: σ_2= 2,700 GM(150 fs)

CS-4: σ_2= 1,300 GM (150 fs)

KS-9
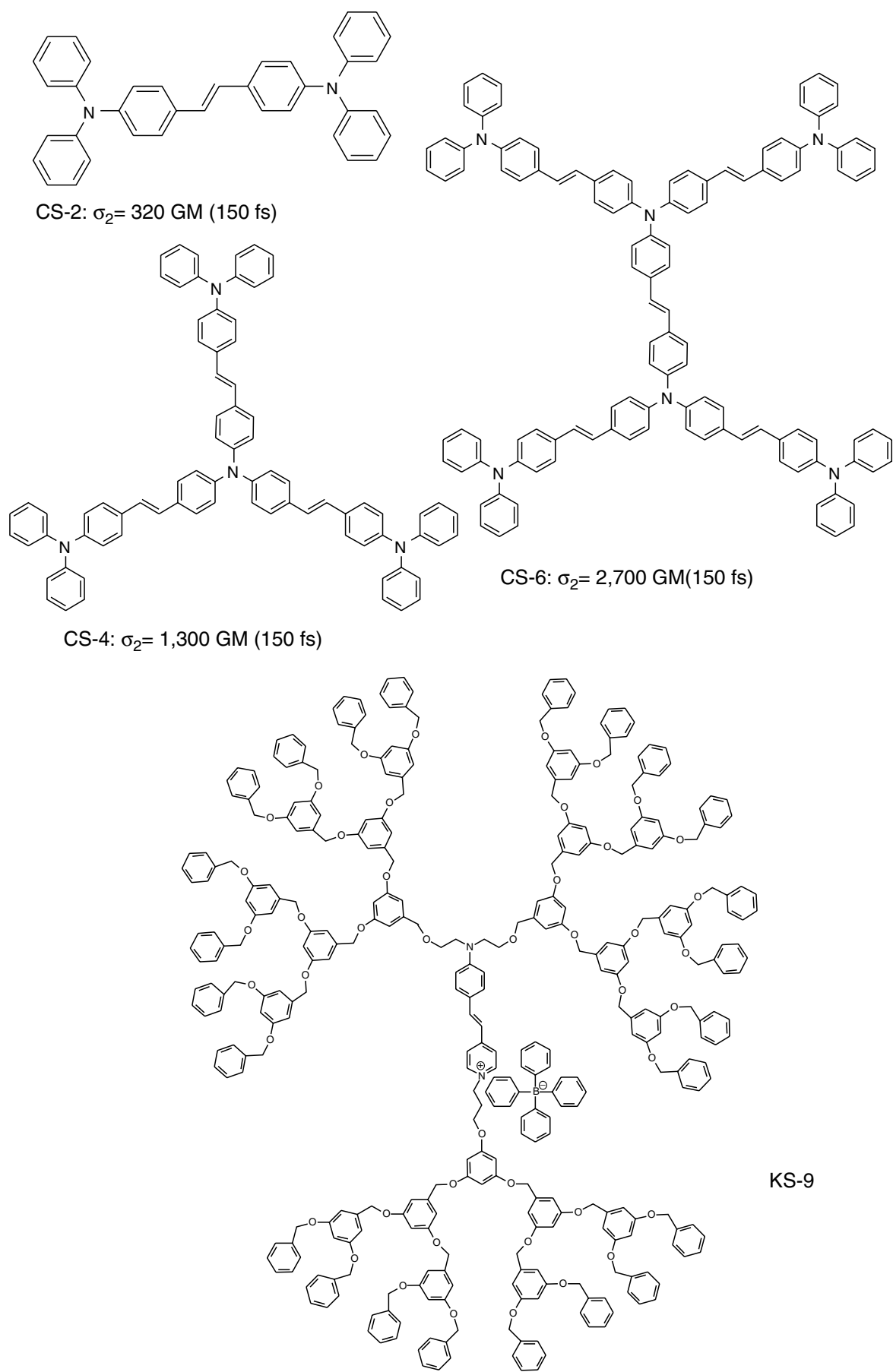
FIGURE 49.20. Chemical structure of two-photon absorbing dendritic molecules.
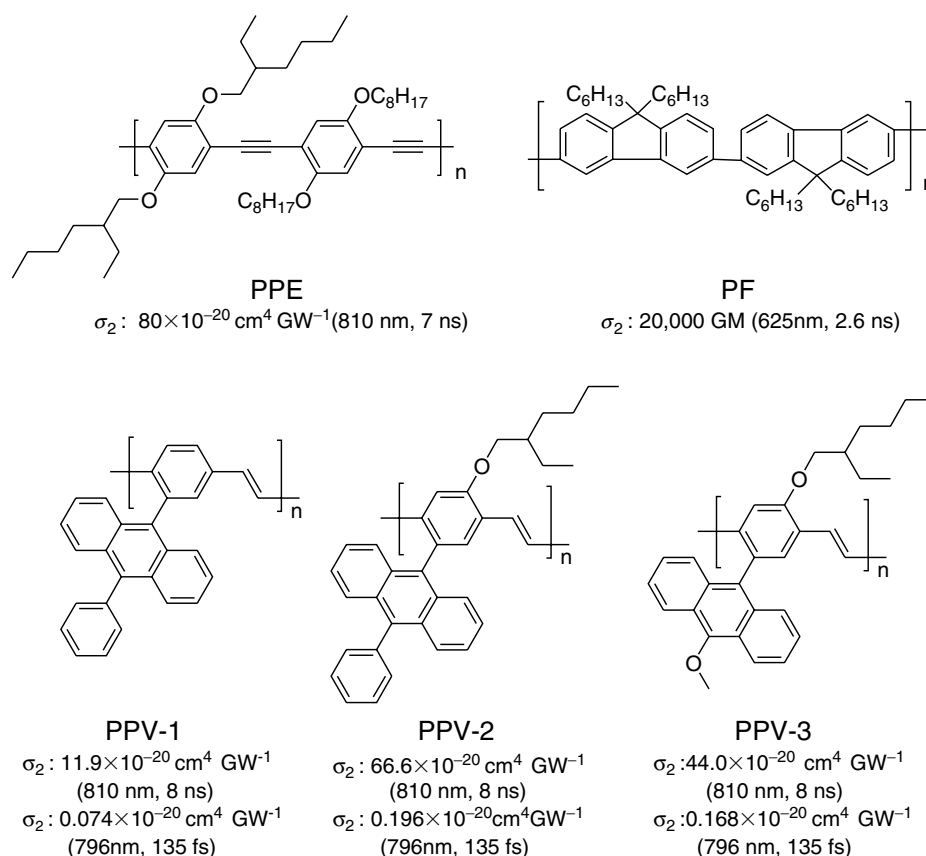
FIGURE 49.21. Molecular structure of TPA polymers.

values of $\chi^{(2)}$ and $\chi^{(3)}$ depend on the resonance contribution. The same compound may exhibit substantially different $\chi^{(2)}$ or $\chi^{(3)}$ values depending on the wavelength at which the measurement is made. Also, the variation in σ_2 values can exist, depending on experimental conditions such as pulse duration of the laser beam, the measured wavelength, laser intensity, the solvent polarity, concentration of samples in solution, and the used σ_2 values of standard materials. Therefore, a comparison of $\chi^{(2)}$, $\chi^{(3)}$, and σ_2 values should be made with caution.

Related information can be found in Chapters 34 and 35.

REFERENCES

1. N. Bloembergen, *Nonlinear Optics* (Benjamin/Cummings, New York, 1965).
2. Y. R. Shen, *Principles of Nonlinear Optics* (Wiley, New York, 1984).
3. P. N. Prasad and D. J. Williams, *Introduction to Nonlinear Optical Effects in Molecules and Polymers* (Wiley, New York, 1992).
4. *Nonlinear Optical Properties of Organic Molecules and Crystals*, edited by D. S. Chemla and J. Zyss (Academic, Orlando, FL, 1987), Vols. I and II.
5. B. F. Levine and C. G. Bethea, J. Chem. Phys. **63**, 2666 (1975).
6. P. D. Maker, R. W. Terhune, M. Nisenoff, and C. M. Savage, Phys. Rev. Lett. **8**, 21 (1962).
7. F. Zernike and J. E. Midwinter, *Applied Nonlinear Optics* (Wiley, New York, 1973).
8. J. Jerphagnon and S. K. Kurtz, J. Appl. Phys. **41**, 1667 (1970).
9. D. A. Kleinman, Phys. Rev. **126**, 1977 (1962).
10. W. M. K. P. Wijekoon, Y. Zhang, S. P. Karna, P. N. Prasad, A. C. Griffin, and A. M. Bhatti, J. Opt. Soc. Am. B **9**, 1832 (1992).
11. M. A. Mitchell, J. E. Mulvaney, H. K. Hall, Jr., C. S. Willand, H. Hampsch, and D. J. Williams, Polym. Bull. **28**, 381 (1992).
12. G. R. Meredith, J. VanDusen, and D. J. Williams, Macromolecules **15**, 1385 (1982).
13. K. D. Singer, J. Sohn, and S. Lalama, Appl. Phys. Lett. **49**, 248 (1986).
14. M. Mortazavi, A. Knoesen, S. Kowel and B. Higgins, J. Opt. Soc. Am. B **6**, 733 (1989).
15. K. D. Singer, M. Kuzyk, W. Holland, J. Sohn, S. S. Lalama, R. Comizzoli, H. Katz, and M. Schilling, Appl. Phys. Lett. **53**, 1800 (1988).
16. H. Katz, K. Singer, J. Sohn, C. Dirk, L. King, and H. Gordon, J. Am. Chem. Soc. **109**, 6561 (1987).
17. G. Gadret, F. Kajzar, and P. Raimond, Proc. SPIE **1560**, 251 (1991).
18. C. Ye, T. J. Marks, J. Yang, and J. K. Wong, Macromolecules **20**, 2322 (1987).
19. Y. Shuto, M. Amano, and T. Kaino, Jpn. J. Appl. Phys. **30**, 320 (1991).
20. M. Eich, H. Looser, D. Yoon, R. Twieg, G. Bjorklund, and G. Baumert, J. Opt. Soc. Am. B **6**, 1590 (1989).
21. C. Ye, N. Minami, T. J. Marks, J. Yang, and J. K. Wong, Macromolecules **21**, 2899 (1988).
22. L. Hayden, G. Sauter, F. Ore, P. Pasillas, J. Hoover, G. Lindsay, and R. Henry, J. Appl. Phys. **68**, 456 (1990).
23. D. Dai, T. J. Marks, J. Yang, P. Lundquist, and G. K. Wong, Macromolecules **23**, 1891 (1990).
24. D. Dai, M. A. Hubbard, J. Park, T. J. Marks, J. Wang, P. Lundquist, and G. K. Wong, Mol. Cryst. Liq. Cryst. **189**, 93 (1990).
25. D. H. Choi, W. M. K. P. Wijekoon, H. M. Kim, and P. N. Prasad, Chem. Mater. **6**, 234 (1994).
26. D. H. Choi, H. M. Kim, W. M. K. P. Wijekoon, and P. N. Prasad, Chem. Mater. **4**, 1253 (1992).

27. M. Amano, T. Kaino, F. Yamamota, and Y. Takeuchi, Mol. Cryst. Liq. Cryst. **182**, 81 (1990).
28. M. A. Hubbard, T. J. Marks, J. Yang, and G. K. Wong, Chem. Mater. **1**, 167 (1989).
29. D. M. Burland, R. D. Miller, C. A. Walsh, Chem. Rev. **94**, 31 (1994).
30. K. Kajikawa, H. Nagamori, H. Takezoe, A. Fukuda, S. Ukishima, Y. Takahashi, M. Iijima, and E. Fukuda, Jpn. J. Appl. Phys. **30**, L1737 (1991).
31. I. Teraoka, D. Jungbauer, B. Reck, D. Yoon, R. Twieg, and C. Wilson, J. Appl. Phys. **69**, 2568 (1991).
32. M. Chen, L. R. Dalton, L. P. Xu, S. Q. Shi, and W. H. Steir, Macromolecules **25**, 4032 (1992).
33. Y. Shi, W. H. Steir, M. Chen, L. Yu, and L. R. Dalton, Appl. Phys. Lett. **60**, 2577 (1992).
34. B. K. Mandal, J. Kumar, J. Huang, and S. Tripathy, Makromol. Chem. Rapid. Commun. **12**, 63 (1991).
35. B. K. Mandal, Y. M. Chen, V. Y. Lee, J. Kumar, and S. Tripathy, Appl. Phys. Lett. **58**, 2459 (1991).
36. C. P. J. Van der Vorst and S. J. Picken, J. Opt. Soc. Am. B **7**, 320 (1989).
37. M. Eich, G. Bjorklund, and G. Yoon, Polym. Adv. Technol. **1**, 189 (1990).
38. C. Xu, B. Wu, L. R. Dalton, P. Ramon, Y. Shi, and W. Steier, Macromolecules **25**, 6716 (1992).
39. M. Chen, L. R. Dalton, L. P. Xu, X. Shi, and W. Steier, Macromolecules **25**, 4032 (1992).
40. J. Lon, M. Hubbard, T. J. Marks, W. Lin, and G. K. Wong, Chem. Mater. **4**, 1148 (1992).
41. D. R. Robello, C. S. Willand, C. S. Scozzafava, A. Ulman, and D. J. Williams, in *Materials for Nonlinear Optics. Chemical Perspectives*, ACS Symposium Series No. 455, edited by S. Marder, J. Sohn, and G. Stucky (American Chemical Society, Washington, D. C. 1991), p. 279.
42. B. K. Mandal, J. Y. Lee, X. Xhu, Y. M. Chen, E. Prakienavincha, J. Kumar, and S. K. Tripathy, Syn. Met. **41–43**, 3143 (1991).
43. B. K. Mandal, Y. M. Chen, V. Lee, J. Kumar, and S. K. Tripathy, Appl. Phys. Lett. **58**, 2459 (1991).
44. H. Hsiung, Appl. Phys. Lett. **59**, 2495 (1991).
45. T. L. Penner, H. R. Motschmann, A. J. Armstrong, M. C. Ezenyilimba, and D. J. Williams, Nature **367**, 49 (1994).
46. K. Clays, N. J. Armstrong, M. C. Ezenyilimba, and T. L. Penner, Chem. Mater. **5**, 1032 (1993).
47. K. Clays, N. J. Armstrong, and T. L. Penner, J. Opt. Soc. Am. B **10**, 886 (1993).
48. H. R. Motschmann, T. L. Penner, A. J. Armstrong, and M. C. Ezenyilimba, J. Phys. Chem. **97**, 3933 (1993).
49. S. H. Ou, J. A. Mann, J. B. Lando, L. Zhou, and K. D. Singer, Appl. Phys. Lett. **61**, 2284 (1992).
50. S. R. Marder, B. Kippelen, A. K.-Y. Jen, and N. Peyghambirian, Nature **388**, 845 (1997).
51. J. L. Oudar and D. S. Chemla, J. Chem. Phys. **66**, 2664 (1977).
52. S. R. Marder, L. T. Cheng, B. G. Tiemann, A. C. Friedli, M. Blanchard-Desce, J. W. Perry, and J. Skindhøj, Science **263**, 511 (1994).
53. F. Kajzar, K.-S. Lee, and A. K.-Y. Jen, Adv. Poym. Sci. **161**, 1 (2003).
54. L. R. Dalton, Adv. Polym. Sci. **158**, 1 (2002).
55. A. K.-Y. Jen, K. Y. Wong, V. P. Rao, K. Drost, and Y. M. Cai, J. Electron. Mater. **23**, 653 (1994).
56. Y. M. Cai and A. K.-Y. Jen, Appl. Phys. Lett. **117**, 7295 (1995).
57. H. Ma, X. Wang, X. Wu, S. Liu, and A. K.-Y. Jen, Macromolecules **31**, 4049 (1998).
58. A. K.-Y. Jen, X. Wu, and H. Ma, Chem. Mater. 10, 471 (1998).
59. H. Ma, A. K.-Y. Jen, J. Wu, S. Liu, C. F. Shu, L. R. Dalton, S. R. Marder, and S. Thayumanavan, Chem. Mater. **11**, 2218 (1999).
60. L. R. Dalton, Opt. Eng. **39**, 589 (2000).
61. C.-K. Park, J. Zieba, C.-F. Zhao, B. Swedek, W. M. K. P. Wijekoon, and P. N. Prasad, Macromolecules **28**, 3713 (1995).
62. S. Jin, M. Wübbenhorst, J. Van Turnhout, and W. Mijs, Macromol. Chem. Phys. **197**, 4135 (1996).
63. K.-J. Moon, H.-K. Shim, K.-S. Lee, J. Zieba, and P. N. Prasad, Macromolecules **29**, 861 (1996).
64. K.-S. Lee, S.-W. Choi, H. Y. Woo, K.-J. Moon, H.-K. Shim, M.-Y. Jeong, and T.-K. Lim, J. Opt. Soc. Am. B **15**, 393 (1998).
65. H. Y. Woo, J.-K. Shim, and K.-S. Lee, Macromol. Chem. Phys. **199**, 1427 (1998).
66. H. Y. Woo, H.-K. Shim, and K.-S. Lee, Polym. J. **32**, 8 (2000).
67. C.-B. Yoon, B.-J. Jung, and H.-K. Shim, Synth. Met. **117**, 233 (2001).
68. T. Beltrami, M. Bösch, R. Centore, S. Concilio, P. Günter, and A. Sirigu, Polymer **42**, 4025 (2001).
69. M. Becker, L. Sapochak, L. R. Dalton, W. Steier, and A. K.-Y. Jen, Chem. Mater. **6**, 104 (1994).
70. H. Saadeh, A. Gharari, D. Yu, and L. Yu, Macromolecules **30**, 5403 (1997).
71. K. Van der Broeck, T. Verbiest, M. Van Beylen, A. Persoons, and C. Samyn, Macromol. Chem. Phys. **200**, 2629 (1999).
72. H. Y. Woo, H.-K. Shim, K.-S. Lee, M.-Y. Jeong, and T.-K. Lim, Chem. Mater. **11**, 218 (1999).
73. W. N. Leng, Y. H. Zhou, Q. H. Wu, and J. Z. Liu, Polymer **42**, 9253 (2001).
74. T.-D. Kim, K.-S. Lee, G. U. Lee, and D.-K. Kim, Polymer **41**, 5237 (2000).
75. T.-D. Kim, K.-S. Lee, Y. H. Jeong, J. H. Ju, and S. Chang, Synth. Met. **117**, 307 (2001).
76. E. Gubbelmans, T. Verbiest, M. Van Beylen, A. Persoons, and C. Samyn, Polymer **43**, 1581 (2002).
77. K. Van der Broeck, T. Verbiest, J. Degryse, M. Van Beylen, A. Persoons, and C. Samyn, Poymer **42**, 3315 (2001).
78. N. Song, L. Men, J. P. Gao, Y. Bai, A. M. R. Beaudin, G. Yu, and Z. Y. Wang, Chem. Mater. **16**, 3708 (2004)
79. J. Y. Do, S. K. Park, J.-J. Ju, S. Park, and M.-H. Lee, Opt. Mater. **26**, 223 (2004).
80. J. Y. Do, S. K. Park, J.-J. Ju, S. Park, and M.-H. Lee, Polym. Adv. Tech. **16**, 221 (2005).
81. K.-S. Lee, K.-J. Moon, H. Y. Woo, and H.-K. Shim, Adv. Mater. **9**, 978 (1997).
82. M.-H. Lee, J.-J. Ju, M.-S. Kim, J. Y. Do, S. K. Park, S. Park, and J. Kim, J. Nonlinear Opt. Phys. Mater. **13**, 391 (2004).
83. N. Nemoto, F. Miyata, Y. Nagase, J. Abe, M. Hasegawa, and Y. Shirai, Chem. Mater. **8**, 1527 (1996).
84. C. Heldann, M. Schulze, and G. Wegner, Macromolecules **29**, 4686 (1996).
85. C. Weder, B. H. Glomm, P. Neuenschwander, U. W. Suter, P. Pretre, P. Kaatz, and P. Günter, Adv. Nonlinear Opt. **4**, 63 (1997).
86. Y.-W. Kim, J.-I. Jin, M. Y. Jin, K.-Y. Choi, J.-J. Kim, and T. Zyung, Polymer **38**, 2269 (1997).
87. F. Miyata, N. Nemoto, Y. Nagase, J. Abe, M. Hasegawa, and Y. Shirai, Macromol. Chem. Phys. **199**, 1465 (1998).
88. N. Nempto, F. Miyata, T. Kamiyama, Y. Nagase, J. Abe, and Y. Shirai, Macromol. Chem. Phys. **200**, 2309 (1999).
89. B.-K. So, K.-S. Lee, S.-M. Lee, M.-K. Lee, and T. K. Lim, Opt. Mater. **21**, 87 (2002).
90. Z. Sekkat, C. S. Kang, E. F. Aust, G. Wegner, and W. Knoll, Chem. Mater. **7**, 142 (1995).
91. N. Nemoto, F. Miyata, Y. Nagase, J. Abe, M. Hasegawa, and F. Shirai, Macromolecules **29**, 2365 (1996).
92. K. Noniewicz and Z. K. Brzozowski, Reat. Funct. Polym. **33**, 343 (1997).
93. J. Luo, J. Qin, and H. Kang, Polym. Int. **49**, 1302 (2000).
94. J.-Y. Lee W.-J. Lee, C. S. Baek, and H.-B. Bang, Bull. Korean Chem. Soc. **25**, 1941 (2004).
95. S. Yokoyama, T. Nakahama, A. Otomo, and S. Mashiko, Thin Solid Films **331**, 248 (1998).
96. S. Yokoyama, T. Nakahama, A. Otomo, and S. Mashiko, J. Am. Chem. Soc. **112**, 3174 (2000).
97. J.-H. Lee and K.-S. Lee, Bull. Korean Chem. Soc. **21**, 847 (2000).
98. H. L. Bozec, T. L. Bouder, O. Maury, A. Bondon, I. Ledoux, S. Deveau, and J. Zyss, Adv. Mater. **13**, 1677 (2001).
99. H. Ma, B. Chen, T. Sassa, L. R. Dolton, and A. K.-Y. Jen, J. Am. Chem. Soc. **123**, 986 (2001).
100. H. Ma and A. K.-Y, Jen, Adv. Mater. 13, 1201 (2001).
101. P. Busson, J. Örtegren, H. Ihre, U. W. Gedde, A. Hult, G. Andersson, A. Eriksson, and M. Lindgren, Macromolecules 35, 1663 (2002).
102. M. E. Van der Boom, Angew. Chem. Int. Ed. **41**, 3363 (2002).
103. H. Ma, S. Liu, J. Luo, S. Suresh, L. Liu, S. H. Kang, M. Haller, T. Sassa, L. R. Dolton, and A. K.-Y. Jen, Adv. Funct. Mater. **12**, 565 (2002).
104. J. Luo, S. Liu, M. Haller, L. Liu, H. Ma, and A. K.-Y. Jen, Adv. Mater. **14**, 1763 (2002).

105. Y. V. Pereverzev, O. V. Prezhdo, and L. R. Dalton, Chem. Phys. Lett. **373**, 207 (2003).
106. T. L. Bouder, O. Maury, A. Bondon, K. Costuas, E. Amouyal, I. Ledoux, J. Zyss, and H. L. Bozec, J. Am. Chem. Soc. **125**, 12284 (2003).
107. O. Y.-H. Tai, C. H. Wang, H. Ma, and A. K.-Y. Jen, J. Chem. Phys. **121**, 6086 (2004).
108. J. Luo, M. Haller, H. Ma, S. Liu, T.-D. Kim, Y. Tian, B. Chen, S.-H. Jang, L. R. Dalton, and A. K.-Y. Jen, J. Phys. Chem. B **108**, 8523 (2004).
109. H. C. Jeong, M. J. Piao, S. H. Lee, M.-Y. Jeong, K. M. Kang, G. Park, S.-J. Jeon, and B. R. Cho, Adv. Funct. Mater. **14**, 64 (2004).
110. A. J. Brouwer and R. M. J. Liskamp, Eur. J. Org. Chem. 487 (2005).
111. Y. Bai, N. Song, J. P. Gao, X. Sun, X. Wang, G. Yu, and Z. Y. Wang, J. Am. Chem. Soc. **127**, 2060 (2005).
112. J. F. Nye, *Physical Properties of Crystals* (Clarendon, Oxford, 1960).
113. S. Cyvin, J. Rauch, and J. Decius, J. Chem. Phys. **43**, 4083 (1965).
114. M. J. Soileau, W. E. Williams, and E. W. Van Stryland, IEEE J. Quantum Electron. **19**, 731 (1983).
115. D. Grischkowsky, Phy. Rev. Lett. **24**, 866 (1970).
116. J. H. Marburger, in *Progress of Quantum Electronics*, edited by J. H. Sandom and S. Stenholm (Pergamon, New York, 1977), p. 35.
117. M. Sheik-Bahae, A. A. Said, and E. W. Van Stryland, Opt. Lett. **14**, 955 (1989).
118. M. Göppert-Mayer, Ann. Phys. **9**, 273 (1931).
119. W. Kaiser and C. G. B. Garret, Phys. Rev. Lett. **7**, 229 (1961).
120. R. Menzel, *Photonics; Linear and Nonlinear Interactions of Laser Light and Matter* (Springer, Berlin, 2001).
121. J. D. Bhawalkar, G. S. He, and P. N. Prasad, Rep. Prog. Phys. **59**, 1041 (1996).
122. T.-C. Lin, S.-J. Chung, K.-S. Kim, X. Wang, G. S. He, J. Swiatkiewicz, H. E. Pudavar, and P. N. Prasad, Adv. Polym. Sci. **161**, 157 (2003); Ref. therein.
123. M. Albota, D. Beljonne, J. C. Bredas, J. E. Ehrlich, J.-Y. Fu, A. A. Heikal, S. E. Hess, T. Kogej, M. D. Levin, S. R. Mader, D. McCord-Maughon, J. W. Perry, H. Rockel, M. Rumi, G. Subranmaim, W. W. Webb, X.-Y. Wu, and C. Wu, Science **281**, 1653 (1998).
124. C. Wu and W. W. Webb, J. Opt. Soc. Am. B **13**, 481 (1996).
125. H.-B. Sun, S. Matsuo, and H. Misawa, Appl. Phys. Lett. **74**, 786 (1999).
126. M. Straub and M. Gu, Opt. Lett. **27**, 1824 (2002).
127. S. Shoji, H.-B. Sun, and S. Kawata, Appl. Phys. Lett. **83**, 608 (2003).
128. H.-B. Sun, T. Suwa, K. Takada, R. P. Zaccaria, M.-S. Kim, K.-S. Lee, and S. Kawata, Appl. Phys. Lett. **85**, 3708 (2004).
129. S. Esener and P. M. Rentzepis, Proc. SPIE **1449**, 144 (1991).
130. J. H. Strickler and W. W. Webb, Opt. Lett. **16**, 1780 (1991).
131. H. J. Strickler and W. W. Webb, Adv. Mater. **5**, 479 (1993).
132. B. H. Cumpston, S. P. Ananthavel, S. Barlow, D. L. Dyer, J. E. Ehrlich, L. L. Erskine, A. A. Heikal, S. M. Kuebler, I.-Y. S. Lee, D. McCord-Maughon, J. Qin, H. Röckel. M. Rumi, X.-L. Wu, S. R. Marder, and J. W. Perry, Natuer **398**, 51 (1999).
133. S. Kawata and Y. Kawata, Chem. Rev. **100**, 1777 (2000).
134. Y. Kawata, M. Nakano, S.-C. Lee, Opt. Eng. **40**, 2247 (2001).
135. B. J. Siwick, O. Kalinina, E. Kumacheva, R. J. D. Miller, and J. Noolandi, J. Appl. Phys. **90**, 5328 (2001).
136. S. Klein, A. Barsella, H. Leblond, H. Bulou, A. Fort, C. Andraud, G. Lemercier, J. C. Mulatier, and K. Dorkenoo, Appl. Phys. Lett. **86**, 211118 (2005).
137. T. Sherwood, C. Young, J. Takayesu, K.A. Jen, L. Dalton, and A. Chen, Proc. SPIE **5724**, 356 (2005).
138. L. Luo, C. Li, S. Wang, W. Huang, C. Wu, H. Yang, H. Jiang, Q. Gong, Y. Yang, and S. Feng, J. Opt. A: Appl. Opt. **3,** 489 (2001).
139. S. Maruo and K. Ikuta, Proc. SPIE **3937**, 106 (2000).
140. H.-B. Sun, T. Kawakami, Y. Xu, J.-Y. Ye, S. Matuso, H. Misawa, M. Miwa, and R. kaneko, Opt. Lett. **25**, 1110 (2000).
141. H.-B. Sun, K. Takada, and S. Kawata, Appl. Phys. Lett. **79**, 3173 (2001).
142. S. Kawata, H.-B. Sun, T. Tanaka, and K. Takada, Nature **412**, 697 (2001).
143. A. Mukherjee, Appl. Phys. Lett. **62**, 3423 (1993).
144. G. S. He, C. F. Zhao, J. D. Bhawalkar, and P. N. Prasad, Appl. Phys. Lett. **67**, 3703 (1995).
145. G. S. He, J. D. Bhawalkar, C. F. Zhao, C.-K. Park, and P. N. Prasad, Opt. Lett. **20**, 2393 (1995).
146. A. Abbotto, L. Beverina, R. Bozio, S. Bradamante, C. Ferrante, G. A. Pagani, and R. Signorini, Adv. Mater. **12**, 1963 (2000).
147. G. Zhou, D. Wang, X. Wang, X. Xu, X. Cheng, Z. Shao, X. Zhao, Q. Fang, and M. Jiang, Opt. Laser Tech. **33**, 529 (2001).
148. A. Abbotto, L. Beverina, R. Bozio, S. Bradamante, G. A. Pagani, and R. Signorini, Synth. Met. **121**, 1755 (2001).
149. D. Wang, G. Zhou, Y. Ren, S. Yang, X. Xu, X. Zhao, Z. Shao, and M. Jiang, Opt. Eng. **41**, 1899 (2002).
150. K. Shirota, H.-B. Sun, and S. Kawata, Appl. Phys. Lett. **84**, 1632 (2004).
151. G. S. He, J. D. Bhawalker, C. F. Zhao, and P. N. Prasad, Appl. Phys. Lett. **67**, 2433 (1995).
152. G. S. He, L. Yuan, N. Cheng, J. D. Bhawalkar, P. N. Prasad, L. L. Brott, S. J. Clarson, and B. A. Reinhardt, J. Opt. Soc. Am. B **14**, 1097 (1997).
153. J. E. Ehrlich, X. L. Wu, L.-Y. Lee, Z.-Y. Hu, H. Roecker, S. R. Marder, and J. Perry, Opt. Lett. **22**, 1843 (1997).
154. C. W. Spangler, J. Mater. Chem. **9**, 2013 (1999).
155. G. S. He, T.-C. Lin, P. N. Prasad, C.-C. Cho, and L.-J. Yu, Appl. Phys. Lett. **82**, 4717 (2003).
156. M. G. Silly, L. Porrès, O. Mongin, P.-A. Chollet, and M. Blanchard-Desce, Chem. Phys. Lett. **379**, 74 (2003).
157. T.-C. Lin, G. S. He, P. N. Prasad, and L.-S. Tan, J. Mater. Chem. **14**, 982 (2004).
158. Z. Yang, Z. Wu, J. Ma, A. Xia, Q. Li, C. Liu, and Q. Gong, Appl. Phys. Lett. **86**, 061903 (2005).
159. W. Denk, J. H. Strikler, and W. W. Webb, Science **248**, 73 (1990).
160. H. Ohata, H. Yamada, T. Niioka, M. Yamamoto, and K. Momose, J. Pharmacol. Sci. **93**, 242 (2003).
161. S. M. Dunham, H. E. Pudavar, P. N. Prasad, and M. K. Stachowiak, J. Phys. Chem. B **108**, 10540 (2004).
162. E. E. Serrano and V. B. Knight, Proc. SPIE **5705**, 225 (2005).
163. K. Baba, T. Y. Ohulchanskyy, Q. Zheng, T.-C. Lin, E. J. Bergey, and P. N. Prasad, MRS Symp. Proc. **845**, 209 (2005).
164. J. D. Bhawalkar, N. D. Kumar, C. F. Zhao, and P. N. Prasad, J. Clin. Med. Surg. **15**, 201 (1997).
165. P. K. Frederiksen, M. Jørgensen, and P. R. Ogiby, J. Am. Chem. Soc. **123**, 1215 (2001).
166. I. Roy, T. Y. Ohulchanskyy, H. E. Pudaver, E. J. Bergey, A. R. Oseroff, J. Morgan, T. J. Dougherty, and P. N. Prasad, J. Am. Chem. Soc. **125**, 7860 (2003).
167. M. Fournier, C. Pépin, D. Houde, R. Oueller, and J. E. van Lier, Photochem. Photobiol. Sci. **3**, 120 (2004).
168. M. Drobizhev, Y. Stepanenko, Y. Dzenis, A. Karotki, A. Rebane, P. N. Taylor, and H. L. Anderson, J. Phys. Chem. B **109**, 7223 (2005).
169. M. A. Oar, J. M. Serin, W. R. Dichtel, M. J. Fechet, T. Y. Ohulchanskyy, and P. N. Prasad, Chem. Mater. **17**, 2267 (2005).
170. C. W. Spangler, J. R. Starkey, F. Meng, A. Gong, M. Drobizhev, A. Rebane, and B. Moss, Proc. SPIE **5689**, 141 (2005).
171. C. Stuteret, J. P. Herman, R. Frey, F. Fradere, J. Ducuing, R. H. Daughman, and R. R. Chance, Phys. Rev. Lett. **36**, 956 (1976).
172. G. M. Carter, J. V. Hryniewicz, M. K. Thakur, Y. J. Chen, and S. E. Mayler, Appl. Phys. Lett. **49**, 998 (1986).
173. J. Bolger, T. G. Harvey, W. Ji, A. K. Kar, S. Molyneux, B. S. Wherrett, D. Bloor, and P. Norman, J. Opt. Soc. Am. B **9**, 1552 (1992).
174. M. Ohsugi, S. Takaragi, H. Matsuda, A. Okada, H. Masaki, and H. Nakanishi, Proc. SPIE **1337**, 162 (1990).
175. P. A. Chollet, F. Kazjar, and J. Messier, in *Nonlinear Optics of Organics and Semiconductors*, edited by T. Kobayashi (Springer, Berlin, 1988), p. 171.
176. P. A. Chollet, F. Kazjar, and J. Messier, Thin Solid Films **132**, 1 (1985).
177. J. M. Nunzi and F. Charra, J. Appl. Phys. **62**, 2198 (1987).
178. T. Doi, S. Okada, H. Matsuda, A. Masaki, N. Minami, H. Nakanishi, and K. Hayamizu, presented at the 52nd Meeting of the Japanese Society of Applied Physics, 1991.
179. P. N. Prasad, Proc. SPIE **1017**, 2 (1988).
180. J. Le Moigne, A. Thierry, P. A. Chollet, F. Kazjar, and J. Messier, J. Chem. Phys. **88**, 6647 (1988).
181. J. Le Moigne, A. Thierry, and F. Kazjar, Proc. SPIE **1125**, 9 (1990).
182. T. Kanetake, K. Ishikawa, T. Hesegawa, T. Koda, K. Takeda, H. Hesegawa, K. Kubodera, and H. Kobayashi, Appl. Phys. Lett. **54**, 2287 (1989).
183. F. Kazjar and J. Messier, Thin Solid Films **132**, 11 (1985).

184. F. Kazjar and J. Messier, Polym. J. **19**, 275 (1987).
185. H. Matsuda, S. Okada, and H. Nakanishi, in Proceedings of the Fifth International Conference on Photoactive Solids, Okazaki, Japan, 1991, p. 264.
186. L. Yang, R. Dorsinville, Q. Wang, W. Zou, P. Ho, N. Yang, R. Alfano, R. Zamboni, R. Danieli, G. Ruini, and C. Taliani, J. Opt. Soc. Am. B **6**, 753 (1989).
187. T. Sugiyama, T. Wada, and H. Sasabe, Synth. Met. **28**, C323 (1989).
188. Y. Pang and P. N. Prasad, J. Chem. Phys. **93**, 2201 (1990).
189. B. P. Singh, M. Samoc, H. Nalva, and P. N. Prasad, J. Chem. Phys. **92**, 2756 (1990).
190. H. Sasabe, T. Wadw, T. Sigiyama, H. Ohkawa, A. Yamada, and A. F. Garito, in *Conjugated Polymeric Materials in Electronics, Optoelectronics and Molecular Electronics*, edited by J. L. Bredas and R. R. Chance (Kluwer, London, 1990), p. 399.
191. H. Matsuda, M. Sato, S. Okada, H. Nakanishi, M. Kato, and T. Nishiyama, Polym. Prepr. Jpn. **28**, 1035 (1989).
192. F. Kazjar, J. Messier, C. Sentein, R. L. Elsenbaumer, and G. G. Miller, Proc. SPIE **1147**, 36 (1989).
193. T. Kaino, K. Kubodra, H. Kobayashi, T. Kurihara, S. Saito, T. Tsutsui, T. Takito, and H. Murata, Appl. Phys. Lett. **53**, 2002 (1988).
194. P. N. Prasad, Thin Sold Films **152**, 275 (1987).
195. P. Logsdon, J. Pfleger, and P. N. Prasad, Synth. Met. **26**, 369 (1988).
196. M. Sinlair, D. McBranch, D. Moses and A. Heeger, Synth. Met. **28**, D645 (1989).
197. E. Wintner, F. Krausz, and G. Leising, Synth. Met. **28**, D159 (1989).
198. G. A. Olah, E. Zadok, R. Edler, D. H. Adamson, W. Kasha, and G. Suryaprakash, J. Am. Chem. Soc. **111**, 9123 (1989).
199. D. Neher, A. Wolf, C. Bubeck, and G. Wegner, Chem. Phys. Lett. **163**, 116 (1989).
200. H. Vanherzeele, J. Meth, S. Jenekhe, and M. Roberts, J. Opt. Soc. Am. B **9**, 524 (1982).
201. B. P. Singh, P. N. Prasad, and F. E. Karasz, Polymer **29**, 1940 (1988).
202. D. D. Bradley and Y. Mori, Jpn. J. Appl. Phys. **28**, 174 (1989).
203. K. Kamiyama, M. Era, T. Tsutsui, and S. Saito, Jpn. J. Appl. Phys. **29**, L840 (1990).
204. Y. Pang, M. Samoc, and P. N. Prasad, J. Chem. Phys. **94**, 5282 (1991).
205. J. Swiatkiewicz, P. N. Prasad, F. E. Krausz, A. A. Druy, and P. Glatkwski, Appl. Phys. Lett. **56**, 892 (1990).
206. C. J. Wung, W. M. K. P. Wijekoon, and P. N. Prasad, Polymer **34**, 1174 (1993).
207. K. Kamiyama, M. Era, T. Tsutsui, and S. Sato, Jpn. J. Appl. Phys. **29**, L840 (1990).
208. K. Wong, S. Han, and Z. Vardeny, J. Appl. Phys. **70**, 1896 (1991).
209. S. K. Goshal, Chem. Phys. Lett. **158**, 65 (1989).
210. J. R. Lindle, F. J. Bartoli, C. A. Hoffmann, O. K. Kim, Y. S. Lee, J. S. Shirk, and Z. F. Kafazi, Appl. Phys. Lett. **65**, 712 (1990).
211. K. S. Lee and M. Samoc, Polymer **32**, 361 (1991).
212. S. A. Jenekhe, J. A. Osaheni, H. Vanherzeele, and J. Meth, Chem. Mater. **4**, 683 (1992).
213. L. Yu, D. W. Polis, M. R. McLean, and L. R. Dalton, in *Electroresponsive Molecular and Polymeric Systems*, edited by T. A. Skotheim (Dekker, New York, 1991), Vol. II, p. 113.
214. H. S. Nalva, T. Hamada, A. Kakuta, and A. Mukoh, Jpn. J. Appl. Phys. **32**, L193 (1993).
215. P. N. Prasad, Proc. SPIE **1328**, 186 (1990).
216. C. J. Wung, Ph.D. dissertation, State University of New York at Buffalo, Buffalo, 1991.
217. P. Shukla, P. M. Cotts, R. D. Miller, S. Ducharme, R. Asthana, and J. Zavislan, Mol. Cryst. Liq. Cryst. **183**, 241 (1990).
218. J. C. Baumert, G. C. Bjorklund, D. H. Dundt, M. C. Jurich, H. Looser, R. D. Miller, J. Rabolt, R. Sooriyakumaran, J. D. Swalean, and R. J. Twieg, Appl. Phys. Lett. **53**, 1147 (1988).
219. F. Kazjar, J. Messier, and C. Rosilio, J. Appl. Phys. **60**, 3040 (1986).
220. L. Yang, Q. Wang, P. Ho, R. Dorsville, R. Alfano, W. Zou, and N. Yang, Appl. Phys. Lett. **53**, 1245 (1988).
221. C. L. Callender, C. A. Carere, J. Albert, L. L. Zhou, and D. J. Worsfold, J. Opt. Soc. Am. B **9**, 518 (1992).
222. K. S. Wong, S. G. Han, Z. V. Vardeny, J. Shinar, Y. Pang, I. Maghsoodi, T. J. Barton, S. Grigoras, and B. Parbhoo, Appl. Phys. Lett. **58**, 1695 (1991).
223. W. J. Blau, H. J. Byrne, D. J. Cardin, T. J. Dennis, J. P. Hare, H. W. Kroto, R. Taylor, and D. R. Walton, Phys. Rev. Lett. **67**, 1423 (1991).
224. X. K. Wong, T. G. Zhang, W. P. Lin, S. Z. Liu, G. K. Wong, M. M. Kappes, R. P. H. Chang, and J. B. Ketterson, Appl. Phys. Lett. **60**, 810 (1992).
225. F. Henari, J. Collaghan, H. Stiel, W. Blau, and D. J. Cardin, Chem. Phys. Lett. **199**, 144 (1992).
226. J. S. Meth, H. Vanherzeele, and Y. Wang, Chem. Phys. Lett. **188**, 492 (1992).
227. Y. Wang and L. T. Chen, J. Chem. Phys. **96**, 1530 (1992).
228. M. J. Rosker, H. O. Mercy, T. Y. Chang, J. T. Khoury, K. Hansen, and R. L. Whetten, Chem. Phys. Lett. **196**, 427 (1992).
229. H. Hoshi, N. Nakamura, Y. Maruyama, T. Nakagawa, S. Suzuki, H. Shiromaru, and A. Achiba, Jpn. J. Appl. Phys. **30**, L1397 (1991).
230. G. B. Talapatra, N. Manickam, M. Samoc, M. E. Orczyk, S. P. Karna, and P. N. Prasad, J. Phys. Chem. **96**, 5206 (1992).
231. S. C. Yang, Q. Gong, Z. Xia, Y. Zou, Y. Wu, D. Qiang, Y. Sun, and Z. Gu, Appl. Phys. B **55**, 51 (1992).
232. Q. Gong, Y. Sun, Z. Xia, Z. Gu, X. Zhou, and D. Qiang, J. Appl. Phys. **71**, 3025 (1992).
233. J. P. Herman, Opt. Commun. **9**, 74 (1973).
234. C. Maloney and W. Blau, J. Opt. Soc. Am. B **4**, 1035 (1987).
235. S. H. Stevenson, D. S. Donald, and G. R. Meridith, in *Nonlinear Optical Properties of Polymers, Materials*, Research Society Symposium Proceedings Vol. 109, edited by A. J. Heeger, J. Orenstein, and D. R. Ulrich (Materials Research Society, Pittsburgh, 1988), p. 103.
236. M. E. Orczyk, J. Swiatkiewicz, N. Manickam, M. Tomoaia-Cotisel, and P. N. Prasad, Appl. Phys. Lett. **60**, 2837 (1992).
237. Z. H. Kafafi, J. R. Lidle, R. G. S. Pong, F. J. Bartoli, L. J. Lingg, and J. Milliken, Chem. Phys. Lett. **188**, 492 (1992).
238. Z. Z. Ho, C. Y. Ju, and W. M. Hetherington III, J. Appl. Phys. **62**, 716 (1987).
239. M. Hosoda, T. Wada, A. Yamada, A. F. Garito, and H. Sasabe, Nonlinear Opt. **3**, 183 (1992).
240. J. S. Shirk, J. R. Lindle, F. J. Bartoli, C. A. Hoffman, Z. H. Kafafi, and A. W. Snow, Appl. Phys. Lett. **55**, 1287 (1989).
241. H. Matsuda, S. Okada, a. Masaki, H. Nakanishi, Y. Suda, K. Shigehara, and A. Yamada, Proc. SPIE 1337, 105 (1990).
242. J. S. Shirk, J. R. Lindle, F. J. Bartoli, and M. F. Boyle, J. Phys. Chem. **96**, 5847 (1992).
243. M. Castevenss, M. Samoc, J. Pfleger, and P. N. Prasad, J. Chem. Phys. **92**, 2019 (1990).
244. H. S. Nalwa, A. Kakuta, and A. Mukoh, Chem. Phys. Lett. **203**, 109 (1993).
245. H. S. Nalwa, A. Kakuta, and A. Mukoh, J. Phys. Chem. **97**, 1097 (1993).
246. J. S. Shirk, J. R. Lindle, F. J. Bartoli, Z. H. Kafafi, A. W. Snow, and M. E. Boyle, Int. J. nonlinear Opt. Phys. **1**, 699 (1992).
247. B. A. Reinhardt, L. L. Brott, S. T. Clarson, A. G. Dillard, J. C. Bhatt, R. Kannan, L. Yuan, G. S. He, and P. N. Prasad, Chem. Mater. **10**, 1683 (1998).
248. O.-K. Kim, K.-S. Lee, H. Y. Woo, K.-S. Kim, G. S. He, J. Swiatkiewicz, and P. N. Prasad, Chem. Mater. **12**, 284 (2000).
249. B. R. Cho, K. H. Son, S. H. Lee, Y.-S. Song, Y.-K. Lee, S.-J. Jeon, J. H. Choi, H. Lee, and M. Cho, J. Am. Chem. Soc. **123**, 10039 (2001).
250. S.-J. Chung, K.-S. Kim, T.-C. Lin, G. S. He, J. Swiatkiewicz, and P. N. Prasad, J. Phys. Chem. B **103**, 10741 (1999).
251. A. Adronov, J. M. J. Frechet, G. S. He, K.-S. Kim, S.-J. Chung, J. Swiatkiewicz, and P. N. Prasad, Chem. Mater. **12**, 2838 (2000).
252. F. E. Hernandez, K. D. Belfield, and I. Cohanoschi, Chem. Phys. Lett. **391**, 22 (2004).
253. O. Mongin, L. Porrès, L. Moreaux, J. Mertz, and M. Blanchard-Dece, Org. Lett. **4**, 719 (2002).
254. L. Porres, O. Mongin, C. Katan, M. Charlot, T. Pons, J. Mertz, and M. Blanchard-Desce, Org. Lett. **6**, 47 (2004).
255. F. Meng, B. Li, S. Qian, K. Chen, and H. Tian, Chem. Lett. **33**, 470 (2004).
256. K. D. Belfield, A. R. Morales, J. M. Hales, D. J. Hagan, E. W. Van Stryland, V. M. Chapela, and J. Percino, Chem. Mater. **16**, 2267 (2004).
257. K. D. Belfield, A. R. Morales, B.-S. Kang, J. M. Hales, D. J. Hagan, E. W. Van Stryland, V. M. Chapela, and J. Percino, Chem. Mater.**16**, 4634 (2004).
258. Y. Lu, F. Hasegawa, T. Goto, S. Ohkuma, S. Fukuhara, Y. Kawazu, K. Torani, T. Yamashita, and T. Watanabe, J. Lumin. **110**, 1 (2004).

259. Y. Iwase, K. Kamada, K. Ohta, and K. Kondo, J. Mater. Chem. **13**, 1575 (2003).
260. Q. Zheng, G. S. He, and P. N. Prasad, J. Mater. Chem. **15**, 579 (2005).
261. M. Charlot, L. Porrès, C. D. Entwistle, A. Beeby, T. B. Marder, and M. Blanchard-Desce, Phys. Chem. Chem. Phys. **7**, 600 (2005).
262. S. K. Lee, W. J. Yang, J. J. Choi, C. H. Kim, S.-J. Jeon, and B. R. Cho, Org. Lett. **7**, 323 (2005).
263. M. Rumi, J. E. Ehrlich, A. A. Heikal, J. W. Perry, S. Barlow, Z. Hu, D. McCord-Maughon, T. C. Parker, H. Röckel, S. Thayumanavan, S. R. Marder, D. Beljonne, and J. L. Brédas, J. Am. Chem. Soc. **122**, 9500 (2000).
264. S. J. K. Pond, O. Tsutsumi, M. Rumi, O. Kwon, E. Zojer, J. L. Brédas, S. R. Marder, and J. W. Perry, J. Am. Chem. Soc. **126**, 9291 (2004).
265. K.-S. Lee, J.-H. Lee, K.-S. Kim, H.-Y. Woo, O.-K. Kim, H. Choi, M. Cha, G. S. He, J. Swiatkiewcz, P. N. Prasad, M.-A. Chung, and S.-D. Jung, Nonlinear Opt. **27**, 87 (2001).
266. K.-S. Lee, M.-S. Kim, H.-K. Yang, H.-B. Sun, S. Kawata, and P. Fleitz, Mol. Cryst. Liq. Cryst. **424**, 35 (2004).
267. M.-S. Kim, H.-K. Yang, R. H. Kim, K.-S. Lee, M. Cha, H. Choi, H.-B. Sun, S. Kawata. J. Nonlinear Opt. Phys. Mater. 13, 467 (2004).
268. H.-K. Yang, M.-S. Kim, S.-W. Kang, K.-S. Kim, K.-S. Lee, S. H. Park, D.-Y. Yang, H. J.Kong, H.-B. Sun, S. Kawata, and P. Fleitz, J. Photopolym. Sci. Tech. **17**, 385 (2004).
269. K.-S. Lee, S.-W. Kang, and J. Y. Kim, unpublished results.
270. W.-H. Lee, H. Lee, J.-A. Kim, J.-H. Choi, M. Cho, S.-J. Jeon, and B. R. Cho. J. Am. Chem. Soc. **123**, 10658 (2001).
271. B. R. Cho, M. J. Piao, K. H. Son, S. H. Lee, S. J. Yoon, S.-J. Jeon, and M. Cho, Chem. Eur. J. **8**, 3907 (2002).
272. W. J. Yang, C. H. Kim, M.-Y. Jeong, S. K. Lee, M. J. Piao, S.-J. Jeon, and B. R. Cho. Chem. Mater. **16**, 2783 (2004).
273. S.-J. Chung, T.-C. Lin, K.-S. Kim, G. S. He, J. Swiatkiewicz, P. N. Prasad, G. A. Baker, and F. V. Bright, Chem. Mater. **13**, 4071 (2001).
274. X. Zhou, A. M. Ren, J.-K. Feng, and X.-J. Liu, Chem. Phys. Lett. **362**, 541 (2002).
275. G. P. Bartholomew, M. Rumi, S. J. K. Pond, J. W. Perry, S. Tretiak, and G. C. Bazan, J. Am. Chem. Soc. **126**, 11529 (2004)
276. W. J. Yang, D. Y. Kim, C. H. Kim, M.-J. Jeong, S. K. Lee, S.-J. Jeon, and B. R. Cho, Org. Lett. **6**, 1389 (2004).
277. C. Li, C. Liu, Q. Li, and Q. Gong, Chem. Phys. Lett. **400**, 569 (2004).
278. S.-W. Kang, J. Y. Kim, R. H. Kim, B.-K. So, K.-S. Lee, I.-W. Hwang, D. Kim, P. Fleitz, H.-B. Sun, and S. Kawata, Proc. SPIE **5621**, 1 (2004).
279. Y.-Z. Cui, Q. Fang, G. Xue, G.-B. Xu, L. Yin, and W.-T. Yu, Chem. Lett. **34**, 644 (2005).
280. A. Adronov, J. M. J. Fréchet, G. S. He, K.-S. Kim, S.-J. Chung, J. Swiatkiewicz, and P. N. Prasad, Chem. Mater. **12**, 2838 (2000).
281. M. Drobizhev, A. Karotki, Y. Dzenis, A. Rebane, Z. Suo, and C. W. Spangler, J. Phys. Chem. B **107**, 7540 (2003).
282. M. Hara, S. Samori, X. Cai, S. Tojo, T. Arai, A. Momotake, J. Hayakawa, M. Ueda, K. Kawai, M. Endo, M. Fujitsuka, and T. Majima, J. Am. Chem. Soc. **126**, 14217 (2004).
283. M. Drobizhev, A. Rebane, Z. Suo, and C. W. Spangler, J. Lumin. **111**, 291 (2005).
284. M. A. Oar, J. M. Serin, W. R. Dichtel, M. J. Fréchet, T. Y. Ohulchanskyy, and P. N. Prasad, Chem. Mater. **17**, 2267. (2005).
285. R. K. Meyer, R. E. Benner, Z. V. Vardeny, M. Liess, M. Ozaki, K. Yoshino, Y. Ding, and T. Barton, Synth. Met. 84, 549 (1997).
286. G. S. He, C. Weder, P. Smith, and P. N. Prasad, J. Quantum Electron. **34**, 2279 (1998).
287. M. G. Harrison, M. Urbasch, R. F. Mahrt, H. Giessen, H. Bässler, and U. Scherf, Chem. Phys. Lett. **313**, 755 (1999).
288. P. Najechalski, Y. Morel, O. Stéphan, and P. L. Baldeck, Chem. Phys. Lett. **343**, 44 (2001).
289. S.-J. Chung, G. S. Maciel, H. E. Pudavar, T.-C. Lin, G. S. He, J. Swiatkiewicz, P. N. Prasad, D. W. Lee, and J.-I. Jin, J. Phys. Chem. A **106**, 7512 (2002).

CHAPTER 50

Refractive Index, Stress-Optical Coefficient, and Optical Configuration Parameter of Polymers

Vassilios Galiatsatos

Leibniz Institute of Polymer Research, 01069 Dresden, Germany*

Refractive index is the ratio of electromagnetic radiation in vacuo to the phase velocity of electromagnetic radiation of a specified frequency in the medium (ISO definition). The definition implies that the refractive index is always greater than unity and that it is dimensionless. For anisotropic materials the state of polarization of the light and its direction must be defined relative to reference axis in the sample.

When an incident ray of light passes from vacuum into another medium, its velocity is reduced and the ray is bent (or refracted) toward the normal to the medium's surface. The angle between the incident ray and the normal is the angle of incidence (i); the angle between the refractive ray and the normal is the angle of refraction (r).

For a given medium the ratio of the sine of the angle of incidence to the sine of the angle of refraction is constant:

$$(\sin i)/(\sin r) = c/v = n. \qquad (50.1)$$

The index of refraction, n, is dependent upon the wavelength of the incident light. If the incident light is not monochromatic, the constituent rays will experience varying amounts of refraction. This effect is known as dispersion. Consequently, measurements of refractive indices require the use of monochromatic incident light. All experimental values of refractive indices compiled here were measured at the Na D line, which has a wavelength of 5,893 Å.

In anisotropic crystals and fibers, the refractive index varies with the direction of (polarized) light through the structure. For example fibers have two principal values one parallel and one perpendicular with respect to the long direction of the fiber. On the other hand isotropic crystals have only one refractive index. Crystals with tetragonal and hexagonal symmetry have two principal values of refractive index. Orthorombic, monoclinic, and triclinic crystals have three principal values. The refractive index varies with frequency, temperature, and degree of polymerization.

The two measurement methods recommended by ISO489 are the Abbe refractometer technique and the Becke line technique. The latter is more useful with powdered or granulated transparent material or even with small chips of material taken from a larger sample. ASTM D542 includes only the Abbe method and it is widely used for characterization of refractive index of polymers.

An Abbe refractometer has a fixed telescope and two right-angle prisms. A thin film of the sample being measured is placed in the gap between the hypotenuses of the right-angle prisms. The monochromatic incident light is refracted through the first prism, the sample, and the second prism. The refracted beam emerges parallel to the incident beam and is viewed with the telescopic eyepiece. The prism assembly is rotated to create a field of view as seen through the telescope in which exactly one-half of the field is dark and the other half is light, with a sharp interface between the two. The refractive index of the sample is read from a graduated scale on the prism assembly. The experimental error is less than 0.01%. Imperfect alignment of the prisms can increase the error. Advances in instrument design have made measurement of refractive index an automated task.

The refractive index of a material is closely related to its polarizability (α). The two are related to each other through the molar refractivity (R_m), which is given as:

$$R_m = \frac{M}{\rho} \frac{n^2 - 1}{n^2 + 2}, \qquad (50.2)$$

* Permanent address: Lyondell Chemical Co. -11530 Northlake Drive, Cincinnati, OH 45249, USA.

where M is the molar mass and ρ is the density of the material. This definition of molar refraction is due to Lorentz and Lorentz. Gladstone and Dale have also proposed a relationship between molar refraction (denoted here as $R_{m,GD}$ to distinguish it from the one given above) and refractive index:

$$n = \frac{1 + R_{m,GD}}{M/\rho,}. \tag{50.3}$$

The relationship between polarizability and molar refractivity is:

$$3\varepsilon_0 R_m = N_A \alpha(\omega) \tag{50.4}$$

where ε_0 is the dielectric constant and N_A is Avogadro's number. The (dynamic) polarizability $\alpha(\omega)$ is a function of frequency (far from an absorption band) and is given as

$$\alpha(\omega) = \frac{2}{3h} \sum_n \frac{\omega_{n0}|\langle 0|\mu|n\rangle|^2}{\omega_{n0}^2 - \omega^2}, \tag{50.5}$$

where ω is frequency, the subscript "0" denotes the ground state, the subscript "n" denotes the excited state, and μ is the electric transition dipole moment from the ground to the excited states. The correlation of optical properties of polymers to fundamental properties such as atomic polarizability is an exciting and useful field of research.

Denbigh established that the molar refraction may be considered as the sum of the bond refractions that make up the molecule. Van Krevelen has assigned chemical group refractivities that can be used to calculate refractive indices of polymers. A similar additivity approach may be used to calculate the refractive indices of semicrystalline polymers of known density, if the crystalline and amorphous densities and refractive indices are also known:

$$n = \nu_{cr} - n_{cr} + (1 - \nu_{cr})n_{nc}, \tag{50.6}$$

$$\nu_{cr} = \frac{\rho - \rho_{nc}}{\rho_{cr} - \rho_{nc}}, \tag{50.7}$$

Refractive indices of polymers and copolymers can be found in Tables 50.1 and 50.2, respectively. In Table 50.1 footnotes have been used extensively. Footnotes containing no additional data are used to list other forms of the material which have the same refractive index according to the reference cited.

Other footnotes show additional data differing from that of the most recent reference cited. Readers are cautioned that some of the data is conflicting, and original references should be consulted when assessing the validity of such data. It should also be kept in mind that refractive indices of polymer products (films, injection molded articles, thermoformed sheets, etc.) will have optical properties that depend on the processing history of the product. Therefore one should distinguish between the fundamental

refractive index of the polymer and those of the final product. The handbook makes an effort to include both types of information.

The stress-optical coefficient C is the ratio of birefringence to true stress:

$$C = \frac{\Delta n}{\tau}, \tag{50.8}$$

The stress-optical coefficient has units of mm^2/N. It is related to the optical configuration parameter, $\Delta\alpha$, a configuration-dependent property of a polymer, through

$$C = \frac{2\pi\Delta\alpha(n^2 + 2)^2}{45kTn}, \tag{50.9}$$

where T is temperature (in Kelvin) and k is the Boltzmann constant. The birefringence, or double refraction, is the difference in refractive indices along the three Cartesian coordinate axes of the polymer sample:

$$\Delta n_{xy} = n_x - n_y, \tag{50.10}$$

$$\Delta n_{xz} = n_x - n_z, \tag{50.11}$$

$$\Delta n_{yz} = n_y - n_z = \Delta n_{xz} - \Delta n_{xy}. \tag{50.12}$$

Strain-induced birefringence is measured with a rheo-optical instrument. Such an instrument may induce orientation of the polymer chains within a sample, generally via uniaxial strain, while monochromatic light passes through the sample on an axis perpendicular to that of the strain. In some other cases the orientation may be induced by an external field (such as flow) acting on the sample, or the sample may already have anisotropy already "frozen-in" as is the case of semicrystalline polymers for example. The retardation of the light passing through the sample may be measured with a Babinet compensator. Modern instruments rely on photoelastic modulators for the task. The birefringence is then calculated from the retardation, and the stress-optical coefficient is calculated from the birefringence and the stress. The experimental error in such procedures is less than 5%.

The optical configuration parameter may be calculated theoretically through the rotational isomeric state model. Its units are typically in cm^3. Stress-optical coefficient and optical configuration parameter data for polymers and copolymers can be found in Tables 50.3 and 50.4, respectively. In both tables wavelength is 6,328 Å. The data in Tables 50.1–50.4 have been compiled from more than 100 references. For consistency the polymeric material names are reported exactly as in the original references. In some cases computer databases, given the material names listed here, may be able to provide structural information about the materials.

Related information can be found in Chap. 23.

TABLE 50.1. *Refractive indices of polymers. All values reported are at a wavelength of 5,893 Å unless otherwise noted.*

Polymer	Refractive index n	Temperature (°C)	Reference
Acrylic (PMMA)	1.49		[1]
Acrylic Cont Poly Acrycal MP (see Ftn. 1)	1.49		[2]
Acrylic Cont Poly Acrycal MP CP-1000 E/E/ exc blend stock material	1.50		[2]
Acrylic Cont Poly Acrycal MP CP-1000 l/l/ best impact str transparency	1.50		[2]
Acrylic Cyro acrylite (see Ftn. 2)	1.49		[2]
Acrylic Degussa Corp. Degalan (see Ftn. 3)	1.49		[2]
Acrylic DuPont USA Lucite L super abrasion resistant exc optical	1.49		[2]
Acrylic high impact grade	1.49	23	[3,13]
Acrylic Polycast acrylic sheet clear sheet color white textured sheet	1.49		[2]
Acrylic Polysar Zylar90/l/clear impact fda exc γ ray recovery	1.52		[2]
Acrylic Polysar Zylar91/E/clear impact acrylic for extrusion	1.52		[2]
Acrylic Rohm & Haas Plexiglass (see Ftn. 4)	1.50		[2]
Acrylic sheet Aristech (see Ftn. 5)	1.49		[2]
Allyl cast resin	1.50–1.575		[4,14]
Allyl diglycol carbonate	1.50	23	[3,18]
Amber	1.538–1.548		[4,14]
Balsam (in stick form)	1.54	23	[4,14]
Balsam, Canada	1.53		[4,14]
Benzylcellulose	1.47–1.52		[4,14]
Butyl rubber (unvulcanized)	1.508		[4,5]
Butylphenol formaldehyde	1.66		[4,5]
Cellulose	1.54		[4,5]
Cellulose acetate (see Ftn. 6)	1.48–1.50		[5]
Cellulose acetate (see Ftn. 7)	1.46–1.50	23	[13,18]
Cellulose acetate butyrate (see Ftn. 8)	1.46–1.49		[5]
Cellulose acetate propionate (see Ftn. 9)	1.47–1.48		[4,14]
Cellulose acetate, highly acetyl	1.46–1.50	23	[6]
Cellulose nitrate (see Ftn. 10)	1.50–1.514		[4,5]
Cellulose propionate	1.47–1.48		[4,14]
Cellulose tripropionate	1.48–1.49		[5]
Cellulosics	1.46–1.50		[1]
Chlorinated diphenyl	1.61–1.70		[4,14]
Chlorinated rubber	1.56		[4,14]
Chlorotrifluoroethylene (CTFE)	1.42		[1]
Congo, hard amber (see Ftn. 11)	1.545 ± 0.003	20	[4,14]
Coumarone-indene resins	1.617–1.66		[4,14]
Cresylic acid-formaldehyde condensation resin	1.645 ± 0.003	20	[4,14]
Damar (see Ftn. 12)	1.535–1.538	25	[4,14]
East India gum	1.537 ± 0.003	20	[4,14]
Epoxy resins (see Ftn. 13)	1.55–1.60		[5]
Ethyl cellulose	1.479	21	[5]
Fluorinated ethylene propylene (FEP)	1.34	23	[13,18]
Glycerol-phthalate, rosin modified	1.557	25	[4,14]
Glycerol phthalate, cast resin	1.57	23	[6]
Gutta percha, α (see Ftn. 14)	1.514	21	[5]
Hexamethylene sebacamide	1.532	25	[4,14]
Hydrochlorinated rubber	1.53–1.55		[4,5]
Kapton Type H Film	1.78	23	[7,15]
Methyl cellulose (low viscosity)	1.497	25	[4,14]
Methyl methacrylate cast resin	1.485–1.50	23	[6]
Methyl methacrylate molding resin	1.49	23	[6]
Methyl rubber	1.525		[4,14]
Methyl siloxane fluids	1.375–1.403		[4,14]
Methylpentene polymer	1.465		[1]
Napthalene–formaldehyde resin	1.696		[4,14]
Natural rubber	1.519–1.52	20	[4,14]

TABLE 50.1. *Continued.*

Polymer	Refractive index *n*	Temperature (°C)	Reference
NBS casting resin (mixture of 2,5-dichlorostyrene and styrene)	1.608	25	[4,14]
Neoprene	1.5512	25	[4,14]
Nylon (see Ftn. 15)	1.566		[1]
Pentabromophenyl methacrylate	1.71		[4,14]
Phenol–formaldehyde and phenol–furfural compounds—no filler	1.58–1.66	23	[6]
Phenol–formaldehyde resins (see Ftn. 16)	1.47–1.70		[5]
Phenylene oxide (Noryl)	1.63	23	[13,18]
Phenylphenol–formaldehyde	1.47–1.7		[4,14]
Poly (2-ethoxyethyl methacrylate)	1.367		[4,14]
Poly[1,1-(1-phenylethane) bis(4-phenyl)carbonate]	1.4833	20	[5]
Poly[1,1-(2-methyl propane) bis(4-phenyl)carbonate]	1.6130	25	[8,17]
Poly[1,1-butane bis(4-phenyl)carbonate]	1.5702	25	[8,17]
Poly[1,1-cyclohexane bis(4-phenyl)carbonate]	1.5792	25	[8,17]
Poly(1,1-cyclohexane bis[4-(2,6-dichlorophenyl)]carbonate)	1.5900	25	[8,17]
Poly(1,1-cyclopentane bis(4-phenyl)carbonate)	1.5857	25	[8,17]
Poly(1,1-diethylpropyl methacrylate)	1.5993	25	[8,17]
Poly(1,1-dihydroperfluorehexyl acrylate)	1.4889	20	[5]
Poly(1,1-dihydroperfluorobutyl acrylate)	1.5937	25	[8,17]
Poly[1,1-ethane bis(4-phenyl)carbonate]	1.5000	20	[5]
Poly(1,2-butadiene)	1.5816	20	[5]
Poly(1,2-diphenylethyl methacrylate)	1.5154	25	[5]
Poly(1,3-butadiene)	1.52		[5]
Poly(1,3-butadiene) (high *cis* type)	1.5180		[5]
Poly(1,3-butadiene) (35% *cis*; 56% *trans*; 7% 1,2 content)	1.5270	20	[5]
Poly(1,3-dichloropropyl methacrylate)	1.527	20	[4,14]
Poly(1,3-dichloropropyl-2-methacrylate)	1.5160	25	[8,17]
Poly(1,4-butadiene)	1.5624	20	[5]
Poly[1-(*o*-chlorophenyl)ethyl methacrylate]	1.4730		[5]
Poly(1-decene)	1.5111	20	[4,5]
Poly(1-methycyclohexyl methacrylate)	1.4710	25	[8,17]
Poly(1-octadecene)	1.5396	20	[5]
Poly(1-phenyl-*n*-amyl methacrylate)	1.5573	20	[5]
Poly(1-phenylallyl methacrylate)	1.5645	20	[4,5]
Poly(1-phenylcyclohexyl methacrylate)	1.5487	25	[8,17]
Poly(1-phenylethyl methacrylate)	1.53		[5]
Poly(1-vinyl-2-pyrrolidone)	1.5660	25	[6,17]
Poly(2,2,2′-trimethylhexamethylene terephthalamide)	1.4185		[5]
Poly(2,2,2-trifluoro-1-methylethyl methacrylate)	1.392	25	[5]
Poly(2,2,3,4,4,4-hexafluorobutyl acrylate)	1.5783	25	[8,17]
Poly(2,2-butane bis[4-(2-methylphenyl)]carbonate)	1.5827	25	[8,17]
Poly[2,2-butane bis(4-phenyl)carbonate]	1.5745	25	[8,17]
Poly[2,2-pentane bis(4-phenyl)carbonate]	1.6056	25	[8,17]
Poly(2,2-propane bis[4-(2,6-dibromophenyl)]carbonate)	1.5739	20	[4,5]
Poly(2,2-propane bis[4-(2,6-dichlorophenyl)]carbonate)	1.5900	25	[8,17]
Poly(2,2-propane bis[4-(2-chlorophenyl)]carbonate)	1.6147	25	[8,17]
Poly(2,3-dibromopropyl methacrylate)	1.525	20	[4,5]
Poly(2,3-dimethylbutadiene) (methyl rubber)	1.6248	20	[4,5]
Poly(2,6-dichlorostyrene)	1.412	25	[5]
Poly[2-(1,1,2,2-tetrafluoroethoxy)ethyl acrylate]	1.5682		[5]
Poly[2-(phenylsulfony)ethyl methacrylate]	1.537	20	[5]
Poly(2-aminoethyl methacrylate)	1.5816	20	[4,14]
Poly(2-β-diphenylethyl methacrylate)	1.50	25	[5]
Poly(2-bromo-4-trifluoromethylstyrene)	1.5426	20	[5]
Poly(2-bromoethyl methacrylate)	1.5270	20	[5]
Poly[2-chloro-1-(chloromethyl)ethyl methacrylate]	1.5179	20	[4,5]

TABLE 50.1. *Continued.*

Polymer	Refractive index n	Temperature (°C)	Reference
Poly(2-chlorocyclohexyl methacrylate)	1.533	25	[5]
Poly(2-chloroethyl α-chloroacrylate)	1.517	20	[5]
Poly(2-chloroethyl methacrylate)	1.4899	20.5	[5]
Poly(2-decyl-1,3-butadiene)	1.4899	25	[8,17]
Poly(2-decyl-1,4-butadiene)	1.5174	20	[5]
Poly(2-diethylaminoethyl methacrylate)	1.471	25	[5]
Poly(2-ethoxyethyl acrylate)	1.4768	20	[5]
Poly(2-fluoroethyl methacrylate)	1.390	25	[5]
Poly(2-heptafluorobutoxy)ethyl acrylate)	1.500		[5]
Poly(2-heptyl-1,3-butadiene)	1.5000	25	[8,17]
Poly(2-heptyl-1,4-butadiene)	1.5119	20	[5]
Poly(2-hydroxyethyl methacrylate)	1.5028	30	[5]
Poly(2-isopropyl-1,3-butadiene)	1.5020	25	[8,17]
Poly(2-isopropyl-1,4-butadiene)	1.463	25	[5]
Poly(2-methoxyethyl acrylate)	1.5028	20	[4,5]
Poly(2-methylcyclohexyl methacrylate)	1.4868	20	[4,5]
Poly(2-nitro-2-methylpropyl methacrylate)	1.5592	20	[5]
Poly(2-phenylethyl methacrylate)	1.5060	24.6	[5]
Poly(2-t-butyl-1,3-butadiene)	1.5060	25	[8,17]
Poly(2-t-butyl-1,4-butadiene)	1.419	25	[5]
Poly(2-trifluoroethoxyethyl acrylate)	1.55	20	[5]
Poly(2-vinyltetrahydrofuran)	1.6376	20	[5]
Poly(2-vinylthiophene)	1.485	20	[4,5]
Poly(3,3,5-trimethylcyclohexyl methacrylate)	1.4580	25	[8,17]
Poly(3-butoxypropylene oxide)	1.465	25	[5]
Poly(3-ethoxypropyl acrylate)	1.4590	25	[8,17]
Poly(3-hexoxypropylene oxide)	1.471	25	[5]
Poly(3-methoxypropyl acrylate)	1.4947	20	[4,5]
Poly(3-methoxypropylene oxide)	1.6330	25	[5,17]
Poly(3-methylcyclohexyl methacrylate)	1.4630	25	[8,17]
Poly[4,4′-isopropylidene diphenoxy di(4-phenylene)sulfone]	1.6500	25	[8,17]
Poly[4,4′-sulfone diphenoxy di(4-phenylene)sulfone]	1.5602	25	[8,17]
Poly[4,4-heptane bis(4-phenyl)carbonate]	1.46		[5]
Poly(4-fluoro-2-trifluoromethylstyrene)	1.5868	20	[5]
Poly(4-methoxy-2-methylstyrene)	1.5967	20	[9]
Poly(4-methoxystyrene)	1.459–1.465		[5]
Poly(4-methyl-1-pentene) (see Ftn. 17)	1.463	20	[10]
Poly(4-methylcyclohexyl methacrylate)	1.546	25	[5]
Poly(abietic acid) (see Ftn. 18)	1.51	20	[10]
Poly(acetal)	1.61		[1]
Poly(acrolein)	1.5270	25	[5]
Poly(acrylate)	1.514	20	[10]
Poly(acrylic acid) (see Ftn. 19)	1.492		[1]
Poly(acrylonitrile) (see Ftn. 20)	1.641	20	[5]
Poly(allomer)	1.64–1.70		[4,14]
Poly(allyl methacrylate) (see Ftn. 21)	1.6411	20	[4,14]
Poly(α-methallyl methacrylate)	1.5573	20	[4,14]
Poly(α-naphthyl carbinyl methacrylate)	1.5396	20	[4,14]
Poly(α-naphthyl methacrylate (see Ftn. 22)	1.651	23	[13,18]
Poly(α-o-chlorophenylethyl methacrylate)	1.568	20	[4,10]
Poly(α-phenyl allyl methacrylate)	1.537	20	[4,14]
Poly(α-phenyl-n-amyl methacrylate)	1.5426	20	[4,14]
Poly(α-phenylethyl methacrylate)	1.533 ± 0.001	25	[4,14]
Poly(amide)	1.4833	20	[4,14]
Poly(arylsulfone)	1.508		[4,14]

TABLE 50.1. *Continued.*

Polymer	Refractive index *n*	Temperature (°C)	Reference
Poly(benzhydryl methacrylate)	1.511	20	[4,14]
Poly(benzyl methacrylate)	1.6298	20	[5]
Poly(β-aminoethyl methacrylate)	1.6298	20	[4,14]
Poly(β-bromoethyl methacrylate)	1.5592	20	[4,14]
Poly(β-chloroethyl chloroacrylate)	1.5682	20	[4,14]
Poly(β-ethoxyethyl methacrylate)	1.5059	20	[5]
Poly(β-methallyl methacrylate)	1.5178	20	[9,10]
Poly(β-naphthyl methacrylate) (see Ftn. 23)	1.4631	30	[5]
Poly(β-phenylethyl methacrylate)	1.50		[1]
Poly(β-phenylsulfone ethyl methacrylate)	1.5390	20	[5]
Poly(bornyl methacrylate) (see Ftn. 24)	1.586	23	[13,18]
Poly(butadiene) (see Ftn. 25)	1.6056		[4,14]
Poly(butene) (isotactic)	1.6290	25	[8,17]
Poly(butyl acetate)	1.554–1.558		[5]
Poly(butyl acrylate) (see Ftn. 26)	1.3900	25	[8,17]
Poly(butyl mercaptyl methacrylate)	1.542	25	[5]
Poly(butylene)	1.4969	20	[5]
Poly(carbonate) from 3,3′,5,5′-tetrachlorodiphenyl (see Ftn. 27)	1.5570	25	[8,17]
Poly(chloro-*p*-xylylene)	1.4990		[5]
Poly(chloroprene)	1.572	20	[4,5]
Poly(chlorotrifluoroethylene) (see Ftn. 28)	1.544		[5]
Poly(cinnamyl methacrylate)	1.4035	25	[8,17]
Poly(cyclohexanediol-1,4-dimethacrylate)	1.403		[11]
Poly(cyclohexyl α-bromoacrylate)	1.395		[11]
Poly(cyclohexyl α-chloroacrylate)	1.403		[11]
Poly(cyclohexyl α-ethoxyacrylate)	1.4035		[11]
Poly(cyclohexyl bromoacrylate)	1.399		[11]
Poly(cyclohexyl methacrylate) (see Ftn. 29)	1.4031		[11]
Poly(cyclohexyl–cyclohexyl methacrylate)	1.4034		[11]
Poly(cyclohexylmethylsilane)	1.388		[11]
Poly(decamethylene glycol dimethacrylate)	1.4015		[11]
Poly(diacetin methacrylate)	1.3935		[11]
Poly(diallyl cinnamate)	1.4025		[11]
Poly[diallyl glycol carbonate (CR-39)]	1.398		[11]
Poly(diallyl phthalate) (see Ftn. 30)	1.6539	25	[8,17]
Poly(dichlorostyrene)	1.4740	20	[5]
Poly(diethylaminoethyl methacrylate)	1.5300	25	[8,17]
Poly(dihydroabietic acid)	1.60		[1]
Poly(dimethylsiloxane)	1.537–1.55	23	[6]
Poly(dimethylsiloxane) hydride terminated M.W. = 17,500	1.53–1.57	23	[6]
Poly(dimethylsiloxane) hydride terminated M.W. = 28,000	1.523–1.54		[5]
Poly(dimethylsiloxane) hydride terminated M.W. = 400	1.50–1.57	23	[13,18]
Poly(dimethylsiloxane) hydride terminated M.W. = 62,000	1.53–1.58	23	[13,18]
Poly(dimethylsiloxane) trimethylsiloxy terminated M.W.>28,000	1.658		[1]
Poly(dimethylsiloxane) trimethylsiloxy terminated M.W. = 13,650	1.4685	20	[5]
Poly(dimethylsiloxane) trimethylsiloxy terminated M.W. = 162	1.5020	25	[5]
Poly(dimethylsiloxane) trimethylsiloxy terminated M.W. = 17,250	1.4903	20	[5]
Poly(dimethylsiloxane) trimethylsiloxy terminated M.W. = 2,000	1.485	20–25	[5]
Poly(dimethylsiloxane) trimethylsiloxy terminated M.W. = 237	1.502 ± 0.001	25	[4,14]
Poly(dimethylsiloxane) trimethylsiloxy terminated M.W. = 28,000	1.555	20	[4,14]
Poly(dimethylsiloxane) trimethylsiloxy terminated M.W. = 340	1.5063	20	[5]
Poly(dimethylsiloxane) trimethylsiloxy terminated M.W. = 3,780	1.455	20	[9]
Poly(dimethylsiloxane) trimethylsiloxy terminated M.W. = 410	1.455	20	[9]
Poly(dimethylsiloxane) trimethylsiloxy terminated M.W. = 550	1.459	20	[9]
Poly(dimethylsiloxane) trimethylsiloxy terminated M.W. = 5,970	1.570 ± 0.003	20–22	[4,14]

TABLE 50.1. *Continued.*

Polymer	Refractive index n	Temperature (°C)	Reference
Poly(dimethylsiloxane) trimethylsiloxy terminated M.W. = 770	1.459	20	[10]
Poly(dimethylsiloxane) trimethylsiloxy terminated M.W. = 9,430	1.459	20	[9]
Poly(dimethylsiloxane) trimethylsiloxy terminated M.W. = 950	1.463	20	[9]
Poly[diphenylmethane bis(4-phenyl) carbonate]	1.465	20	[9]
Poly(diphenylmethyl methacrylate)	1.467	20	[9]
Poly(dodecyl methacrylate)	1.455	20	[10]
Poly(ε-caprolactam)	1.462	20	[10]
Poly(ester carbonate) (polyphthalate)	1.56–1.57		[4,14]
Poly(ester) cast resin, rigid (see Ftn. 31)	1.4840	25	[8,17]
Poly(etherimide)	1.52–1.53	20	[5]
Poly(ethersulfone)	1.545	20	[5]
Poly(ethyl acrylate)	1.54		[1]
Poly(ethyl α-chloroacrylate) (see Ftn. 32)	1.54	23	[13,18]
Poly(ethyl glycolate methacrylate)	1.51	23	[13,18]
Poly(ethyl methacrylate)	1.51	23	[13,18]
Poly(ethyl sulfide methacrylate)	1.51	23	[13,18]
Poly(ethylene chlorohydrin methacrylate)	1.54	23	[13,18]
Poly(ethylene dimethacrylate)	1.54	23	[13,18]
Poly(ethylene glycol benzoate methacrylate)	1.448	20	[9]
Poly(ethylene glycol dimethacrylate)	1.452	20	[9]
Poly(ethylene glycol fumarate)	1.451	20	[9]
Poly(ethylene glycol methyl ether) M.W. = 350	1.453	20	[9]
Poly(ethylene glycol methyl ether) M.W. = 550	1.454	20	[9]
Poly(ethylene glycol methyl ether) M.W. = 750	1.455	20	[9]
Poly(ethylene glycol monomethacrylate)	1.459	20	[9]
Poly(ethylene glycol phthalate) (see Ftn. 33)	1.5300	25	[8,17]
Poly(ethylene glycol) (see Ftn. 34)	1.547	20	[5]
Poly(ethylene glycol) (Carbowax)	1.51		[5]
Poly(cyclohexyl-α -chloroacrylate)	1.40		[11]
Poly(cyclohexyl-α -ethoxyacetate)	1.3825		[11]
Poly(ethylene glycol) M.W. = 300	1.5381		[5]
Poly(ethylene glycol) M.W. = 400	1.575 ± 0.003	20	[4,14]
Poly(ethylene glycol) methyl ester	1.4750	30	[5]
Poly(ethylene glycol) tetrahydrofurfuryl ester	1.5300	25	[8,17]
Poly(ethylene maleate)	1.481	20	[10]
Poly(ethylene oxide)	1.505–1.51		[5]
Poly(ethylene succinate)	1.477	20	[5]
Poly(ethylene terephthalate) (PET)	1.5045	20	[10]
Poly(ethylene terephthalate) grounded (PETG)	1.5050	25	[8,17]
Poly(ethylene) (see Ftn. 35)	1.521	20	[5]
Poly(ethylene) (density 0.914 g/cm^3)	1.5191	20	[9]
Poly(ethylene) (density 0.94–0.945 g/cm^3)	1.4728	20	[5]
Poly(ethylene) (density 0.965 g/cm^3)	1.645	20	[4,14]
Poly(ethylene); type 1—lower density, melt index 0.3–3.6	1.6006	20	[4,14]
Poly(ethylene); type 1—lower density, melt index 200	1.52		[5]
Poly(ethylene); type 1—lower density, melt index 6–26	1.472–1.48		[5]
Poly(ethylene); type 2—med. density, melt index 1.0–1.9	1.5672	20	[4,5]
Poly(ethylene); type 2—med. density, melt index 20	1.517	20	[5]
Poly(ethylene); type 3—higher density, melt index 0.1–12.0	1.52	20	[5]
Poly(ethylene); type 3—higher density, melt index 0.2–0.9	1.4893	23	[5]
Poly(ethylene); type 3—higher density, melt index 1.5–15	1.49	20	[9]
Poly(ethyleneglycol) 200 monononylether	1.383		[11]
Poly(ethyleneglycol) 300 monononylether	1.381		[11]
Poly(ethyleneglycol) 300 monononylether (fractionated, fraction 2)	1.382		[11]
Poly(ethyleneglycol) 300 monononylether (fractionated, fraction 4)	1.379		[11]

TABLE 50.1. *Continued.*

Polymer	Refractive index *n*	Temperature (°C)	Reference
Poly(ethyleneglycol) 300 mononylether (fractionated, fraction 5)	1.5172	20	[4,14]
Poly(ethyleneglycol) 400 mononylether (at 6,563 Å)	1.5155		[4,14]
Poly(ethyleneglycol) 600 mononylether (at 4,861 Å)	1.5248		[4,14]
Poly(ethylidene dimethacrylate) (see Ftn. 36)	1.5118	20	[4, 14]
Poly(ethylmercaptyl methacrylate)	1.451		[11]
Poly(eugenol methacrylate)	1.3979	20	[9]
Poly(fluorenyl methacrylate)	1.398	20	[10]
Poly(furfuryl methacrylate)	1.396		[11]
Poly(glycerol phthalate)	1.382		[11]
Poly(glycerol rosin–maleate)	1.397		[11]
Poly(glycol maleate)	1.443		[11]
Poly(glycol succinate)	1.445		[11]
Poly(heptafluorobutyl acrylate)	1.463		[1]
Poly(hexadecyl methacrylate)	1.455		[11]
Poly(hexamethylene adipamide)	1.43	23	[6]
Poly(hexamethylene glycol dimethacrylate) (see Ftn. 37)	1.5857	20	[5]
Poly(hexamethylene sebacamide)	1.5476	20	[4,5]
Poly(hexyl methacrylate)	1.5965	20	[4,5]
Poly(isobutene)	1.5246	20	[4,14]
Poly(isobutyl methacrylate) (see Ftn. 38)	1.4830	25	[8,17]
Poly(isobutylene) (see Ftn. 39)	1.4813	20	[4,5]
Poly(isoprene) (see Ftn. 40)	1.4840	25	[4,8]
Poly(isopropyl methacrylate) (see Ftn. 41)	1.360	25	[5]
Poly(lead dimethacrylate)	1.5823	20	[4,5]
Poly(*m*-cresyl methacrylate)	1.6040		[5]
Poly(*m*-nitrobenzyl methacrylate)	1.6098	20	[4,5]
Poly(methacrylate methyl salicylate)	1.5707	20	[5]
Poly(methacryl phenyl salicylate)	1.507	20	[4,14]
Poly(methacrylic anhydride)	1.5705	20	[4,5]
Poly(methacrylonitrile) (see Ftn. 42)	1.5932	20	[4,5]
Poly(methyl acrylate) (see Ftn. 43)	1.5750	25	[8,17]
Poly(methyl α-bromoacrylate)	1.6400	25	[8,17]
Poly(methyl α-chloroacrylate)	1.4630	25	[8,17]
Poly(methyl isospropenyl ketone)	1.4800	25	[8,17]
Poly(methyl isopropenyl ketone)	1.4900	25	[8,17]
Poly(methyl methacrylate)	1.5500	25	[8,17]
Poly(methyl methacrylate)	1.5600	25	[8,17]
Poly(methyl methacrylate)	1.4430	25	[8,17]
Poly(methyl methacrylate), beads	1.4450	25	[8,17]
Poly(methyl phenyl siloxane), trimethylsiloxy terminated	1.4510	25	[8,17]
Poly(methyl-3,3,3-trifluoropropylsiloxane), M.W. = 14,000	1.4550	25	[8,17]
Poly(methyl-3,3,3-trifluoropropylsiloxane), M.W. = 2,350	1.3830	25	[8,17]
Poly(methyl-3,3,3,-trifluoropropylisoxane), M.W. = 4,600	1.3970	25	[8,17]
Poly(methyl-3,3,3-trifluoropropylsiloxane), silanol terminated	1.465	50	[5]
Poly(methyl-α-chloroacrylate) (see Ftn. 44)	1.5671		[5]
Poly(methyl-α-methylene butyrolactone)	1.5745		[5]
Poly(methylene-α-valerolactone)	1.5602		[5]
Poly(methylhexadecylsiloxane)	1.5827		[5]
Poly(methylhydrosilane)	1.5792		[5]
Poly(methylhydrosiloxane)	1.5900		[5]
Poly(methylhydrosiloxane) trimethylsilyl terminated M.W. = 1,500	1.6539		[5]
Poly(methylhydrosiloxane) trimethylsillyl terminated M.W. = 2,270	1.5937		[5]
Poly(methylhydrosiloxane) trimethylsilyl terminated M.W. = 360–420	1.5702		[5]
Poly(methylhydrosiloxane) trimethylsilyl terminated M.W. = 4,500–5,000	1.5850		[5]
Poly(methyloctadecylsiloxane)	1.6056		[5]

TABLE 50.1. *Continued.*

Polymer	Refractive index n	Temperature (°C)	Reference
Poly(methyloctylsiloxane)	1.43		[5]
Poly(methylpentene)	1.4563	30	[5]
Poly(methyltetradecylsiloxane)	1.51–1.54		[5]
Poly(monochlorotrifluoroethylene)	1.555	20	[5]
Poly(monofluorethyl methacrylate)	1.4840	25	[5]
Poly[N(-2-methoxythyl)methacrylamide]	1.4744	25	[5]
Poly[N-(2-phenylethyl)methacrylate]	1.5750	20	[5]
Poly(N-allyl methacrylamide)	1.48	20	[5]
Poly(N-benzyl methacrylamide)	1.4690	25	[8,17]
Poly(N-β-methoxyethyl methacrylamide)	1.5840	20	[5]
Poly(N-β-phenylethyl methacrylamide)	1.4495		[5]
Poly(n-butyl methacrylate) (see Ftn. 45)	1.5559	20	[4,5]
Poly(N-butyl-methacrylamide)	1.5575	20	[4,5]
Poly(n-hexyl methacrylate)	1.6150	20	[4,5]
Poly(N-methyl-methacrylamide)	1.554	20	[4,5]
Poly(n-propyl methacrylate)	1.552	20	[4,5]
Poly(N-vinylphthalimide)	1.5967	20	[4,5]
Poly(nonafluoropentyl acrylate)	1.6690	25	[8,17]
Poly(o-chlorobenzhydryl methacrylate)	1.71	20	[5]
Poly(o-chlorobenzyl methacrylate)	1.608	20	[4,5]
Poly(o-chlorodiphenylmethyl methacrylate)	1.339	25	[5]
Poly(o-chlorostyrene)	1.584 ± 0.003	20	[4, 14]
Poly(o-cresyl methacrylate) (see Ftn. 46)	1.385	25	[5]
Poly(o-methoxyphenyl methacrylate)	1.612	25	[4,5]
Poly(o-methoxystyrene)	1.5624	20	[4,5]
Poly(o-methoxystyrene)	1.5706	20	[4,5]
Poly(octafluoropentyl acrylate)	1.6300	25	[8,17]
Poly(octylmethylsilane)	1.447	20	[10]
Poly[oxy(2,6-dimethyl-1,4-phenylene)]	1.4570	25	[8,17]
Poly[oxy(2,6-diphenyl-1,4-phenylene)]	1.5960	25	[8,17]
Poly[oxy(acryloxypropylmethylsilylene)]	1.49	20	[10]
Poly[oxy(dicyanopropylsilylene)]	1.49		[1]
Poly[oxy(mercaptopropylmethylsilylene)]	1.4735	20	[5]
Poly[oxy(methyl m-chlorophenylethylsilylene)]	1.5030	20	[5]
Poly[oxy(methyl m-chlorophenylsilylene)]	1.541	20	[10]
Poly[oxy(methyl n-hexadecylsilylene)]	1.542	25	[5]
Poly[oxy(methyl n-hexylsilylene)]	1.500	25	[4,5]
Poly[oxy(methyl n-octadecylsilylene)]	1.6568	25	[8,17]
Poly[oxy(methyl n-octylsilylene)]	1.59–1.592	20	[5]
Poly[oxy(methyl n-tetradecyl silylene)]	1.59–1.60		[4,14]
Poly[oxy(methyl-t-trifluoropropylsilylene)]	1.5901	25	[4,14]
Poly[oxy(methylhydrosilylene)]	1.5858		[4,14]
Poly[oxy-1-oxopentamethylene]	1.5916	20	[10]
Poly(oxy-2,6-dimethylphenylene)	1.59–1.60		[1]
Poly[oxycarbonyloxy-1,4(2,6-dichloro)phenylne-isopropylidene-1,4(2,6-dichloro)phenylene]	1.57–1.60		[1]
Poly(oxycarbonyloxy-1,4-phenylene-1,3-dimethyl-butylidene-1,4-phenylene)	1.59–1.60	23	[6]
Poly(oxycarbonyloxy-1,4-phenylene-1-methyl-butylidene-1,4-phenylene)	1.6	23	[13,18]
Poly(oxycarbonyloxy-1,4-phenylene-1-propyl-butylidene-1,4-phenylene)	1.6–1.7		[4,5]
Poly(oxycarbonyloxy-1,4-phenylene-sec-butylidene-1,4-phenylene)	1.633		[1,5]
Poly(oxycarbonyloxy-1,4-phenylenebutylidene-1,4-phenylene)	1.4638	25	[8,17]
Poly(oxycarbonyloxy-1,4-phenylenecyclohexylidene-1,4-phenylene)	1.4638	20	[10]
Poly(oxycarbonyloxy-1,4,phenylenediphenyl-methylene-1,4-phenylene)	1.4746	30	[5]
Poly(oxycarbonyloxy-1,4-phenyleneethylidene-1,4-phenylene)	1.346	25	[5]
Poly(oxycarbonyloxy-1,4-phenyleneisobutylidene-1,4-phenylene)	1.348	25	[5]
Poly(oxycarbonyloxy-1,4-phenyleneisopropylidene-1,4-phenylene)	1.360	25	[5]

TABLE 50.1. *Continued.*

Polymer	Refractive index *n*	Temperature (°C)	Reference
Poly(oxycarbonyloxybis[1,4(3,5-dichlorophenylene)])	1.35	20	[9]
Poly(oxydimethylsilylene)	1.35	23	[13,18]
Poly(oxyethylene) (see Ftn. 47)	1.35		[12]
Poly[(oxyethylene)-α-benzoate-ω-methacrylate]	1.35		[1]
Poly(oxyethyleneoxymaleoyl) [poly(ethylene maleate)]	1.46	20	[10]
Poly(oxyethyleneoxysuccinoyl) [poly(ethylene succinate)]	1.465	20	[10]
Poly(oxyethyleneoxyterephthaloyl) [poly(ethylene terephthalate)]	1.466	20	[10]
Poly(oxymethylene)	1.5096	20	[5]
Poly(oxyoctamethylene)	1.4889	20	[5]
Poly(oxypentaerythritoloxyphthaloyl)	1.43	23	[3,13]
Poly(oxypropylene)	1.407	25	[5]
Poly(*p,p′*-xylyenyl dimethacrylate)	1.437		[5]
Poly(*p*-bromophenyl methacrylate)	1.4177	20	[5]
Poly(*p*-cyclohexylphenyl methacrylate)	1.375	25	[5]
Poly(*p*-divinylbenzene)	1.356		[5]
Poly(*p*-isopropylstyrene)	1.5–1.6		[5]
Poly(*p*-methoxybenzyl methacrylate)	1.4628	30	[5]
Poly(*p*-methoxystyrene)	1.48–1.50		[5]
Poly(*p*-xylylene)	1.4665	20	[5]
Poly(pentabromophenyl methacrylate)	1.45–1.47	23	[6]
Poly(pentachlorophenyl methacrylate)	1.49–1.53		[5]
Poly(pentadecafluorooctyl acrylate)	1.49–1.53	23	[6]
Poly(pentaerythritol phthalate)	1.5775	20	[4,5]
Poly(pentaerythritol tetramethacrylate)	1.4563	20	[5]
Poly(pentafluoropropylacrylate)	1.485	20	[9,10]
Poly(pentafluorovinyl propionate)	1.47–1.49	23	[6]
Poly(phenyl α-bromoacrylate)	1.48–1.49	23	[6]
Poly(phenyl cellosolve methacrylate)	1.52–1.53	23	[6]
Poly(phenyl methacrylate)	1.54–1.55		[5]
Poly(phenylmethylsilane)	1.52–1.55		[12]
Poly(propylene glycol)	1.52		[5]
Poly(propylene oxide)	1.55		[5]
Poly(propylene sulfide)	1.54–1.55	23	[6]
Poly(propylene) (see Ftn. 48)	1.512	25	[5]
Poly(propylene) (density 0.9075 g/cm^3)	1.502	20	[5,10]
Poly(propylene), atactic (density 0.8575 g/cm^3)	1.454	20	[10]
Poly(propylene), chlorinated	1.50	23	[6]
Poly(sec-butyl α-bromoacrylate)	1.4750	20	[5]
Poly(sec-butyl α-chloroacrylate)	1.4591	30	[5]
Poly(styrene sulfide)	1.4507	30	[5]
Poly(styrene) (see Ftn. 49)	1.5129	20	[5]
Poly(sulfides) (Thiokol)	1.466	20	[10]
Poly(sulfone)	1.474	30	[5]
Poly(*t*-butyl methacrylate) (see Ftn. 50)	1.683	20	[4,5]
Poly(terpineyl methacrylate)	1.55	20	[5]
Poly(tetradecyl methacrylate)	1.60–1.63	23	[3,13]
Poly[tetrafluoro-3-(heptafluoropropoxy)propyl acrylate]	1.60–1.63	23	[6]
Poly[tetrafluoro-3(pentafluoroethoxy)propyl acrylate]	1.42	25	[5]
Poly[tetrafluoro-3(trifluoromethoxy)propyl acrylate]	1.42	23	[13,18]
Poly(tetrafluoroethylene) (PTFE) (see Ftn. 51)	1.6818	20	[5]
Poly(tetrahydrofuran) M.W. = 250	1.52		[4,14]
Poly(tetrahydrofuran) M.W. = 650	1.5196	20	[4,14]
Poly(tetrahydrofuran), with oxirane	1.54		[4,14]
Poly(tetrahydrofurfuryl methacrylate)	1.5059	20	[4,14]
Poly(triethoxyl silicol methacrylate)	1.4631	30	[4,14]

TABLE 50.1. *Continued.*

Polymer	Refractive index n	Temperature (°C)	Reference
Poly(triethylcarbinyl methacrylate) (see Ftn. 52)	1.4634	25	[4,14]
Poly(trifluorochloroethylene) (PTFCE)	1.554	20	[4,14]
Poly(trifluoroethyl acrylate)	1.39–1.43		[4,14]
Poly(trifluoroethyl methacrylate)	1.394	20	[4,14]
Poly(trifluoroisopropyl methacrylate) (see Ftn. 53)	1.5067	20	[4,14]
Poly(trifluorovinyl acetate)	1.5066	20	[4,14]
Poly(undecafluorohexyl acrylate)	1.5099	23	[4,14]
Poly(urethane), rigid (see Ftn. 54)	1.65		[1]
Poly(vinyl acetal) (see Ftn. 55)	1.4855	20	[4,14]
Poly(vinyl acetate) (at 6,563 Å) (see Ftn. 56)	1.5013	20	[4,14]
Poly(vinyl alcohol) (see Ftn. 57)	1.483–1.485	25	[4,14]
Poly(vinyl benzoate)	1.51–1.52		[4,14]
Poly(vinyl butyl ether)	1.517	20	[4,14]
Poly(vinyl butyral) (see Ftn. 58)	1.5063	20	[4,14]
Poly(vinyl chloride acetate) molding compound—rigid	1.5119	20	[4,14]
Poly(vinyl chloride) (PVC) rigid (see Ftn. 59)	1.52–1.57		[1]
Poly(vinyl chloride–acetate)	1.477	25	[4,14]
Poly(vinyl chloroacetate) (see Ftn. 60)	1.4728	20	[4,14]
Poly(vinyl cychlohexene dioxide)	1.5228	20	[4,14]
Poly(vinyl decyl ether)	1.499	20	[4,14]
Poly(vinyl dodecyl ether)	1.52		[4,14]
Poly(vinyl ethyl ether) (see Ftn. 61)	1.4725	20	[4,14]
Poly(vinyl formal) molding compound (see Ftn. 62)	1.4893	23	[4,14]
Poly(vinyl formate) (see Ftn. 63)	1.4768		[4,14]
Poly(vinyl hexyl ether)	1.5117	20	[4,14]
Poly(vinyl isobutyl ether) (see Ftn. 64)	1.514	20	[4,14]
Poly(vinyl methacrylate) (see Ftn. 65)	1.376	25	[4,14]
Poly(vinyl methyl ether) (see Ftn. 66)	1.5096	20	[4,14]
Poly(vinyl methyl ketone)	1.4177	20	[4,14]
Poly(vinyl naphthalene)	1.48–1.50		[4,14]
Poly(vinyl octyl ether)	1.47–1.49		[4,14]
Poly(vinyl pentyl ether)	1.4667	24	[4,14]
Poly(vinyl phenyl sulfide)	1.545–1.555	25	[4,14]
Poly(vinyl propionate) (see Ftn. 67)	1.51–1.55		[4,14]
Poly(vinyl sec-butyl ether) (isotactic)	1.47–1.49		[4,14]
Poly(vinyl triophene)	1.54–1.56		[4,14]
Poly(vinyl-2-ethylhexyl ether)	1.565	40	[4,14]
Poly(vinylcarbazole)	1.525–1.529	21	[4,14]
Poly(vinylfuran) (see Ftn. 68)	1.5303	20	[4,14]
Poly(vinylidene chloride) molding compound (see Ftn. 69)	1.4757	20	[4,14]
Poly(vinylidene-fluoride) (PVDF) (see Ftn. 70)	1.5129	20	[4,14]
Poly(vinylnaphthalene)	1.467	20	[4,14]
Poly(vinylpyrrolidone)	1.55	20	[4,14]
Poly(vinylsulfonic acid) (sodium salt)	1.53		[4,14]
Propylmethyl homopolymer, vinyldimethyl terminated	1.43		[11]
Pyralin Polyimide Film-Pl-2540	1.78		[7,16]
Pyralin Polyimide Film-Pl-2550	1.70		[7,16]
Rosin (grade M, wood)	1.525 ± 0.003	20	[4,14]
Rosin ester	1.496 ± 0.003	21–23	[4,14]
Rubber (hard, 32% S)	1.60	25	[4,5]
Rubber hydrochloride (Pilofilm)	1.540–1.550	25	[4,14]
Shellac, bleached, dry	1.534 ± 0.003	20–22	[4,14]
Shellac, orange	1.516 ± 0.003	20–22	[4,14]
Silicone, Dow-Corning 2102	1.419		[4,14]
Sulfonamide resins	1.56–1.596		[4,14]

TABLE 50.1. *Continued.*

Polymer	Refractive index *n*	Temperature (°C)	Reference
Terpene resin (Piccolyte S-10)	1.506		[4,14]
Terpene resin (Piccolyte S-40)	1.515	25	[4,14]
Toluenesulfonamide formaldehyde	1.596	25	[4,14]
Urea formaldehyde	1.54–1.56		[1,14]
Urea–thiourea formaldehyde	1.66	25	[4,14]

Footnote 1
CP-41/l/ gen. purpose, lowest heat resistance
CP-51/IE/ gen. purpose, medium heat resistance
CP-61/IE/ gen. purpose, medium heat resistance
CP-71/l/ gen. purpose, maximum heat resistance
CP-75/l/ gen. purpose, maximum heat resistance, medium flow
CP-80/E/ gen. purpose, unlubed
CP-81/E/ gen. purpose, high heat resistance
CP-82/l/ gen. purpose, maximum heat resistance
CP-924/l/ good impact str. exc. light trans.
CP-927/I/ better impact str. exc. surface gloss
Footnote 2
H-11/IE/ highest heat resistance water white
H-12/IE/ improved flow properties water white
H-15-011/IE/ UV absorbing automotive applications
H-15-012/I/ UV transmitting automotive applications
H-15/IE/ increased toughness maximum service temp. white
L-40/IE/ improved flow easy molding water white
M-30/IE/ improved flow easy molding water white
Footnote 3
6/I/ thin walled and complicated parts
6E/EI/ good flow, tough technical parts
7/I/ good flow dimen. stability
7E/EI/ high melt viscosity
8/I/ good surface hardness
8E/E/ high melt viscosity, good stab.
Footnote 4
DR G/I/ high-impact γ radiation
DR M/I/ high-impact, low reflectance
DR/IE/ high-impact acrylic molding
G-UVT// gen. purpose optical quality
G// gen. purpose cellcast unshrunk nat.
HFI-10/I/ high-impact high-flow pellets
HFI-7/I/ medium-impact high-flow pellets
II-UVA// gen. purpose preshrunk
II-UVT// gen. purpose increases uv stab
K// superior thermoformability
MC// plastic sheet economical material
MI-7/I/ medium-impact high flow
MI-7G/IE/ medium-impact light transmission
UF-3// ultraviolet radiation
V-044/E/ high heat resistance
V-045/IE/ high heat resistance
V-052/I/ high heat resistance
V-811/IE/ maximum heat resistance
V-825/IE/ maximum heat resistance
V-920/IE/ high heat resistance
VM/IE/ medium heat resistance
VS/I/ maximum flow lowest heat resistance

TABLE 50.1. *Continued.*

Polymer	Refractive index n	Temperature (°C)	Reference
Footnote 5			
300// cross-linked commercial continuous cast			
Acrysteel I-GP// continuous cast impact clear			
GPA// gen purpose cast acrylic sheet clear			
Footnote 6			
Cellulose acetate (partly saponified)	1.54		[4,14]
Cellulose acetate-molding	1.46–1.50	23	[6]
Cellulose acetate-sheet	1.49–1.50	23	[6]
Footnote 7			
ASTM Grade: H2-1			
ASTM Grade: H4-1			
ASTM Grade: H6-1			
ASTM Grade: MH-1, MH-2			
ASTM Grade: MS-1, MS-2			
ASTM Grade: S2-1			
Footnote 8			
ASTM Grade: H4	1.46–1.49		[13,18]
ASTM Grade: MH	1.46–1.49		[13,18]
ASTM Grade: S2	1.46–1.49		[13,18]
Cellulose acetate butyrate	1.46–1.50		[4,14]
Cellulose acetate butyrate	1.494	21	[4,14]
Footnote 9			
Cellulose acetate propionate; ASTM Grade: 1	1.46–1.49	23	[13,18]
Footnote 10			
Cellulose nitrate	1.501	21	[4,14]
Footnote 11			
Congo copal	1.540–1.541	25	[4,14]
Congo ester	1.506 ± 0.003	20	[4,14]
Footnote 12			
Damar No. 1 (Singapore)	1.515 ± 0.003	20	[4,14]
Footnote 13			
Epoxy resins	1.57–1.61		[4,14]
Epoxy, diglycidyl ether of bisphenol A, cast flexible or molded	1.61	23	[13,18]
Footnote 14			
Gutta percha, alpha	1.514	50	[4,14]
Gutta percha, beta	1.509	50	[4,5]
Footnote 15			
Nylon 6 (Poly[imino(1-oxohenamethylene)])	1.53		[5]
Nylon 6,10 [Poly(iminoadipoyliminotetramethylene)]	1.53		[5]
Nylon 6,6 [Poly(iminoadipoylaminohexamethylene)]	1.53		[5]
Nylon molding compound	1.53–1.55		[4,14]
Nylons (polyamide) type 11	1.52		[1]
Nylons (polyamide) type 6,6	1.53		[1]
Footnote 16			
Phenol–formaldehyde	1.5–1.7		[4,14]
Footnote 17			
Poly(4-methyl-1-pentene)	1.4975	20	[4,5]
Footnote 18			
Poly(abietic acid)	1.529		[5]
Footnote 19			
Poly(acrylic acid)	1.5196	20	[5]
Footnote 20			
Poly(acrylonitrile)	1.4917	20	[4,14]
Poly(acrylonitrile)	1.63		[4,5]
Footnote 21			
Poly(allyl methacrylate)	1.5624	20	[4,14]

TABLE 50.1. *Continued.*

Polymer	Refractive index *n*	Temperature (°C)	Reference
Footnote 22			
Poly(α-naphthyl methacrylate)	1.5487	20	[4,14]
Poly(α-naphthyl methacrylate)	1.5933	20	[4,14]
Footnote 23			
Poly(β-naphthyl methacrylate)	1.466	20	[5]
Footnote 24			
Poly(bornyl methacrylate)	1.467	20	[10]
Footnote 25			
Poly(butadiene)	1.585		[4,14]
Footnote 26			
Poly(butyl acrylate)	1.5951	20	[4,14]
Poly(butyl acrylate)	1.5067	20	[5]
Footnote 27			
Poly(carbonate)	1.532 ± 0.001	25	[4,14]
Poly(carbonate) of bisphenol-A	1.4969	20	[4,14]
Poly(carbonate) of bisphenol-A	1.5857	25	[8,17]
Footnote 28			
Poly(chlorotrifluoroethylene)	1.571–1.572	20	[4,14]
Poly(chlorotrifluoroethylene)	1.62–1.64		[4,14]
Footnote 29			
Poly(cyclohexyl methacrylate)	1.375		[11]
Footnote 30			
Poly(diallyl phthalate)	1.5933	20	[5]
Footnote 31			
Poly(ester) cast resins—flexible	1.4539	20	[10]
Poly(ester) cast resins—rigid	1.4744	25	[8,17]
Poly(ester) cast, flexible	1.64		[1]
Poly(ester) cast, rigid	1.51	20	[5]
Poly(ester) resin, rigid (ca. 50% styrene)	1.567		[1]
Footnote 32			
Poly(ethyl α-chloroacrylate)	1.51	23	[6]
Footnote 33			
Poly(ethylene glycol phthalate)	1.4831	20	[5]
Footnote 34			
Poly(ethylene glycol)	1.5714	20	[4,14]
Footnote 35			
Poly(ethylene)	1.5191	20	[10]
Poly(ethylene) Ionomer	1.533		[11]
Poly(ethylene) molding cmpd.	1.5705	20	[4,14]
Footnote 36			
Poly(ethylidene dimethacrylate)	1.5431	20	[4,14]
Footnote 37			
Poly(hexamethylene glycol dimethacrylate)	1.5246	20	[5]
Footnote 38			
Poly(isobutyl methacrylate)	1.5857	20	[4,14]
Footnote 39			
Poly(isobutylene)	1.4831	25	[4,14]
Footnote 40			
Poly(isoprene)	1.5398	20	[4,5]
Poly(isoprene) *cis*	1.6200	20	[4,5]
Poly(isoprene)	1.5219	20	[4,14]
Footnote 41			
Poly(isopropyl methacrylate)	1.604	20	[4,14]

TABLE 50.1. *Continued.*

Polymer	Refractive index *n*	Temperature (°C)	Reference
Footnote 42			
Poly(methacrylonitrile)	1.5874	20	[5]
Footnote 43			
Poly(methyl acrylate)	1.380	25	[5]
Poly(methyl acrylate)	1.4780	25	[8,17]
Footnote 44			
Poly(methyl-α-chloroacrylate)	1.575		[5]
Poly(methyl-α-chloroacrylate	1.6056		[5]
Footnote 45			
Poly(*n*-butyl methacrylate)	1.5964	20	[4,5]
Footnote 46			
Poly(*o*-cresyl methacrylate)	1.364	25	[5]
Footnote 47			
Poly(oxyethylene) (high molecular weight)	1.35	23	[6]
Footnote 48			
Poly(propylene)	1.4640	30	[5]
Poly(propylene)	1.4540	30	[5]
Footnote 49			
Poly(styrene)	1.467	20	[5,10]
Poly(styrene)	1.4700	30	[5]
Poly(styrene)	1.5000	20	[8,10]
Poly(styrene)	1.6818	20	[4,14]
Poly(styrene) (general purpose)	1.4613	30	[5]
Poly(styrene) (general purpose)	1.4665	20	[5]
Poly(styrene) (heat and chemical)	1.4581	30	[5]
Poly(styrene) modified molding compound—heat and chemical resistance type	1.57–1.60	23	[6]
Poly(styrene) molding compound—unfilled	1.6568	20	[4,5]
Footnote 50			
Poly(*t*-butyl methacrylate	1.6376		[4,14]
Poly(*t*-butyl methacrylate)	1.4626	30	[5]
Footnote 51			
Poly(tetrafluoroethylene) (PTFE)	1.389	20	[10]
Poly(tetrafluoroethylene) (PTFE)	1.356		[4,14]
Poly(tetrafluoroethylene) (PTFE)	1.4638	20	[4,14]
Poly(tetrafluoroethylene) (PTFE)	1.546	25	[4,14]
Poly(tetrafluoroethylene) (PTFE)	1.527	25	[4,14]
Poly(tetrafluoroethylene) (PTFE) molding compound	1.529		[4,14]
Footnote 52			
Poly(triethylcarbinyl methacrylate)	1.539	20	[4,14]
Footnote 53			
Poly(trifluoroisopropyl methacrylate)	1.547 $\pm$ 0.001	25	[4,14]
Footnote 54			
Poly(urethanes)	1.525	20	[4,14]
Footnote 55			
Poly(vinyl acetal)	1.5001	20	[4,14]
Footnote 56			
Poly(vinyl acetate) (at 4,861 Å)	1.5100	20	[4,14]
Poly(vinyl acetate)	1.5174	20	[4,14]
Poly(vinyl acetate) (medium acetate type)	1.4903	20	[4,14]
Poly(vinyl acetate) (low acetate type)	1.523–1.57		[4,14]
Poly(vinyl acetate) molding compound	1.4685	20	[4,14]

TABLE 50.1. *Continued.*

Polymer	Refractive index n	Temperature (°C)	Reference
Footnote 57			
Poly(vinyl alcohol) molding compound)	1.547	20	[4,14]
Poly(vinyl alcohol) molding compound)	1.512–1.519	25	[4,14]
Footnote 58			
Poly(vinyl butyral)	1.4563	30	[4,14]
Poly(vinyl butyral) molding compound—flexible, unfilled	1.51–1.54	25	[4,14]
Poly(vinyl butyral) molding compound—rigid	1.514	25	[4,14]
Footnote 59			
Poly(vinyl chloride) (PVC)	1.4831	20	[4,14]
Poly(vinyl chloride) (PVC)	1.5381	20	[4,14]
Poly(vinyl chloride) (PVC)	1.541	25	[4,14]
Poly(vinyl chloride) (PVC) rigid	1.484	25	[4,14]
Poly(vinyl chloride) (PVC) + 40% dioctyl phthalate	1.4744	25	[4,14]
Poly(vinyl chloride) (PVC) + 40% tricrexyl phosphate	1.5048	23	[4,14]
Poly(vinyl chloride) (PVC) molding compound—rigid	1.5066	20	[4,14]
Poly(vinyl chloride) (PVC) rigid	1.52–1.55		[1]
Footnote 60			
Poly(vinyl chloroacetate)	1.505–1.51		[4,14]
Footnote 61			
Poly(vinyl ethyl ether)	1.48	25	[4,14]
Poly(vinyl ethyl ether), low molecular weight	1.52	20	[4,14]
Footnote 62			
Poly(vinyl formal)	1.485–1.49		[4,14]
Footnote 63			
Poly(vinyl formate)	1.49	20	[4,14]
Footnote 64			
Poly(vinyl isobutyl ether)	1.49		[4,14]
Footnote 65			
Poly(vinyl methacrylate)	1.35–1.38		[4,14]
Footnote 66			
Poly(vinyl methyl ether)	1.436	20	[4,14]
Poly(vinyl methyl ether) (isotactic)	1.4889	20	[4,14]
Footnote 67			
Poly(vinyl propionate)	1.49–1.53		[4,14]
Footnote 68			
Poly(vinylfuran)	1.512	25	[4,14]
Footnote 69			
Poly(vinylidene chloride)	1.454		[4,14]
Footnote 70			
Poly(vinylidene fluoride) (PVDF)	1.452		[4,14]

TABLE 50.2. *Refractive indices of copolymers. All values reported are at a wavelength of 5,893 Å.*

Copolymer	Refractive index n	Temperature (°C)	Reference
Acrylics multipolymer	1.52		[12]
Acrylonitrile butadiene styrene copolymer (ABS), transparent	1.536		[1]
Arylef U100 (equimolar random copolymer of bisphenol-A terephthalate and bisphenol-A isophthalate)	1.61	25	[8]
Dimethyl (48–52%)–phenylmethyl siloxane (48–52%) copolymer, trimethylsiloxy terminated	1.5		[11]
Dimethyl (70%)–dodecyl (15%)–tetradecyl siloxane (15%), terpolymer	1.43		[11]
Dimethyl (70%)–methyloctadecyl siloxane (30%), copolymer	1.44		[11]
Dimethyl (79–82%)–diphenylsiloxane (18–21%) copolymer, silanol terminated	1.485		[11]
Dimethyl (79–82%)–diphenylsiloxane (18–21%) copolymer, trimethylsiloxy terminated	1.488		[11]
Dimethyl (82–88%)–diphenylsiloxane (12–18%) copolymer, silanol terminated	1.473		[11]
Dimethyl (88–92%)–phenylmethyl siloxane (18–12%) copolymer, trimethylsiloxy terminated	1.425		[11]
Dimethyl (94–96%)–diphenylsiloxane (4–6%) copolymer, trimethylsiloxy terminated	1.422		[11]
Dimethyl (97–98%)–diphenylsiloxane (2–3%) copolymer, silanol terminated	1.42		[11]
Dimethyl–tetrachlorophenyl siloxane, copolymer, branched, trimethylsiloxy terminated	1.428		[11]
Diphenyl (76.5%)–dimethyl (23.5%) copolymer, vinyl terminated, M.W. = 13, 200	1.493	22–25	[11]
Diphenyl (84%)–dimethyl (16%) copolymer, vinyl terminated, M.W. = 9,300;18,600; 18,900;19,500;35,300;54,900	1.465	22–25	[11]
Diphenyl (95%)–dimethyl (5%) copolymer, vinyl terminated, M.W. = 17,300; 49,000;80,400	1.432	22–25	[11]
Diphenyl (97%)–dimethyl (3%) copolymer, vinyl terminated, M.W. = 15,600;62,300	1.420	22–25	[11]
Diphenyl (97%)–dimethyl (3%) copolymer, vinyl terminated, M.W. = 78,000	1.421	22–25	[11]
Methyl hydro (3–4%)–cyanopropylmethylsiloxane copolymer	1.446		[11]
Methyl hydro (0.5–1.0%)–dimethylsiloxane copolymer, trimethylsilyl terminated, M.W. = 10,000,13,000	1.404		[11]
Methyl hydro (30–35%)–dimethylsiloxane copolymer, trimethylsilyl terminated, M.W. = 2,000–2,100	1.399		[11]
Methyl hydro (15–18%)–dimethylsiloxane copolymer, trimethylsilyl terminated, M.W. = 25–35	1.4		[11]
Methyl hydro (50–55%)–dimethylsiloxane copolymer, trimethylsilyl terminated, M.W. = 900–1,000	1.394		[11]
Methyl hydro (25–30%)–methyloctyl siloxane copolymer	1.44		[11]
Methyl hydro (40–60%)–methyloctyl siloxane copolymer	1.435		[11]
Methyl hydro (45–50%)–phenylmethylsiloxane copolymer, dimethylsiloxy terminated	1.5		[11]
Methyloctyl (35–40%)–vinylmethyl (3–4%)–dimethylsiloxane (56–64%), terpolymer	1.437		[11]
Methylphenyl (45–55%)–diphenylsiloxane (45–55%) copolymer, trimethylsiloxy terminated	1.582		[11]
Poly(butadiene-*co*-acrylonitrile)	1.52		[5]
Poly(butadiene-*co*-styrene) (∼30% styrene) block copolymer	1.53		[5]
Poly(butadiene-*co*-styrene) (75%–25%)	1.535		[5]
Poly(ethylene-*co*-propylene) (EPR-rubber)	1.4748–1.48		[5]
Poly(ethylene–*co*-vinyl acetate)	1.47–1.5		[5]
Poly(methyl-3,3,3-trifluoropropylsiloxane–50% dimethyl siloxane) copolymer	1.387		[11]
Poly(oxyethyleneoxymaleoyl) [poly(ethylene maleate)]	1.4840	25	[5]
Poly(oxyethyleneoxysuccinoyl) [poly(ethylene succinate)]	1.4744	25	[5]
Poly(oxyethyleneoxyterephthaloyl) [poly(ethylene terephthalate)]	1.5750	20	[5]
Poly(styrene-*co*-acrylonitrile) (75%–25%)	1.57		[5]
Poly(styrene-*co*-maleic anhydride)	1.564	21	[5]
Poly(tetrafluoroethylene-*co*-hexafluoropropylene)	1.338		[5]

TABLE 50.2. *Continued.*

Copolymer	Refractive index *n*	Temperature (°C)	Reference
Poly(vinyl chloride + 40% dioctyl phthalate	1.52		[5]
Poly(vinyl chloride) + 40% tricrexyl phosphate	1.55		[5]
Poly(vinyl chloride-*co*-vinyl acetate) (95/5-90/10)	1.525–1.535		[5]
Styrene acrylonitrile (SAN)	1.565–1.569	23	[3]
Styrene acrylonitrile copolymer (unfilled)	1.56–1.57		[1]
Styrene butadiene	1.571		[1]
Styrene butadiene thermoplastic elastomers	1.52–1.55		[1]
Styrene maleic anhydride (SMA)	1.6		[1]
Styrene methylmethacrylate (SMMA)	1.56		[1]

TABLE 50.3. *Optical configuration parameters ($\Delta\alpha$) and stress-optical coefficients (C) of polymers. All values reported are at a wavelength of 6,328 Å, D.S. denotes degree of substitution, and v^2 is the polymer volume fraction.*

Polymer	$\Delta\alpha$ (Å³)	Diluent	Temp (°C)	v2	Stress optical coefficient C (10^9 Pa^{-1})	Reference
Benzyl cellulose, D.S. = 2.5	294	Dioxane				[65]
Cellulose acetate D.S. = 2.4	0	Pyridene				[65]
Cellulose acetate D.S. = 3.0	− 34	Tetrachloroethane				[65]
Cellulose acetate D.S. = 3.0	35	Bromoform				[65]
Cellulose acetate D.S. = 3.0	61	Dioxane				[100]
Cellulose acetate D.S. = 3.0	144	Methyl ethyl ketone				[65]
Cellulose benzoate D.S. = 3.0	− 617	Dimethylformamide				[65]
Cellulose benzoate D.S. = 3.0	− 763	Chloroform				[65]
Cellulose benzoate D.S. = 3.0	− 914	Bromobenzene				[65]
Cellulose benzoate D.S. = 3.0	− 830	Dimethyl phthalate				[65]
Cellulose benzoate D.S. = 3.0	− 447	Dioxane				[100]
Cellulosedimethylphosphonocarbamate D.S. = 2.0	710	0.1 M NaCl				[101]
Cellulose dimethylphosphonocarbamate D.S. = 2.0	640	0.2 M NaCl				[101]
Cellulose diphenylacetate	1,360	Acetophenone				[102]
Cellulose diphenylacetate	1,030	Dioxane				[100]
Cellulose diphenylphosphonocarbamate D.S. = 2.0	626–640	Dioxane				[65]
Cellulose monophenylacetate D.S. = 2.8	600	Bromobenzene				[65]
Cellulose monophenylacetate D.S. = 2.8	478	Bromoform				[65]
Cellulose nitrate D.S. = 1.9	− 62	Cyclohexanone				[65]
Cellulose nitrate D.S. = 1.9	149	Dioxane				[65]
Cellulose nitrate D.S. = 2.3	− 330	Cyclohexanone				[65]
Cellulose nitrate D.S. = 2.7	− 540	Cyclohexanone				[65]
Cellulose nitrate D.S. = 2.7	− 320	Amyl acetate				[65]
Cellulose nitrate D.S. = 2.7	− 115	Acetone				[65]
Cellulose nitrate D.S. = 2.7	− 300	Butyl acetate				[65]
Cellulose nitrate D.S. = 2.7	− 140	Ethyl acetate				[65]
Cellulose nitrate D.S. = 2.8	− 820	Cyclohexanone				[65]
Cellulose phenylcarbamate	− 1,100	Acetophenone				[102]
Cellulose phenylcarbamate D.S. = 2.2	− 1,880	Dioxane				[65]
Cellulose phenylcarbamate D.S. = 3.0	− 742	Benzophenone				[103]
Cellulose phenylcarbamate D.S. = 3.0	− 572	Benzophenone				[103]
Cellulose phenylcarbamate D.S. = 3.0	− 1,830	Dioxane				[65]
Cellulose phenylcarbamate D.S. = 3.0	− 872	Dioxane				[65]
Cellulose phenylcarbamate D.S. = 3.0	− 560	Ethyl acetate				[65]

TABLE 50.3. *Continued.*

Polymer	$\Delta\alpha$ (A^{**3})	Diluent	Temp (°C)	v 2	Stress optical coefficient C (10^9 Pa^{-1})	Reference
Cellulose stearate D.S. = 2.0	− 500	Tetrachloroethane				[104]
Cyanoethyl cellulose D.S. = 26	900	Cyclohenanone				[65]
Cyanoethylacetyl cellulose	15	Cyclohexanone				[105]
Cyanoethylacetyl cellulose	390	Acetone				[65]
Cyanoethylacetyl cellulose	90	Dimethylformamide				[65]
Cyanoethyltrityl cellulose	220	Cyclohexanone				[105]
DNA	− 30,000	Aqueous 0.2 M NaCl				[65]
Ethyl cellulose	430	Carbon tetrachloride				[106]]
Ethyl cellulose D.S. = 2.5	512	Dioxane				[65]
Poly(1,2,3-trimethyl-2,3-dihydro-1,6-indendiyl-1,4-phenylene-ethylene)	142	Bromoform				[85]
Poly(1,2,3-trimethyl-2,3-dihydro-1, 6-indenedinyl)	78	Bromoform				[85]
Poly(1-butene) atactic	33.4	Toluene				[30]
Poly(1-butene) isotactic	25.2	Toluene				[30]
Poly(1-decene) isotactic	− 82.5	Toluene				[30]
Poly(1-dodecene) isotactic	− 120	Toluene				[30]
Poly(1-heptene) isotactic	− 24.5	Toluene				[30]
Poly(1-hexadecene)	(− 205)–(− 213)	Toluene				[30]
Poly(1-hexene) atactic	12.1	Toluene				[30]
Poly(1-hexene) isotatic	− 6.5	Toluene				[30]
Poly(1-octadecene) isotactic	− 257	Toluene				[30]
Poly(1-octene) isotactic	− 39	Toluene				[30]
Poly(1-pentene) isotactic	8.0	Toluene				[30]
Poly(1-pentene) isotactic	9.3	Toluene				[30]
Poly(1-tetradecene) isotactic	− 176	Toluene				[30]
Poly(1-tetradecene) isotactic	− 171	Toluene				[30]
Poly(2.5-dichlorostyrene)	− 265	Bromoform				[67]
Poly(2.5-dimethylstyrene)	− 180	Bromoform				[67]
Poly(2-methyl-5-vinyl-N-butylpyridinium bromide)	− 900	0.01 M NaCl				[72]
Poly(2-methyl-5-vinyl-N-butypyridinium bromide)	− 270	0.1 M NaCl				[72]
Poly(2-methyl-5-vinyl-pyridine)	− 260	Bromoform				[73]
Poly(2-methyl-5-vinyl-pyridinium chloride)	− 300	0.1 M HCl				[74]
Poly[2-propenoic acid-4-(phenylazoxy)phenyl ester]	− 450	Tetrachloroethane				[65]
Poly(2-propenoic acid-4-[(4-butylphenyl)azoxy]-phenyl ester)	− 510	Tetrachloroethane				[65]
Poly(3,4-dichlorostyrene)	− 300	Tetrabromoethane				[69]
Poly(3-methyl tetrahydrofuran); isotactic, planar, *trans* config	2.473		20		1.25	[21]
Poly(3-methyl tetrahydrofuran); isotactic, planar, *trans* config	2.563		30		1.20	[21]
Poly(3-methyl tetrahydrofuran); isotactic, planar, *trans* config.	2.653		40		1.16	[21]
Poly(3-methyl tetrahydrofuran); isotactic, planar, *trans* config.	2.750		40		1.13	[21]
Poly(3-methyl tetrahydrofuran); isotactic, planar, *trans* config.	2.835		60		1.10	[21]
Poly(3-methyl-1-butene-silsesquioxane)	− 570	Benzene				[65]
Poly(3-methyl-1-butene-silsesquioxane)	− 400	Butyl acetate				[65]
Poly[4-(4-nonyloxy-benzamido) styrene]	− 2,500	Benzene				[65]

TABLE 50.3. *Continued.*

Polymer	$\Delta\alpha$ (A^{**3})	Diluent	Temp (°C)	v2	Stress optical coefficient C (10^9 Pa^{-1})	Reference
Poly(4-(hexadecyloxy)-benzoic acid-4-[(2-methyl-1-oxo-2-propenyl) oxy]phenyl ester)	− 1,000	Bromoform				[66]
Poly (4-(hexadecyloxy)-benzoic acid-4-[(2-methyl-1-oxo-2-propenyl) oxy]phenyl ester)	− 1,600	Benzene				[66]
Poly(4-(hexadecyloxy)-benzoic acid-4-[(2-methyl-1-oxo-2-propenyl) oxy]phenyl ester)	− 1,400	Chloroform				[66]
Poly(4-(hexadecyloxy)-benzoic acid-4-[(2-methyl-1-oxo-2-propenyl) oxy]phenyl ester)	− 2,700	Carbon tetrachloride				[65]
Poly(4-(hexadecyloxy)-benzoic acid-4-[(2-methyl-1-oxo-2-propenyl) oxy]phenyl ester)	− 890	Tetrahydrofuran				[66]
Poly(4-(hexadecyloxy)-benzoic acid-4-[(2-methyl-1-oxo-2-propenyl) oxy] phenyl ester)	− 4,200	Benzene/heptene, 52/48, 66/34				[67]
Poly(4-(hexadecyloxy)-benzoic acid-4-[(4-[(2-methyl-1-oxo-2-propenyl) oxy]benzoyl)oxy]phenyl ester)	− 4,900	Chloroform				[65]
Poly(4-(hexadecyloxy)-benzoic acid-4-[(4-[(2-methyl-1-oxo-2-propenyl) oxy]benzoyl)oxy]phenyl ester)	− 3,000	Benzene				[65]
Poly(4-(hexyloxy)-3-nitro-benzoic acid-4-[(2-methyl-1-oxo-2-propenyl) oxy]phenyl ester)	− 1,200	Dioxane				[65]
Poly(4-(hexyloxy)-benzoic acid-4-[(2-methyl-1-oxo-2-propenyl) oxy]phenyl ester)	− 370	Benzene				[65]
Poly(4-(nonyloxy)-benzoic acid-4-[(2-methyl-1-oxo-2-propenyl) oxy]phenyl ester)	− 600	Carbon tetrachloride				[65]
Poly(4-[(1-oxo-2-propenyl)oxy]-benzoic acid-4-butoxyphenyl ester)	− 800	Tetrachloroethane				[65]
Poly(4-[(1-oxo-2-propenyl)oxy]-benzoic acid-4-ethoxyphenyl ester)	− 630	Tetrachloroethane				[65]
Poly(4-[(1-oxo-2-propenyl)oxy]-benzoic acid-4-methoxyphenyl ester)	− 520	Tetrachloroethane				[65]
Poly(4-[(1-oxo-2-propenyl)oxy]-benzoic acid-4-propoxyphenyl ester)	− 810	Tetrachloroethane				[65]
Poly(4-[(1-oxo-2-propenyl)oxy]-benzoic acid-phenyl ester)	− 520	Tetrachloroethane				[65]
Poly(4-[(2-methyl-1-oxo-2-propenyl)oxy]-benzoic acid-4-(dodecyloxy) phenyl ester)	− 2,350	Carbon tetrachloride				[65]
Poly(4-[(2-methyl-1-oxo-2-propenyl)oxy]-benzoic acid-4-(nonyloxy)phenyl ester)	− 2,700	Carbon tetrachloride				[65]
Poly(4-[(2-methyl-1-oxo-2-propenyl) oxy]-benzoic acid-4-cyanophenyl ester)	− 240	Dimethylformamide				[65]
Poly(4-[(2-methyl-1-oxo-2-propenyl) oxy]-benzoic acid-4-methoxyphenyl ester)	− 500	Tetrachloromethane				[65]
Poly(4-[(2-methyl-1-oxo-2-propenyl) oxy]-benzoic acid-hexadecyl ester)	− 445	Carbon tetrachloride				[65]

TABLE 50.3. *Continued.*

Polymer	$\Delta\alpha$ (A^{**3})	Diluent	Temp (°C)	v2	Stress optical coefficient C (10^9 Pa^{-1})	Reference
Poly(4-[(11-[(2-methyl-1-oxo-2-propenyl)oxy]-1-oxoundecyl)oxy]-benzoic acid-4-butoxyphenyl ester)	-90	Dioxane				[65]
Poly(4-[2-(2-methyl-1-methylene-allyloxy)-ethoxy]-benzoic acid-4-methoxy-phenyl ester]	-117	Carbon tetrachloride				[65]
Poly(4-propoxy-benzoic acid-4-[(2-methyl-1-oxo- 2-propeny)oxy]phenyl ester)	-320	Dimethylformamide/toluene				[65]
Poly(4-vinylpyridene)	-240	Bromoform				[75]
Poly(4-vinylpyridinium chloride)	-260	0.1 M HCl				[75]
Poly(4-vinylpyridinium chloride)	-440	0.05 M HCl				[75]
Poly(acenaphthylene) helix 4/1	-300	Bromoform				[83]
Poly(acenaphthylene) *trans*	-300	Bromoform				[83]
Poly(acrylic acid)	-0.5	Dioxide				[42]
Poly(acrylic acid), sodium salt	-20	0.0012 M NaCl, pH 7				[43]
Poly(acrylic acid), sodium salt	(-4)–(-10)	water, pH 6.1				[43]
Poly(acrylonitrile)	-23	Dimethylformamide				[64]
Poly(α-methylstyrene); glass					0.002	[17,68]
Poly(α-methylstyrene)	-133	Tetrabromoethane				[70]
Poly(benzimidizole-2,6-diyl-1,4-phenylenebenzimidazol-6,2-diyl-iminoterephthaloylimino)	490	Sulfuric acid				[65]
Poly(benzimidizole-2,6-diyl-iminoterephthaloylimino-1, 4-phenylene)	5,080	Sulfuric acid				[65]
iminoterephthaloylimino-1,3-(4-hydroxyphenylene)	2,340	Sulfuric acid				[65]
Poly(benzoxazole-2,6-diyl-iminoterephth-aloylimino-1, 4-(3-hydroxyphenylene)	5,940	Sulfuric acid				[65]
Poly(benzoxazole-2,6-diyl-iminoterephth-aloylimino-1, 4-phenylene)	5,940	Sulfuric acid				[65]
Poly(benzyl methacrylate); glass					0.025–0.045	[17,50]
Poly(β-naphthyl methacrylate)	-60	Tetrabromoethane				[64]
Poly(β-vinylnapthalene)	-440	Bromoform				[83]
Poly(β-vinylnapthalene)	-4.4	Benzene				[27]
Poly(butadiene) 1,4-cis	61.3–63	Benzene				[24]
Poly(butadiene) 1,4-cis	53.5	Carbon tetrachloride				[24]
Poly(butadiene) 1,4-*cis*	57.3	Cyclohexane				[24]
Poly(butadiene) 1,4-*cis*	72	Toluene				[24]
Poly(butadiene) 1,4-*cis*	86.9	*p*-Xylene				[24]
Poly(butadiene) 1,4-*trans*	71	Benzene				[25]
Poly(butadiene) 1,4-*trans*	61.1	Carbon tetrachloride				[24]
Poly(butadiene) 1,4-*trans*	57.3	Cyclohexane				[24]
Poly(butadiene) 1,4-*trans*	81.6	Toluene				[24]
Poly(butadiene) 1,4-*trans*	101	*p*-Xylene				[24]
Poly(butadiene); (isotactic) melt			22		3.3	[17,26]
Poly(butyl acrylate); fraction of *meso* dyads, Wm = 0.3	-0.95		50	1.0		[20,49]
Poly(carbonate) of bisphenol-A			170–230		3.5–3.7	[17,29]
Poly(carbonate) of bisphenol-A, benzyl substituted			220		40	[17,29]
Poly(carbonate) of bisphenol-A, phenyl substituted			250		1.8–2.1	[17,29]
Poly(carbonate) of bisphenol-A; glass				0.111		[17,50]

TABLE 50.3. *Continued.*

Polymer	$\Delta\alpha$ (A^{**3})	Diluent	Temp (°C)	v2	Stress optical coefficient C (10^9 Pa^{-1})	Reference
Poly(carbonate) of bisphenol-A; melt			200	1.0	3.5	[22]
Poly(cetyl acrylate)	− 141	Decalin				[46]
Poly(cetyl acrylate)	− 164	Toluene				[45]
Poly(cetyl methacrylate)	− 160	Benzene				[56]
Poly(chloroethyl methacrylate); glass					− 0.0056	[17,57]
Poly(chlorohexyliminocarbonyl)	3,000	Carbon tetrachloride				[92]
Poly(chloroprene)	110	α-Bromonaphthalene				[27]
Poly(chloroprene)	33	Carbon tetrachloride				[27]
Poly(chloroprene)	64	Chlorobenzene				[27]
Poly(chloroprene)	39	Dichloromethane				[27]
Poly(chloroprene)	99	α-Methylnaphthalene				[27]
Poly(chloroprene)	46	Tetrachloromethane				[27]
Poly(chloroprene)	67	Toluene				[27]
Poly(chloroprene)	88	p-Xylene				[27]
Poly(cholestryl acrylate)	− 360	Benzene				[47]
Poly(cis-1,4-cyclohexane dimethanol sebacate)	9.15		40	1.0	0.352	[20,111]
Poly(cis-1,4-cyclohexane dimethanol sebacate)	8.76		50	1.0	0.326	[20,111]
Poly(cis-1,4-cyclohexane dimethanol sebacate)	8.5		60	1.0	0.306	[20,111]
Poly(cis-1,4-cyclohexane dimethanol sebacate)	8.37		70	1.0	0.292	[20,111]
Poly(cis-1,4-cyclohexane dimethanol sebacate)	8.28		80	1.0	0.280	[20,111]
Poly(cis-1,4-cyclohexane dimethanol sebacate)	7.5	1,3,5-Triethylbenzene	40	0.336		[20,111]
Poly(cis/trans-1,4-cyclohexane dimethanol-alt-formaldehyde) network; M_n = 4,700 g/mol; trans content = 10%	7.344		70		2.560	[23]
Poly(cis/trans-1,4-cyclohexane dimethanol-alt-formaldehyde) network; M_n = 4,700 g/mol; trans content = 10%	7.300		60		2.626	[23]
Poly(cis/trans-1,4-cyclohexane dimethanol-alt-formaldehyde) network; M_n = 4,700 g/mol; trans content = 10%	7.310		50		2.719	[23]
Poly(cis/trans-1,4-cyclohexane dimethanol-alt-formaldehyde) network; M_n = 4,700 g/mol; trans content = 10%	7.234		40		2.783	[23]
Poly(cis/trans-1,4-cyclohexane dimethanol-alt-formaldehyde) network; M_n = 4,700 g/mol; trans content = 10%	7.238		30		2.884	[23]
Poly(cis/trans-1,4-cyclohexane dimethanol-alt-formaldehyde) network; M_n = 4,700 g/mol; trans content = 10%	7.237		20		2.989	[23]
Poly(cis/trans-1,4-cyclohexane dimethanol-alt-formaldehyde) network; M_n = 4,700 g/mol; trans content = 10%	7.229		10		3.099	[23]
Poly(cis/trans-1,4-cyclohexane dimethanol-alt-formaldehyde) network; M_n = 6,000 g/mol; trans content = 70%	9.978		70		3.414	[23]
Poly(cis/trans-1,4-cyclohexane dimethanol-alt-formaldehyde) network; M_n = 6,000 g/mol; trans content = 70%	9.819		60		5.553	[23]
Poly(cis/trans-1,4-cyclohexane dimethanol-alt-formaldehyde) network; M_n = 6,000 g/mol; trans content = 70%	9.969		50		3.727	[23]
Poly(cis/trans-1,4-cyclohexane dimethanol-alt-formaldehyde) network; M_n = 6,000 g/mol; trans content = 70%	9.849		40		3.8.8	[23]

TABLE 50.3. *Continued.*

Polymer	$\Delta\alpha$ (A^{**3})	Diluent	Temp (°C)	v2	Stress optical coefficient C (10^9 Pa^{-1})	Reference
Poly(*cis/trans*-1,4-cyclohexane dimethanol-*alt*-formaldehyde) network; $M_n = 6{,}000$ g/mol; *trans* content $= 70\%$	9.988		30		3.957	[23]
Poly(*cis/trans*-1,4-cyclohexane dimethanol-*alt*-formaldehyde) network; $M_n = 6{,}000$ g/mol; *trans* content $= 70\%$	9.714		20		4.029	[23]
Poly(*cis/trans*-1,4-cyclohexane dimethanol-*alt*-formaldehyde) network; $M_n = 6{,}000$ g/mol; *trans* content $= 70\%$	9.435		10		4.060	[23]
Poly(*cis/trans*-1,4-cyclohexane dimethanol-*alt*-formaldehyde); fraction of rings in *trans* configuration $= 0.1$	7.24		30			[20,23]
Poly(*cis/trans*-1,4-cyclohexane dimethanol-*alt*-formaldehyde); fraction of rings in *trans* configuration $= 0.7$	9.99		30			[20,23]
Poly(cyclohexyl methacrylate); glass					− 0.059	[17,57]
Poly(decyl acrylate)	− 74	Decalin				[45]
Poly(decyl acrylate)	− 95	Toluene				[45]
Poly(dichlorophenyl-silsesquioxane)	− 4,450	Bromoform				[65]
Poly(dichlorophenyl-silsesquioxane)	− 4,700	Tetrabromoethane				[65]
Poly(diethylene glycol terephthalate)	19.8		70	1.0		[20,111]
Poly(diethylene glycol terephthalate)	26.5	Tricresylphosphate	70	0.58		[20,111]
Poly(diethylene glycol *trans*-1,4-cyclohexane dicarboxylate)	7.4			1.0		[20,111]
Poly(dimethyl siloxane)	0.81		70	1.0		[20,32]
Poly(dimethyl siloxane)	0.68		70	1.0		[20,105]
Poly(dimethyl siloxane)	0.3–0.7		70	1.0		[20,108]
Poly(dimethyl siloxane)	0.51	Decalin	70	0.25		[20,32]
Poly(dimethyl siloxane)	0.38	Cyclohexane	70	0.16		[20,32]
Poly(dimethyl siloxane)	0.18	Carbon tetrachloride	70	0.16		[20,32]
Poly(dimethyl siloxane)	0.15–0.20	Carbon tetrachloride	70	0.35–0.71		[20,109]
Poly(dimethyl siloxane)			20–190		0.135–0.260	[17,29]
Poly(dimethyl sil-methylene)	4.27		50	1.0		[20,110]
Poly(dimethyl sil-methylene)	2.5	1,3,5-Triethylbenzene	50			[20,110]
Poly(diphenylpropylene)	80	Bromoform				[39]
Poly(epsilon, *N*-carbobenzoxy-L-lysine) helix	3,600	Dimethylformamide				[93]
Poly(ethyl acrylate)	3.0	Benzene				[48]
Poly(ethyl acrylate)	10	Bromobenzene				[48]
Poly(ethyl acrylate)	− 37	Bromoform				[48]
Poly(ethyl acrylate)	− 14	Dibromoethane				[48]
Poly(ethyl acrylate)	− 11	Dimethylformamide				[48]
Poly(ethyl acrylate); fraction of *meso* dyads, Wm $= 0.3$	− 0.82		50	1.0		[20,49]
Poly(ethylene)	60	Tetralin, xylene				[31]
Poly(ethylene)	30	Decalin				[31]
Poly(ethylene)	7.8		150	1.0		[20,35]
Poly(ethylene)	8.4		150	1.0		[20,34]
Poly(ethylene)	6.5	*n*-C22H$_{46}$	150	0.41		[20,32]
Poly(ethylene)	5.1	*n*-C12H$_{26}$	150	0.44		[20,32]
Poly(ethylene)	40	Decalin	150	0.33		[20,32]
Poly(ethylene)	3.9–4.0	Decalin	150	0.33		[20,33]
Poly(ethylene), cross-linked			130–180		1.5–2.2	[17,29]
Poly(ethylene), linear melt			150–190		1.8–2.4	[17,29]
Poly(gamma-benzyl-L-glutamate) coil	230	Dichloroacetic acid				[65]

TABLE 50.3. *Continued.*

Polymer	$\Delta\alpha$ (A^{**3})	Diluent	Temp (°C)	v2	Stress optical coefficient C (10^9 Pa^{-1})	Reference
Poly(gamma-benzyl-L-glutamate) helix	25,000	Dichloroethane				[65]
Poly(glycol methacrylate)	1.0	Dimethylformamide				[58]
Poly(glycol methacrylate)	− 6.0	Ethyl alcohol				[58]
Poly(glycol methacrylate)	− 6.0	Water				[58]
Poly(hexyl methacrylate)	− 40	Benzene				[59]
Poly(hexyl methacrylate)	− 9.7	Carbon tetrachloride				[59]
Poly(hydrazocarbonyl-1,4-phenylene-iminoterephthaloyl)	3,630	Dimethylsulfoxide				[65]
Poly(imino-1,3-phenyleneimino-sophthaloyl)	360	Sulfuric acid				[65]
Poly(imino-1,4-phenyleneimino-terephthaloyl)	5,250	Sulfuric acid				[65]
Poly(imino-1,4-terephthaloylimino-1, 4-phenylenediphenylmethyl-1,4-phenylene)	130	Sulfuric acid				[65]
Poly(iminocarbonyl,1,4-phenylene)	10,500	Sulfuric acid				[65]
Poly(iminocarbonyl-cyclohexylene)	390	Sulfuric acid				[65]
Poly(isobutene)	45–59	Tetrachloroethylene, *m*-Xylene				[27]
Poly(isobutene)	35	Carbon tetrachloride				[27]
Poly(isobutene)	30	Decalin				[31]
Poly(isobutene)	69	*p*-Xylene				[27]
Poly(isobutylene)	4.10		30	1.0		[20,37]
Poly(isobutylene)	3.5		30	1.0		[20,38]
Poly(isobutylene)	3.36	Carbon tetrachloride	30	0.16		[20,37]
Poly(isobutylene)	3.79	Cyclohexane	30	0.17		[20,37]
Poly(isobutylene)	2.84	Bromotrichloromethane	30	0.19		[20,37]
Poly(isobutylene) Vistanex B-100		Decalin	25	0.03	1.7	[36]
Poly(isobutylphenyl-silsesquioxane) (1:1)	− 840	Benzene				[65]
Poly(isohexylphenyl-silsesquioxane) (1:1)	− 980	Benzene				[65]
Poly(isoprene) *cis*	48	Benzene				[25]
Poly(isoprene) *cis*	53.1	Squalene				[28]
Poly(isoprene) *trans*	49	Benzene				[25]
Poly(isoprene); melt			22		1.9	[17,26]
Poly(isoprene); natural rubber (cross-linked)			20–100		1.80–2.05	[17,29]
Poly(isoprene); *trans*, gutta percha (cross-linked)			85–250		3.0	[17,29]
Poly(L-glutamic acid) coil	136	Phosphate buffer, 0.1 M, pH = 12.5				[93]
Poly(L-glutamic acid) helix	1,900	Phosphate buffer, 0.1 M, pH = 4.2				[93]
Poly(*m,p*-aromatic ester) *m/p* = 1/3	750	Dichloroacetic acid				[91]
Poly(*m*-chlorophenyl-silsesquioxane)	− 4,700	Carbon tetrachloride				[65]
Poly(methacrylic acid)	50	Methanol				[61]
Poly(methacrylic acid)	150	0.002 M HCl				[61]
Poly(methacrylic acid), sodium salt	150	0.012 M NaCl, pH = 7				[61]
Poly(methacrylic acid), sodium salt	400	0.0012 M NaCl, pH = 7				[61]
Poly(methacrylic acid), sodium salt	56–300	Water				[62]
Poly(methyl acrylate)	17	Benzene				[44]
Poly(methyl acrylate)	16	Toluene				[45]
Poly(methyl acrylate)	26	Toluene				[44]
Poly(methyl acrylate); fraction of *meso* dyads, Wm = 0.3	− 0.34			50	1.0	[20,49]
Poly(methyl acrylate); fraction of *meso* dyads, Wm = 0.5	− 0.84			50	1.0	[20]
Poly(methyl methacrylate) atactic	2.0	Benzene				[63]

TABLE 50.3. *Continued.*

Polymer	$\Delta\alpha$ (A^{**3})	Diluent	Temp (°C)	v 2	Stress optical coefficient C $(10^9\ Pa^{-1})$	Reference
Poly(methyl methacrylate) isotactic	25	Benzene				[63]
Poly(methyl methacrylate), glass					(-0.0033) – (0.0045)	[17,50]
Poly(methyl phenyl siloxane); fraction of *meso* dyads, Wm = 0.5	− 12.1		25	1.000		[20,113]
Poly(methyl phenyl siloxane); fraction of *meso* dyads, Wm = 0.5	− 11.5	Decalin	25	0.673		[20,113]
Poly(methyl phenyl siloxane); fraction of *meso* dyads, Wm = 0.5	− 9.12	Decalin	25	0.488		[20,113]
Poly(methyl phenyl siloxane); fraction of *meso* dyads, Wm = 0.5	− 8.32	Decalin	25	0.350		[20,113]
Poly(methyl phenyl siloxane); fraction of *meso* dyads, Wm = 0.5	− 8.10	Decalin	25	0.211		[20,113]
Poly(methyl phenyl siloxane); fraction of *meso* dyads, Wm = 0.5	− 8.50	Decalin	25	0.204		[20,113]
Poly(N,N-piperazindiyl-2,5-diketo-1,3-pyrrolidindiylhexamethylene-2,5-diketo-1,3-pyrrolidindiyl)	56	Benzyl alcohol				[98]
Poly(N,N-piperazindiyl-2,5-diketo-1,3-pyrrolidindiylhexamethylene-2,5-diketo- 1,3-pyrrolidindiyl)	30	Bromoform/cyclohexanol, 60/40				[98]
Poly(N-2,4-dimethylphenylmaleimide)	− 200	Bromoform				[65]
Poly(n-butyl acrylate)	− 11	Benzene				[44]
Poly(n-butyl acrylate)	− 17.8	Decalin				[45]
Poly(n-butyl acrylate)	− 10.1	Toluene				[45]
Poly(n-butyl acrylate)	− 6.5	Toluene				[44]
Poly(n-butyl methacrylate) atactic	− 14	Benzene				[51]
Poly(n-butyl methacrylate) isotactic	− 2.0	Benzene				[52]
Poly(n-butyliminocarbonyl) a.k.a. poly(butyl isocyanate)	4,100	Carbon tetrachloride				[65,107]
Poly(n-butyliminocarbonyl) a.k.a. poly(butyl isocryanate)	800	Pentafluorophenol 0.9/0.1				[65]
Poly(N-isobutylmaleimide)	160	Chlorobenzene				[65]
Poly(N-methylcitraconimide)	150	Bromoform				[97]
Poly(N-phenylmathacrylamide)	− 103	o-Toluidine				[69]
Poly(n-tolyliminocarbonyl)	− 39	Bromoform				[65]
Poly(ocatdecyl acrylate)	− 190	Decalin				[45]
Poly(ocatdecyl acrylate)	− 232	Toluene				[45]
Poly(octyl acrylate)	− 57.4	Decalin				[45]
Poly(octyl acrylate)	− 47.9	Toluene				[45]
Poly(octyl acrylate; fraction of *meso* dyads, Wm = 0.3)	− 1.1		50	1.0		[20,49]
Poly(octyl methacrylate)	− 47	Benzene				[59]
Poly(octyl methacrylate)	− 12.5	Carbon tetrachloride				[59]
Poly(oxadiazole-2,5-diyl-1,4-phenylene)	1,750	Sulfuric acid				[65,112]
Poly(oxycarbonyloxy-1,4-phenylenecyclcohexylidene-1,4-phenylene)	− 114	Bromoform				[88]
Poly(oxydecamethyleneoxycarbonyl-phenyleneoxyterephthaloyloxy phenylenecarbonyl)	200	Dichloroacetic acid				[90]
Poly(oxydimethysilyene)	4.7	Petroleum ether				[94]
Poly(oxyethyleneoxyterephthaloyl)	70	Dichloroethane/phenol 1/1				[89]
Poly(oxyethyleneoxyterephthaloyl)	48.7	Dichloroacetic acid				[90]

TABLE 50.3. *Continued.*

Polymer	$\Delta\alpha$ (A^{**3})	Diluent	Temp (°C)	v2	Stress optical coefficient C (10^9 Pa^{-1})	Reference
Poly(oxyhexamethyleneoxycarbonylphenylene-oxyterephthaloyloxyphenylenecarbonyl)	250	Dichloroacetic acid				[90]
Poly(oxymethylphenylsilylene) (50–62.5)/(50–37.5)	− 36	Decalin				[95]
Poly(oxymethylphenylsilylene) 50/50	− 36	Decalin				[95]
Poly(oxymethylphenylsilylene) 75/25	− 13.6	Benzene				[96]
Poly(oxymethylphenylsilylene) 75/25 1	− 2	Decalin				[95]
Poly(oxymethylphenylsilylene) 87.5/12.5	− 10	Decalin				[95]
Poly(oxymethylphenylsilylene) 90/10	− 2.3	Petroleum ether				[94]
Poly(oxymethylphenylsilylene) atactic	− 25.5	Benzene				[96]
Poly(oxymethylphenylsilylene) atactic	− 82	Decalin, tetralin				[95]
Poly(oxymethylphenylsilylene) isotactic	− 82	Decalin, tetralin				[95]
Poly(oxyphenysilylene)	− 85	Benzene				[96]
Poly(oxypropylene)	− 18	Cyclohexane				[86]
Poly(oxypropylene); $M_c = 2,000$	4.66±0.04		25	1.0		[20,87]
Poly(oxypropylene); $M_c = 3,000$	4.33±0.09		25	1.0		[20,87]
Poly(oxypropylene); $M_c = 3,000$	3.05	Decalin	25			[20,87]
Poly(oxypropylene); $M_c = 3,000$	3.87	POP oligomers	25			[20,87]
Poly(oxytetramethyleneoxy-carbonylphenylene-oxyterephthaloylo-xyphenyleneoxycarbonyl)	280	Dichloroacetic acid				[90]
Poly(p-carboxyphenyl methacrylate)	180	Dioxane				[55]
Poly(p-carboxyphenyl methacrylate)	370	0.1 M NaCl				[55]
Poly(p-carbethoxy-N-phenylmethacrylamide)	− 230	o-Toluidine				[54]
Poly(p-chloro-N-phenylmethacrylamide)	− 160.0	o-Toluidine				[54]
Poly(p-chlorostyrene)	− 230	Bromoform				[67]
Poly(p-chlorostyrene); glass					0.024	[17,68]
Poly(p-methylcarboxy–phenyl methacrylate)	− 77	Dibromoethane				[55]
Poly(p-methylstyrene) atactic	− 147	Bromoform				[71]
Poly(p-methylstyrene) isotactic	− 140	Bromoform				[71]
Poly(p-t-butyl styrene); glass				0.011		[17,68]
Poly(p-t-butylphenyl methacrylate)	− 90	Bromobenzene				[53]
Poly(p-tolymaleiimide)	− 160	Bromoform				[99]
Poly(phenyl methacrylate)	− 10.5	Bromobenzene				[64]
Poly(phenyl methacrylate); glass					0.040	[17,57]
Poly(phenyl-silsesquioxane)	(− 1,060)–(− 1,800)	Bromoform				[65]
Poly(propylene)	0.3					[20,41]
Poly(propylene) atactic	45	Benzene, xylene				[31]
Poly(propylene) atactic	30	Carbon tetrachloride				[40]
Poly(propylene) atactic	30	Decalin				[31]
Poly(propylene) atactic	55	Toluene				[30]
Poly(propylene) isotactic	30	Carbon tetrachloride				[31]
Poly(propylene); isotactic (melt)			210		0.9	[17,29]
Poly(propylene); M.W. = 43,000–48,000			210		0.9	[19,36]
Poly(S-carbobenzoxymethyl-L-cystein)	22	Dichloroacetic acid				[93]
Poly(styrene)	− 1.7					[20,41]
Poly(styrene)					(− 4.1)–5.2	[17,29]
Poly(styrene) atactic	− 145	Bromoform				[67]
Poly(styrene) isotactic	− 224	Bromoform				[76]
Poly(styrene); atactic, M.W. = 9,000,000		Bromoform	25	0.01	− 6.9	[19,36]
Poly(styrene); glass					0.010	[17,50]

TABLE 50.3. *Continued.*

Polymer	$\Delta\alpha$ (A^{**3})	Diluent	Temp (°C)	v2	Stress optical coefficient C (10^9 Pa^{-1})	Reference
Poly(styrene); M.W. = 50,000–860,000			153–215	1.0	(− 4)–(− 5)	[19,36]
Poly(t-butyl methacrylate) atactic	2.1	Benzene				[44]
Poly(t-butyl methacrylate) isotactic	19.3	Benzene				[44]
Poly(triethylene glycol terephthalate)	13.3		1.0			[20,111]
Poly(vinyl acetate)	− 20	Acetone				[77]
Poly(vinyl acetate)	4.0–5.9	Benzene				[27]
Poly(vinyl acetate)	9.4	Bromobenzene				[78]
Poly(vinyl acetate)	− 20	Bromoform				[77]
Poly(vinyl acetate)	− 16	Carbon tetrachloride				[27]
Poly(vinyl acetate)	− 26	Carbon tetrachloride				[79]
Poly(vinyl acetate)	14	Chlorobenzene				[27]
Poly(vinyl acetate)	− 34.9	Chloroform				[79]
Poly(vinyl acetate)	− 24	Chloroform				[27]
Poly(vinyl acetate)	− 23	Cyclohexane				[27]
Poly(vinyl acetate)	− 36	Dichloroethane				[27]
Poly(vinyl acetate)	− 39	Dichloroethane				[27]
Poly(vinyl acetate)	− 25	Tetrabromoethane				[27]
Poly(vinyl acetate)	− 33	Tetrabromoethane				[77]
Poly(vinyl acetate)	10	Toluene				[27]
Poly(vinyl acetate)	13.5	Toluene				[44]
Poly(vinyl acetate)	19	Toluene				[79]
Poly(vinyl acetate)	2.0	o-Xylene				[27]
Poly(vinyl acetate)	81	Chloroform				[27]
Poly(vinyl acetate)	− 2.68		50	1.0		[20,80]
Poly(vinyl acetate)	− 1.90	1,3,5-Triethylbenzene	50	0.6		[20,80]
Poly(vinyl butyral)	173	Toluene–phenol, 79–21				[27]
Poly(vinyl butyral)	− 80	Benzene				[27]
Poly(vinyl butyrate)	− 36	Carbon tetrachloride				[27]
Poly(vinyl butyrate)	− 48	Chloroform				[27]
Poly(vinyl butyrate)	40	Tetrahydrofuran				[81]
Poly(vinyl chloride)	− 420	Bromoform				[82]
Poly(vinyl chloride)					− 0.5	[17,29]
Poly(vinyl chloride); M.W. = 14,000			210	1.0	− 0.5	[19,36]
Poly(vinyl cinnamate)	− 430	Tetrabromoethane				[64]
Poly(vinyl propionate)	− 31	Carbon tetrachloride				[27]
Poly(vinyl propionate)	− 40	Chloroform				[27]
Poly(vinyl propionate)	1.3	Toluene				[27]
Poly(vinyl stearate)	− 130	Carbon tetrachloride				[84]
Poly(vinyl toluene); glass					0.015	[17,68]
Poly(vinylpyrrolidone)	− 75	Benzyl alcohol				[64]
Poly([1,3,5,7-tetraoxo-2,3,6,7-tetrahydro-1H, 5H-benzo-(1,2-c:4,5-c′) dipyrrol- 2,6-diyl]-1,4-phenylene)	250–440	Sulfuric acid				[65]
Poly[(2,2′-diphenyl(6,6′-biquinoxaline)-3,3′-diyl)(1,1′-biphenyl)-4,4′-diyl]	175	Tetrachloroethane, chloroform				[65]
Poly[(3-β)-cholest-5-en-3-ol-2-propenoate]	− 300	Benzene				[65]
Poly[(ar,ar′-diphenyl(biquinoxaline)-ar, ar′-diyl]-1, 4-phenyleneoxy (1,1′-biphenyl)- 4,4′diyloxy-1,4-phenylene)	106	Tetrachloroethane, chloroform				[65]
Poly[(imino-4,6-dicarboxyisophthaloylimino) biphenyl-4-4′-diyl]	75	Dimethylacetamide				[65]

TABLE 50.3. *Continued.*

Polymer	$\Delta\alpha$ (A**^{3})	Diluent	Temp (°C)	v2	Stress optical coefficient C (10^9 Pa^{-1})	Reference
Poly[(phenylquinoxalinediyl) oxy (phenylquixalinediyl)-1, 4-phenyleneoxy (1,1′-biphenyl)-4,4′-diyloxy-1,4-phenylene]	65	Tetrachloroethane, chloroform				[65]
Poly[imino(1-oxohexamethylene)] a.k.a. [Poly(epsilon-caprolactam)]	63	Sulfuric acid				[65]
Poly[imino-1,4-phenyleneimino-(4,6-dicarboxy-isophthaloylimino)−1,4, phenylene-terephthaloyl]	88	Dimethylacetamide				[65]
Sulfate cellulose, sodium salt D.S. = 0.4	634	Aqueous NaCl 0.2 M				[65]
Sulfate cellulose, sodium salt D.S. = 0.4	645	Aqueous NaCl 0.15 M				[65]
Sulfate cellulose, sodium salt D.S. = 0.4	680	Aqueous NaCl 0.10 M				[65]
Sulfate cellulose, sodium salt D.S. = 0.4	980	Aqueous NaCl 0.01 M				[65]
Sulfate cellulose, sodium salt D.S. = 0.4	1,300	Aqueous NaCl 0.005 M				[65]
Sulfate cellulose, sodium salt D.S. = 0.4	1,750	Aqueous NaCl 0.001 M				[65]

TABLE 50.4. *Optical configuration parameters of copolymers. All values reported are at a wavelength of 6,328 Å.*

Copolymer	$\Delta\alpha$(A^3)	Diluent	Reference
Poly(methyl methacrylate-*co*-*p*-*tert*-butylphenyl methacrylate) 25/75 mol %	− 44	Chlorobenzene	[5]
Poly(methyl methacrylate-*co*-*p*-*tert*-butylphenyl methacrylate) 50/50 mol %	− 30.4	Chlorobenzene	[5]
Poly(methyl methacrylate-*co*-*p*-*tert*-butylphenyl methacrylate) 80/20 mol %	− 7.4	Chlorobenzene	[5]
Poly(methyl methacrylate-*co*-*p*-*tert*-butylphenyl methacrylate) 91/9 mol %	1.5	Chlorobenzene	[5]
Poly(methyl methacrylate-*graft*-styrene) (70–90)/(30–10) mol %	100–1,100	Bromoform	[39]
Poly(methyl methacrylate-*graft*-styrene) 10/90 mol %	700–7,000	Bromoform	[114]
Poly(methyl methacrylate-*graft*-styrene) 87/13 mol %	30	Bromoform	[115]
Poly(*n*-butyl methacrylate-*graft*-styrene) 8/92 mol %	1,190	Bromoform	[115]
Poly[*p*-(4-cetoxybenzoxy)-phenyl methacrylate-*co*-cetyl methacrylate] 15/85 mol %	− 277	Carbon tetrachloride	[116]
Poly[*p*-(4-cetoxybenzoxy)-phenyl methacrylate-*co*-cetyl methacrylate] 22/78 mol %	− 400	Carbon tetrachloride	[116]
Poly[*p*-(4-cetoxybenzoxy)-phenyl methacrylate-*co*-cetyl methacrylate] 39/41 mol %	− 540	Carbon tetrachloride	[116]
Poly[*p*-(4-cetoxybenzoxy)-phenyl methacrylate-*co*-cetyl methacrylate] 4/96 mol %	− 16	Carbon tetrachloride	[116]
Poly[*p*-(4-cetoxybenzoxy)-phenyl methacrylate-*co*-cetyl methacrylate] 60/40 mol %	− 920	Carbon tetrachloride	[116]
Poly[*p*-(4-cetoxybenzoxy)-phenyl methacrylate-*co*-cetyl methacrylate] 8/92 mol %	− 180	Carbon tetrachloride	[116]
Poly[*p*-(4-cetoxybenzoxy)-phenyl methacrylate-*co*-cetyl methacrylate] 81/19 mol %	− 2,000	Carbon tetrachloride	[116]
Poly(phenylbutyl isocyanate-*co*-choral) 50/50 mol %	12	Carbon tetrachloride	[92]
Poly(propylene-*graft*-atactic styrene) 30/70 mol %	22	Chlorobenzene	[117]
Poly(styrene-*block*-propylene), atactic, 64/36 mol %	− 8	Chlorobenzene	[118]

TABLE 50.4. *Continued.*

Copolymer	$\Delta\alpha(A^3)$	Diluent	Reference
Poly(styrene-*co*-chlorostyrene) 39.5/60.5 mol %	− 226	Bromoform	[119]
Poly(styrene-*co*-chlorostyrene) 55/45 mol %	− 202	Bromoform	[119]
Poly(styrene-*co*-chlorostyrene) 68.7/31.3 mol %	− 198	Bromoform	[119]
Poly(styrene-*co*-chlorostyrene) 83.2/16.8 mol %	− 172	Bromoform	[119]
Poly(styrene-*co*-chlorostyrene) 89.7/10.3 mol %	− 165	Bromoform	[119]
Poly(styrene-*co*-methyl methacrylate) 30/70 mol %	− 34	Chlorobenzene	[120]
Poly(styrene-*co*-methyl methacrylate) 50/50 mol %	− 68	Bromobenzene	[120]
Poly(styrene-*co*-methyl methacrylate) 70/30 mol %	− 88	Bromobenzene	[120]
Poly(styrene-*co*-*N*-methylcitraconimide) 48/52 mol %	− 34	Bromoform	[97]
Poly(styrene-*co*-*N*-methylcitraconimide) 54/46 mol %	− 26	Bromoform	[97]
Poly(*tert*-butyl methacrylate-*graft*-styrene) 8/92 mol %	540	Bromoform	[121]
Poly(vinyl chloride-*graft*-styrene) 12.1/87.9 wt%	155	Benzene	[81]
Poly(vinyl chloride-*graft*-styrene) 30.7/69.3 wt%	110	Benzene	[81]
Poly(vinyl chloride-*graft*-styrene) 5.2/94.8 wt%	330	Benzene	[81]
Poly(vinyl chloride-*graft*-styrene) 5.6/94.4 wt%	180	Benzene	[81]
Poly[(imino-1,4-phenyleneimino-terephthaloyl)-*co*-(iminocarbonyl-1,4-phenylene)] (ratio 1/9)	4,380	Sulfuric acid	[65]
Poly{[(4-(hexadecyloxy)-benzoic acid-4-[(2-methyl-1-oxo-2-propenyl)oxy]phenyl ester)]-*co*-cetylmethacrylate} 50/50 mol %	− 680	Carbon tetrachloride	[65]
Poly{[(4-(hexadecyloxy)-benzoic acid-4-[(2-methyl-1-oxo-2-propenyl)oxy]phenyl ester)]-*co*-cetyl methacrylate}-70/30 mol %	− 1,050	Carbon tetrachloride	[65]

REFERENCES

1. D. V. Rosato, *Plastics Encyclopedia and Dictionary*, Hanser, New York, 1993, p. 781.
2. Nunez, Nunez, and Mann eds. *CenBASE/Materials in Print*, Wiley, New York, 1990.
3. J. F. Shackelford and W. Alexander, eds. *CRC Materials Science and Engineering Handbook*, CRC, Boca Raton, 1992, p. 776.
4. H. F. Mark, N. G. Gaylord, and N. M. Bikales, eds. *Encyclopedia of Polymer Science and Technology: Plastics, Resins, Rubbers, Fibers*, Interscience, New York, 1964.
5. J. Brandrup and E. H. Immergut, eds. *Polymer Handbook*, 3rd ed. Wiley, New York, 1989, pp. 451–461.
6. C. L. Mantell, ed. *Engineering Materials Handbook* (McGraw-Hill, New York, 1958), Sec. 33.
7. S. H. Goodman, *Handbook of Thermoset Plastics*, Noyes Park Ridge, NJ, 1986, p. 281.
8. J. Bicerano, *Prediction of Polymer Properties*, Dekker, New York, 1993, pp. 179–197.
9. *Janssen Chimica Catalog*, Janssen, Belgium, 1990.
10. *Aldrich Catalog*, Aldrich Chemical, Milwaukee, WI, 1990.
11. R. Anderson, G. L. Larson, and C. Smith, eds., *Huls Silicon Compounds Register and Review*, Huls, Piscataway, N.J., 1991.
12. C.A. Harper, ed. *Handbook of Plastics and Elastomers*, McGraw-Hill, New York, 1975.
13. C. T. Lynch, ed., *CRC Handbook of Materials Science*, CRC Press, Boca Raton, FL, 1975, Vol. 3.
14. G. M. Kline, *Analytical Chemistry of Polymers*, Interscience, New York, 1962, Part III.
15. E. I. duPont de Nemours and Co., Kapton, Summary of Property Report No. E-50533, 1982.
16. E. I. duPont de Nemours and Co., Preliminary Process Bulletin No. PC-1.
17. D. W. van Krevelen, *Properties of Polymers*, 2nd ed. Elsevier, Amsterdam, 1976.
18. *Engineering Plastics*, Vol.2 of *Engineering Materials Handbook*, ASM International, Metals Park, OH, 1988.
19. G. Allen and J. C. Bevington, *Comprehensive Polymer Science*, Pergamon, Oxford, 1989, p. 639.
20. E. Riande and E. Saiz, *Dipole Moments and Birefringence of Polymers*, Prentice-Hall, New Jersey, 1992, pp. 288–289.
21. E. Saiz, M. P. Tarazona, E. Riande, J. J. Guzman, Polym. Sci. Polym. Phys. Ed. **22**, 2165, 1984.
22. R. Wimberger-Friedl, Rheol. Acta **30**, 329, 1991.
23. E. Riande, J. Guzman, E. Saiz, and M. P. Tarazona, J. Polym. Sci., Polym. Phys. Ed., **23**, 1031, 1985.
24. M. Fukuda, G. L. Wilkes, and R. S. Stein, J. Polym. Sci. A **2**, 1417, 1971.
25. I. Ja. Poddubnyi, E. G. Erenburg, and M. A. Eryomina, Vysokomol. Soedin. **10A**, 1381, 1968.
26. G. V. Vinogradov, A. I. Isayev, D. A. Mustafaev, Y. Y. Podolosky, J. Appl. Polym. Sci. **22**, 665, 1978.
27. E. V. Frisman and A. K. Dadivanyan, J. Polym. Sci. C **16**, 1001, 1967.
28. H. Wilski, Kolloid Z. Z. Polym. **238**, 426, 1970.
29. H. Janeschitz-Kriegl, *Integration of Fundamental Polymer Science and Technology—2*, edited by P. J. Lemstra and L. A. Kleintjens Elsevier Applied Science London, 1988, pp. 405–409.
30. W. Philippoff and E. G. M. Tornqvist, J. Polym. Sci. C **N23**, 881, 1968.
31. T. I. Garmonova, Leningrad Univ. Vestnik, Ser. Fiz. Khim. **22**, 72, 1962.
32. M. H. Liberman, Y. Abe, and P. J. Flory, Macromolecules, **5**, 550, 1972.
33. A. N. Gent and V. V. Vickroy, Jr., J. Polym. Sci. A **2**, 47, 1967.
34. D. W. Saunders, D. R. Lightfoot, and D. A. Parsons, J. Polym. Sci. A **2**, 1183, 1968.
35. A. N. Gent and T. H. Kaun, J. Polym. Sci. A **2**, 927, 1971.
36. H. Janeschitz-Kriegl, *Polymer Melt Rheology and Flow Birefringence*, Springer, Berlin, 1983.
37. M. H. Liberman, L. C. DeBolt, and P. J. Flory, J. Polym. Sci. Polym. Phys. Ed. **12**, 187, 1974.
38. R. S. Stein, F. H. Holmes, and A. V. Tobolsky, J. Polym. Sci. **14**, 443, 1954.
39. P. Gramain, J. Leray, and H. Benoit, J. Polym. Sci. C **16**, 3983, 1968.

40. V. N. Tsvetkov, O. V. Kallistov, E. V. Korneeva, and I. K. Nekrasov, Vysokomol. Soedin. **5**, 1538, 1963.
41. Y. Abe, A. E. Tonelli, and P. J. Flory, Macromolecules **3**, 294, 1970.
42. V. N. Tsvetkov, S. Ya. Ljubina, and T. V. Barskaya, Vysokomol. Soedin. **6**, 806, 1964.
43. W. Kuhn, H. Oswald, and H. Kuhn, Helv. Chim. Acta **36**, 1209, 1953.
44. V. N. Tsvetkov, N. N. Boitsova, and M. G. Vitovskaja, Vysokomol. Soedin. **6**, 297, 1964.
45. V. N. Tsvetkov, L. N. Andreeva, E. V. Korneeva, and P. N. Lavrenko, Dokl. Akad. Nauk. SSSR **205**, 895, 1972.
46. V. N. Tsvetkov, L. N. Andreeva, E. V. Korneeva, P. N. Lavrenkov, N. A. Plate, V. P. Shibaev, and B. S. Petrukhin, Vysokomol. Soedin. **13A**, 2226, 1971.
47. V. N. Tsvetkov, E. V. Korneeva, I. N. Shtennikova, P. N. Lavrenko, G. F. Kolbina, D. Hardi, and K. Nitrai, Vysokomol. Soedin. **14A**, 427, 1972.
48. A. E. Grishchenko and E. P. Vorobjeva, Vysokomol. Soedin. **15A**, 895, 1973.
49. M. Ilavsky, E. Saiz, and E. Riande, J. Polym. Sci. Polym. Phys. Ed. **27**, 743, 1989.
50. A. A. Askadskii, Pure Appl. Chem. **46**, 19, 1976.
51. V. N. Tsvetkov and S. Ja. Ljubina, Vysokomol. Soedin. **1**, 577, 1959.
52. V. N. Tsvetkov, M. G. Vitovskaja, and S. Ja. Ljubina, Vysokomol. Soedin. **4**, 577, 1962.
53. V. N. Tsvetkov and I. N. Shtennikova, Zh. Tekh. Fiz. **29**, 885, 1959.
54. V. N. Tsvetkov and V. E. Bychokova, Vysokomol. Soedin. **6**, 600, 1964.
55. E. N. Zakharova, P. N. Lavrenko, G. A. Formin, and I. I. Konstanti-nov, Vysokomol. Soedin. **13A**, 1870, 1971.
56. V. N. Tsvetkov, D. Hardi, I. N. Shtennikova, E. V. Korneeva, G. F. Pirogova, and K. Nitral, Vysokomol. Soedin. **11A**, 329, 1969.
57. J. F. Rudd and R. A. Andrews, J. Appl. Phys. **29**, 1421, 1958; **31**, 818, 1960.
58. A. E. Grishchenko and R. I. Esrielev, Vysokomol. Soedin **14A**, 521, 1972.
59. A. E. Grishchenko, M. G. Vitovskaja, V. N. Svetkov, and L. N. Andreeva, Vysokomol. Soedin. **8**, 800, 1966.
60. V. N. Tsvetkov, S. Ya. Ljubina, and K. L. Boleskii, Vysokomol. Soedin. Sb. Karbotsepnie, Soedin. **4**, 26, 1963.
61. V. N. Tsvetkov, S. Ya. Ljubina, and K. L. Boleskii, Vysokomol. Soedin. Sb. Karbotsepnie, Soedin. **4**, 33, 1963.
62. W. Kuhn, O. Kuenzle, and A. Katchalsky, Helv. Chim. Acta **31**, 1994, 1948.
63. V. N. Tsvetkov and N. N. Boitsova, Vysokomol. Soedin. **2**, 1176, 1960.
64. V. N. Tsvetkov, V. E. Eskin, and S. Ya. Frenkel, *Structure of Macro-molecules in Solutions*, Nauka, Moskow, 1964.
65. V. N. Tsvetkov, *Rigid-Chain Polymer Molecules*, Nauka, Moskow-Leningrad, 1985.
66. V. N. Tsvetkov, I. N. Shtennikova, E. I. Rjumtsev, G. F. Kolbina, I. I. Konstantinov, Ju. B. Amerik, and B. A. Krentsel, Vysokomol. Soe-din. **11A**, 2528, 1969.
67. E. V. Frisman, A. M. Martsinivsky, and N. A. Domnitcheva, Vyso-komol. Soedin. **2**, 1148, 1960.
68. H. Lamble and E. S. Dahmouch, Br. J. Appl. Phys. **9**, 388, 1958.
69. V. N. Tsvetkov, V. E. Bychokova, S. M. Savvon, and I. K. Nekrasov, Vysokomol. Soedin. **1**, 1407, 1959.
70. L. N. Andreeva, E. V. Beliaeva, A. A. Boikov, P. N. Lavrenko, and V. N. Tsvetkov, Vysokomol. Soedin. **25A**, 1631, 1983.
71. V. N. Tsvetkov and N. N. Boitsova, Vysokomol. Soedin. **5**, 1263, 1963.
72. V. N. Tsvetkov, S. Ya. Ljubina, V. E. Bychkova, and I. A. Strelina, Vysokomol. Soedin. **8**, 846, 1966.
73. I. N. Shtennikova, E. V. Korneeva, V. E. Bychokova, I. A. Strelina, and G. S. Sogomonyants, Vysokomol. Soedin. **14B**, 118, 1972.
74. S. Ja. Ljubina, I. A. Strelina, G. S. Sogomonyants, S. I. Dmitrieva, O. Z. Korotkina, G. V. Tarasova, V. S. Skazka, and V. M. Jamshchi-kov, Vysokomol. Soedin **12A**, 1560, 1970.
75. S. Ya. Lyubina, I. A. Strelina, V. S. Skazka, G. V. Tarasova, and V. M. Jamshchikov, Vysokomol. Soedin. **14A**, 1371, 1972.
76. V. N. Tsvetkov and S. Ja. Magarik, Dokl. Akad. Nauk SSSR **127**, 840, 1959.
77. E. V. Frisman and A. B. Chzu, Vysokomol. Soedin. **4**, 1564, 1962.
78. V. N. Tsvetkov, A. E. Grishchenko, L. E. De-Millo, and E. N. Rostovskii, Vysokomol. Soedin. **6**, 384, 1964.
79. E. V. Frisman and V. A. Andreichenko, Vysokomol. Soedin. **4**, 1559, 1962.
80. E. Riande, E. Saiz, and J. E. Mark, J. Polym. Sci. Polym. Phys. Ed. **22**, 863, 1984.
81. S. P. Micengendler, K. I. Sokolova, G. A. Andreeva, A. A. Korotkov, T. Kadirov, S. I. Klenin, and S. Ja. Magarik, Vysokomol. Soedin. **9A**, 1133, 1967.
82. V. N. Tsvetkov, E. N. Zakharova, G. A. Fomin, and P. N. Lavrenko, Vysokomol. Soedin. **14A**, 1956, 1972.
83. V. N. Tsvetkov, M. G. Vitovskaja, P. N. Lavrenko, E. N. Zakharova, I. F. Gavrilenko, and N. N. Stefanovskaja, Vysokomol. Soedin. **13A**, 2532, 1971.
84. V. S. Skazka, G. A. Fomin, G. V. Tarasova, I. G. Kirillova, V. M. Jamshchikov, A. E. Gryshchenko, and I. A. Alekseeva, Vysokomol. Soedin. **15A**, 2561, 1973.
85. V. N. Tsvetkov and S. Ja. Magarik, Dokl. Acad. Nauk. SSSR **115**, 911, 1957.
86. V. N. Tsvetkov, T. I. Garmonova, and R. P. Stankevitch, Vysokomol. Soedin. **8**, 980, 1966.
87. A. L. Andrady, M. A. Llorente, and E. Saiz, J. Polym. Sci. Polym. Phys. Ed. **25**, 1935, 1987.
88. T. I. Garmonova, M. G. Vitovskaja, P. N. Lavrenko, V. N. Tsvetkov, and E. V. Korovina, Vysokomol. Soedin. **13**, 884, 1971.
89. S. M. Savvon and K. K. Turoverov, Vysokomol. Soedin. **6**, 205, 1964.
90. V. N. Tsvetkov, L. N. Andreeva, P. N. Lavrenko, E. V. Baleiva, O. V. Okatova, A. Yu. Bilibin, and S. S. Skorokhodov, Eur. Polym. J. **20**, 817, 1984.
91. V. N. Tsvetkov, L. N. Andreeva, P. N. Lavrenko, O. V. Okatova, E. V. Baleiva, A. Yu. Bilibin, and S. S. Skorokhodov, Eur. Polym. J. **21**, 933, 1985.
92. V. N. Tsvetkov, I. N. Shtennikova, E. I. Rjumtsev, and Ju. P. Get-manchuk, Eur. Polym. J. **1**, 767, 1971.
93. V. N. Tsvetkov, I. N. Shtennikova, V. S. Skazka, and E. I. Rjumtsev, J. Polym. Sci. C **16**, 3205, 1968.
94. V. N. Tsvetkov, E. V. Frisman, and N. N. Boitsova, Vysokomol. Soedin. **2**, 1001, 1960.
95. V. N. Tsvetkov, K. A. Andrianov, E. L. Vinogradov, S. E. Yakush-kina, and Ts. V. Vardasanidze, Vysokomol. Soedin. **9B**, 893, 1967.
96. V. N. Tsvetkov, K. A. Andrianov, E. L. Vinogradov, V. I. Pakhomov, and S. E. Yakushkina, Vysokomol. Soedin. **9A**, 1967.
97. M. G. Vitovskaja, V. N. Tsvetkov, L. I. Godunova, and T. V. Sher-emeteva, Vysokomol. Soedin. **9A**, 1682, 1967.
98. T. I. Garmonova, M. G. Vitoskaja, S. V. Bushin, and T. V. Shereme-teva, Vysomokol. Soedin. **16A**, 265, 1974.
99. V. N. Tsvetkov, N. N. Kupriyanova, G. V. Tarasova, P. N. Lavrenko, and I. I. Migunova, Vysomokol. Soedin. **12A**, 1974, 1970.
100. V. N. Tsvetkov, E. I. Rjumtsev, I. N. Shtennikova, T. V. Peker, and N. V. Tsetkova, Dokl. Akad. Nauk. SSSR **207**, 1173, 1972.
101. E. N. Zakharova, L. I. Kutsenko, V. N. Tsvetkov, V. S. Skakza, G. V. Tarasova, and V. M. Jamshchikov, Leningrad Univ. Vestnik, Ser. Fiz. Khim. **N16**, 55, 1970.
102. G. I. Okhmenko, Thesis, Inst. Macromolecular Compounds Acad. Sci. SSSR, Leningrad, 1969.
103. H. Janetchitz-Kriegl and W. Burhard, Adv. Polym. Sci. **6**, 170, 1969.
104. V. N. Tsvetkov, S. Ja. Ljubina, I. A. Strelina, S. I. Klenin, and V. I. Kurljankina, Vysomokol. Soedin. **15A**, 691, 1973.
105. V. N. Tsvetkov and A. E. Grishchenko, J. Polym. Sci. C **6**, 3195, 1968.
106. V. N. Tsvetkov and I. N. Shtennikova, Vysomokol. Soedin. **2**, 808, 1960.
107. V. N. Tsvetkov and A. V. Grishchenko, Polym. Sci. USSR **7**, 902, 1965; J. Polym. Sci. C **16**, 3195, 1968.
108. N. J. Mills and D. W. Saunders, J. Macromol. Sci. B. **2**, 369, 1968.
109. N. J. Mills, Polymer **12**, 658, 1971.
110. M. A. Llorente, J. E. Mark, and E. Saiz, J. Polym. Sci. Polym. Phys. Ed. **21**, 1173, 1983.
111. E. Riande, J. Guzman, and J. G. de la Campa, Macromolecules **21**, 2128, 1988.
112. S. Ja. Magarik and V. N. Tsvetkov, Zh. Fiz. Khim. **33**, 835, 1959.
113. M. Llorente, I. Fernandez de Pierola, and E. Saiz, Macromolecules **18**, 2663, 1985.

114. V. N. Tsvetkov, S. Ja. Magarik, T. Kadirov, and G. A. Andreeva, Vysokomol. Soedin. **10A**, 943, 1968.

115. V. N. Tsvetkov, G. A. Andreeva, I. A. Branovskaja, V. E. Eskin, S. I. Klenin, and S. Ja. Magarik, J. Polym. Sci. C **6**, 239, 1967.

116. V. N. Tsvetkov, E. I. Rjumtsev, I. N. Shtennikova, E. V. Korneeva, Okhrimenko, N. A. Mikhailova, A. A. Baturin, Ju. A. Amerik, and B. A. Krentsel, Vysokomol. Soedin. **15A**, 2570, 1973.

117. V. N. Tsvetkov, E. I. Rjumtsev, I. N. Shtennikova, E. V. Korneeva, Okhrimenko, N. A. Mikhailova, A. A. Baturin, Ju. A. Amerik, and B. A. Krentsel, Vysokomol. Soedin. **15A**, 2570, 1973.

118. A. Romanov, S. Ja. Magarik, and M. Lazar, Vysokomol. Soedin. **9B**, 292, 1967.

119. T. M. Birshtein, V. P. Budtov, E. V. Frisman, and N. K. Janoskaja, Vysokomol. Soedin. **4**, 455, 1962.

120. E. V. Frisman and N. N. Boitsova, Leningrad Univ. Vestnik. **N4**, 26, 1959.

121. V. N. Tsvetkov, G. A. Andreeva, I. A. Branovskaja, V. E. Eskin, S. I. Klenin, and S. Ja. Magarik, J. Polym. Sci. C **16**, 239, 1967.